Ulm University

Institute for Applied Physiology

Director: Prof. Dr. Birgit Liss

Electrophysiological and behavioural investigation of the circuits underlying cognitive functions in humans and the *Gria1* mouse model of schizophrenia

Dissertation to achieve the medical doctoral degree of the medical faculty of Ulm University

Daniel Strahnen

Neu-Ulm

2021

Current dean of the faculty: Prof. Dr. Thomas Wirth

1. Supervisor: Prof. Dr. Dennis Kätzel

2. Supervisor: Prof. Dr. Wolfgang Kelsch

3. Supervisor: Prof. Dr. Pico Caroni

Day doctorate awarded: 17.02.2023

Declaration with reference to the Creative Commons Attribution License

Parts of this thesis have already been published in

Strahnen D, Kapanaiah SKT, Bygrave AM, Kätzel D. Lack of redundancy between electrophysiological measures of long-range neuronal communication. *BMC Biol* 19. doi: 10.1186/s12915-021-00950-4

and

Strahnen D, Kapanaiah SKT, Bygrave AM, Liss B, Bannerman DM, Akam T, Grewe BF, Johnson EL, Kätzel D. 2021. Highly task-specific and distributed neural connectivity in working memory revealed by single-trial decoding in mice and humans. *bioRxiv*. doi: 10.1101/2021.04.20.440621

and are protected under the Creative Commons Attribution License (CC BY 4.0). For both articles, reuse is allowed, and copyright is retained by the author(s). The affected figures and tables are indicated with the following term: CC BY 4.0, https://creativecommons.org/licenses/by/4.0/

TABLE OF CONTENTS

ABBREVIATIONS

1 INTRODUCTION

1.1 SCHIZOPHRENIA

The term Schizophrenia etymologically stems from the Greek roots *schizein* ("to split") and *phren* (diaphragm) which was believed to be the place of the soul. The term was shaped by swiss psychiatrist Eugen Bleuler in 1908 who was first to detach the disease from the term *dementia praecox* which was introduced first as a description of what is today known as Schizophrenia by the German psychiatrist Emil Kraepelin in 1893 [217]. It has a point prevalence of 4.6 per 1000, a life-time prevalence of 0.7% and manifests itself most often in young adulthood accompanied by big personal and societal burdens whereas men are slightly more often affected than women [124, 177, 251, 304, 344]. Due to current occasion, it is noteworthy that schizophrenia constitutes a significant risk factor of dying from Covid-19, only being exceeded by age, but surpassing (pre-)conditions like diabetes mellitus and heart failure [329]. Despite new treatment options, schizophrenia remains a devastating and prognostically serious psychiatric disorder with few possibilities to predict the outcome of individual patients. From a diagnostic point of view, schizophrenic symptoms are described as heterogeneous but can be generally divided into three groups: positive, negative, and cognitive. Positive symptoms are called as such because they present as characteristics that are non-existent in healthy individuals such as psychotic manners like delusions, hallucination, and disorders of thought. Most reported manifestations of positive symptoms include hearing voices, persecutory delusions and disorganized communication which are commonly known as psychosis. Negative symptoms include disordered emotional stability which presents itself through reduced drive to engage in activities and diminished emotional expression. Cognitive symptoms consist of lessened executive functions, e.g., processing of everyday social interactions, attention problems and declining working memory (WM). WM is a core syndrome in schizophrenia [267], but it is also impaired in various other psychiatric conditions such as major depression and bipolar disorder that are characterizes by severe and pharmaco-resistant impairments of WM [308]. In general, WM refers to the capacity to maintain and manipulate contents of perception and thought at the forefront of attention over seconds to minutes [21, 22]. Attention and WM are closely intertwined since it is crucial to select the relevant information which should be remembered and not to be side-tracked by surrounding distractors [334]. In general, tests in human psychology demand from the subject to remember a certain number of words, numbers, or other symbols which are presented in a sample phase (SP) and then maintain the information over a short period of time (delay) after which the item must be retrieved in a choice phase (CP). Therefore, one can distinguish subcomponents of WM in humans based on the presented stimuli, e.g., verbal, or visual-spatial WM. If stimuli are repeatedly presented over multiple trials with the same outcome, associations are established as a *reference memory* (RM) for the given task or problem, which in humans can be referred to as mid- to long-term memory [209]. Besides WM deficits, schizophrenia is often associated with anxiety disorders [60] and their negative effect on morbidity has already been described by Bleuler [49].

The onset of manifest psychotic symptoms is often preceded by a prodromal state which is characterized by negative or nonspecific symptoms, such as depressive episodes, social withdrawal, anxiety and educational or occupational failure [303]. This typically occurs in the late teens or early twenties and is frequently overlooked and thus falsely classified by relatives and friends as a “normal” adolescence crisis. Since schizophrenia is yet an incurable disease the need to correctly identify prodromal symptoms is obvious in order to develop preventions and early interventions [278, 303, 409, 481].

Depending on which symptoms prevail, the disease can be further divided into subtypes which are no definite entities but rather merge into each other. The most common subtype is the paranoid-hallucinatory type in which psychotic symptoms like delusions and hallucinations dominate the clinical picture. Other subtypes include the *catatonic type* (which has been separated from schizophrenia in DSM-V) with psychomotor symptoms like hyperkinesia and stupor, the *hebephrenic type* which occurs in teenage years and is characterised by affective and social abnormalities, the *residual type* after experiencing psychotic episodes and personality changes, *post-schizophrenic depression* and *Schizophrenia simplex*, which is dominated by negative symptoms.

This description of the disease – as for most psychiatric diseases – is purely symptom based which is due to the fact that scientific insights into the aetiology of these disorders followed much later. Even though schizophrenia is often seen as a unique disease entity in clinical practice its uniformity is often questioned because of the variability of the symptoms and genetic traits [17, 218, 425]. A clear difference between schizophrenia and other mental illnesses is often difficult to determine because psychotic symptoms are not exclusive to schizophrenia. Recent studies strengthen more integrated approaches to mental diseases in presenting new evidence for genetic relationships between schizophrenia, bipolar disorder and schizoaffective disorders which frequently show indistinguishable patterns of the symptoms described above [84, 274, 321]. In this regard, it is important to note that, as for other psychiatric disorders, many patients show comorbidities, i.e., they meet criteria for more than one mental disorder, and also many patients do not show the full range of symptoms required by classical diagnostic symptoms leading to their exclusion in clinical trials. Although schizophrenia is not a monogenetic disease, studies have revealed a strong heritability and a large genome-wide association study (GWAS) has identified more than a hundred schizophrenia-associated genomic loci [382]. Environmental and social risk factors as well as the gut microbiome also seem to contribute to the genesis of schizophrenia, which is why schizophrenia should be seen as a complex and multifactorial illness [183, 369, 425].

An alternative to the purely symptom-based classification of mental disorders – which is, as described above, often insufficient in adequately assigning distinct disease diagnoses and tailored treatments – is the *Research Domain Criteria* (RDoC) project of the National Institute of Mental Health (NIMH) [113]. In contrast to classical diagnostic systems such as the *Diagnostic and Statistical Manual of Mental Disorders* (DSM) and the *International Classification of Diseases* (ICD), RDoC does not aim to strictly classify mental disorders [113]. It rather uses neurobiological and behavioural scientific results and thus is not solely based on the combination of presenting symptoms. However, its goal is not to serve as a new diagnostic system but rather as a research framework that may inform future versions of classification systems [113, 114]. RDoC was therefore proposed as a new approach to investigating mental disorders, i.e., not focusing on clinical syndromes but rather on fundamental psychological functions. Specifically, RDoC proposes six major domains of human psychological functioning: negative valence, positive valence, cognitive systems, systems for social processes, arousal/regulatory systems and sensorimotor systems [114]. Different units of analysis such as genes, circuits or behaviour can be studied to uncover the pathophysiology of parts of these domains. This trans-diagnostic approach is backed by findings of a recent study that found considerable genetic overlap between multiple psychiatric illness and directly questions the classical, categorical classification of mental disorders [269]. Furthermore, current medication for psychiatric disorders is effective for a large body of patients, but is rather unprecise, e.g., anti-psychotics can be used in schizophrenia, bipolar disorder, and other severe circumstances such as delirium and anti-depressants can be used to treat depression, anxiety, and mood disorders [113]. This manifoldness reduces the efficacy of psychiatric drugs because pathophysiological mechanisms differ in such heterogenous syndromes as classified in the *ICD* and *DSM* which is why drug development may profit from a more symptom-based and neurobiologically informed scrutinization of the diseases [113].

1.1.1 Treatment options for schizophrenia

Current medication for patients with schizophrenia primarily consists of antipsychotic drugs which aim to alleviate positive symptoms but mostly fail to improve negative and cognitive symptoms. Besides the fact that they often come along with considerable side effects, their efficacy – even against psychotic symptoms - is far from optimal which urges the necessity of new treatments [279]. Since patients suffering from schizophrenia often behave non-adherent towards therapy it is important to keep side-effects as minimal as possible and to address negative and cognitive symptoms as well to actually improve the patients well-being and everyday functioning which is mostly not achieved with antipsychotic drugs [2, 279].

The first discovered antipsychotic drug was Chlorpromazine, brought to market in the 1950s. Following this, more antipsychotic substances were discovered which are classified today as either typical or atypical antipsychotics. The former are also known as first-generation antipsychotics and often show severe extra-pyramidal side-effects like dystonia and parkinsonism. The latter are known as second-generation antipsychotics and show little extra-pyramidal symptoms with equivalent or even better therapeutic effects. The mechanism of action of antipsychotic drugs is not fully understood but they primarily block dopamine D_2 receptors. This blockade is likely associated with the extra-pyramidal side effects because dopamine D_2 receptors are an important component of the nigrostriatal pathway. Even though the receptor profile of atypical antipsychotics is not obviously distinct from first generation antipsychotics, they do not appear to severely reduce dopaminergic activity in the nigrostriatal pathway, which may explain the reduced extrapy-

ramidal side-effects they cause.
However, these drugs are still associated with adverse effects such as weight gain, metabolic disturbances and cardiometabolic risk factors which often contribute to morbidity and mortality in patients [273]. Just recently, the novel drug Lumateperone finished its first three phase clinical trials, was approved by the FDA and showed evidence of being safe and effective in alleviating positive, negative and cognitive symptoms without most of the side effects of usual antipsychotics [108]. The mechanism of action of Lumateperone comprises a combination of strong 5-HT2A antagonism, together with weaker serotonin reuptake inhibition, dopamine D2 and D1 receptor antagonism. However, results are still to be considered preliminary since long-term studies evaluating the safety profile and alleviation in negative and cognitive symptoms might be due to the improvements in positive symptoms [108].

1.1.2 Dopamine and the aberrant salience theory in schizophrenia

Dopamine receptors are G-protein coupled receptors (GPCRs) [39] and are divided into two groups: D_1-like receptors and D_2-like receptors [39]. The D_1 family contains D_1 and D_5 receptors and the D_2 family contains D_2, D_3 and D_4 [39]. The first discovery that dopamine-receptor blockade might play a crucial role for the mechanism of action of antipsychotics [375] and the experimental confirmation that their affinity to dopamine D_2 receptors positively correlates with their effective clinical dose in 1975 [393] were the founding stones of the dopamine-hypothesis of schizophrenia. These receptors were initially called “neuroleptic receptors” and studies in which patients were given psychostimulant drugs such as amphetamine, which upregulate dopamine in the CNS, showed that psychosis could be intensified [277].

However, Davis et al. discussed that a state of hyperdopaminergia alone fails to explain all facets of the disease [115]. The reasons given for this included the observation that the atypical antipsychotic drug Clozapine showed higher efficacy then other antipsychotics despite lower affinity to dopamine D_2 receptors [115, 234]. Also, unexpectedly, cerebrospinal fluid amine metabolites were not elevated in patients compared to normal controls [356]. Therefore, rather than being caused by a general state of elevated dopamine release, schizophrenia was considered to be caused by an unbalanced dopaminergic innervation across the brain. Indeed, especially the frontal cortex shows lower dopamine release [362] and lower blood flow in general in patients with schizophrenia [214]. Davis et al. hypothesised that a *hyper*dopaminergic state in the striatum leads to psychotic symptoms (and constitutes the effective target of antipsychotic drugs) whereas *hypo*dopaminergia in frontal cortex results in negative symptoms [115]. This idea was backed up by findings that the destruction of dopaminergic synapses in the PFC increased dopamine in the striatum of the rat [360].

However, as Davis et al. acknowledged, these findings also fell short in fully explaining the link between altered dopamine levels and the clinical manifestations of schizophrenia [115, 207]. In their review in 2009, Howes and Kapur tackled the emerging question how disturbances in a single neurotransmitter lead to such profound deficits in patients [207]. According to the multidimensionality and heterogeneity of schizophrenia, Howes and Kapur proposed that dopaminergic abnormalities are caused by upstream deviations in genetic, developmental and environmental factors [82, 207, 382]. The authors therefore conclude that schizophrenia unlikely has one basic cause, but the clinical symptoms are rather a composition of different biological alterations [207]. Striatal hyperdopaminergia was suggested as a marker for psychosis, but it is not confined to schizophrenia as it was observed in patients who suffered from psychotic episodes but were no diagnosed with schizophrenia [365]. Striatal hyperdopaminergia is tightly linked to the PFC since lesioning dopamine neurons in the PFC led to increased dopamine levels in the striatum and application of dopamine agonists to the PFC reduced dopamine in the striatum [207]. Dopamine is known to be crucial in reward signalling and pleasure seeking and a loss of it in the PFC could explain symptoms like anhedonia, social withdrawal and loss of interest [207]. It is important to notice that Howes and Kapur did not conclude that dopamine is the sole cause of psychosis, but rather an observed final common pathway and some other brain disturbances might also be involved [207].

Considering discoveries about dopamine, its crucial role in motivation and reward seeking and the ability of amphetamine to initiate psychotic symptoms, M. Spitzer was first to argue that dopaminergic and noradrenergic overactivity could be the reason for an increased signal to noise ratio when it comes to assessing everyday-stimuli resulting in unproper attribution of significance to ordinary and insignificant things which consequently leads to delusional symptoms [414]. S. Kapur and colleagues further elaborated this hypothesis and formulated the concept of aberrant salience [207, 235, 236], suggesting that abnormally elevated activity of dopamine neurons in the ventral tegmental area (VTA) of the dopamine system correlates with aberrant assignment of salience to harmless or otherwise irrelevant stimuli [235, 236]. Notably, dopamine in other areas was also linked to attribute the salience of stimuli, namely in mesolimbic, nigrostriatal and mesocortical regions [52, 195, 206]. Importantly, however, Kapur argued that acute altered dopaminergic signalling cannot be the sole criterion that leads to positive symptoms, but possibly chronically increased dopaminergic signalling [235]. This notion is supported by the observation that acute administration of amphetamine to healthy humans did not results in psychotic symptoms [486], but in medically treated patients with schizophrenia [13, 486]. The brain consequently attempts to construct a fitting narrative surrounding its perception of stimuli which is impossible when a proper assignment of importance is impaired and psychotic symptoms might be the consequent reaction of the brain [207, 235, 414]. Furthermore, many psychotic symptoms are based on the misconception between the patient's own thoughts and actions and the inability to see them as their own [281]. For instance, it was observed that patients may perceive their own sub-vocals as auditory hallucinations [179]. This only applies to a fraction of the positive symptoms that patients suffering from schizophrenia show which includes, as an example, the observation that other people can hear and control one's own thoughts but fails to explain patient's lack of proper decision-making and attribution of significance. Consequently, patients assign improper significance to a random or arbitrary stimulus and psychotic symptoms such as delusions and hallucinations arise over time as an explanation for the importance of the stimulus [207, 235, 236].

Building on this, a further approach has been discussed to characterise the positive symptoms of schizophrenia, namely the Bayesian approach [107, 143]. The Bayes-Theorem is a universal method that updates the probability of certain future events based upon new evidence about the implications of the present state conditions and is mainly applied in mathematical statistics, machine learning (ML), philosophy and engineering, but also found its way into describing processes in the brain [38, 252]. In neuroscience, it assumes that the brain actively tries to construct explanations for sensory inputs based on the weighing of generally known evidence and the persons own prior experiences [252]. Importantly, this makes perception an *active* process, as originally proposed by Herrmann von Helmholtz based on his studies on visual stimulus processing where he was the first to demonstrate that humans are susceptible to optical illusions [196]. The natural and autonomous tendency of humans to always trying to make sense of everything happening around them – which is comprehensibly impossible – earned the brain the nickname *inference and prediction machine* [156, 252] and led to the hypothesis that perception is merely a "controlled hallucination" [98, 396]. With regards to schizophrenia it is believed that the perception machinery is heavily disrupted, because patients with schizophrenia have immense difficulties with probabilistic inferences and additionally defend their misled and implausible convictions and fears with greatest efforts [143, 479].

Accordingly, increased aberrant salience was observed in patients suffering from delusions (despite medication) as well as in prodromal patients (highlighting the possible causal relationship between aberrant salience attribution and psychosis), but was reduced in effectively medicated patients [370, 371]. Following on from this, Katthagen et al. found that patients incorrectly assign predictive value to non-predictive stimuli in a task where they had to associate stimuli with certain outcomes and that their abnormal salience correlated with increased negative symptoms [238, 239]. As another example for aberrant salience attribution, a recent paper showed that patients with schizophrenia drastically overestimate immediate, personal experiences compared to information obtained from others, which also might explain social isolation, false beliefs and inappropriate behaviour observed in patients with schizophrenia [402].

1.1.3 Glutamate in schizophrenia

Besides the crucial role that dopamine supposedly plays, glutamate was also identified to be of high importance in the aetiology of schizophrenia. Glutamate is the most abundant neurotransmitter in the mammalian CNS and therefore plays a crucial role in many neural processes. Its dysfunction has been linked to several neurodegenerative and neurodevelopmental disorders [185]. Glutamatergic receptors are divided into ionotropic and metabotropic receptors where ionotropic receptors form an ion channel and are excitatory and metabotropic receptors are signal through G-proteins and therefore may be either activating or inhibitory depending on if they couple to G_q or G_i-proteins, respectively. Ionotropic glutamate receptors include the N-methyl-D-aspartate receptor (NMDAR), the α-amino-3-hydroxy-5-methyl-4-isoxazolepropionic acid receptor (AMPAR) and kainate receptors. Analysis of de novo copy number variations and exome sequencing have established a genetic connection between NMDARs and schizophrenia [249, 282, 439], and a GWAS linked the NMDAR subunit NR2a and the glutamate ionotropic receptor AMPA type subunit 1 (GluA1) to schizophrenia [367, 382]. AMPA receptors and their relevance to schizophrenia are described in more detail in 1.5. Metabotropic glutamate receptors (mGluR) are classified into three groups and are named $mGluR_{1\text{-}8}$. mGluRs were found to be a potential therapeutic targets in schizophrenia research by their ability to directly modulate ionotropic glutamate signalling, including presynaptic glutamate release [105, 106, 352].

Analogous to the dopamine hypothesis of schizophrenia which was formulated because of the mechanism of action of antipsychotic drugs, the glutamate hypothesis was originally proposed because of the psychotomimetic effects of the NMDAR antagonist phencyclidine (PCP, “angel dust”) [289, 290]. Importantly, PCP mimics schizophrenic symptoms without excessive dopaminergic activity [87] and in the presence of dopamine antagonists [255]. Later studies confirmed the importance of NMDAR in schizophrenia by showing that ketamine administration in patients without schizophrenia leads to schizophrenic symptoms [257] and deteriorates symptoms in patients stabilized with antipsychotics [261]. These findings led to the assumption that NMDAR agonists might be a new therapeutic target which was supported by studies that found that PCP-induced effects can be reversed by a $mGluR_2$ agonist in rats [314] and humans [256]. Further clinical studies with the drug bitopertin, a reuptake inhibitor of the NMDA co-agonist glycine, and D-Amino acid oxidase (DAAO), which is responsible for degrading NMDAR amino acids, yielded partially promising results [64, 263, 352]. Still, cognitive symptoms were alleviated only with mixed success which might be explained with insufficient cognitive stimulation from the environment of patients with schizophrenia [242]. However, the glycine transporter 1 inhibitor BI 425809 that boosts the concentration of glycine in the synaptic cleft and serves as a co-agonist for NMDA receptors [374], was shown to be safe and efficacious and could improve cognition in patients with schizophrenia and is currently in phase three clinical trials [142].

1.2 Oscillations in the brain

Electrophysiology is a fundamental field in medicine and biology ever since Luigi Galvani discovered the electric properties of nerves and muscles in the 18th century and Hans Berger observed oscillations in the electrical potential above the scalps in humans. Since then, research on this topic advanced rapidly and technological progress allows today's scientists to study electrical signals in multiple ways. The fundamental procedure in electrophysiology involves the measurement of voltage changes that arise because of a difference of the electric potential measured at two different points, e.g., two compartments with different ion concentrations that are separated by the equivalent of a non-permeable membrane. In neuroscience, one can distinguish between to different approaches: Intra- and extracellular recordings. Intracellular recording comprises measuring differences in electric potentials across the membrane of individual cells. Studies which examined the electric properties of neurons by inserting an electrode inside the target cell led to the discovery of the action potential – the temporary depolarisation of the membrane potentials by about 100 mV [202]. Further developments like the patch-clamp technique allow scientists to investigate distinct features of cells such as membrane properties, synaptic inputs, and ion channel activity [328].

Electric current can also be measured in the extracellular medium surrounding brain cells because action potentials and post-synaptic potentials perturb the electric field around the respective neuron [208]. Focussing on the brain's bioelectricity there are the following methods for its measurement. Non-invasive approaches) are magnetoencephalography (MEG), which records magnetic fields produced by electric current and electroencephalography (EEG), a widely used technique especially in epilepsy patients where multiple electrodes are placed all around the patient's scalp. Other methods require craniotomy and therefore are rather invasive; this includes electrocorticography (ECoG) which can be also called intracranial electroencephalography (iEEG) using grid or stripe electrodes, which are placed on the surface of the cerebral cortex and deliver spatially more precise signal analysis than extracranial techniques because the limiting factor of low bone conductivity is eliminated. Stereo encephalography (SEEG) / intracerebral electrodes are depth electrodes which are able to detect local field potentials (LFP) and, with a sufficient sampling rate, even extracellular action potentials (spikes). Signals obtained from extracellular electrodes can be divided into two frequency ranges: LFPs (mostly <100Hz) and spiking activity (multiunit activity (MUA), >300Hz) [70]. It is possible to precisely identify individual neurons if the electrode is placed in close proximity to a neuron and multiple recording sites record the same neuron activity. If this is not the case, the recording mostly consists of the summed activity of multiple cells recorded simultaneously (MUA) which can be quantified by thresholding or template-matching (selecting template spike shapes and then assign the detected waveforms) [70, 167].

LFPs are the sum of all ionic processes surrounding the recording electrode, e.g., transmembrane currents from synaptic activity or action potentials [70, 312]. The spectrum of the LFP can be further divided into specific frequency ranges. In humans the EEG waveform is typically separated into five frequency bands: Delta (δ: 1-4 Hz), Theta (θ: 4-8 Hz), Alpha (α: 8-15 Hz), Beta (β: 15-30 Hz) and Gamma (γ: > 30 Hz). In rodents, however, this classification differs slightly so that the α-range is included into the θ-range which is from 5 to 12 Hz (or from 4-12 Hz). Beta and gamma are considered as high frequency oscillations and are involved in short- as well as in long-range networks, i.e. in neural communication within and between brain regions, respectively [445, 476]; delta and theta / alpha are considered as low frequency oscillations and usually modulate long-range synchronization [417].

Several studies showed that the firing of neurons in the cats visual cortex is correlated with the phase and amplitude of the LFP recorded from the same electrode as a response to light stimuli which expanded the horizon of electrophysiology by not confining to single cell analysis [134, 181, 182]. Building on this work, further studies confirmed the importance of synchronous neural oscillations for communication in the brain [298, 299] and in 2005 P. Fries proposed the influential concept of “Communication through Coherence” (CTC) which states that coherent oscillations in interactive brain regions are necessary for proper spiking input and output and therefore essential for long-range communication [154]. Furthermore, LFPs were increasingly seen as neural activity that can influence behaviour together with spiking activity, rather than being an epiphenomenal by-product [487]. However, it is important to note that the analysis of action potentials and LFP differ fundamentally with regards to a phenomenon called volume conduction: When recording spiking of single neurons one can be sure to only record data from that specific

neuron, but, however, when analysing the sum of the extracellular current as for LFP the exact source localization proves difficult [135, 197, 230]. Two electrodes – although placed in different brain regions - may record the same signal which was conducted passively as an electrical field from a single source through the tissue. In this case, the data is corrupted because both signals will have a phase lag of zero or π resulting in spuriously high coherence values that do not reflect actual neural processes. Despite their name, LFPs are suspected of not being particularly local and the term is mainly used because of its widespread use in the neuroscientific community [230]. Especially in rodent brains it was shown that low frequency potentials generated in the hippocampus can be measured in neocortical areas [403]. Therefore, it is important to question the reference location and the respective methodology with which to analyse the signals, because some were proven to be less susceptible to volume conduction (see 1.2.1 and 2.5).
With reference to schizophrenia, symptoms are thought not to arise solely because of a malfunction in a single brain region but rather because of fundamental impairments in multiple neural circuits. As a consequence of the numerous pathologic alterations in the brain of patients with schizophrenia, the communication between brain regions – as indicated by synchrony of their neural activities - are disrupted [159, 411]. It is important to note that up to this date it is not completely clarified to what extent certain oscillatory processes in distinct frequency ranges contribute to specific brain diseases such as schizophrenia and that similar aberrant patterns are observable in multiple diseases [447]. In fact, it seems to be more likely that the complex interaction between different frequencies and their rhythmic relationship to neuronal spiking seems to form a solid basis on which the brain communicates [69]. Also, most observations of abnormal oscillatory activity are correlative and causal relationships to behavioural deficits are generally very difficult to establish. However, surveying all oscillatory abnormalities associated with a given disease is a necessary first step.

Therefore, in the following subchapters, the most commonly used measures of neural communication are introduced (1.2.1), and subsequently, key findings regarding abnormalities in distinct frequency ranges seen in patients with schizophrenia and animal models are presented, and their relevance to specific cognitive functions is discussed (1.2.2 - 1.2.3).

1.2.1 Measures of neural communication

To adequately capture the neural communication between two or more anatomically separated networks, researchers developed a variety of different measures (see Table 1.2.1). Theoretically, an ideal measure would identify all activity by excitatory, inhibitory and interneurons in both regions and then extract and quantify equalities and differences. Yet, this proved to be particularly difficult in behaving mice which is why in most cases metrices based on LFPs or spike-LFP synchrony are used. However, LFPs come with the natural disadvantage of being the summed input from multiple neural processes. Considering that most brain regions are built of diverse cell layers, the precise locations of the recording electrodes are crucial and requires prior knowledge of anatomical connections. For example, it is intuitive to measure informational flow between the somatic layer of one region and the dendritic layer of another region, but it is questionable if the reverse conveys any biologically relevant information. Table 1.2.1 contains the most widely used metrices to assess inter-regional neural communication in rodents, mostly involving recordings from the hippocampus and PFC [4, 123, 229, 401], but also increasingly from the thalamus [56, 349], and the amygdala [394].

In the following subchapters (1.2.1.1 - 1.2.1.4) and in the methods section (2.5), these measures will be described in broader detail.

1.2.1.1 Non-directed coupling, synchrony

Oscillations in the brain – like any other oscillation – consist of amplitude, period and phase and contain many frequency domains which consequently can be decomposed into their components. The conversion from the time domain to the frequency domain is achieved by estimating the power spectrum which plots the frequency on the x-axis against the power at a given frequency on the y-axis. The power spectrum represents merely oscillatory features in brain region A. These characteristics might be also found in brain region B, but in order to investigate neural circuits one is also interested in interdependencies between A and B. Hence, one could investigate how the phases of both signals are related, e.g., if both regions strongly oscillate in the theta-range with a constant phase relationship. The phase difference between two signals is essential to understand the relation of two oscillations and can be calculated via conjugate multiplication of complex numbers obtained from each power spectrum resulting in a data structure called the cross-spectrum. The cross spectrum divided by the product of the power spectra of the individual signals returns a dimensionless number between 0 and 1 which is commonly referred to as coherence. It therefore represents a static phase relationship between two signals. As described above, coherence was shown to play an important role in the visual cortex [134, 181, 182] and further findings led to the concept of CTC which was proposed by P. Fries in 2005 [154]. It declares that long-range communication between different regions in the brain is dependent on phase-locked oscillations between them and thus proper communication is not possible in the absence of coherence. This statement is supported by the presumption that oscillations are a basic feature of neurons and play an important role not only in facilitating the output of the "sending" region but also in enhancing the excitability of the receiving neurons. Consequently, communication between brain regions is the most effective if input and output are timed which is believed to be coordinated by coherence [6, 154, 155, 476].

The biggest point of criticism of the metric of coherence that has been raised is the issue of volume conduction. Since coherence consists of a real and an imaginary component, Nolte et al. demonstrated in 2004 that using only the *imaginary component of coherence* (ImC) reduces the influence of a volume-conducted signal originating from a common source [332]. Further improvement was made by Stam et al. in 2007 by proposing the *phase lag index* (PLI) which was publicised to be more precise in detecting phase synchronization and reducing susceptibility to volume conduction [416]. This was due to the fact that the PLI ignores the magnitude of the phase by which one brain region leads or lags another brain region and only estimates a consistent, non-zero phase lag [416]. Vinck et al. insisted that the PLI lacks accuracy in correctly sensing small changes in phase synchronization which compromises the validity of the results [454]. Therefore, the *weighted phase-lag index* (wPLI) takes the detected phase lead or lag and weighs it by the magnitude of the ImC which was proven to eliminate these small noise perturbations [454]. Another limitation related to measures of phase synchronization like the ImC, PLI and wPLI is sample-size bias, i.e., the observation of spurious non-zero synchrony even in the absence of real connections which usually increases with a lower number of samples. To solve this issue, Vinck et al. introduced a debiased estimator of the wPLI which is more independent from sample size and thus has a higher statistical power than previous measures [454]. As the classical coherence metric, wPLI ranges between zero (no synchrony) and one (total synchrony). The described outdated measures (ImC, PLI, biased wPLI) are not applied here and, for the sake of clarity, the debiased wPLI will be referred to as wPLI throughout this thesis.

Besides the already described measures for phase synchronization, other metrics are also widely applied such as the phase-locking value (PLV) [260] and pairwise phase consistency (PPC) [455]. They either compute a Hilbert, wavelet, or Fourier transform to calculate the constancy of the difference between the instantaneous phases of two signals and to quantify the distribution of phase differences either by taking the vector average or by determining the distribution of phase differences across observations, respectively. While PPC and PLV are usually considered as roughly equal, the key benefit of the PPC metric is that it is not biased by sample size and therefore more suited for comparing datasets with differing sample size as reviewed in [36].

1.2.1.2 Directed synchrony based on leads and lags

The stated measures of phase synchronization are attempts to quantify *non-directed* connectivity. This means that the quantification of coupling is essentially based on correlation analysis, ignores its temporal structure, and assumes no direction of the influence from one region to another [36, 157]. However, LFP data contain patterns from which *effective* or *directed connectivity* can be inferred [157, 158]. This can be achieved by analysing recurring pairwise patterns in the time series obtained from any region and by quantifying the causal impact that the activity in one region exerts on another region. A computationally straightforward metric to uncover directionality between two time series is *cross-correlation*. That means that correlations are calculated as the LFP-signals are incrementally shifted against one another which could results in a high cross-correlation at a certain temporal shift (lags). Adhikari et al. developed a method termed *amplitude cross-correlation* in which the instantaneous amplitudes of two oscillatory signals filtered in a certain frequency range are cross-correlated to determine if one is leading or lagging the other [3]. If the lags at which the peak of the amplitude cross-correlation function occur is significantly different from 0ms, it is indicated that one region leads or lags the other one with a certain consistency (peak of the cross-correlation function), which was hypothesized to represent a directed influence from the leading onto the lagging region. This method helped to detect directed connectivity in the brain related to WM and fear processing [56, 280, 423].

1.2.1.3 Directed synchrony based on causal influences

A different measure of directed influence is Granger causality (GC). It infers directed causation based on the notion that one signal is helpful in predicting the other. It was initially proposed by Norbert Wiener in 1956 who stated that in case the information of one of two simultaneously measured signals can help predicting the second signal, the first one is causal to the second [472]. This in particular makes it a useful complement to estimate the distribution of influence in the observed neural networks. This concept was later put to practical use by nobel laureate Clive Granger in 1969 to detect information flow between time series in economics using autoregressive modelling [180]. In *parametric* GC, two separate autoregressive models (ARMs) are calculated and statistically compared: a univariate ARM, where the signal is predicted by a weighted combination of its own past values, and a bivariate ARM where the signal is additionally predicted by the second signal. If the inclusion of the bivariate AR leads to a reduction of variance of the autoregressive prediction error, one signal is said to Granger-cause the other [126]. GC can also be computed with *non-parametric* methods where the same information is obtained by first calculating the cross-spectral density matrix and then applying Wilson's spectral matrix factorization as input to the GC algorithm [121]. Overall, this approach has been demonstrated to be equivalent to parametric GC and to uncover the same network characteristics [121]. The mathematical foundations of GC and its application to neuroscience has been reviewed extensively in [62, 63, 126, 397]. Related measures that can either be based on *multivariate* ARMs or on non-parametric methods for directionality estimation and allow analysis of more than two channels include the directed transfer function (DTF) [233] and partial directed coherence (PDC) [19]. These measures are reviewed comprehensively in [50].

1.2.1.4 Directed cross-frequency coupling and spike-LFP synchrony

Other indicators of inter-regional communication that partly circumvent volume conduction and are typically interpreted as causal directed influence include those that measure *different types* of neural activity in the different regions, i.e., a low-frequency LFP oscillation (typically in the theta-range) in the presumed sending region and a local and high-frequency activity at the receiving end. In contrast to the metrics introduced before, historically, such measures were introduced by way of an actual *biological* discovery of such coupling phenomena, rather than by *a priori* mathematical considerations on how to best assess inter-regional communication. For instance, one could quantify the degree to which oscillations of *distinct* frequencies are coupled to each other, a phenomenon called cross-frequency coupling (CFC) [81]. Particularly, local phase-amplitude coupling (PAC) - the statistical relationship between the phase of a low-frequency and the amplitude of a high-frequency component – was repeatedly associated with memory processing in the hippocampus of rats [102, 441] and humans [18]; see 1.2.3 for further description of the relevance of PAC for WM. However, albeit to a lesser extent, *cross-regional* PAC between the hippocampus and prefrontal cortex (PFC) has also been used and was associated with directed information flow and cognitive functions [326, 403, 442, 489]. As high-frequency brain oscillations mainly reflect local aspects of information processing whereas low-frequency brain rhythms are relevant for inter-regional communication, CFC might represent a mechanism of transferring information from large scale neural networks to local processes [81, 287].

Another very widely used measure is based on the recording of spikes in one (potentially the *influenced*) region alongside the LFP in another (potentially the *influencing*) region. Spikes are generally not considered to be confounded by volume conduction or referencing (assuming that reference electrodes are placed several hundred microns away from the recording site), and they represent a more direct readout of the actual neuronal activity of a region. For example, phase-locking of neuronal firing to theta-frequency hippocampal oscillations was shown in the PFC [229, 400], entorhinal cortex (EC) [148] and the amygdala [347]. That means, that it was observed that action potentials in these brain regions occurred rhythmically at the same phase of the hippocampal theta rhythm. This coupling is known as spike-phase coupling (SPC) and was correlated to performance in multiple cognitive tasks [41, 229, 400], and has been used to reveal coupling deficits in mouse models related to schizophrenia [123, 401, 434].

Table 1.2.1: Overview of commonly used measures of neural communication
Adapted from [420], open access article: CC BY 4.0, https://creativecommons.org/licenses/by/4.0/

Category	Acronym	Metric	Description	Reference
Non-directed coupling, synchrony	-	coherence (magnitude)	Magnitude of the complex cross-spectrum	[229, 401]
	ImC	imaginary part of coherence	Discards the real component of the cross-spectrum	[332]
	PLI	phase-lag index	Disregards the magnitude of the cross-spectrum and averages the sign of phase differences	[416]
	wPLI	Weighted phase-lag index	Phase lags are weighed by the magnitude of the imaginary component of the cross-spectrum	[454]
	PLV	phase-locking value	Circular resultant vector length of the phase differences	[260]
	PPC	pairwise phase-consistency	Computed based on the distribution of phase differences	[455]
Directed (lead/lag, LFP-based)	-	coherence (phase angle)	Angle of the complex cross-spectrum	[88, 473]
	CC	cross-amplitude coupling, amplitude cross-correlation	Instantaneous amplitudes of two filtered LFPs are cross-correlated and the lag at which the peak occurred is determined	[3]
Directed (causal influence)	GC	Granger causality	Quantifies if the past of one time series can predict the future of another time series using autoregressive modelling	[62, 63, 126, 397]
	npGC	non-parametric Granger causality	Granger Causality based on spectral matrix factorization	[120, 121]

	PDC	partial directed coherence	Normalized metric based on GC that measures direct influence from one time series to another	[19]
	DTF	direct transfer function	Adaptation to multiple input variables closely related to PDC	[50, 233]
Directed (phase-locking of local activity)	SPC, MRL	spike-phase coupling, Mean resultant vector length	Circular concentration of the phase distribution at which spikes occurred	[4, 123, 400, 401]
	PAC, CFC, MI	phase-amplitude coupling, cross-frequency coupling, modulation index	Modulation of the amplitude of high-frequency oscillations in one area by the phase of low-frequency oscillations from another area	[403, 442, 489]
Directed (lead-lag, spike-based)	-	Phase angle of MRL	Mean phase at which spikes occurred	[123]
	-	Phase-shifted MRL	Calculation of the MRL based on phases at shifted lags	[400, 401]

1.2.2 High-frequency oscillations and their aberration in schizophrenia

Gamma oscillations were shown to play an important role in proper communication between brain regions and were observed during awake and sleep states [74, 75]. The generation of gamma oscillations is tightly linked to gamma-aminobutyric acid (GABA)-ergic parvalbumin (PV) positive interneurons [110, 300]. For example, optogenetic inhibition of these neurons could strongly suppress cortical gamma activity [406]. Since GABAergic markers, including PV, were found to be reduced in post mortem tissue of patients with schizophrenia, it strongly suggests that the GABA network and the gamma rhythm are tightly correlated with the pathophysiology of schizophrenia [176]. Also, intact interhemispheric gamma synchrony between prefrontal PV interneurons was recently shown to be important for behavioural adaptation during rule-shifting as optogenetic disruption of gamma led mice to persevere, highlighting the importance of gamma synchrony for reattributing the behavioural attention to novel rules [94].

Alterations in gamma oscillations have been related to sensory-processing deficits in schizophrenia in multiple studies [305] and were proposed as potential biomarkers for the disease [438]. Work by Kwon et al. [259] examined the synchronization of the EEG to auditory stimulation at a frequency of 40 Hz and were able to show, for the first time, that patients display impairments in entrainment and synchronization of gamma-frequency oscillations in the auditory cortex. This auditory paradigm is called auditory steady-state responses (ASSR) and alterations were replicated and linked to reduced expression of PV mRNA in GABAergic interneurons not only in the above mentioned brain regions, but also in auditory cortices in patients with schizophrenia [189]. Furthermore, spontaneous gamma activity was found to be increased during ASSR-stimulation in patients with schizophrenia [200]. This can be connected to previous findings in animal models in which it was already shown that hypofunction of NMDARs led to increased spontaneous gamma power in rats administered with NMDAR-antagonists [355] and in mice in which NMDARs were ablated in PV cells [86] suggesting that spontaneous gamma power could serve as a potential biomarker for NMDA dysfunction in schizophrenia. Optogenetic studies endorsed the importance of the interplay between NMDA-receptors, PV-interneurons and gamma-oscillations by showing that oscillations in the gamma-range where increased during stimulation of PV-interneurons [83], but reduced when PV-interneurons lacked NMDA-receptors [86]. These findings highlight the possible importance of synchronous gamma oscillations in sensory processing which might be disrupted in patients with schizophrenia.

Furthermore, patients with schizophrenia showed reduced gamma-band oscillations in an auditory oddball (mismatch-negativity) paradigm where participants were confronted with frequent standard tones and rare, deviant tones [165]. In a study in which patients were confronted with Mooney faces – a series of black and white photographs where faces can be detected, a phenomenon known as Gestalt perception – they showed significant desynchronization in the gamma and beta band compared to healthy control subjects [446]. These results suggest that dysfunction in sensory processing shown by patients with schizophrenia are associated with impaired gamma and beta oscillations. Additionally, enhanced gamma and beta band activity and synchrony was linked to the positive symptoms of schizophrenia, especially to auditory hallucinations [270, 412, 413]. It was hypothesized that increased oscillatory activity leads to impairment of corollary discharge, a mechanism for distinguishing between self and externally generated perceptions by generating an efferent copy of the motor plan which is supposedly disrupted in schizophrenia [146, 447].

In rodents, beta and gamma oscillations were tightly linked to WM as the former was shown to play a critical role in orchestrating thalamo-prefrontal and hippocampal-prefrontal connectivity [76, 349] and the latter was correlated to correct memory choices in various studies [138, 199, 316, 483]. For a tabular overview of oscillations and their correlation with WM in rodent studies please see Table 1.6.1.

1.2.3 Low-frequency oscillations and their aberration in schizophrenia

Although abnormalities in high-frequency oscillations are more extensively documented, alteration have also been revealed for low-frequency oscillations such as δ, α and θ [283]. Theta-band oscillatory activity in the awake state was found to be generated and to be most dominant in the hippocampus and its afferents from the medial septum [67, 184, 449]. Unlike high-frequency oscillations, low-frequency oscillations like theta can travel further distances in the brain and therefore connect more distant brain areas [71]. It is important to note that theta oscillations in the awake state have been primarily studied in rodents where they are associated with voluntary movement [449]. They have been reliably observed in learning tasks [392] and spatial navigation [65] which led to the assumption that theta oscillations are crucial for a variety of rodent behaviour [68, 72].

Theta is believed to play an important role in synchronising activities of the hippocampus and the PFC in cognitive tasks [229]. In the hippocampus, the firing of place cells, excitatory neurons with spatial receptive fields, is phase-locked to the local theta rhythm (see 1.2.1.4 and [336]). Findings in rodents underline the importance of theta synchrony between several brain regions such as the PFC and hippocampus for WM [1, 137, 229, 341, 410, 433]. In 2010, Sigurdsson et al. investigated theta-band connectivity between the PFC and the hippocampus in Df(16)A+/- mice – a model for a microdeletion on human chromosome 22 (22q11.2), one of the largest known genetic risk factors for schizophrenia – and found significant reductions during memory retrieval compared to healthy control animals [401].

In contrast to impaired theta activity in WM tasks in rodents, elevated and sustained theta activity is consistently associated with psychotic symptoms in humans [11, 320, 415, 490]. This is consistent with the recent finding in a genetic mouse model of schizophrenia that increased fronto-temporal theta-coherence was correlated to novelty-induced hyperactivity, a potential marker for psychosis in rodents (see 1.4.1) [76]. Both could be restored by viral re-introduction of the respective gene which highlights the close connection between theta and short-term habituation [76]. Also, novelty resets theta-band connectivity between the ventral hippocampus (vHC) and the mPFC by weakening this connection, however, connectivity is strengthened during subsequent adaptation to the new task [348]. In this study, the authors also proved a link to D1 receptors as blocking these receptors prevented these adaptations [348] which highlights the importance of novelty adaptation in schizophrenia and potentially explains a functional role of elevated theta as the cause of failed short-term habituation.

Likewise, as already introduced in 1.2.1.4 as CFC and mostly quantified as PAC, the phase of the theta rhythm was found to be associated with the amplitude of gamma-band oscillations in the brain of rodents [61, 287, 403, 407] and humans [80, 287] which was hypothesised to be a general coding scheme, especially for WM [284, 286, 287]. Lisman and Jensen therefore proposed the “Theta-Gamma Neural Code” which implicates that distinct spatial information is coded in different gamma subcycles of a theta cycle which can be observed within or between brain regions [287]. Analogous to this, patients with schizophrenia which showed WM deficits, also displayed impaired theta-gamma coupling during a WM task [34].

Generally, it was observed that low-frequency oscillations in patients with schizophrenia display lower task-related increases decreased during cognitively demanding tasks and elevated during rest compared to healthy control subjects [318]. Unlike gamma oscillations, the theta-frequency range itself and its connection to schizophrenia has been less explored so far and results do not seem to be completely unambiguous. On the one hand, theta-range coherence recorded between neocortical regions using EEG was explicitly correlated with auditory hallucinations in a study where patients without auditory hallucinations and healthy controls showed increased theta coherence between frontal and temporal electrodes, whereas patients with schizophrenia with auditory hallucinations had significantly reduced patterns of theta coherence [147]. On the other hand, increased theta-range connectivity was found in resting-state EEG recordings [11, 320, 415, 490].

1.3 Brain regions with relevance to schizophrenia

The first studies about changes in gross brain anatomy in patients with schizophrenia using magnetic resonance imaging (MRI) reported an enlarged ventricular system [117], and grey matter reductions most prominent in the temporal lobe and in the dorsolateral [480]. Additionally, it was shown that brains of patients with schizophrenia display abnormalities already before mental symptoms occur, suggesting that schizophrenia is a neurodevelopmental disorders [322, 467]. Since it is hypothesized that schizophrenia is not a disease that can be traced back to a deficit in a single brain region, functional connections between the PFC and other brain regions were investigated and patterns of strongly altered connectivity were observed among patients [100]. However, it was recently shown that the same brain abnormalities seen on MRI scans are not equally observable in all patients with diagnosed schizophrenia, leading the authors to conclude that there might be different subtypes of the disease which display different neuroanatomical phenotypes [90].

Three of the most relevant brain regions, the PFC, the hippocampus, and the thalamus, will be discussed in the following since they are of particular bearing for the rest of this work.

1.3.1 The prefrontal cortex

The PFC is located in the anterior part of the hemispheres and receives major inputs from the mediodorsal nucleus of the thalamus (MD). The PFC is ascribed great importance in cognitive functions which are a necessity to coordinate a wide variety of behaviours [175]. As a first key finding, it was shown that persistent firing of neurons in the dorsolateral PFC (dlPFC) was associated with WM performance in primates [161]. Human neuroimaging studies further suggested relevance of the PFC in regulating attention [346] and WM [301].

Regarding the relevance of the PFC in schizophrenia, it was already described in 1.1.2 that reduced dopamine in the PFC can lead to symptoms of the disease. Neuropathological studies of the brains of patients with schizophrenia revealed the same number of neurons but in smaller volume resulting in elevated neuronal density and in reduced neuropil which might lead to diminished connectivity [48, 395]. Based on the fact that WM is impaired in patients [469] imaging studies revealed no specific activation of the PFC during cognitive tasks in patients with the illness compared to healthy controls [468]. Interestingly, however, the disease onset is characterised by a state of increased PFC connectivity revealed by comparing resting-state functional MRI (fMRI) of patients with early-course schizophrenia and healthy subjects [15].

Even before being aware of these alterations in schizophrenia, the main treatment for schizophrenia and other mental diseases associated with deviant behaviour often was frontal lobotomy, i.e., the surgical severing of connections in the PFC [150]. This procedure was fortunately abandoned since it left the patients with strongly damaged intelligence, emotion, and social behaviour [150]. Interestingly, one of its critics was American mathematician Norbert Wiener who was introduced in 1.2.1.3 and who would later pave the way for future discoveries regarding whole brain connectivity with his works on communication and causality [62].

Since the PFC is considered exclusive in primates because of its outstanding role in cognition, decision making, speech and linking present experiences to possible future outcomes [163, 175], it is particularly difficult to transfer animal findings into human brain research. Historically, the PFC of primates was defined based on the presence of a cortical granular layer IV rostral to the agranular motor areas which differentiates it from non-primates as they lack a granular layer IV [448]. However, the cytoarchitecture as a sole criterium was soon abandoned and replaced by connectivity and functions. For example, reciprocal thalamocortical connections, which, for the PFC, are mainly formed with the MD (see 1.3.3), are an important tool for classifying cortical areas [288, 373] and are also seen in rodents [186, 448]. However, a precise anatomical definition of the PFC in mice is still not available resulting in varying delineations and proposed subregions as summarized in [265]. Therefore, the authors conclude that it is important to report the exact stereotactic locations in order to avoid miscommunication of scientific findings [265].

1.3.2 The hippocampus

The hippocampus is part of the limbic system in the temporal lobe and because of the rotational movement during development shows an S-shaped structure. It receives major cortical input from the EC and consists of the dentate gyrus (DG), the cornu ammonis (CA) with its subfields CA1-4 and the subiculum. The main excitatory pathway, the classic trisynaptic loop, was described as the following: EC → DG, DG → CA3 and CA3 → CA1. The EC serves as the main interface between the hippocampus and the neocortex and forwards information along the perforant path to the granule cells in the DG [8]. Axons called mossy fibres mainly project to CA3, and axons of CA3, called Schaffer collaterals (SC), project to CA1 [8]. The circuitry is completed by a connection from CA1 to the subiculum and back to the EC [474]. Afferent and efferent connections of the hippocampus are mainly transmitted through the EC and the subiculum [474]. In addition to the trisynaptic path, CA1 also receives monosynaptic glutamatergic input from the EC forming synapses in a layer called stratum lacunosum moleculare (SLM) whereas the SC end in the stratum radiatum (SR). Besides the known connection from CA3 and EC to CA1, CA2 neurons were also shown to be excited by direct EC and SC input and to strongly excite CA1 neurons [92]. Also, the subiculum was shown to not be the only output channel of the hippocampus as a functional circuit from CA3 to the dopaminergic neurons of the VTA via the lateral septum was discovered [291] and CA3 was revealed to also receive afferents from the medial septum [42]. Further literature on anatomical connections within the hippocampus and to other brain regions is extensively reviewed in [37].

Regarding functional tasks, early studies showed that bilateral hippocampal lesions lead to an impairment in acquiring new, explicit memories (anterograde amnesia) which was first documented in the famous patient H.M. [391]. However, general knowledge such as vocabulary which was learned well ahead of the hippocampal damage remained intact and led to the assumption that these older memories become transferred to the neocortex [391]. Lesioning the EC, DG, CA3 and CA1 emphasized their role in learning and memory formation [323, 324, 424, 444] whereas the CA2 subfield was shown to be of particular importance regarding social memory [127, 201, 418]. The discovery of place cells in rats in 1951 by John O'Keefe shed light into the observation that hippocampal damage resulted in spatial memory deficits [335]. Each place cell in the hippocampus has its place field and fires when the subject is at a distinct place in a known surrounding, which is known as the spatial mapping theory [335, 337]. Besides the function of the hippocampus for spatial, object-related and social associative long-term memory the hippocampus is involved in long-term fear memory [247], and (short-term) working memory indicating that it contains various circuits for different types of memory [422]. With special emphasis on WM, studies linked neuronal activity in the medial temporal lobe (MTL,

which includes the hippocampus, EC and the amygdala) in humans [57, 232, 253] and hippocampal neuronal activity in monkeys [78, 153, 465] to WM. In rodents, hippocampal lesions led reduced hippocampal-prefrontal connectivity an WM performance [66] and analyses of (mainly theta- (5-12 Hz) and gamma- (30-50 Hz) band) oscillatory synchrony between the hippocampus and the PFC were found to strongly correlate with WM [41, 213, 229, 400, 401, 410]. Notably, Spellman et al. found that direct projections from the vHC to the mPFC and gamma synchrony were associated with successful WM performance which could be disrupted by inhibiting the vHC terminals [410].
Aside from the role in memory, the hippocampus is also a key structure for the processing of salience associated with sensory stimuli. This includes a prominent role in regulating anxiety [26, 204] and the adjustment of novelty-related salience assignment [29, 76, 128, 240, 456].

Abnormalities in the structure and function of the hippocampus in schizophrenia are among the most solid and reproduced findings of the neuropathology of the disease. These include atrophy and atypical hypermetabolism [54, 275] and upregulated cerebral blood flow in the hippocampus [275]. Hippocampal hyperactivity was also found to occur at rest [306, 388, 389, 429–431, 443] and was associated with cognitive symptoms of schizophrenia such as memory deficits [193, 443]. Additionally, patients with schizophrenia showed elevated activation of the hippocampus while they fail to habituate to repeated exposure to fearful faces, which illustrates an aberrant representation of salience attribution in the hippocampus [204]. Anterior hippocampal hyperactivity could serve as a potential biomarker since it often is observable in subjects with high risk for transition to overt schizophrenia which later display symptoms of the disease [276, 388]. Regarding the underlying pathophysiology of hippocampal hyperactivity, the reduction of non-pyramidal (GABAergic) neurons and the resulting excitation-inhibition imbalance were discussed as possible mechanisms [43, 192, 194, 285]. In addition, hippocampal hyperactivity was linked to the hyperactivation of the dopamine system since elevated blood flow in the hippocampus could be normalized by D_2-antagonists [306].

1.3.3 The thalamus

The thalamus represents the largest part of the diencephalon and sits nearly in the centre of the brain as its medial area constitutes the side wall of the third ventricle. It is composed of many individual nuclei which in part have separate functions but relate to numerous association fibres. The thalamus' most prominent feature is its intense reciprocal connections to the cerebral cortex which stresses its necessity for cognition and emotion processing [398]. The thalamus is widely considered to be a hub for all kinds of stimuli and therefore a gating function has been attributed to him [101, 398]. Recalling the importance of sensory processing in the cognitive pathology of schizophrenia it seems plausible to assume abnormalities in patients with schizophrenia. Imaging studies mostly revealed reduced thalamic volume in patients [9, 171]. Particularly the MD, which receives most of its input from the PFC, showed reliable abnormalities across studies [170].

The MD was first linked to schizophrenia in imaging studies that showed its decreased activation during cognitive tasks [12] and its reduced connection to the PFC [311, 478]. However, it remains elusive if these electrophysiological findings are the cause of their cognitive symptoms because results from lesion studies in rodents yielded controversial results so far. For example, one study found that rats with lesioned MDs scored significantly worse in a WM task than non-lesioned controls [144], but another study could not replicate this finding [44]. Recent studies in humans using fMRI found that decreased MD – PFC connectivity is linked to psychosis and might serve as a prognostic marker since prodromal patients with strongly decreased MD - PFC connectivity patterns had elevated risk of developing schizophrenia in their adulthood [14, 477, 478].

To investigate the connectivity between the MD and the PFC, Parnaudeau et al. used a chemogenetic approach in mice to selectively and transiently inhibit neurons in the MD in mice [349]. They found that inhibiting neurons in the MD led to impairments in cognitive flexibility (reversal learning) and a form of WM and reduced task-dependent MD-PFC beta-synchrony [349]. These results imply that the MD and its synchronous activity with the PFC in the beta frequency range are important for cognitive function [349]. Based on this work, optogenetic studies revealed that inhibiting input neurons from the MD into the medial PFC (mPFC) and *vice versa* input neurons from the mPFC in the MD worsened performance in a spatial WM (SWM) task [56]. Notably, inhibiting connections from the MD to the orbitofrontal cortex (OFC) in the same way did not have any impact on the task performance which underlines the importance of the MD – mPFC circuit [56]. Interestingly, using temporally limited optogenetic inhibition Bolkan et al. could demonstrate that functional interaction between the MD and the mPFC is dependent on the task phase [56]. While input from the MD to the mPFC support the maintenance of SWM during a delay period, signals from the mPFC to the MD are important for memory retrieval [56]. Moreover, another study using optogenetics showed that MD activation amplifies local PFC activity and cortical connectivity and improves performance and in a sustained attention task, but activation of the PFC directly resulted in inappropriate connectivity and worsened behavioural performance [384].

1.4 DO MICE HAVE SCHIZOPHRENIA?

This chapter discusses if symptoms of psychiatric diseases like schizophrenia as described in 1.1 can be translated to or from rodent models. Also, the most commonly used rodent behavioural test paradigms are described and linked to schizophrenic symptoms in humans.

To begin with, mice most likely do not have schizophrenia analogously to the respective disease seen in humans. In any case, since schizophrenia can only be diagnosed from first-person accounts describing experiences of psychotic symptoms using human language, schizophrenia cannot be diagnosed in an animal, by definition. So, the question arises what we hope to achieve by studying schizophrenia in supposed mouse models of this disease, both for scientific and ethical reasons. Although mice resemble humans in many ways, some disparities remain fundamental. Differences in gross anatomy, genes and behaviour allow scientists only to speak of models of diseases and not to replicate an entire syndrome in an animal. Consequently, it appears folly to speak of a *mouse model* of a multifactorial disease like schizophrenia; it is more accurate to speak of the pursuit of understanding how certain genetic mutations or other manipulations increase the risk for schizophrenia and how the discovered mechanisms might be a target for medication. In accordance with the RDoC project introduced in 1.1, animal models allow researchers to precisely test candidate genes, neural circuits, and drugs for specific aspects of the abnormal functioning of certain domains of the diseases and evaluate their suitability for future treatment options. Therefore, schizophrenia-related research has been centred around identifying suitable animal models that express certain endophenotypes of the disease and then trying to understand the physiological basics of the respective model [76, 349, 401, 434].

1.4.1 Correlates of positive symptoms in mice

It is not known if or to what extent mice can experience positive symptoms such as delusions and hallucinations. Elevated locomotor activity which includes hyperactivity and increased stereotypic movements has been reported in various rodent models of schizophrenia, such as mice with a genetic downregulation of dopamine transporters and therefore elevated dopamine levels [164] as well as mice with reduced NMDA receptor expression [315]. Psychomimetic drugs such as ketamine, PCP and amphetamine increase locomotor activity in rodents and this effect can be reverted by the administration of antipsychotic drugs [340]. The suggests a certain predictive validity: the shared responsiveness of psychotic symptoms and novelty- or drug-induced hyperlocomotion to antipsychotic medication renders the latter as a first-pass rodent correlate of aspects of positive symptoms in humans, even though it is insufficient on its own to draw strong conclusions [16]. The theory of aberrant salience and the Bayes theorem highlight the importance of correct stimulus processing in the aetiology of positive symptoms (see 1.1.2). The proper processing and integration of sensory stimuli are altered in patients with schizophrenia as they display oversensitivity to sensory stimuli and the inability to predict them [59]. One measure for this is prepulse inhibition (PPI), i.e., a non-startling prepulse stimulus shortly before a startling stimulus attenuates the startle response in healthy subjects as it warns and prepares the nervous system. PPI was repeatedly shown to be diminished in patients and related mouse models [58, 59, 351]. Another function that is reduced in patients suffering from schizophrenia is the proper processing of acoustic stimuli during auditory oddball paradigms [20] or sensory gating, the processes of filtering out redundant or unnecessary stimuli throughout information processing [357], which suggest that these patients have trouble processing auditory stimuli which in return might foster the emergence of psychotic symptoms (see 1.2.2).

Importantly, a recent study was able to measure hallucination-like perception in mice which could be elevated by administration of hallucinogenic drugs like ketamine and was tightly linked to the Bayesian theorem of faulty belief-updating in schizophrenia [383]. In this study they trained mice to report if they hear a tone signal embedded in a noisy background by poking into one of two choice ports. Mice were trained over a long time period in order to avoid false alarms and to correctly adapt them to a reward according to their invested time duration. If mice spent a longer time to earn the award after reporting a tone signal it was interpreted as high confidence, analogously to humans with schizophrenia which defend their faulty beliefs with greatest efforts as described in 1.1.2. It was also found that elevated dopamine in the striatum preceded these hallucination-like perceptions in mice and even could be induced by optogenetic stimulation of mesostriatal dopamine projections which in return was rescued by the D2 antagonist haloperidol [383].

1.4.2 Correlates of negative symptoms in mice

It is proving challenging to specifically mimic negative symptoms in animals since they are not unique for schizophrenia and show overlaps with other neuropsychiatric disorders such as depression and anxiety disorders. One measure for negative symptoms is the nesting behaviour in rodents. Rodents typically tend to build a nest out of cotton sheets, which is impaired in mice which are pre-treated with psychomimetic drugs [387] and in some genetic mouse models of schizophrenia [23, 313]. One more characteristic of negative symptoms of schizophrenia is anhedonia, i.e., the inability to experience pleasure during activities that are usually joyful. This is tested in mice assessing the preference for sucrose intake whereby mice normally show a strong tendency towards a sweet sucrose solution over water [109]. As an example, the NMDAR antagonist MK-801 produces a deficit in sucrose preference analogous to the observed blunted affection in humans [77, 450].

As described above, anxiety is often present in patients with schizophrenia, which is why it can be tested in mouse models of the disease as an important comorbidity [89]. The most used behavioural assay is the elevated plus maze (EPM) in which the tendency towards open versus closed environments is analysed (see2.3.4) [354, 462].

Negative symptoms of schizophrenia often also include social withdrawal which often occurs before the onset of positive symptoms and serves as a childhood risk factor for later schizophrenia [338]. Social functioning can be tested in mice by assessing multiple parameters. Sociability can be assessed reciprocally (direct interaction between two mice) or non-reciprocally (the test mouse can inspect the other mouse only through a grid). For reciprocal sociability, the test mouse is exposed to the novel stimulus mouse in an open-field environment and social interactions starting from the test mouse are counted over a certain time period. Subsequent to this, one can evaluate social memory by introducing a delay period after the sociability test and then starting two consecutive phases in which mice are exposed either to the identical or a new stimulus mouse [201]. Non-reciprocal sociability is usually tested by putting the test mouse in an apparatus where it is confronted with two equally sized, separated compartments, one occupied with another mouse and the other one empty or with an object within [201]. Following this, the preference to visit a novel rather than an already familiar mouse like their cage mate can be assessed measuring social novelty preference [201]. This test was originally developed to measure anxiety [139] and revealed abnormal behaviours in mouse models of schizophrenia, for instance in calcineurin knockout (KO) mice [313]. Also, it can be assessed if mice remember a mouse that they previously met after a short delay, but which is not their cage mate (social short-term memory). Healthy mice rather visit the novel mouse because their social memory informs them that they already know the other mouse. These tasks are described in broader detail in 2.3.3.

1.4.3 Cognitive symptoms in mice

Patients with schizophrenia suffer from a variety of cognitive impairments which include WM, attention and information processing and are mainly unaffected by antipsychotic treatment [10]. *Selective attention*, the capability to attend to a particular stimulus or activity in the presence of additional distracting stimuli, is severely impaired in patients [264]. This is measured in rodent research by several, mostly indirect attention tasks, including possibly the 5-choice serial reaction time task (5-CSRTT, which also exists for humans) [368]. In this task, animals are confronted with a wall with five holes of which one is briefly illuminated, and a reward is given for reporting the correct hole by poking it. Notably, the 5-CSRTT consequently rather assesses *sustained* than *selective attention*, the ability to attend to a stimulus or activity over an extended period of time.

In rodent studies, WM is often tested as a form of SWM. At the present time, the delayed non-match to sample (DNMTS) T-maze test of rewarded alternation [339] is a gold standard test in rodents [116, 244]. Briefly, on a T-shaped maze, animals must remember the arm they visited during a sample run and are rewarded for alternating to the previously unknown choice arm (win-shift strategy, see 2.3.7). However, it was argued that this principle of rewarded alternation is confounded by the mice' natural preference to explore novel spaces [377]. This is likely to be facilitated by short-term habituation - the decrease of attributed salience to repeated stimuli – and especially in schizophrenia this must be seen critical since deficits in short-term habituation are present [204, 377]. Importantly, healthy mice seem to rather use a passive form of WM since they tend to perform above chance level even in their very first trial without being able to have learned the win-shift strategy and rewarded alternation [76, 77, 437]. Besides short-term habituation, a variety of other cognitive functions such as motivation and attention can confound the performance on this task. Therefore, Sanderson and Bannerman stated that the T-maze might produce false-negative results in mice with a WM deficit which is, however, obscured by their WM-independent solving strategies [377]. As depicted in Table 1.6.1, many neural correlates for WM based on the T-maze were found, involving various brain regions.

Additionally, the T-maze usually comes with low trial numbers, lack of delay-independent challenges (e.g., sound, or light distraction) and is generally used as a DNMTS-paradigm, because rodents cannot be trained to follow a the delayed match to sample (DMTS) rule in this task because of their natural tendency to explore novel spaces. DMTS paradigms have, however, been widely used in the research of human WM, e.g. in autistic patients [35], patients with Alzheimer's and Parkinson's disease [376] and also schizophrenia [271]. A DMTS task usually involves three phases, i.e., the SP, during which the stimulus which has to be memorized is presented; a delay phase during which participants must maintain information about the stimuli; a CP during which the sample stimulus is presented together with other stimuli and the participant has to make a verdict about which is the sample stimulus. Variations of this sequence could contain different kind of decisions that have to be made about the sample stimulus or stimuli, e.g., participants may be asked to tell which of the stimuli was presented first (temporal relationship) or which one was previously on top or below (spatial relationship) (see Figure 3.2.13a and [225, 226]).

In the rodent literature, operant tests have been used to implement DMTS paradigms using two retractable levers [129, 405, 484]. One lever is presented during the SP and during the CP both levers are presented, whereupon the subject receives a reward when pushing the lever from the SP. This approach, however, has a drawback since mice do not have to move during each trial which entails the possibility to not engage WM to obtain the reward but to learn to stick to a certain body position [437]. Operant DMTS tasks in rodents aiming to overcome these concerns were initially developed for rats [96, 97] and later adopted to mice [245, 437]. In the latter, inspired by the 5-CSRTT, animals pass through three phases: a SP, during which one hole gets illuminated, a delay phase during which the animal has to return to the opposite wall to collect a reward and wait in total darkness, and a CP where the animal is rewarded if it pokes into the previously illuminated hole while another hole is presented as alternative option in a wide variety of configurations (see 2.3.5). In principle, this whole setup can also be used to implement a DNMTS paradigm by changing the rule for the CP reward to be delivered when subjects poke into the previously non-illuminated hole – however, in practice neither mice nor rats have so far been trained successfully in such a DNMTS paradigm. Also, the operant design allows for various sorts of challenges such as delayed prolongation, distraction by sound, and light, or (although not done so far) variations of the number of stimuli presented in the CP. Furthermore, other cognitive capabilities can be assessed, e.g., attention from the choice accuracy in the SP and motivation by measuring the reward latency which would resemble the analysis done with the 5-CSRTT (see 2.3.5, Table 2.3.1 and [27, 368]). Also, mice must rotate around their body axis between task phases strongly reducing the possibility to encode the correct choice by a specific body position or habitual behaviour rather than using WM.

1.5 *GRIA1* MOUSE MODEL OF SCHIZOPHRENIA

GWASs identified variants in the locus of the *Gria1* (glutamate receptor, ionotropic, AMPA 1) gene – which encodes the AMPAR subunit GluA1 – as being associated with a higher risk for schizophrenia [367, 382]. AMPARs are postsynaptic heterotetrameric glutamate receptors, consisting of a combination of the four subunits GluA1, GluA2, GluA3 and GluA4. Those subunits can form seven different subtypes of AMPARs with GluA1A2, GluA2A3 and GluA2A4 being the principal subtypes on excitatory neurons [470]. The homomeric GluA4 receptor is the least expressed subunit in the adult brain [491] and plays an important role in glutamate signalling in interneurons [353], but not in AMPAR-mediated signalling in excitatory neurons [317]. Long-term potentiation (LTP) or depression (LTD) can be *induced*, inter alia, by NMDARs, whereas the modification, addition, or removal of AMPARs is the primary means of the *expression* of synaptic plasticity at the postsynapse of pyramidal neurons given that they are the also the main mediators of excitatory synaptic transmission [297]. Riedel et al. infused the AMPA antagonist LY326325 into the hippocampus and observed a reduction in excitatory transmission and deficits in spatial memory [366], which suggests AMPAR-mediated LTP as a correlate of learning. However, these findings must be met with caution since the observed effects reached by pharmacological antagonism do not necessarily equate to the genetic lack of the respective receptor and might be depending on memory training protocols, as shown for NMDARs [24].

The most distinguishing feature between the different AMPAR subunits is their C-terminus and associated function: GluA1 has a long C-terminus and can easily be trafficked to or from the postsynapse which alters synaptic strength [399]; GluA2 and GluA4 display splicing-dependent variable length of their C-termini and GluA3 generally has a short C-terminus which makes them unsuited for mediating synaptic plasticity [491].

Post-mortem studies revealed decreased expression of GluA1 mRNA and GluA1 in the hippocampus of patients with schizophrenia [131, 132, 190]. Importantly, these findings do not seem to be induced by prior antipsychotic treatment [133, 343]. Although GluA1 receptors are found throughout the brain, they show their highest expression in the hippocampus [243].

1.5.1 Electrophysiological phenotype of *Gria1*$^{-/-}$ mice

The GluA1 subunit was found to be crucial for LTP at hippocampal synapses [408] which is believed to be important for learning and memory [51]. Zamanillo et al. found that excitatory postsynaptic potentials (EPSP) in *Gria1* KO (*Gria1*$^{-/-}$) mice are unaltered, suggesting that GluA1 is not essential for synaptic transmission or there are compensatory mechanisms [488]. However, further studies revealed a reduced EPSP in *Gria1*$^{-/-}$ mice [222, 372], indicating that the complex contribution of GluA1 to synaptic transmission must be scrutinized by applying different methodologies:

Zamanillo et al. showed that in *in vitro* recordings the application of 100 Hz tetanic stimulation failed to induce LTP at SC – CA1 pyramidal cell synapses in *Gria1*$^{-/-}$ mice [488]. This protocol results in peak synaptic efficacy rapidly (1-3 minutes). A further study found that stimuli that are too weak to induce LTP, but induce short-term potentiation (STP) in healthy mice, failed to induce STP in *Gria1*$^{-/-}$ mice [136]. Romberg et al. observed that hip-

pocampal LTP contains two components: The long-lasting, GluA1-independent phase and a short, rapidly decaying, GluA1-dependent phase [372].
Long-term synaptic transmission can also be induced by theta-burst pairing (TBP) and leads to quick potentiation that develops over time [203]. Using this protocol, Hoffman et al. showed that TBP induced a slower developing, delayed potentiation which did not differ in *Gria1*-KOs from wildtype (WT) animals 25 minutes after induction and therefore seemed to be GluA1-independent [203]. However, the *initial* phase (first 25 minutes) of TBP was markedly reduced in *Gria1*$^{-/-}$ mice [203]. These findings have the important implication that GluA1 seems to be crucial for the early and short-lasting phase of LTP that occurs within seconds after induction and might be relevant to attentional processing (especially via short-term habituation to sensory stimuli) or other forms of short-term memory [29, 136, 203, 372] that involve the hippocampus [456].

A previous study using in vivo LFP recordings revealed that sustained elevation of hippocampal-prefrontal theta-coherence in *Gria1*$^{-/-}$ mice is correlated with protracted selective attention in novel environments [76]. Strikingly, the electrophysiological and the behavioural abnormalities could be restored by viral reintroduction of GluA1 into the CA2/CA3 subfields of the hippocampus [76]. This underlined the notion that GluA1-containing AMPARs in the hippocampus – more specifically the CA3 region – seems to be an important regulator of the theta rhythm and the adjustment of novelty-related selective attention [76]. This suggested that short-lasting LTP may be a mechanism to regulate selective attention and, hence, salience attribution – as has been hypothesized by Olga Vinogradova decades earlier [456].

1.5.2 Behavioural phenotype of *Gria1*$^{-/-}$ mice

Gria1$^{-/-}$ mice develop phenotypically as their WT littermates, have similar life expectancy and show no difference in the structure of synapses and dendrites [488]. They do, however, display increased learned helplessness and decreased serotonin levels which links the *Gria1*-gene to the negative symptoms of schizophrenia and renders them a possible model for schizoaffective disorder [95, 141]. Based on the LTP-deficits described in 1.5.1 the hypothesis was formulated that *Gria1*$^{-/-}$ mice might display deficits in learning and memory [488]. Accordingly, findings of *Gria1*$^{-/-}$ related behavioural deficits will be reviewed in the following.

The first study tested these KO mice in the Morris water maze test [319, 488] where the mice have to remember the place of a hidden platform in a water pool. Interestingly, *Gria1*$^{-/-}$ mice did not show significant impairment in this task, suggesting that GluA1-dependent LTP might not be critical for spatial RM. This contrasts with animals with hippocampal lesions which show impaired performance in a water maze and other tests of spatial RM [364, 488]. Studies also revealed deficits of SWM in the T-maze DNMTS task (see 2.3.7) [364] and a radial maze task [385]. In the latter, mice were tested in a radial maze with six arms from which three arms had a milk reward and the other three did not. In paradigm one, mice had to recall these three baited arms and since every arm was closed by a door after the mouse entered it, this part of the assay tested RM In paradigm two, however, SWM was tested by leaving arms open and allowing the mice to re-enter an arm within a trial, which would indicate a violation of the win-shift (rewarded alternation) rule and hence a WM-deficits [385]. Therefore, this assay represents the most direct comparison of WM and RM, possible, and in this study *Gria1*$^{-/-}$ mice showed selective impairments in WM but intact RM [385]. By extension, this also demonstrates that the profound SWM deficits of *Gria1*-KOs are not caused by a more basic impairment in the processing of spatial cues. These results led to the assumption that short-term and long-term memory are based on different neural processes, hypothesizing that only short-term memory is dependent on GluA1. Further studies questioned, however, that the impairment in *Gria1*-KOs was limited to WM – as a form of short-term memory – or rather a more passive form termed short-term habituation. Short-term habituation essentially is a form of attentional control whereby less and less attention is paid to stimuli as they become familiar (which may also be regarded as novelty-related salience attribution that decreases with familiarity). This was evident in multiple assays of short-term habituation [378]. One example is spatial novelty preference which is assessed in a non-rewarded Y-maze task where mice are allowed to explore one arm of a Y-shaped maze for a few minutes after which the previously blocked arm is opened and their tendency to visit the new arm is assessed (see 2.3.2). Here, *Gria1*$^{-/-}$ mice showed no preference to visit the previously blocked arm of the maze indicating impaired spatial short-term habituation [379]. Interestingly, when the interval between exposure to one arm of the Y-maze and revisiting the maze for both arms was extended up to 24 hours, *Gria1*$^{-/-}$ mice showed even enhanced novelty-preference [378]. These discrepancies between short- and long-term habituation fit in line with a model proposed by Wagner in 1976 where he presumes that short-term and long-term memory processes are independent from one other and even compete [461]. According to this theory, Sanderson et al. hypothesised that *Gria1*$^{-/-}$ mice trumped WTs because the accumulation of short-term memories did not interfere with long-term memory [378].

Confirming this, *Gria1*$^{-/-}$ mice also showed impaired short-term habituation in a novel object recognition task [380]. This task consists of a SP during which mice are confronted with two copies of the same object which they are allowed to explore freely and a test phase where one familiar copy is replaced by a novel object (see 2.3.8, Figure 3.5.2d and [380]). WTs usually recognize the two objects during the SP as familiar and will prefer to visit the novel object throughout the test phase whereas *Gria1*$^{-/-}$ mice show no preference towards the novel object reflecting their lack of short-term habituation [380]. However, the same study demonstrated the *Gria1*$^{-/-}$ mice do not suffer from long-term habituation deficits as they were shown not to be impaired in a context-dependent object recognition task where specific objects are presented to the mice several times in a distinctive context [380]. Consistent with these findings, orienting responses of *Gria1*$^{-/-}$ mice were shown to differ markedly from those of WT mice in the **h**abituation of the **o**rienting **r**esponse to **n**eutral **s**timuli (HORNS) task where animals were exposed to one certain visual stimulus and after a delay of 30 seconds either to the same or to a different visual stimulus [381]. WT mice showed a stimulus-specific habituation, indicated by a significantly lower responding rate when the second stimulus was the same as the first stimulus, but with a similar responsiveness if the second stimulus was novel [381]. In *Gria1*$^{-/-}$ mice orienting to the stimulus was enhanced when the second matched the first stimulus, but activity was reduced when the second stimulus differed from the first [381]. These results show that *Gria1*$^{-/-}$ mice not only lack short-term habituation, but display a stimulus-specific *sensitization*, i.e. a stronger reaction to the second stimulus compared to the first, which is the reverse pattern of that seen in healthy control mice [381].

Results from these habituation and memory studies led to the conclusion that *Gria1*$^{-/-}$ mice seem to have troubles with short-term habituation and WM in non-associative settings, whereby, to date it remains unclear to what extent their alternation deficits are actually indicative of a genuine WM impairment or driven by the same short-term habituation deficit seen in the other tasks [29, 377]. However, when the task is associative, i.e., context-dependent, and persistent behaviour is assessed, they show no difference compared to WT mice or even enhanced learning. This lack of short-time habituation can be interpreted as a cause of aberrant salience and puts the *Gria1*$^{-/-}$ mice in position as a model for psychosis in rodents [29]. Supporting this, Wiedholz et al. found that the velocity of striatal dopamine clearance was delayed in *Gria1*$^{-/-}$ mice and reduced hyperactivity and normal PPI (see below) was found in *Gria1*$^{-/-}$ mice after administration of a dopamine D2 antagonist [471]. However, the actual mechanistic link between GluA1, dopamine regulation and psychological mechanisms of salience attribution or short-term habituation remain to be elucidated. Also, *Gria1*$^{-/-}$ mice display deficiencies in PPI of the acoustic startle reflex [471], just like patients with schizophrenia [58, 351]. Another prominent feature of *Gria1*$^{-/-}$ mice has been distinct locomotor hyperactivity, which is evident when exposed to an unknown territory, but not in a familiar home-cage environment [25, 76, 141, 471]. Furthermore, when confronted with a novel environment, *Gria1*$^{-/-}$ mice show elevated theta power in the dorsal hippocampus (dHC) and coherence between the dHC and the PFC [76] which is akin to broadly elevated theta-band connectivity seen in EEG-studies in patients with schizophrenia [11, 20, 490] and other mouse models of the disease [464]. Again, such increased locomotor activity may be the result of a failure to habituate to a new setting and novel spatial stimuli as they become familiar [451]. Specifically the dHC seems to play a major role in regulating hyperactivity in *Gria1*$^{-/-}$ mice, since this part of the brain is most active during novelty-induced hyperactivity [358] and a chemogenetic approach of inhibiting neurons in the dHC was able to restore hyperactivity of *Gria1*-KOs without affecting the behaviour of WT mice [5]. These findings were reinforced by a study which used a viral approach to rescue *Gria1* in the hippocampus and found that these rescue mice were less hyperactive and only partly impaired in the Y-maze, but performance on the T-maze was also only partially restored [152]. In line with these findings, it was found that selective knockdown of GluA1 in the dHC or vHC was not sufficient to completely extinguish SWM [151]. The aforementioned study from our lab achieved a more specific viral reintroduction only to CA2/CA3 areas in the hippocampus and showed that this was sufficient to restore hyperactivity, spatial novelty-preference, and abnormal theta coherence, but could only partially restore SWM [76]. It was argued that these findings relate to the idea that CA3 might serve as a comparator to control salience attribution [76]. Elevated dHC theta oscillations were suggested to be associated with elevated and inflexible attention which is adjusted by GluA1-dependent plasticity in CA3 and/or CA2, which in turn, mediates short-time habituation. In that view, the hippocampus might act as a novelty sensor spotting discrepancies between incoming and stored information which might underlie exploratory behaviour [76, 205, 456]. Notably, GluA1 in other circuits might also contribute to the same functions. For example, Schmitt et al. found that transgenic restoration of GluA1 in excitatory forebrain neurons (including those of the hippocampus) could also, at least partially, restore performance on the T-maze in *Gria1*$^{-/-}$ mice [386] and Fuchs et al. discovered that selective ablation of GluA1 in PV-positive interneurons led to deficits in exploratory behaviour during the novel object recognition test and mild impairment on the T-maze [160].

1.5.3 GluA1 as a possible pharmaceutical target

Regarding the therapeutic suitability, molecules that activate AMPA-receptors are thought to be a possible target for schizophrenia [272]. Research in rodents showed that novelty-induced hyperlocomotion in *Gria1*$^{-/-}$ mice could be normalised by the AMPAR antagonist NBQX, but not the AMPA potentiator CX546 [358]. This seemingly unexpected finding could be explained by the finding that novelty is known to increase glutamate in the hippocampus which is why NBQX could relieve hyperlocomotion [358]. Also, the mGluR2/3 agonist LY354740 was shown to reduce hyperlocomotion in *Gria1*$^{-/-}$ mice [359].

Until now, no substance reached clinical relevance, even though AMPA-receptor modulators (*ampakines*) were found to be cognitive enhancers [292] and a drug called *aniracetam* is sold in Europe as a prescription drug for Alzheimer's disease but is not approved by the FDA. One study showed that the AMPAR modulator piracetam in combination with haloperidol alleviated positive and negative symptoms of patients with schizophrenia more than haloperidol and placebo [333]. However, this study was in small scale and therefore only yields preliminary results. Additionally, another AMPAR modulator, *CX516*, improved short-term memory in healthy humans [215] but did not improve any symptoms of schizophrenia when administered in addition to standard medication [173]. Recently, another ampakine, *PF-04958242*, was able to attenuate ketamine-induced impairment in verbal learning and memory in healthy subjects [361]. The AMPAR potentiator *TAK-137* was recently assessed preclinically in rodents and non-human primates where it improved psychostimulant-induced (NMDA-blockade through ketamine and MK-

801) hyperlocomotion in rats and mice, social deficits, deficits on the 5-CSRTT and cognitive flexibility in rats and WM both in rats and monkeys [435]. This study suggests that treatment with minimally agonistic AMPAR modulators rather than their blunt enhancement could yield beneficial results [435].

1.6 AIMS OF THIS THESIS

1.6.1 Assessment of redundancy between electrophysiological measures of long-range neural communication

The measures described in 1.2.1 and Table 1.2.1 have been widely used for two decades to assess inter-regional neural communication in rodents during a variety of cognitive tasks and disease-related manipulations, mostly involving recordings from the hippocampus and PFC [4, 123, 229, 401], but also increasingly from the thalamus [349], and the amygdala [394]. However, on average only one or two measures of coupling are evaluated and interpreted as sufficient surrogate to quantify task- or manipulation-related differences in actual information exchange between the analysed regions. Besides, these measures are usually regarded as equally informative and redundant and therefore, the contingency of the attained conclusions on the selection of the coupling measure are typically not exhaustively assessed. Often, simulated data is used to assess the ability of a measure to characterize the complexity of neurophysiological data which is difficult given the variability of these data. The implicit assumption that results can be easily translated between studies using different measures is not justified given the mathematical and partly biological differences between these constructs. Thus, our goal was to assess the redundancies and contingencies of such coupling metrics. To this end we recorded data during a simple behavioural assay – novelty-induced locomotion and its habituation over time – in *Gria1*$^{-/-}$ mice and their littermate controls. As described in 1.5.1, the *Gria1*-KO model, which models some behavioural deficits relevant to schizophrenia, shows profound and state-dependent aberrations of hippocampal-prefrontal coupling in this task [76]. We focused on the most widely used connectivity measures – coherence magnitude and phase angle, wPLI, PPC, PLV, cross-amplitude coupling, parametric and non-parametric GC (npGC), PDC, DTF, cross-regional PAC, SPC and SPC-related directionality (Table 1.2.1) – with respect to three "*litmus tests*" for redundancy: First, detection of KO-related alterations of coupling across the 10 min test, second, detection of KO-related changes of a measure over time, and third, bivariate within-animal correlation of the examined measures. Signals obtained from the mPFC, dHC and vHC were used to calculate connectivity between these regions. For the most part of the analysis, four commonly used frequency bands, delta (δ, 1-4 Hz), theta (θ, 5-12 Hz), beta (β, 15-30 Hz) and low gamma (γ, 30-48 Hz) are distinguished, whereby the analysis of theta and gamma may be regarded as particularly revealing due to the existence of spectral peaks indicating actual underlying oscillatory processes.

As for the choice of examined measures of neural connectivity, the dependence of the conclusions on the exact placements of electrodes within the analysed regions and the choice of reference are often not evaluated either [36, 135, 230, 231]. We therefore determined the exact placement of the recording electrodes in order to identify possible signal differences within each brain region and used to distinct reference locations to detect related dependencies. To this date, this is not routinely done which can be problematic especially when interpreting negative data, i.e., the supposed absence of differences in coupling.

To summarize, the goal of the first part of this work was to analyse redundancies between widely used functional connectivity measures and to precisely evaluate electrode and reference locations, opening the possibility for seemingly contradicting findings and inconclusive null results when comparing non-redundant measures, which in return should be avoided in further, more complex, analyses. This study was published in [420].

1.6.2 Single-trial decoding of working memory in mice and humans based on electrophysiological measures

Studies in humans, non-human primates, and rodents [262] have centrally implicated the PFC [112, 119, 174, 188, 226, 350, 419, 485], the parietal cortex [226, 228], the MD [162, 349], and the hippocampus [79, 187, 225, 337, 466, 485] in WM processes. In particular, connectivity between these brain structures correlates with performance [309] (see Table 1.6.1 for an overview on rodent studies), and dysfunctional connectivity may underlie WM impairments in schizophrenia [310].

However, it still remains elusive which kind of neural information transfer actually mediates WM. Several - partially conflicting and remarkably distinct - reports exist on which brain regions, frequency bands [76, 229, 483] and types of inter-regional coupling (or metrics to analyse) are essential to WM. Studies in rodents have implicated network oscillations in either the delta [130], theta [229, 401], beta [76, 349], or gamma [138, 316, 483] frequency, in coupling between such frequency bands (esp. theta-gamma) [433] or between oscillations and local spiking of neurons [229, 349, 410, 432, 433], or in interactions between either the ventral [410, 433] or dorsal hippocampus [76, 295, 401] and PFC. On a T-maze rewarded-alternation task, both vHC→PFC connectivity [410], and dHC-PFC coupling via the thalamic nucleus reuniens [295] have been argued to mediate the encoding of WM-contents using optogenetic inhibition experiments. In addition to this diversity of findings in rodents - which mainly originate from recordings in spatial alternation tasks (Table 1.6.1) - it remains largely unknown to what extent the discovered associations generalize across different WM tasks and species.

Table 1.6.1: Measures of long-range neural connectivity associated with WM in rodents
Studies that have attempted to identify an electrophysiological WM correlate in form of coupling of activity in two brain regions are listed, in so far as the association between WM performance and metric have been proven by some analysis, e.g., bivariate correlations, linear regression, or comparison between correct and incorrect trials or between SP and CP phases. Studies that merely noted connectivity and WM differences due to some manipulations independently were not included. Abbreviations**:** T, T-maze; H, H-maze; 8, 8-shaped maze; RA rewarded delayed alternation; SPC, spike-phase-coupling (usually assessed by mean resultant vector length, MRL); CC, cross-correlation of amplitudes to determine temporal leading or lagging of oscillation in one region *vis-a-vis* the other; CFC (PAC) cross-frequency-coupling (phase-amplitude-coupling); PDC, partial directed coherence; MUA, multi-unit activity; SUA, single-unit activity; dMEC, dorsal medial EC; dCA1/vCA1, dorsal/ventral CA1; dHC/vHC, dorsal/ventral hippocampus; MD, medio-dorsal thalamus; PFC, medial prefrontal cortex (usually prelimbic area); Re/Rh, Ncl. reuniens / Ncl. rhomboideus of the midline thalamus; VTA, ventral-tegmental area. Adapted from [421], open access article: CC BY 4.0, https://creativecommons.org/licenses/by/4.0/

Task	Metric	Frequency	Connection	Ref.
T (RA)	Phase synchrony	γ, MUA bursts	dMEC - dCA1	[483]
T (RA)	SPC, coherence	β	PFC (β) - MD (spikes or β)	[349]
T (RA)	Coherence	β	PFC - dHC	[76]
T (RA)	CFC (PAC)	low $\gamma - \theta$	PFC (γ) - vHC (θ)	[188, 433]
T (RA)	SPC	γ, SUA	PFC (spikes) - vHC (γ)	[410, 432]
H (RA)	SPC, coherence	θ, SUA	PFC (spikes, θ) - vHC (θ)	[229]
T (RA)	SPC, coherence	θ, SUA	PFC (spikes, θ) - vHC (θ)	[188, 341, 401]
T (RA)	SPC, SPC-based directionality	θ, SUA	Delay: MD → PFC, CP: PFC → MD	[56]

T (RA)	CC directionality (lead/lag), coherence	θ, γ	PFC - (Re/Rh) - dHC	[188]
8 (RA)	PDC	θ, α, β	vCA1 → PFC, PFC → vCA1	[85]
T (RA)	SPC, coherence	δ (4 Hz)	VTA (δ) - PFC (δ)	[130]
2-lever operant DNMTS	SPC	θ, SUA	PFC (spikes) - vHC (θ)	[213]
Delayed tactile discrimination	SPC, coherence	θ, SUA	PFC (θ) → S1(spikes, θ)	[137]

Moreover, it remains unclear if this variety of reported associations between specific neural activity and WM performance reflects the complexity of the biological reality, i.e., that, indeed, several types of connectivity and connections are engaged in WM, defying the desire for mono-causal conceptualizations. Alternatively, it could be caused by differences between used task paradigms, rodent models, species, or analysis procedures. Several factors may explain the current uncertainty regarding the physiological correlate of WM. With respect to the state of rodent studies, this includes a pre-dominance of the use of the T-maze rewarded-alternation assay (or its derivatives; Table 1.6.1) [377] which also entails the difficulty of separating correlates of more basic functions like motivation, spatial processing, and attention from the actual WM component of the task as described in 1.4.3. Further uncertainty arises from the typical analytical approach of correlating within-subject averages of performance (WM accuracy score) [76, 401, 433], trial type (correct vs. incorrect) [410], or trial phase (sample vs. choice phase) [341, 410] with a within-subject average of a select connectivity measure. Such correlations do not necessitate mechanistic causation but could be indirect or even epiphenomenal. Finally, the *street-light effect* has recently been highlighted as a rather principal limitation of studies of physiological correlates of psychological function [111]. I.e., when only focusing on descriptive analyses of averaged data, many important aspects are often overlooked since the obvious brightness entices to only search around the light source. In our context, this term denotes the missing of neurophysiological correlates due to a biased selection of only few investigated brain regions, connections, or activity parameters.

Therefore, we aimed to improve on these points in several respects in order to highly reliably identify forms of inter-regional neural communication that are linked to WM in mice and humans:

(*a*) We comparatively assessed three distinct visual WM tasks in each species. In mice, we build on our recent advances in establishing an operant DMTS 5-SCWM assay that features intrinsic control variables for stimulus-directed attention and motivation and minimizes the possibility for mediation, in addition to using the T-maze rewarded alternation and an operant 2-choice DNMTS task. In humans, we analysed an existing, openly available dataset where three distinctive task types were inter-mixed within one session and featured a very similar temporal structure [225]. Therefore, in each species, the non-WM related differences between the applied tasks are relatively little, which benefits an optimal comparison of the neurophysiological basis of different types of WM.

(*b*) In mice, we used a recently developed pyControl-based operant box that allows to record neural activity while mice are performing operant tasks and to align all behavioural events with electrophysiological recordings [7]. During WM tasks in both species, LFPs were simultaneously recorded from four sites (PFC, dHC, vHC, and MD) in rodents, and from three sites (PFC, MTL, and OFC) in humans.

(*c*) To maximize the connectivity-related information obtained from these multi-site recordings, we extracted a large set of measures of inter-regional neural coupling including coherence, wPLI, GC, PDC and theta-gamma PAC – together with measures of local activity. The results from the study described in 1.6.1 were used as indication to maximize information by incorporating only largely non-redundant LFP-based coupling metrics [420]. Each metric was determined in three or four task phases, four or five frequency bands (where sensible), and as both absolute and relative measure (absolute value divided by the preceding inter-trial interval (ITI)). This yielded a minimum amount of 720 and 1344 neural connectivity measures in mice and humans, respectively, in addition to at least 180 measures of local activity, whose association with WM were analysed.

(*d*) Most importantly, we applied ML to predict WM choices on a single-trial basis from these high-dimensional patterns of functional connectivity. The use of ML in neuroscience is increasing rapidly and expanded to various parts of the field ranging from brain-computer interfaces, serving as a model of the brain over to identifying predictive variables [172, 460]. More data-driven approaches have recently been deployed to reduce the *streetlight effect* and to offer a hypothesis-free approach to analysing complex data [111, 210, 211, 248]. These studies have applied *unsupervised* classification procedures to extract electrophysiological correlates of stress responses [210], depression vulnerability [211], and anxiety [111] from connectivity patterns obtained from multi-site LFP-recordings in mice, collectively termed the *electome* (electrical functional connectome factors/networks). These LFP-patterns containing coherence and phase leads/lags were shown to be highly predictive of the respective behavioural outcome. However, these approaches cannot easily be applied to analyse brain-wide correlates of high-level cognition that is assessed in behavioural assays with temporally complex, multi-trial task structure and pre-determined values of the subject's choices. We translated the supervised, trial-based nature of WM tasks (pre-defining choices as correct or incorrect) into our analysis in order to establish a largely unbiased quest for WM correlates within high-dimensional oscillatory patterns by implementing a *supervised* decoding analysis to harness the power of prediction to prove the presence of behaviourally relevant information in those complex signals [104]. The possibility of trial-by-trial prediction of WM-based choices in a rewarded-alternation task from the spiking activity of large ensembles of neurons in rodent PFC [410, 419], monkey inferior temporal cortex [475] and human MTL [57] has recently been demonstrated. In these attempts however, prediction was done with classifiers that were trained specifically for a single animal and session since the predictor variables are the individual neurons. In contrast, we merged datasets from multiple subjects and sessions and used connectivity and activity metrics from multiple sites as predictor variables which generally entails high generalisation potential. In this way, we were able to subsequently quantify the trial-by-trial predictive power of each electrophysiological variable in order to identify connectivity patterns associated with WM in mice and humans in a largely unbiased manner. Results from this study were published as a preprint in [421].

1.6.3 Assessment of *Gria1*$^{-/-}$ mice on different paradigms of working memory and identification of electrophysiological alterations

Gria1$^{-/-}$ mice simultaneously underwent the same experimental procedure as their WT littermates, i.e., they were also implanted with electrodes in the same brain regions in order to obtain multi-site recordings and to measure inter-regional neural communication and tested on the newly designed operant DMTS, DNMTS and the T-maze. As argued in

1.5.2, it remains elusive, if the deficit of *Gria1*$^{-/-}$ mice on the T-maze truly reflects impaired WM or it is a potential by-product of their impaired short-term habituation as the mice lose their ability to regard recently visited (more familiar) spaces as less salient. We initially applied the same analytical pipeline as presented in 1.6.2 and then further extended our ML-approach to compare the genotype-related differences of trial-by-trial prediction and to possibly identify correlates of impaired WM linked to schizophrenia.

1.6.4 Selective knockout of *Gria1* in the CA2 and CA3 subregion of the hippocampus

To evaluate the relevance of certain hippocampal cell populations for the behavioural phenotype of *Gria1*$^{-/-}$ mice (see 1.5), we transgenically restricted the *Gria1* knockout to CA2 (*Gria1*$^{\Delta Amigo2}$ cohort; see 2.1) or CA3 (*Gria1*$^{\Delta Grik4}$ cohort). In order to develop adequate treatment strategies, it is important to know through which cell types and neural circuits GluA1-hypofunctionen leads to psychiatric deficits. It was recently shown that spatial short-term habituation in global *Gria1*-KO mice could be restored by viral re-introduction into the CA2/CA3 subfield of the hippocampus [76]. To further elucidate these findings, both cohorts underwent the same experiments at roughly the same age to ensure comparability. Experiments included the open field test (see 2.3.1), Y-maze (see 2.3.2), EPM (see 2.3.4), NOR (see 2.3.8), and tests for social interaction and memory (see 2.3.3). Both cohorts were not implanted with recording electrodes and will be referred to as the *Gria1*$^{\Delta Grik4}$ and *Gria1*$^{\Delta Amigo2}$ cohort throughout this thesis.

2 MATERIALS AND METHODS

2.1 MICE

All experiments were performed in accordance with the German Animal Rights Law (Tierschutzgesetz) 2013 and were approved by the Federal Ethical Review Committee (Regierungsprädsidium Tübingen) of Baden-Württemberg, Germany (licence number TV1399). Mice were bred at the animal facility of Ulm University. Three cohorts of mice were used to generate the data in this thesis. The first was a cohort of male and female *Gria1* KO (*Gria1*^{tm1Rsp}; MGI:2178057) [488] mice (N = 15, 9 males) and WT littermate controls (N = 12, 8 males) which were bred from heterozygous parents. Homologous recombination and transient expression of Cre recombinase in embryonic stem cells was used to delete exon 11, the encoding region of the GluA1 protein [488]. For the other two cohorts, to enable region- and excitatory cell-type selective *Gria1*-ablation, mice with a homozygously floxed *Gria1*-locus (f*Gria1*, B6N.129-*Gria1*tm2Rsp/J; also known as GluR-A^{2lox}, Jax stock# 019012) were cross-bred with Cre-driver lines in which promoters direct Cre-expression to excitatory cells of CA2 (Amigo2-Cre, B6.Cg-Tg(Amigo2-cre)1Sieg/J, Jax-stock# 030215) [201] or CA3 (Grik4-Cre, C57BL/6-Tg(Grik4-cre)G32-4Stl/J, Jax-stock# 006474) [325]. Mixed male-female cohorts were used and Cre-negative littermate controls with homozygous f*Gria1*-locus were used in all cases.

Mice were housed in a temperature- and humidity-controlled holding room at Ulm University (Institute for Applied Physiology) on a 13/11-hour light-dark cycle. All experiments were conducted during the light-period. Mice were kept in individually ventilated cages (IVC, Type II, Tecniplast, Germany) together with their littermates whenever possible. IVCs contained saw dust, a cardboard house and sizzle nest (Datesand, UK) whereas the cardboard house was removed after mice underwent surgery and was replaced by smaller pieces of cardboard enabling the mice to hide with minor injury risks. All cages were cleaned, and content was exchanged habitually.

Mice had access to water ad libitum and as soon as no reward-based experiments were performed mice were put on a free food schedule consisting of pellet food (Ssniff, Germany). In case of bigger weight discrepancies between animals in the same cage the respective mouse was transferred to an extra-feeding cage for a couple of hours. Feeding practices for surgeries and behavioural experiments can be found in the following chapters.

2.2 Surgeries in *Gria1*$^{-/-}$ mice

Surgeries for electrode implantation were only conducted in the *Gria1* cohort. Mice were implanted with electrodes at ca. nine months of age. The days prior to the surgery mice were put on a free food schedule and received high-caloric food to get used to the post-operation food. Before and after surgery mice were weighed to appropriate drug doses and monitor their recovery. To prevent aggressive behaviour, entire cages underwent surgery the same day or, when this was not possible due to time constraints, operated mice were temporally kept in a separate cage.
Mice were anesthetized with 4-5% isoflurane (Forene® 100 %inhalation solution, AbbVie, Germany) with a flow rate of 1 ml/min in an induction chamber. The head was shaved and cleaned diligently with Decontaman (Dr. Schumacher, Germany). 0.2 ml of Marcaine® (active ingredient Bupivacaine) were injected under the skin at the shaved area to provide local anaesthesia. The following substances were applicated subcutaneously at the back: Metacam® (active ingredient Meloxicam, Boehringer Ingelheim, Germany), a non-steroidal anti-inflammatory drug with a dosage of 0.25ml/g; Vetergesic® (active ingredient Buprenorphine, Champion Alstoe Animal Health, UK) for pain relief and Saline (0.5ml) for proper hydration.
The surgical area was largely cleaned and sterilized before surgery. The mouse was fixated into a manual stereotaxic frame with ear-bars (World Precision Instruments, USA). Body temperature was upheld by a feedback-loop heating blanket (Harvard Apparatus, USA) and anaesthesia was maintained by an average of 1.5% isoflurane. The depth of the anaesthesia was constantly checked by the surgeon assessing the breathing rate and the absence of the hind-paw pedal-reflex. The eyes were covered by Bepanthen (Bayer, Germany) to avoid desiccation. After an anterior-posterior incision was made starting from the rear of the head up to the level between the eyes the skull surface was cleaned with cotton buds. Bregma was identified and used as the basic position. The three-dimensional position of lambda respective to bregma was determined to verify the correct positioning of the mouse in the stereotaxic frame. Inclination in the longitudinal axis was measured

evaluating the depth of two points on the skull 2 mm behind bregma and 1 mm left and right from the longitudinal axis.

In total six craniotomies were conducted with a Micro Drill (Harvard Apparatus, USA). Four of them were used as introduction holes for the recording electrodes listed in Table 2.2.1 and two were used for ground and reference. For the recording electrodes Teflon-coated 50 µm tungsten wires (WireTronic, USA) were used; for the ground and reference silver wires (Stainless steel, 0.125 mm diameter of the bare wire with a coating thickness of 0.025 mm, Advent Research Materials, UK) and metal screws (M1.2x2 SLOT CSK MACHINE SCREW DIN 963 A2 ST/ST, Precision Technology Supplies, UK) were inserted. The recording end of the wires were determined by a cut with a serrated scissor to remove the insulation. Surgeries were mostly performed by Sampath K. T. Kapanaiah.

The following coordinates were used:

Table 2.2.1: Coordinates used for electrode implantation.
a/p = anterior/posterior, m/l = medial/lateral, d/v = dorsal/ventral; distances in millimetres

	A/P	**M/L**	**D/V**
mPFC	1.9	0.3	1.9 / 1.4
MD	- 1.2	0.3	2.7
vHC	- 3.2	3.0	3.9 / 3.4
dHC	- 2.0	1.5	1.4

The D/V plain of the mPFC and the vHC contain two coordinates because two electrodes were glued together (RS Components super-glue, UK) so that the recording ends of the wires have a length difference of 0.5 mm and different placements can be analysed. Dual electrodes were used in 26 mice and single electrodes were used in 10 mice. In 21 mice the electrodes were implanted in the right hemisphere and in 17 mice in the left hemisphere. Both the ground screw and the reference electrode were placed in the contralateral hemisphere. The coordinates used for the reference electrode and screw were A/P 4 mm and M/L 1 mm and A/P -5.5 mm and M/L 1 mm for the ground electrode and screw. Both were placed above the respective brain region, the cerebellum for the ground and the PFC for the reference. The recording electrodes, the reference electrode and screws were fixed by Breeze™ self-adhesive Resin Cement and (Pentron, USA) and then connectorized to a dual row socket (Mill-Max Mfg. Corp., USA) using gold pins (Mill-Max Mfg. Corp., USA).

After surgery mice were injected with a 0.5 ml glucose/saline - solution and received Metacam injections for three consecutive days. The post-operation period was one week in which the mice were weighed and monitored according to a standardized scoring sheet. They received jelly-food and mesh food or oatmeal with Müller® strawberry milk and in case of severe weight loss were injected with a glucose/saline solution.

2.3 Behavioural tasks in mice

After a recovery time after surgery of 3-5 weeks and ad libitum food mice were weighed at three consecutive days to determine the average weight. For the operant chamber WM tasks and the T-maze experiment, animals were put on food deprivation to sustain motivation and to ensure reward-driven behaviour. The weight of the mice was closely monitored with target weight of 80-90 % of the before measured average weight. For the other behavioural tests, mice had unrestricted access to food supply to ensure only exploratory-driven behaviour. Unrestricted water supply was ensured at all times and all training and experiments were conducted in a ventilated laboratory room. Animals were transferred from their holding room to the experiment room at least 30 minutes before the start of the task for habituation. The *Gria1* cohort underwent the following experiments: Novelty-induced locomotor activity (open field, 2.3.1), EPM (2.3.4), operant DMTS 5-CSWM (2.3.5) and DNMTS 2-CSWM task (2.3.6) and T-maze (2.3.7). The *Gria1*$^{\Delta\mathrm{Amigo2}}$ and *Gria1*$^{\Delta\mathrm{Grik4}}$ cohort were tested on following experiments: Novelty-induced locomotor activity (open field, 2.3.1), spatial novelty preference (Y-maze, 2.3.2), social interaction and memory (2.3.3), NOR (2.3.8) and EPM (2.3.4).

2.3.1 Novelty-induced locomotor activity

For animals of the *Gria1* cohort, mice were tethered to obtain electrophysiological data and moved from their home cage into a novel differently sized plastic cage (Typ III, Tecniplast, Germany) containing fresh sawdust. Mice were given ten minutes to freely explore the new environment and were observed with a CCTV camera connected to the behavioural tracking software AnyMaze (San Diego Instruments, USA). To investigate safety and anxiety behaviour the experiment cage was divided into a centre, periphery, and transi-

tion zone. Mice normally tend to avoid the centre and rather stay close to the walls of the periphery. Behavioural parameters were analysed as average values and as a function of time. Those parameters included the total distance travelled, mean speed, the average distance to the border of the cage and the number of rotations.
Since the *Gria1*$^{\Delta\mathrm{Amigo2}}$ and *Gria1*$^{\Delta\mathrm{Grik4}}$ cohort were not tethered, the protocol was extended so that mice had 90 minutes to explore the novel cage.

2.3.2 Spatial novelty preference

To assess spatial novelty preference Y-maze experiment was conducted in a transparent, three arm 120° angle maze. Mice were given five minutes time in a separate box before putting them in the maze. The maze floor was covered with sawdust consisting of clean sawdust and sawdust obtained from same-sex mouse cages.
The experiment is divided into two phases, namely the sample and test phase. During the former one arm of the maze is blocked and mice have 5 minutes time to explore the unclosed arm. The number of times the right / left arm was blocked were equally distributed within genotypes. After finishing the sample phase mice were returned to the habituation box for an inter trial interval of one minute. To eliminate olfactory hints the sawdust was shuffled and redistributed in the maze. During the following test phase, the previously closed arm was opened, and mice were again given five minutes time to now visit both arms. Animals were tracked using the AnyMaze software.

2.3.3 Social interaction and memory

All social interaction tests used adult, but younger mice of the same sex and strain as stimulus mice. For reciprocal social interaction, the test mouse was exposed to the novel stimulus mouse in a familiar open field (dark but transparent Type III cage; Tecniplast, Germany). Interactions were video-monitored and scored in 2 min intervals for 12 min. A second 12 min interaction test was conducted at an older age which was followed by two consecutive 4 min phases 1 h later during which mice were exposed either to the same or a new stimulus mouse (order counterbalanced within subgroup) to assess social memory (Figure 3.5.3a) [201]. Additionally, a modified three-chamber task was conducted to assess non-reciprocal social interaction and social short-term memory, similarly as applied previously to assess sociability in mice with ablated synapses of CA2 excitatory cells (see Figure 3.5.3f) [201]: All mice were habituated to the situation of a stimulus mouse by remaining in half-circular compartments (9 cm radius, perforated metal) at each end of the 3-chamber box (50 cm long, 20 cm wide, 25 cm high grey PVC walls) for 2x 5 min on the prior day and once more 5 min 1-2h before testing on the first test day. In the first test session, mice were habituated first to the arena without metal compartments (5 min), then to the arena with empty metal compartments (5 min) and were then exposed to a cage-mate in one of the empty metal compartments while a mouse-sized piece of black foam was introduced to the other (social preference test). The second testing session was conducted on the subsequent day and consisted of four phases: 5 min habituation to the 3-chamber box with metal compartments, 5 min exposure to an unfamiliar stimulus mouse in one compartment and the same cage-mate as seen on the previous day in the other (position counter-balanced within sub-group; assessing social novelty-preference), 10 min habituation to the novel mouse from phase 2 (other compartment empty), 5 min exposure to the mouse from phase 2 and an unfamiliar stimulus mouse (position counter-balanced), assessing social short-term memory.

2.3.4 Elevated plus maze

The EPM is a widely used behavioural experiment to assess anxiety in rodents [354, 462]. It consists of a plus-shaped maze consisting of two open and two closed arms which are opposite of each other (see Figure 3.4.1a). The setup is placed 72cm above ground and the movements of the mice are taped by a CCTV camera on the ceiling and recorded via AnyMaze. Before the experiment mice were habituated to a novel cage for about 5 minutes and were then placed at the junction of the four arms of the maze facing an open arm. Increased entries to the open arms are considered a marker for reduced anxiety. The main parameters were the ratio of entries and time spent in the open arms divided by the total entries and time spent in all arms excluding the centre area. Spontaneous motor activity (total distance travelled, travelling speed, and entries to all arms) was measured in order to potentially identify novelty induced hyperactivity.

2.3.5 Operant DMTS 5-CSWM task

A 5-Choice-Spatial-Working-Memory test (5-CSWM) was conducted as described in [437]. The setup included an inner box consisting of a wall with 5 poke holes on the one side and a reward receptacle on the other side and an outer box for insulation (design files are openly available at https://github.com/KaetzelLab/Operant-Box-Design-Files). This arrangement is based on the 5-CSRTT which is commonly used for the assessment of attention and impulsivity control in rodents [27] and the task protocols were adapted from the combined attention and memory task (CAM) for rats [97]. The task was conducted in custom-designed pyControl-based operant boxes that were optimized for both simultaneous electrophysiological recordings and the acquisition of the 5-CSWM task (operant box task-scripts implementing all task paradigms used in this thesis are available from https://github.com/KaetzelLab/Operant-Box-Code; initial operant box setup and task programming was performed by Sampath K. T. Kapanaiah) [7]. Before starting training, mice were accustomed to the strawberry-milk reward (Müller®, GER) in their home cages and were given time accordingly to get used to the experiment box. Also, a fan for proper ventilation was constantly turned on.

Each trial of the task is divided into a SP, a delay-phase (delay) - which is further subdivided into a pre-delay and a post-delay by the time point of reward collection - the CP, and the ITI. In the default state, the task is conducted in the dark (house-light off) with the only illumination deriving from the poke- and receptacle holes in certain task phases. The SP is identical to that of the 5-CSRTT, except that premature responses are not punished: one of the 5 holes in the 5-choice wall is illuminated for a certain stimulus duration (SP-SD) and mice need to poke into that hole within the limited hole time (SP-SD plus 1 s) in order to obtain a small reward (20 μl or, in stages 2 and onwards, 10 μl strawberry milk) at the receptacle at the opposite end of the wall during the pre-delay time. The reward-collection (receptacle exit) starts the post-delay (2 s in all cases) after which the originally presented hole and one randomly assigned other hole is illuminated (thereby starting the CP) for a certain SD (CP-SD, 5 s for all protocols shown in Figure 3.2.1). Mice have to poke into the same hole as in the SP, realizing a DMTS-rule, in order to obtain a large reward (60 μl). After a 5 s ITI a new trial starts with the SP. Incorrect pokes or omissions in the SP or CP led to a 5 s time-out period (house-light illuminated; reward omitted) and the start of a new trial after an ITI of 5 s. Before training, mice were habituated to the operant box, to consuming the strawberry milk (Müller®, Germany) reward from the receptacle, and to poking into the 5-choice wall to obtain a reward (acquisition of the basic operant cycle).

Subsequently, training was conducted through multiple stages across which the task became incrementally more difficult due to a shortening of SDs and an increase in the number of CP-stimulus configurations (see Table 2.3.1). During pre-surgery training – in order to compare performance between groups – no performance-based staging was applied, but instead all mice were trained on the stage 1 for the same number of 21 days, and then transitioned through the remaining three training stages (2-4) with 2-3 d of training per stage. Parameters defining the stages are found in Table 2.3.1. Sessions lasted 30 min throughout and were conducted on 5 d/week. Training was continued ~4-5 weeks after surgery on the baseline stage (4) for 5 weeks to allow the mice to approach asymptotic performance. Subsequently, mice were trained further for 3 weeks in a tethered mode, with the head stage (see below) mounted on their heads, in a baseline protocol with shorter SD in SP (10 s) and CP (5 s; stage 5) to increase the number of obtained trials and better standardize the encoding time. Subsequently, mice were taken through three series of challenge protocols with intermittent training on the baseline stage 5. The same challenge was conducted on 2-3 consecutive days in order to obtain sufficient trials for later analysis. The three series were *(a)* pure delay challenges, where the pre-delay was extended from 0 to 5 and 10 s, *(b)* a distraction challenge with an illumination of the house-light for 0.5 s starting randomly timed between 0.8-1.3 s of the 2 s post-delay phase, and *(c)* a combined attention (SP) and WM challenge with an SP-SD of 1 s (instead of the 2 s of the specific baseline stage 6 of this challenge) and a pre-delay of 5 s, which was preceded by a sole attention challenge (1 s SP-SD, 0 s pre-delay). Most of the analysis shown uses the data from the final (combined) challenge, although decoding analysis (see 2.6) was also conducted for the other challenges in order to replicate the analysis and, additionally, to assess the capacity of cross-prediction between classifiers from entirely different challenge-conditions (Figure 3.2.5). The post-delay remained 2 s, starting with the exit from the reward receptacle and spent in darkness, throughout all challenge and baseline protocols.

Note that, on *all* stages, the *post-delay* is 2 s, the *CP reward* is 60 μl, the *limited hold time* - that is the time in which a response is registered - exceeds the SD by 1 s, the *ITI* is 5 s, and the time-out time after incorrect responses or omissions is *5 s*. The CP configurations indicate the two holes of the 5-choice wall that can be illuminated; note that the actual configurations when considering the correct hole is double than what is stated (i.e., 2-4 is different from 4-2, which is not listed). Stage 4 served a pre-surgery baseline and post-surgery training stage without tether. Stage 5 was only conducted with simultaneous re-cordings (or tether) and served as baseline for all challenge conditions conducted with simultaneous recordings, except that – for habituation to shorter stimulus intervals – the last challenges (with SP-SD 1 s) had their own baseline as reference, featuring an SP-SD of 2 s: stage 6.

Table 2.3.1: 5-CSWM training stages

			Parameters of training and baseline stages			
Stage	SP-SD, s	CP-SD, s	Pre-delay, s	Post-delay, s	Reward (µl)	CP configurations
1	20	20	0	2	20	1-3, 2-4, 3-5
2	20	20	0	2	10	1-3, 2-4, 3-5
3	20	20	0	2	0	1-2, 2-3, 3-4, 4-5
4	20	20	0	2	10	1-2, 1-3, 1-4, 2-3, 2-4, 2-5, 3-4, 3-5, 4-5
5	10	5	0	2	10	1-2, 1-3, 1-4, 2-3, 2-4, 2-5, 3-4, 3-5, 4-5
6	2	5	0	2	10	1-2, 1-3, 1-4, 2-3, 2-4, 2-5, 3-4, 3-5, 4-5
			Parameters of challenge stages			
Delay 5s	10	5	5	2	10	As baseline
Delay 10s	10	5	10	2	10	As baseline
Distraction	10	5	0	2 (Distract.)	10	As baseline
Attention	1	5	0	2	10	As baseline
Combined	1	5	5	2	10	As baseline

For behavioural assessment, the following parameters were mainly assessed:

a) Sample phase:

- % Accuracy: Percentage of pokes into the lit hole versus pokes in not-illuminated holes
- % Correct: Percentage of pokes into the lit hole respective to all other trials
- # Correct: Number of pokes into the illuminated hole
- % Omissions: Number of trials without any poke respective to the total amount of sample phases
- Reward latency: time between correct poke and entering of the receptacle
- Correct latency: time between start of the sample phase and correct response

b) Choice phase:

- % Accuracy lit: Percentage of pokes into the sample hole against the additionally lit hole
- % Accuracy: Percentage of pokes into the sample hole respective to the number of pokes into any other hole (lit and not-lit holes)
- % Correct: Percentage of pokes into the sample hole respective to all other trials
- # Correct: Number of pokes into the sample hole
- % Omissions: Number of choice phases without any poke respective to the total amount of choice phases
- Reward latency: time between correct poke and poking the receptacle
- Correct latency: time between start of the choice phase and correct response

2.3.6 Operant DNMTS 2-CSWM task

The operant DNMTS task followed the same principal trial-schedule as the 5-CSWM task except for two modifications: the implementation of a *non*-match-to-position rule (i.e. animals are rewarded for choosing the illuminated CP poke-hole that is not the one, that they poked in the SP) and a simplified set of choice options using always only holes 2 and 4 of the 5-choice wall (making it similar to a task developed by Goto & Ito [178]). Mice were trained in this task only after the T-maze (2.3.7) in order to ease the switching from the prior, opposite task-rule. All mice were trained for 30 training sessions on the 2-choice DNMTS task, then were tested in two delay challenges, in which the pre-delay was extended to 5 and then 10 s (2 d each). A subset was then trained in a 5-choice version of the same task (i.e., the DNMTS-version of the 5-CSWM task) for 12 d *without* and for 3 d *with* head stage mounted, but performance in many mice was not sufficient, and hence mice were returned to the 2-choice version and trained for a further 5 d with mounted head stage. The other subset moved directly to 5 d of training with mounted head stage. Then, recordings were conducted on two days with baseline training and two days each for two delay challenges, in which the pre-delay was extended to 5 and then 10 s. Given the relatively low performance in the delay challenges, the data from the two baseline days was used for further analysis of electrophysiology data. In all protocols, the SP-SD was 8 s, the CP-SD was 5 s, the limited hold time exceeded the SD by 1 s, ITI and time-out were each 5 s, the post-reward delay was 2 s (spent in darkness), the SP reward was

10 μl, and the CP reward 60 μl. The same parameters were mainly analysed as described in 2.3.5.

2.3.7 Non-matching to sample T-maze test of rewarded alternation

SWM as rewarded alternation was tested in a red-colour plastic T-maze with transparent walls and food wells placed in the end of all three arms. Before testing mice were habituated to the surroundings and to the condensed milk reward (10% Ja! ®-Kondensmilch, diluted 1:1 with drinking water) at first cage-wise and later independently.

The experiment involved ten trials per day each consisting of a SP and a CP. During the SP mice were placed at the beginning of the arm facing the experimenter with one of the goal arms blocked. Mice then should run towards the reward in the non-blocked sample arm and then return motivated by a smaller reward in the start arm. After a delay period of 5 s the previously blocked arm was made accessible by the experimenter and mice were given the choice to either visit the familiar, now unrewarded sample arm or the previously unvisited, rewarded choice arm. It was considered a correct choice when mice entered the novel arm and a wrong choice when they visited the sample arm. Trials were separated by an ITI of 20 s and the choice arm for each trial was determined pseudo-randomly. It was made sure that the distribution of both arms was equal and that the choice arm was not the same for more than three consecutive trials.

For the above-described baseline protocol eight testing days were carried out followed by four days during which the delay period was prolonged to 30 s.

2.3.8 Novel object recognition test

The NOR test of object-related novelty preference was used to assess short-term habituation (memory) for objects. Mice were habituated to the square open-field (dark-red floor, grey PVC walls of 25 cm height, 40 cm length and width) over the two days before testing; the first 5 min habituation session was conducted with the cage mates, all subsequent ones – one time 5 min on the same day, one time 5 min and one time 10 min on the next day, and one time 10 min on the morning of the test day – were conducted with each mouse individually. On the test day, mice were habituated to a holding cage for ca.

20 min and then introduced to the familiar open field in which two copies of the same unfamiliar object were placed (sample phase). After 10 min, the subject was removed into the holding cage for 2 min so that both objects could be replaced, whereby one was re-

placed by an identical object and the other one by a novel object. Subsequently, mice were introduced to the open field again for the 5 min test phase. Mice were video-monitored and thereby their interaction with objects scored manually, in addition to tracking with AnyMaze. Data from manual scores was used for further analysis. Novelty preference was analysed by calculating the *time* spent in with the novel object divided by the sum of the time spent with either object. Additionally, the same preference score was calculated based on the *number of contacts*.

2.4 Human intracranial electrophysiology data during working memory

A publicly available open-access dataset of multi-site intracranial recordings during three WM tasks [225] was downloaded from http://dx.doi.org/10.6080/K0VX0DQD within the framework of the CRCNS.org data sharing program in computational neuroscience initiated by the University of California, Berkeley [436]. The openly available data in the repository is anonymous and was originally acquired for the experiments described in [225] and the online dataset was already used for other publications [166, 237]. As stated in [225], ethics approvals were submitted. Accordingly, all subjects gave informed written consent in accordance with the University of California, Berkeley Institutional Review Board (#2010-01-520); Regional Committee for Medical Research Ethics, Region South (#2015/175/REK); or Stanford University Medical Centre Institutional Review Board (Protocol ID 11354, IRB Number 4593, panel 5); and also, in agreement with the Declaration of Helsinki [225].

It includes data from 10 human adult subjects (mean ± SD [range]: 37 ± 13 [22–69] y; 7 males) who were implanted with intracranial electrodes to identify epileptic foci for surgical resection. Electrode placements were in the MTL (i.e., CA1; CA3/DG; subiculum; or parahippocampal, perirhinal, or entorhinal area), lateral PFC (inferior, middle, or superior frontal area), and OFC (orbitofrontal, frontal polar, or medial prefrontal area). Only subjects with electrodes localized in all three regions were included in the present analyses ($N = 8$). For details on data acquisition and pre-processing, and a detailed description of the behavioural experimental setup see [225, 226]. Three different WM tasks were conducted, whereby subjects had to either identify a previously indicated object identity, location, or temporal order of two visual stimuli (see Figure 3.2.13a). Trials from all these three tasks were pseudo-randomly mixed from trial to trial in a single test session. Each trial started with a 1 s pre-trial fixation interval, after which a screen indicated whether in the respective trial would be tested for object identity or spatiotemporal position (800ms). Subsequently, the SP started in which two shapes were presented subsequently for 200ms each, separated by 200ms. After a subsequent pre-cue delay (900 or 1150ms, varied pseudo-randomly), a cue appeared for 800ms that specified which of the two shapes would need to be identified in the later CP according to a rule of identity (same/different), spatial location (top/bottom) or temporal order (first/second). After a post-cue delay (900 or 1150ms, varied pseudo-randomly), the CP started as two shapes were presented, of which the participant had to choose the one that was correct according to the prior cue. All trials from all patients were merged for subsequent analyses, just as was done for the mouse WM data.

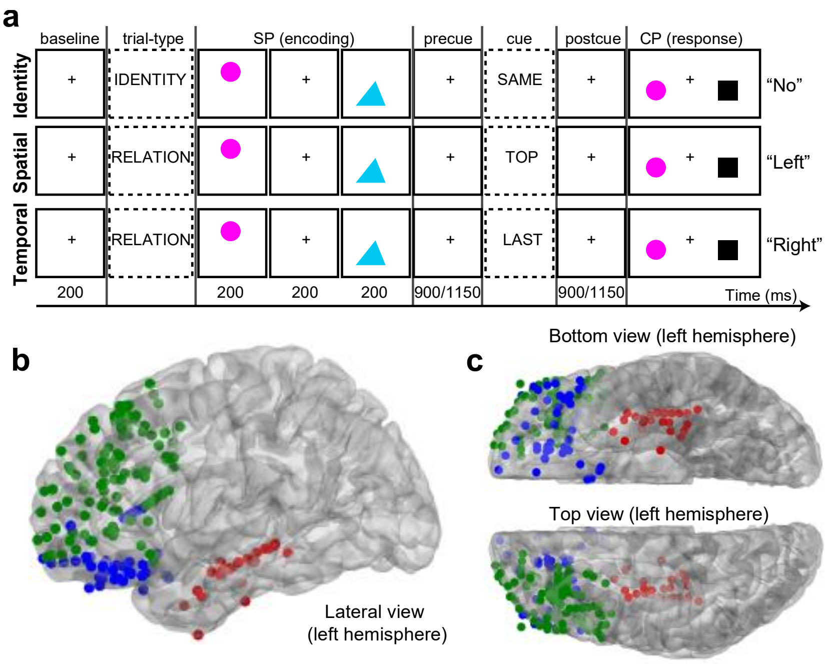

Figure 2.4.1: Human data overview
(**a**) Display of the structure of the three human WM tasks, according to [225]. (**b, c**) Placements of electrodes as projected onto the left hemisphere, irrespective of actual hemisphere of each electrode. Adapted from [421], open access article: CC BY 4.0, https://creativecommons.org/licenses/by/4.0/

2.5 ELECTROPHYSIOLOGICAL DATA PROCESSING

Electrophysiological data was acquired at a sampling rate of 10 or 20 kHz via a 32 – Channel RHD2132 amplifier board (Intan Technologies, USA) containing a 12-pin Omnetics polarized nano connector and a 36-pin Omnetics nano strip connector where the former is connected to a light-weight SPI interface cable (Intan Technologies, USA) and the latter with the recording electrodes using a custom-made adaptor. The adaptor was wired so that all signals were referenced to the ground-signal obtained from above the contralateral cerebellum, while the signal from the additional frontal reference screw was recorded separately (for later offline re-referencing) like the LFP channels, i.e., also referenced to ground. Data was transferred to an Open E-Phys acquisition board and the Open E-Phys acquisition software (Open E-Phys, USA) where a bandpass-filter was applied (0.1 – 250 Hz), although the unfiltered data was also saved. For GC and MUA analysis the unfiltered data was used and further sampled down to 250 Hz for GC [33]. In operant tasks, all individual task- and behavioural events were recorded by pyControl [7]. Additionally, all events relevant to time-locked electrophysiological analysis of WM task-phases and choices (e.g., correct SP and CP responses) were encoded as patterns of transistor-transistor logic (TTL) signals by pyControl and recorded as timestamps with the electrophysiological data by the Open-EPhys acquisition software using the 8 analogue inputs of the acquisition board and a dedicated BNC-HDMI interface board (Open-EPhys). For the T-maze task, AnyMaze was used to track the position of the animal in the different subdivisions of the maze, and this positional information was encoded in patterns of TTL-signals recorded via an AMi-interface board and a BNC-HDMI interface board as timestamps with the electrophysiological signals in the Open-EPhys acquisition software. For WM-tasks, trials were excluded from further analyses if the amplitude exceeded the 5^{th} standard deviation within each channel for more than 10% of the trial duration. PFC and vHC were partially recorded with dual electrodes in some mice (see 2.2). If both electrodes had equally good placement (as inferred from lesion sites) all further connectivity analysis was performed for both signals. For the open field experiment, the data from each electrode was regarded as the unit of observation (N), so that a single mouse could contribute up to an N = 4 for vHC-PFC connections and up to an N = 2 for dHC-vHC, PFC-vHC, MD-PFC and MD-vHC connections. For WM experiments, results were averaged between electrodes in a single mouse in order to keep the trail-based structure. Analogously, for local activity measures, each single metric was calculated for every electrode and the resulting value was averaged across all electrodes of a given area for each subject.

For the human dataset, iEEG data were sampled at either 1kHz or 512Hz and were resampled offline to 1kHz. As described in [225] raw electrophysiology data were carefully inspected, epileptiform activity or artefactual signals were excluded, filtered between 1 and 200Hz, demeaned and 60Hz line noise harmonics were removed using discrete Fourier transform. The number of electrodes per site varied between 1 and 28 per area. Therefore, for connectivity measures, each single metric was calculated for every possible interregional pair of electrodes and the resulting value was averaged across all combinations of a single connections. Analogously, for local activity measures, each single metric was calculated for every electrode and the resulting value was averaged across all electrodes of a given area for each subject.

All signal analyses were done in MatLab (MathWorks, USA). Data were exported to MatLab and, for all LFP analyses, down-sampled to 1 kHz (or 250Hz for GC analysis) and analysed with custom-written scripts. To reduce low frequency drift, signals were first detrended using the *locdetrend* function of the Chronux signal processing toolbox (http://chronux.org/, [55]) with 1 s of data and a sliding window of 0.5s. MatLab scripts are publicly available at http://doi.org/10.5281/zenodo.4384980 and https://github.com/KaetzelLab/LFP_analysis.

2.5.1 Spectral power and coherence

Power and coherence spectra were calculated with routines implemented in the chronux signal processing toolbox using the multitaper method [55]. Power values were expressed as $10*\log_{10}$ values for all analyses and the range of frequencies was set from 0.1 to 48Hz. For the open-field experiment, a bandwidth of 0.2Hz and a total of 220 tapers were used to calculate power and coherence over the course of the 10 min exploration time. To analyse the temporal development of spectral features, power and coherence were also calculated in 10 s bins using a bandwidth of 1Hz and 19 tapers. For WM-experiments (operant DMTS 5-CSWM, DNMTS 2-CSWM and T-maze), a time-bandwidth product of 9 and 17 tapers were used to calculate power and coherence during defined time-periods during ITI, SP, delay (if applicable) and CP. Time-frequency spectral analyses were performed with routines from the FieldTrip toolbox using Morlet wavelets with a width of 3 cycles steps of 10ms [342]. Time periods before and after the time frame of interest were padded with real data to avoid artifacts of too long wavelets at low frequencies.

2.5.2 Weighted phase lag index

The wPLI was calculated using the routines implemented in the FieldTrip toolbox [342]. For the open-field experiment, the 10 min exploration time was cut into non-overlapping 1 s bins and padded to the next power of two. The complex cross-spectrum was computed using a Hann taper with a spectral smoothing of 0.5 Hz. For temporal analysis wPLI was averaged for each minute of the 10 min period using the same spectral parameters. For WM-experiments, the original trials were further divided into 99% overlapping "pseudo trials" with a length of 600ms and padded to the next power of two. The complex cross-spectrum was computed using a Hann taper with a spectral smoothing of 2 Hz. As in 2.5.1, time-frequency wPLI analysis was performed with routines from the FieldTrip toolbox using Morlet wavelets with a width of 3 cycles steps of 10 ms [342] and time periods before and after the time frame of interest were padded with real data to avoid artifacts of too long wavelets at low frequencies.

2.5.3 Phase-amplitude coupling

CFC [81] was assessed using the measure of PAC, the statistical relationship between the phase of a low-frequency and the amplitude of a high-frequency component, in a cross-regional analysis [403, 442]. For the open field experiment, the 10 min recording was split into 1 min bins during which the PAC was calculated using the Modulation Index (MI, [442, 457]). Briefly, time series data is first band-pass filtered in the desired frequency range, followed by a Hilbert transform using the MatLab function *hilbert* which calculates the real and imaginary part of the signal to obtain the instantaneous amplitude and phase at any given time point. Theta phases were binned into 18 20° intervals and the mean gamma amplitude was calculated in each phase bin. The distribution across bins was assessed using the Kullback-Leibler divergence [258] and normalized between 0 and 1. The MI is close to zero if the mean gamma amplitude is uniformly distributed over the theta phases and close to one if the mean gamma amplitude is exceptionally higher within one phase bin [442].

For WM-experiments, intra- and inter-regional PAC were determined by calculating the modulation of γ-amplitude by θ-phase using the phase-locking technique proposed by Voytek et al. with routines described in [458, 459]. The suitability of single-trial PAC for behavioural decoding has been demonstrated in previous studies [125, 220, 427].

2.5.4 Cross-correlation of instantaneous LFP amplitudes

To determine whether one signal was leading or lagging the other, amplitude cross-correlations of instantaneous amplitudes of LFP oscillations between all brain regions were performed according to [3]. First, the two signals were bandpass filtered in the respective frequency range; the Hilbert transform was computed using the MatLab function *hilbert* to calculate the instantaneous amplitude and the envelope of the signal; cross-correlation between the amplitudes of the two signals was calculated with the MatLab function *xcorr* over lags ranging from -100 ms to + 100 ms; the lag at which cross-correlation peaked was determined [3]. The amplitude of the correlation represents the resemblance of both signals, and one signals leads the other by a delay. It quasi corresponds to coherence whereas coherence is in the frequency, but cross-correlation takes place in the time domain.

To determine if the obtained lags significantly differ from zero, a Wilcoxon Signed Rank test were performed. Amplitude cross-correlation was only analysed during the open-field experiment, since single-trial analysis can yield spurious and non-informative results [3].

2.5.5 Granger causality measures

Parametric GC was calculated using the multivariate GC (MVGC)-toolbox [32]. GC mainly applies to stationary signals which means that the variances are not excessively changing over time [63, 168]. Therefore for the open-field experiment, the 10 min period was divided into 1 min bins and the in-built trial averaging function was used to calculate GC in non-overlapping 10 s sections to ensure reasonable stationarity [145, 198, 219]. The 1 min bins were used for the analysis of GC over time and then averaged to obtain a GC value for the whole 10 min testing period. Raw LFP data was sampled down to 250 Hz to ensure a reasonable model order for autoregressive modelling [31, 32, 397]. The model order was obtained using the Bayesian Information Criterion (BIC, [390]) as it was shown to provide the best fit to electrophysiological data [32]. The model order was fixed to 27 across all animals and trials to obtain comparable results [99]. Non-prefiltered data were used because empirical analyses have shown that filtering time series data increases the ARM order and leads to high variances making it unsuitable for GC analysis [31]. To obtain GC values for specific frequency bands we first computed GC up to the Nyquist-frequency and then integrated over the desired frequency range [31]. A permutation procedure implemented in the MVGC-toolbox was performed to test the null hypothesis that values obtained by GC estimation occurred by chance [32, 63]. npGC, DTF, and PDC were calculated using the FieldTrip toolbox [342]. The same temporal configurations were used as described above for parametric GC and raw LFP data was sampled down to 250 Hz as well. Instead of deriving the noise covariance matrix and transfer function by autoregressive modelling (as done for parametric GC), these were obtained by applying Wilson's spectral matrix factorization to complex Fourier-spectra. This non-parametric approach was shown to be better at capturing all spectral features, less error prone because no model order had to be chosen and computationally faster [121, 122]. For WM-experiments, the original trials were further divided into 50% overlapping "pseudo trials" with a length of 1 s and padded to the next power of two, differing from power and non-directed synchrony measures because 99% overlap did not provide substantially different results but came with a much higher computational effort. The complex cross-spectrum was computed using a Hann taper with a spectral smoothing of 2 Hz. The noise covariance matrix and transfer function were obtained by applying Wilson's spectral matrix factorization to complex Fourier-spectra. This non-parametric approach was shown to be better at capturing all spectral features, less error prone because no model order had to be chosen, computationally faster than applying autoregressive modelling [120, 121], and to deliver virtually same results when used on our LFP data [420]. Time-frequency representations of npGC and PDC were obtained by Morlet wavelets using the same configurations as described above for non-directed measures.

2.5.6 Spike-phase coupling

MUA was extracted by high pass filtering the raw signal above 800 Hz and applying a threshold at 3.5 standard deviations from the mean. Spikes were excluded if the threshold exceeding was longer than 2 ms and if spikes occurred within 1 ms. LFP of the second brain region was filtered between 5 and 12 Hz using the MatLab function *eegfilt* from the EEGLAB-toolbox [118]. To account for speed-dependent waveform asymmetry in the theta oscillation, the theta phase was defined by linear interpolation between consecutive troughs within each cycle [73, 302, 400]. Only periods in which the theta amplitude was above 0.25 standard deviations of its mean were included to ensure sufficient theta rhythm. Each spikes was than assigned a theta phase and the mean resultant vector length (MRL) was calculated as an indicator for the strength of coupling using the CircStat-

Toolbox [45, 401]. The number of spikes was fixed to 1000 for each recording to prevent spuriously high MRL values and fluctuations in the firing rate. To determine the directionality between MUA and theta oscillations, phase locking was calculated for 50 different temporal offsets ranging from -100 ms to 100 ms in steps of 4 ms using custom written MatLab scripts. If the MRL peaked at a positive offset, spikes were most strongly phased to the next theta cycle of the past, suggesting that theta drives spiking activity [400, 401]. A Wilcoxon sign rank test was applied to determine if the lag or lead was significantly different from zero. SPC was only analysed during the open-field experiment since single-trial analysis was not possible due to too erratic appearance of spikes.

2.6 SUPERVISED MACHINE LEARNING

To validate the calculated measures of neural connectivity and to identify predictive variables of WM we employed supervised ML algorithms. Spectrally resolved parameters (e.g., γ-coherence, γ-power) from each inter-regional connection (e.g., dHC-PFC) and local brain region (e.g., dHC) were analysed separately using different classifiers. For classification, we used the absolute parameter values as well as the ratio of each parameter relative to the preceding ITI. In mice, 240 connectivity metrics per connection and 56 local activity metrics per region were used in the 5-CSWM DMTS task (1184 for all connections and regions combined; 296 per task-phase), and 180 connectivity metrics and 42 local activity metrics were used on the operant 2-CSWM DNMTS task and the T-maze (888 combined). The difference originates from the usage of 4 task phases, including pre- and post-delay phases, in the 5-CSWM task, but only 3 phases (one delay phase) in the two DNMTS tasks, which was the post-delay in the 2-CSWM task. For all predictor matrices, the pre- and post-delay phases were combined to allow uniform comparisons between all three tasks. In humans, 448 connectivity metrics per connection and 80 local activity metrics were generated, using all 4 task phases including SP, pre-cue delay, post-cue delay, and CP (classifiers omitting the CP were also calculated, see Figure 3.2.14). Note that, in humans more predictors arise because frequency bands have been determined additionally in the alpha-band (8-12 Hz), and in a higher gamma-band (50-100 Hz) in addition to the low gamma band (30-49 Hz) used in rodent analysis. We also included the combined band (30-100 Hz) as separate predictor. To ensure a sufficient number of trials for classification and the general validity of the identified predicting variables, we merged data from all subjects of one group, i.e., from all mice of a given genotype (KO or WT) provided correct electrode placement or from the subset of human subjects with coverage of all three regions, respectively.

Since rodent and human subjects performed proficiently above chance level (except for *Gria1*-KOs on the T-maze) resulting in more correct than incorrect trials (see Figure 3.3.2 for behavioural results in mice; mean accuracies (%) and standard deviation in humans: 0.90/0.04 (identity), 0.92/0.09 (spatial), 0.89/0.09 (temporal) [225]), we used a *synthetic minority over-sampling technique* (SMOTE) to construct a balanced dataset with five nearest neighbours to consider [91]. All electrophysiological predictor variables of a classifier were normalized between 0 and 1, setting the maximum empirical value for each metric to 1. We used 90% of the data as a training set and the remaining 10% for testing. Allocation to the training and test set was done randomly and repeated 100 times to obtain a mean and its variance for the achieved decoding accuracy the predictor weights. To identify the classification algorithm which fits our data best we assessed the 25 most used classifiers implemented in MatLab (Figure 3.2.4). Focussing on easy interpretability and high predictive accuracy we chose random subspace ensembles on a linear discriminant analysis (LDA) template (subspace discriminant classifier) for our further analysis, which achieved the highest prediction accuracies compared to all other tested linear classifiers. Briefly, LDA aims to identify a hyperplane that maximizes the mean distance between the mean of the two classes while minimizing variance between them. Since the sample size of our data was relatively small compared to the number of features, we used the *random subspace method,* which is a valid approach to resolve this issue and has been shown to be superior to single classification algorithms [404, 440]. It operates by creating a classifier ensemble where each classifier is trained with a reduced, randomly sampled number of input features, e.g., they are projected into a new subspace which leads to a relative increase of the number of samples. The number of features to sample in each classifier and the number of learning cycles were set to half of the total number of features and 30, respectively. The coefficient magnitudes of each feature obtained by each subspace LDA classifier were averaged across learning cycles to get a solid quantification of its predictive value. Because the accuracy alone does not always give a full representation of an ML model's performance, we used the prediction accuracy, the area under the curve (AUC) of the receiver operating characteristic (ROC) and the F1-score which is defined as follows: F1 = (2*class1precision * class1recall) / (class1precision + class1recall). Precision is defined as the True Positives / (True Positives + False Positives) for class 1 and as the True Negatives / (True Negative + False Negative) for class 2. Recall is defined as True Positives / (True Positives + False Negatives) for class1 and as True Negatives / (True Negatives + False Positives) for class2. The sensitivity refers to the percentage of positives that are correctly identified which equals the recall for class1, whereas the specificity describes the proportion of negatives that are correctly identified which equals the recall for class2.

The ROC represents a probability curve between the True positive rate (= Recall/Sensitivity) and the False positive rate (= False Positives / (False Positives + True Negatives)). The AUC of such a curve therefore indicates the separability of the classes, i.e., an excellent model has AUC close to one, whereas a poor model has AUC near to zero and an AUC of 0.5 means that the model has no class separation capability at all.

During this study, classifier performance for binary grouping is reported as the F1 and as the prediction accuracy for multiclass calculation. To be transparent about the performance of the classifier performance we report all the mentioned indicators of performance in order to avoid disbalances towards one of the classes. However, throughout all measures showed high percentages, indicating that the classifiers fitted the data well without any imbalances (see Suppl. Table 2, Suppl. Table 3 and Suppl. Table 4 for mice data and Suppl. Table 5, Suppl. Table 6 and Suppl. Table 7 for human data). Since it has been shown that the theoretical chance level of 50% should not be expected and it is favourable to obtain an empirical chance level, we randomly shuffled the data labels (e.g. correct / incorrect) and repeated the analysis described above to create an empirical null distribution [103]. A direct comparison between the actual values and the respective chance level distribution was employed to attain the associated p-value.

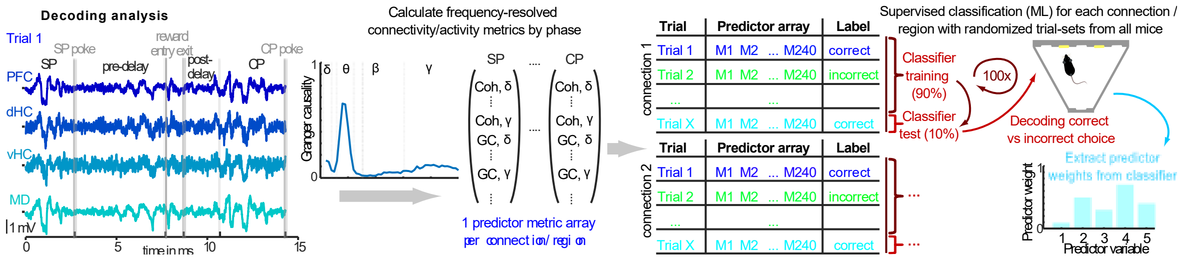

Figure 2.6.1: Illustration of ML-based decoding analysis
From left to right: Exemplary time series of the four analysed brain regions over the course of one trial with time points of interest. Frequency-resolved GC spectrum between two signals highlighting frequency-band specific information and arrays containing frequency-averaged connectivity metrics. Matrix containing predictor arrays from each trial with the respective labelling (correct/incorrect). The fraction of trial that is used for training and testing the classifier is indicated in red and the experimental setup for mice is exemplified. Blue bar graph illustrates exemplary weights assigned by the classifier for each predictor (e.g., δ Coh). Adapted from [421], open access article: CC BY 4.0, https://creativecommons.org/licenses/by/4.0/

2.7 Perfusion of mice

Mice were sacrificed by injecting a ketamine (100 mg/ml, WDT, G) / medetomidine (1mg/ml, Domitor, Orion Pharma, Finland) solution intraperitoneally. To validate the correct placements of the electrodes miniature lesions were made by applying electrical current on the recording electrodes immediately after the death of the mouse. After this, the mouse was perfused with phosphate-buffered saline (PBS) followed by 4 % paraformaldehyde (PFA). After decapitation and removal of the brain, the same was post-fixed in 4 % PFA for at least 24 h and then cut with a vibratome (VT1000, Leica) into 60 µm slices.

2.8 Statistical analysis

Statistical analyses were performed with SPSS version 25 (IBM, USA) and MatLab 2020 (Mathworks, USA).

For the open-field experiment, genotype-related differences within the same metric and frequency range were assessed by independent-sample *t*-test or, in the case of GC, by Sidak paired post-hoc tests conducted after a significant effect of genotype or interaction in the prior repeated-measures analysis of variance (ANOVA). For circular data (spike and coherence phase angles) the Watson-Williams two-sample test was used to assess genotype-related differences. A p-value < 0.05 was used as indicator for statistical significance; no further correction for multiple comparisons were applied, given that we aimed to emulate the situation that only a single measure is used to characterise connectivity, and false-negatives were to be avoided given the analytical goal of detecting redundancies between metrics. Bivariate correlations were calculated using Spearman's rho. To detect correlations between circular and circular and between circular and linear data we used circular-circular correlation and circular-linear correlation as implemented in [45].

For WM-experiments, behavioural training and challenge data were analysed with repeated-measures ANOVA and pairwise Sidak post-hoc tests for simple main effects. To determine the importance of individual connectivity or activity measures (predictors), we used a two-step procedure: First, pre-classification, we performed a paired *t*-test for each feature comparing its value in correct vs. incorrect trials. Second, post-classification, we used the magnitude of the weight of each predictor as delivered by the subspace discriminant classifiers to perform a paired *t*-test between the obtained magnitudes and the magnitudes from the shuffled dataset. Features were only recognized as significantly important if both criteria were met. *P*-values were Bonferroni-corrected within-species for the total number of used features across all classifiers calculated in mice (1184; $P < 0.05/1184$) and humans (1584; $P < 0.05/1584$) in the most conservative analysis; additional analysis was conducted to evaluate the dependency of the number of obtained significant predictors with less stringent adjustments.

For the experiments conducted in the *Gria1*$^{\Delta\mathrm{Amigo2}}$ and *Gria1*$^{\Delta\mathrm{Grik4}}$ cohort, one-way univariate or repeated measures ANOVAs were used with a simple between-subjects design.

Variability in the data is displayed as standard error of mean (SEM) throughout.

3 RESULTS

3.1 LACK OF REDUNDANCY BETWEEN ELECTROPHYSIOLOGICAL MEASURES OF LONG-RANGE NEURAL COMMUNICATION

3.1.1 Elevated locomotor activity in *Gria1*-KO mice during measurement of interregional communication

To measure inter-regional coupling, we implanted 15 adult *Gria1*$^{-/-}$ mice and 12 littermate WT controls unilaterally with LFP electrodes in 4 regions, PFC (2 electrodes), MD (1 electrode), dHC (1 electrode) and vHC (2 electrodes), and inserted screws for ground and reference above the cerebellum and frontal cortex, respectively (Figure 3.1.1a). After successful recovery from surgery, recordings from all regions were made during a 10 min test of novelty-induced locomotor activity where we could replicate the previously shown hyperlocomotion-phenotype of *Gria1*$^{-/-}$ mice (Figure 3.1.1b-c; [76]).

After finishing all experiments (see Figure 3.2.1a for a timeline), placements of all electrodes were evaluated through electrolytically lesioning the respective sites and misplaced electrodes were eliminated from the dataset (number of all included electrodes are depicted in Figure 3.1.2); data from the MD was discarded for most of the subsequent analysis because of the low number of animals with accurate placements.
In accordance with previous study in this mouse line [76], the ground screw above the cerebellum was used as the primary reference for subsequent analyses but we also used the data from the frontal reference screw for a separate analysis (displayed in Figure 3.1.8). Besides extracting LFP signals (Figure 3.1.1d-e) from all electrodes we also obtained MUA spikes from the prefrontal wires. For PAC, amplitude cross-correlations and SPC, the theta-phase angle was extracted using a Hilbert-transform for the two former or linear interpolation between consecutive cycles for the latter (Figure 3.1.1f-g).

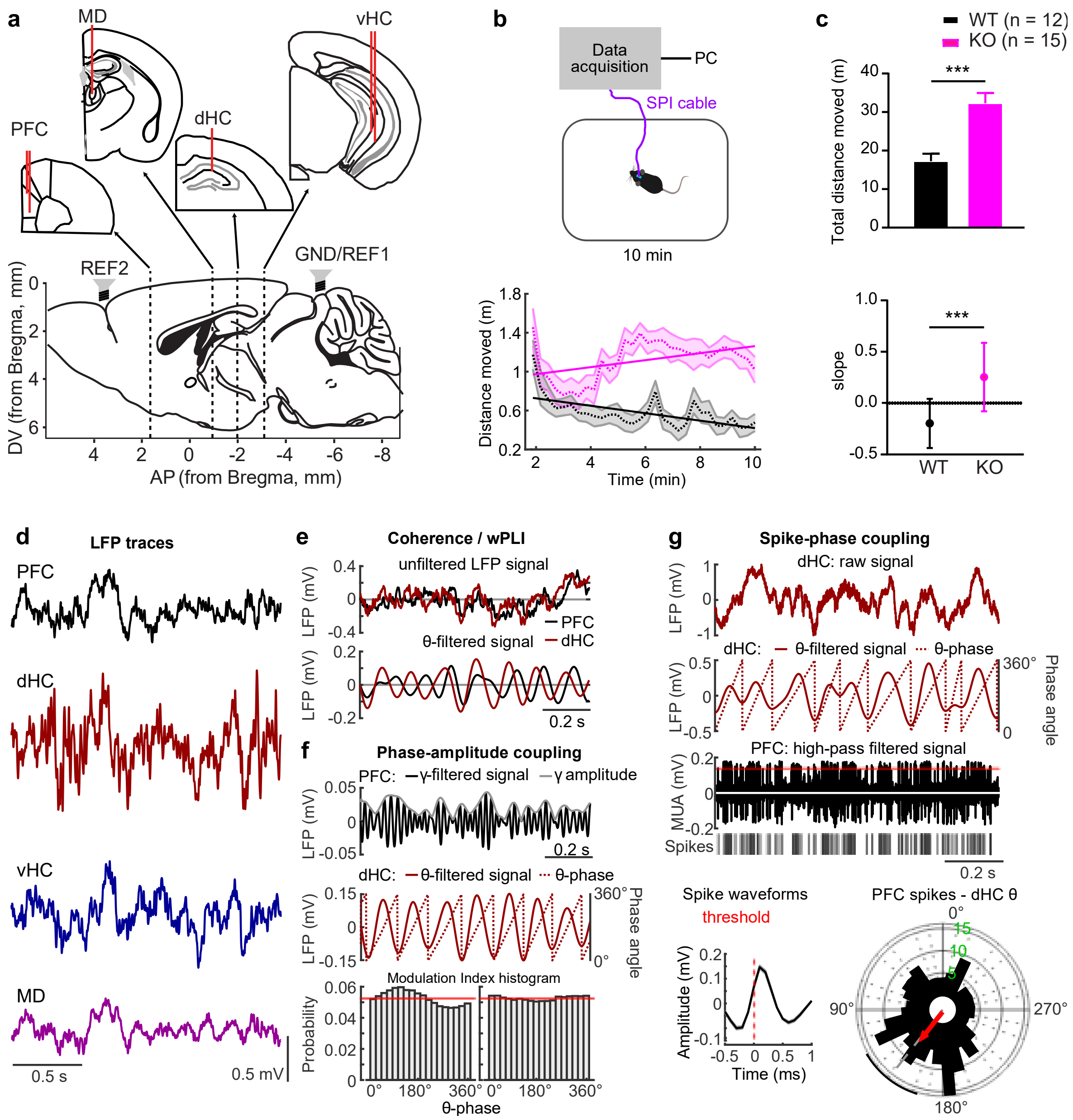

Figure 3.1.1: Experimental set-up, behaviour, and recorded signals

(**a**) Placement of LFP and screw electrodes. (**b**) Top, experimental set-up; bottom, distance moved in 20 s bins by *Gria1*$^{-/-}$ (KO, purple) and wildtype controls (WT, black), dashed line indicating mean, shaded region representing SEM, solid overlaid line representing linear interpolations across time. (**c**) Same data as in (b) but displayed as total distance moved in 10 min (top) and slope of the interpolated line (bottom). *** $p <$ 0.001, *t*-test. (**d**) Examples of unfiltered LFP traces recorded in the four brain regions. (**e**) Illustration of the processing for connectivity measures using the same LFP frequency-band in both regions; raw LFP signal (top) and LFP signal filtered in a specific frequency-range (bottom). (**f**) Illustration of cross-regional θ–γ PAC, whereby the signal in one region is filtered in the low–γ range and the amplitude is extracted (top), while the signal in the other region is filtered in the θ-range and Hilbert-transformed to extract the θ-phase (middle). The coupling-strength is derived as MI measuring the phase-related change of γ -amplitude (bottom). Left histogram depicts solid modulation, whereas right histogram depicts no modulation (**g**) Illustration of SPC; the hippocampal LFP (top) is filtered in the theta-range and the phase angle is extracted by linear interpolation (below, brown); the prefrontal high-pass-filtered signal reveals MUA from which spikes are extracted by thresholding (below, single spikes, and bottom left, average of all extracted PFC spikes, black). A circular histogram is computed by assigning each spike to its theta-phase angle and the average of all vectors is calculated as mean resultant vector (red) whose length (MRL) is taken as indicator of SPC strength (bottom right). Adapted from [420], open access article: CC BY 4.0, https://creativecommons.org/licenses/by/4.0/

3.1.2 Differences in detecting delta and gamma-range coupling in *Gria1*-KO mice across measures of synchrony and differences in detecting elevated inter-regional theta-range coupling in *Gria1*-KO mice across measures of directed communication

First, we analysed phase-synchronization along the two prefrontal-hippocampal connections (PFC-dHC and PFC-vHC) and within the hippocampus (vHC-dHC) using coherence, wPLI, PLV, and PPC (Figure 3.1.2a-r). We were able to validate results of a previous study [76] showing that PFC-dHC theta coherence is strongly elevated in *Gria1*-KOs in a novel environment. Also, this pattern further increases with time which likely reflects the spatial exploration behaviour of this genotype (Figure 3.1.1b-c, Figure 3.1.2a, d). Still, this phenotype was by no means specific to the PFC-dHC coupling, but also re-appeared in the PFC-vHC and vHC-dHC connections suggesting a broader deficit of excessive theta-range connectivity (Figure 3.1.2b-c, e-f). Reassuringly, the same phenotype was revealed by the wPLI, PLV and PPC metric across connections (Figure 3.1.2g-r). However, when inspecting the other frequency bands, findings were not particularly consistent between wPLI and the other three measures (which appeared very similar to each other). While all indicators revealed a reduced gamma-range PFC-dHC coupling in KOs, a sole analysis with wPLI suggested further differences in the delta (PFC-dHC, vHC-dHC) and gamma (PFC-vHC) ranges that would have gone undetected, if using the other metrics (Figure 3.1.2d-f, j-r). Also, qualitatively, wPLI resulted in spectra with quite different shape compared to the other ones, especially in the low frequency range.

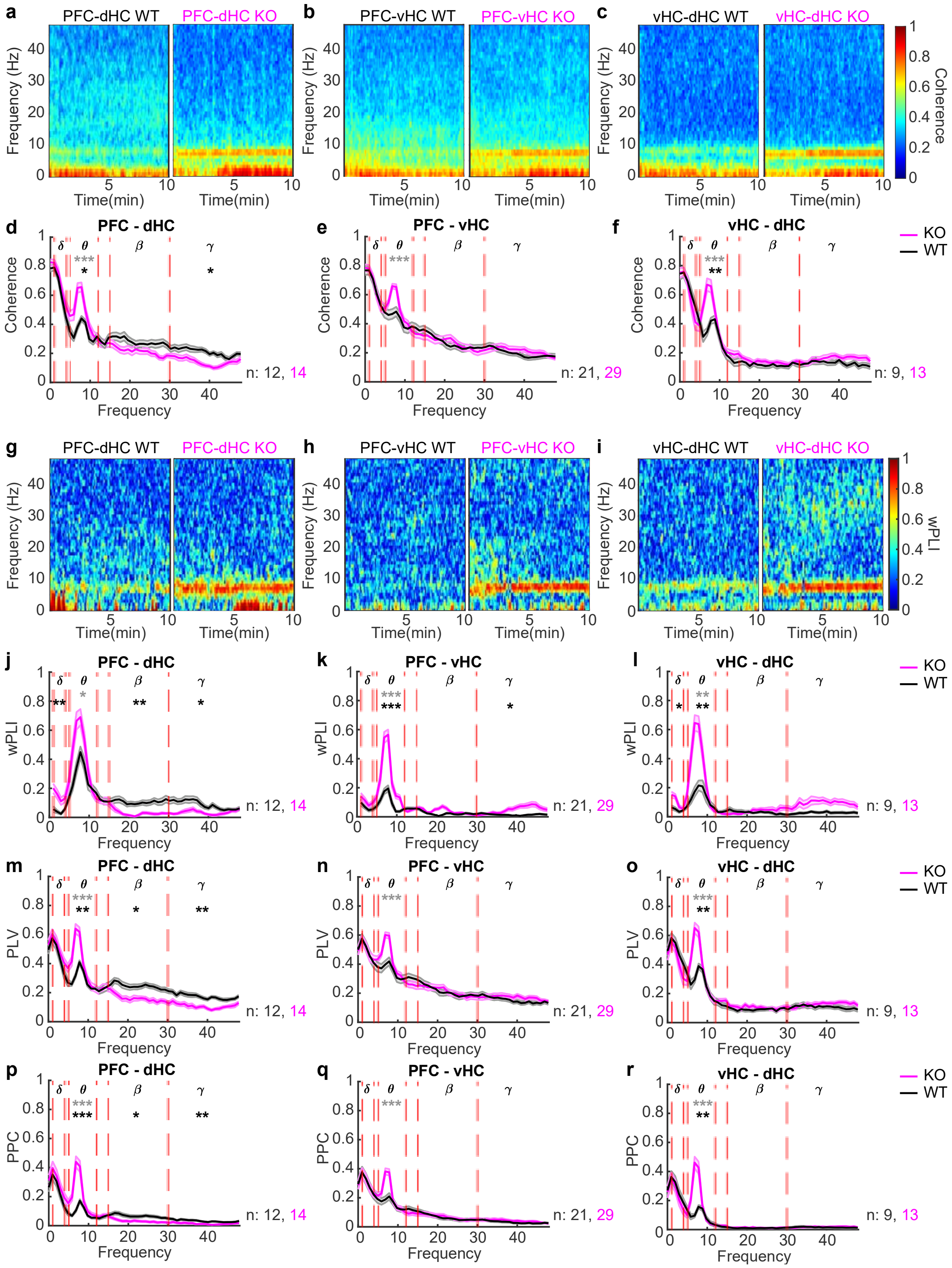

Figure 3.1.2: Non-directed measures of synchrony in *Gria1*$^{-/-}$ and wildtype controls across 10 min novelty-induced activity

(**a-l**) Spectrograms (a-c, g-r) and frequency-spectra (d-f, j-r) displaying coherence (a-f), wPLI (g-l), PLV (m-o), and PPC (p-r) along the PFC-dHC (a, d, g, j, m, p), PFC-vHC (b, e, h, k, n, q) and vHC-dHC (c, f, i, l, o, r) connections. Dotted red lines in spectra indicate boundaries of the analysed frequency bands named by the Greek letters at the top. Stars indicate significant differences between genotypes (*t*-test) in mean (black) or peak (grey) synchrony metrics. Lines display mean ± SEM. # $p < 0.1$; * $p < 0.05$; ** $p < 0.01$; *** $p \leq 0.001$. Adapted from [420], open access article: CC BY 4.0, https://creativecommons.org/licenses/by/4.0/

An analysis of directed connectivity with parametric GC revealed a confirmatory but much more fine-grained picture with KO-induced aberrations in all four frequency bands depending on the connection and direction (Figure 3.1.3a-c). Most prominently, we found strongly elevated theta-range GC in KOs for all projections departing in either subdivision of the hippocampus. This confirms the hippocampal (as opposed to prefrontal) origin of the theta hyper-connectivity phenotype in *Gria1*-KO mice, that was postulated before based on the normalization of this phenotype in mice with hippocampal rescue of GluA1-expression [76]. Likewise, beta/gamma dHC→PFC GC was strongly reduced in KOs (Figure 3.1.3a), in line with reduced phase-synchronization measures (Figure 3.1.2d, j, m, p), while PFC→dHC beta and gamma GC were even mildly elevated. This again suggests a hippocampal origin of the observed reduced synchrony in this frequency range. The most prominent GC was found in the delta range, with PFC→d/vHC GC being significantly larger than the delta GC in the opposite direction in both genotypes. Further, genotype-related differences in vHC→PFC and dHC→vHC delta GC were found that did not match with results from the non-directed synchrony metrics (Figure 3.1.2).

In contrast to GC, significantly elevated theta *PDC* in KOs was only detected in the dHC→PFC/vHC connections, but not in the vHC→PFC/dHC projections. And in the beta/gamma-ranges there were virtually no matches between PDC and GC *at all* regarding genotype-related differences (except for a minority of null-results and trends; Figure 3.1.3a-f). Assessing *SPC* using the MRL representing average spike-occurrence in theta-phase space [4], we found the *opposite* of what would have been assumed from the PDC metric: locking of PFC spikes to *vHC* theta was higher in *Gria1*-KOs, but phase-locking of PFC spikes to *dHC* theta showed no difference between genotypes (the latter also contrasts with GC and all synchrony measures; Figure 3.1.3g).

Further discrepancies appeared when analysing consistent phase-differences (leads and lags) between potentially coupled oscillations in different regions to assess directionality. We investigated two directed measures obtainable from the SPC: the average theta-phase of the MRL [123] and analysis of the effect of incremental shifts of the MUA relative to the theta-cycle on the MRL [400, 401]. The MRLs of PFC spikes relative to the dHC – but not vHC - theta phase was significantly shifted between genotypes: while they occurred during the rising phase of theta in KOs, they occurred at its through in WTs (Figure

3.1.3h). Leading of PFC spikes relative to dHC and vHC theta was seen with phase shifted MRL analysis in KOs, but no significant difference between genotypes was detectable in this metric (Figure 3.1.3i). The equivalent analysis but conducted with PFC *LFP* (instead of spikes) using cross-amplitude coupling showed the *opposite*, namely a lead of dHC and vHC theta relative to prefrontal theta in KOs, and significant differences between genotypes in both connections (Figure 3.1.3j). In reverse, in the gamma range, PFC led both hippocampal regions exclusively in KOs (Figure 3.1.3j), which is not consistent with GC, but – at least for the PFC-vHC connection – with PDC. Lastly, we examined the coherence phase angle. This showed a characteristic ~90°-shift between the theta, beta, and gamma oscillations of the PFC *vis-à-vis* the dHC, particularly in WT mice. In contrast to other directed metrics, significant genotype-related differences were only seen in the gamma-range, and they were prominent in the two HC-PFC-connections (Figure 3.1.3k).

Finally, dHC- and vHC-*gamma oscillations* were coupled stronger to theta oscillations in PFC and the mutually coupled part of the hippocampus in KOs (gamma-theta cross-regional PAC; Figure 3.1.3l). However, PFC-gamma to hippocampal theta coupling was even *reduced* in KOs (Figure 3.1.3l) which contrasts sharply with the results from all other measures.

In summary, while the identification of genotype-related differences in coupling was similar between some measures (especially coherence, PLV, PPC, and GC), there was also a considerable lack of redundancy across the different measures of interregional connectivity (see overview in Table 3.1.1).

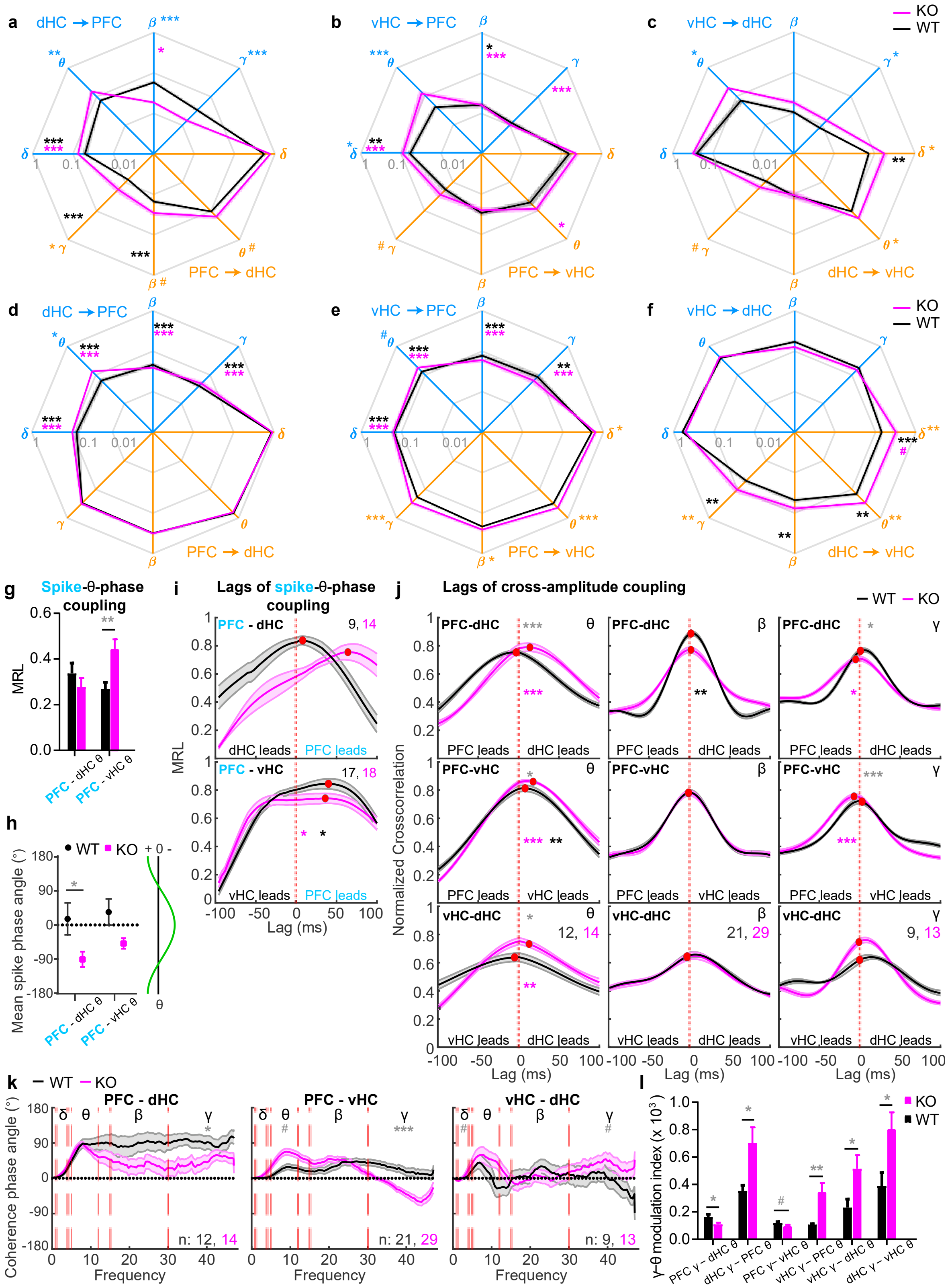

Figure 3.1.3: Directed metrics of inter-regional coupling in *Gria1*$^{-/-}$ and wildtype controls across 10 min novelty-induced activity

(**a-c**) Parametric GC on $\log_{10}$-scale in the frequency bands indicated by Greek letters and along the directed connections identified by the colour (blue: dHC→PFC (a), vHC→PFC (b), vHC→dHC (c); orange: reverse of the before). Statistical indicators in the same colour identify a difference between genotypes (Sidak); statistical indictors in black (WT) or purple (KO) refer to a significant difference between the GC-values of the two opposing directions within the colour-coded genotype whereby the location of the indicator identifies the direction with *smaller* average GC. (**d-f**) Same display as (a-c) but for PDC. (**g**) MRL as indicator of SPC of prefrontal spikes to hippocampal theta. (**h**) Average theta-phase angle of the mean resultant vector from SPC analysis. The theta-phase corresponding to the degree-value is shown on the right (horizontal axis illustrates voltage of LFP). (**i**) MRL as a function of lag between prefrontal MUA and hippocampal LFP. Some data was excluded based on lag-amplitudes above 100ms; contributing *N*-numbers are stated; statistics identical to (g). (**j**) Cross-correlation functions of instantaneous amplitude curves in the connections and frequency bands named at the top of each sub-panel with peak values indicated by a red dot. Statistical indictors in black (WT) or purple (KO) refer to a significant difference of the lag (temporal shift) from 0ms (Wilcoxon's signed rank test). (**k**) Spectra of coherence phase angle along the named connection. Dotted red lines and Greek letters indicate analysed frequency bands. (**l**) Theta-gamma cross-regional PAC for the named directed connections. Solid lines display means and shaded area SEM throughout; bars display mean ± SEM throughout. Grey stars in (g-l) indicate genotype-differences (*t*-test in g,i-j,l; Watson-Williams test in h,k). # $p < 0.1$, * $p < 0.05$; ** $p < 0.01$; *** $p \leq 0.001$. Adapted from [420], open access article: CC BY 4.0, https://creativecommons.org/licenses/by/4.0/

3.1.3 Differences in detecting increases of inter-regional coupling over time in *Gria1*-knockouts across measures

As a second indicator for redundancy between connectivity measures, we investigated potential physiological correlates of the characteristic divergence of exploratory drive between the two genotypes over time (Figure 3.1.1b-c). To allow for an efficient analysis, we captured the change of a given parameter over time in a single number, namely the slope of the linear interpolation across the time series over the 10 min of the test. It was previously found that both local theta power in the dHC and also dHC-PFC theta coherence displayed a characteristic divergence between the groups, that mirrored exploratory behaviour [76]. In this novel dataset and analysis, this pattern emerged much more broadly, namely across multiple power and coherence measures in all three connections (compare Figure 3.1.1b-c with Figure 3.1.4a-d). This included local PFC power in all analysed frequency bands, and gamma and (at trend-level) theta-peak power in the hippocampal regions (Figure 3.1.4a-b). For *coherence*, the KO-related increase in slopes was limited to the delta and theta range and was apparent in the hippocampal-prefrontal connections (confirming earlier results) and marginally for intra-hippocampal coupling (Figure 3.1.4c-d). In the beta and gamma range, either no group-difference occurred or – for PFC-dHC beta coherence – it was even inversed with a higher slope in WT mice. Stunningly, this pattern was not reproduced by the *wPLI* analysis (Figure 3.1.4e-f) – even in the one case where the coupling slope was increased in KOs in *both* metrics (PFC-vHC, theta), the metrics differed in the respect that, in WT controls, theta-wPLI remained constant, while theta-coherence decreased over time.

GC remained largely constant or decreased slightly over time in WT mice, irrespective of connection or frequency band (Figure 3.1.4g-i). In *Gria1*$^{-/-}$ mice, in contrast, GC *increased* over time in the delta and theta range in most connections leading to genotype-related differences in the vHC→PFC (δ, θ), vHC→dHC (θ), dHC→vHC (δ, θ), PFC→vHC (δ, γ), and PFC→dHC (δ, θ) projections. Thus, except for an isolated match in the vHC→PFC theta-connectivity, the GC metric did not align with the wPLI-based slope assessment but provided a near perfect match to the coherence slope pattern (Table 3.1.1). The latter observation even extends to the one instance of PFC-dHC beta coupling where the slope is *higher* in *WT* than in KO mice (Figure 3.1.4g-i). The slope of the *gamma-theta PAC* also showed the expected divergence between genotypes in coupling-strength along vHC-connections, but not in the PFC-dHC connections (Figure 3.1.4j). This pattern matched neither with coherence and GC (as they detected temporal changes in the PFC-dHC connection) nor with wPLI (which detected no changes in the vHC-dHC connection). Likewise, cross-correlational lags did not change in any pattern that resembled the other measures (Figure 3.1.4k). The slopes of MUA-related metrics were not determined because SPC analysis requires a considerable and equal number of spikes (not suitable for short intervals), and PDC and other lag-metrics were not further regarded given that they already differed from the other metrics in the first comparison (Figure 3.1.3).

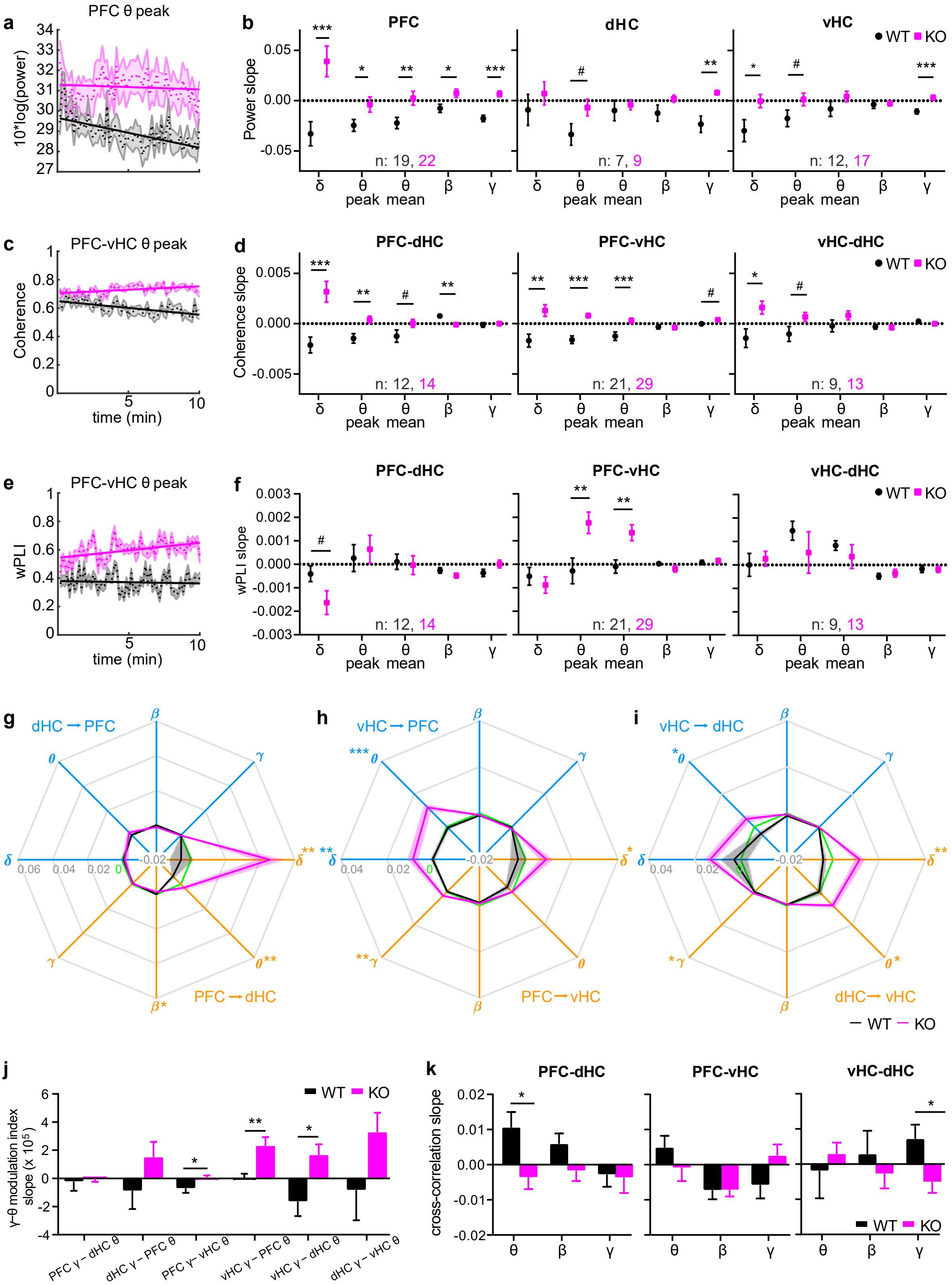

Figure 3.1.4: Changes of power and coupling strength over time during the 10 min open-field test

(**a, c, e**) Examples of individual measures of power (a), coherence (c), and wPLI (e) as they behave as population overage over the 10 min of novelty-induced activity in the open field (dashed line, mean; shaded area, SEM) with linear interpolation between time points overlaid (solid line) to determine the slope as indicator of temporal changes. (**b, d, f**) Average slope (temporal change) of power (b), coherence (d) and wPLI (f) in the indicated regions or connections (top of sub-panel) and frequency bands (x-axis). (**g, h, i**) Slope of GC in the frequency bands indicated by Greek letters and along the directed connections identified by the colour (blue: dHC→PFC (g), vHC→PFC (h), vHC→dHC (i); orange: reverse of the before). Statistical indicators in the same colour identify a difference between genotypes (*t*-test). (**j**) Slope of theta-gamma PAC in the stated directed connections. (**k**) Slope of cross-correlation lags indicating putative changes of temporal shifts of the oscillations in the named frequency bands. Black stars indicate significant differences between genotypes (*t*-test), and error bars or shaded regions indicate SEM throughout. # $p < 0.1$; * $p < 0.05$; ** $p < 0.01$; *** $p \leq 0.001$. Adapted from [420], open access article: CC BY 4.0, https://creativecommons.org/licenses/by/4.0/

Table 3.1.1: Pairwise comparison between wildtype and *Gria1*-knockouts
Overview over genotype-related statistical comparisons of the data displayed in Figure 3.1.2, Figure 3.1.3 (average metric) and Figure 3.1.4 (slope metric). GC and PDC results are derived from Sidak post-hoc test after repeated-measures ANOVA across both directions of a connection and genotypes; MRL-phase and coherence phase-angle are compared with the Watson-Williams test [123]; all other *P*-values are derived from independent-sample *t*-tests. For LFP-based measures (coherence, wPLI, PLV, PPC, GC, PDC) the *P*-values in the theta-range refer to peak-theta (not mean-theta). Arrows in directed measures indicated direction of coupling, → direction labelled in column name (e.g., PFC→ dHC in the PFC-dHC column), ← opposite direction. For MI and MRL measures, the region named first corresponds to the region that contributes the theta-oscillation to the analysis. White background, no measure available or assessed; grey background alone, $p \geq 0.1$; # $p < 0.1$; * $p < 0.05$, ** $p < 0.01$, *** $p \leq 0.001$. Adapted from [420], open access article: CC BY 4.0, https://creativecommons.org/licenses/by/4.0/

	KO vs. WT	delta			theta			beta			gamma		
		PFC-dHC	PFC-vHC	vHC-dHC	PFC-dHC	PFC-vHC	vHC-dHC	PFC-dHC	PFC-vHC	vHC-dHC	PFC-dHC	PFC-vHC	vHC-dHC
average metric	Coherence				***	***	***				*		
	wPLI	**		*	*	***	**	**	#		*	*	#
	PLV				***	***	***	*			**		
	PPC				***	***	***	*			**		
	GC →				#		*	#			*	#	*
	GC ←		*	*	**	***	*	***			***		#
	PDC →		*			***			*			***	
	PDC ←			**	*	#	**						**
	MRL ←					**							
	MI/PAC →				*	**	*						
	MI/PAC ←				*	#	*						
	Coherence phase			#		#					*	***	#
	CC				***	*	*				*	***	
	MRL-phase ←				*								
	MRL-lag ←												
slope metric	Coherence	***	**	*	**	***	#	**				#	
	wPLI	#				**							
	GC →	**	*		**		*	*				**	
	GC ←		**	**		***	*						*
	MI/PAC →					**							
	MI/PAC ←					*	*						
	CC				*			#					*

3.1.4 Lack of redundancy between most coupling measures revealed by bivariate correlation analysis

Given that the above analysis of comparing genotype-related differences across measures ultimately allows only a *qualitative* judgement about the epistemological redundancy of interregional coupling metrics, we supplemented our analysis by a more quantitative analysis in form of bivariate Spearman correlations between pairs of parameters and within genotypes and connections using the average value for each parameter in each electrode pair as dependent variable. We included all metrics analysed in Figure 3.1.2 and Figure 3.1.3 and also DTF and npGC.

This revealed multiple levels of complexity when analysing the relation between the metrics. On the one hand, at the level of isolated observations, the correlations supported the commonalities between measures already seen with the two prior analyses. For example, PFC-dHC theta coherence correlated strongly with dHC→PFC theta-GC in WTs (Figure 3.1.5a). However, this correlation did neither exist in the *KOs* in the same connection (Figure 3.1.5a) nor in the same genotype but the PFC-*vHC* connection (Figure 3.1.5b). Indeed, PFC-vHC theta coherence, did correlate highly with GC in the opposite, i.e. PFC→vHC, direction but not in the vHC→PFC direction – and it did so across all frequency bands - which was not the case in the other two connections (Figure 3.1.5a-b, Figure 3.1.6a, also see Additional File 1, Tables S1 and S2 from [420] for the full correlation tables in WT mice including all metrics and four frequency bands, which is too large to be included in this thesis). In general, when carefully examining each pair of metrics, it became apparent that a correlation seen in one genotype and connection would rarely reappear in another one (Figure 3.1.5a-b, Figure 3.1.6a).

In order to evaluate this systematically, we calculated the *average* correlation coefficient for each pair *across the three connections* and indicated its significance only if it was present in all of them (Figure 3.1.6b). Reassuringly, the three pairs of mathematically closely related metrics showed consistent correlations in each connection and frequency band: PPC and PLV, parametric and non-parametric GC, and PDC and DTF. Beyond that, however, there was not a single pair of distinct metrics that achieved a significant correlation in all three connections in WT mice in the theta band, and only two (coherence correlating with PPC and PLV) in the gamma band (Figure 3.1.6b, also see Additional File 1: Table S4 from [420], which is too large to be included in this thesis). In *Gria1*-KOs, the picture was similar, except that here coherence correlated significantly with PLV and PPC in both the theta and the gamma band, and additionally gamma wPLI correlated with coherence, PPC, and PLV, across connections. The latter result contrasts sharply with the absence of such wPLI-correlations in WT mice, illustrating that some observed correlations may depend on the genotype, and are hence not reflecting *a priori* redundancies.

We further examined correlations that were not significant in all three connections, but yet achieved a high correlation coefficient on average. In the theta-range, *coherence* also correlated strongly with PPC and PLV (average rho ≥ 0.8) - in alignment with our first analysis (Figure 3.1.2, Figure 3.1.3), the correlation result in KOs, and the gamma-band in both genotypes (Figure 3.1.6b) - and with coherence phase angle (average rho > 0.7); further correlations yielded a medium (0.6-0.7) average rho: (a) *coherence phase angle* with PPC, PLV, PDC, DTF, GC, and npGC, and (b) *PPC/PLV* with wPLI, PDC, and DTF. In the *gamma* range, *coherence phase angle* also showed the largest number of medium average correlations with other measures, namely wPLI (average rho = 0.77) and coherence magnitude, PPC, PLV, PDC, DTF, GC and npGC (average rho 0.6-0.7); the only remaining medium average correlations (0.6-0.7) in the gamma range were wPLI with PDC and DTF (Figure 3.1.6b, also see Additional File 1: Table S4 from [420], which is too large to be included in this thesis). Also, in KOs, the *coherence phase angle* showed average medium correlations with most other LFP-based metrics in the theta and gamma range (Figure 3.1.6b). It should be noted that this combined analysis may overlook correlations with directed metrics in case they occur in only one direction. For example, theta GC (and npGC) did actually correlate with theta PDC (and DTF) in each of the three connections but only in one direction each: PFC→vHC, dHC→PFC and vHC→dHC which is difficult to interpret given that we always recorded significant GC and PDC in both directions. Results from the SPC (MRL), PAC, and amplitude cross-correlation (lag) analyses did not correlate with any other measure consistently in any genotype. This synopsis largely aligns with the redundancy patterns seen with the two former analyses (averages and slopes, Table 3.1.1).

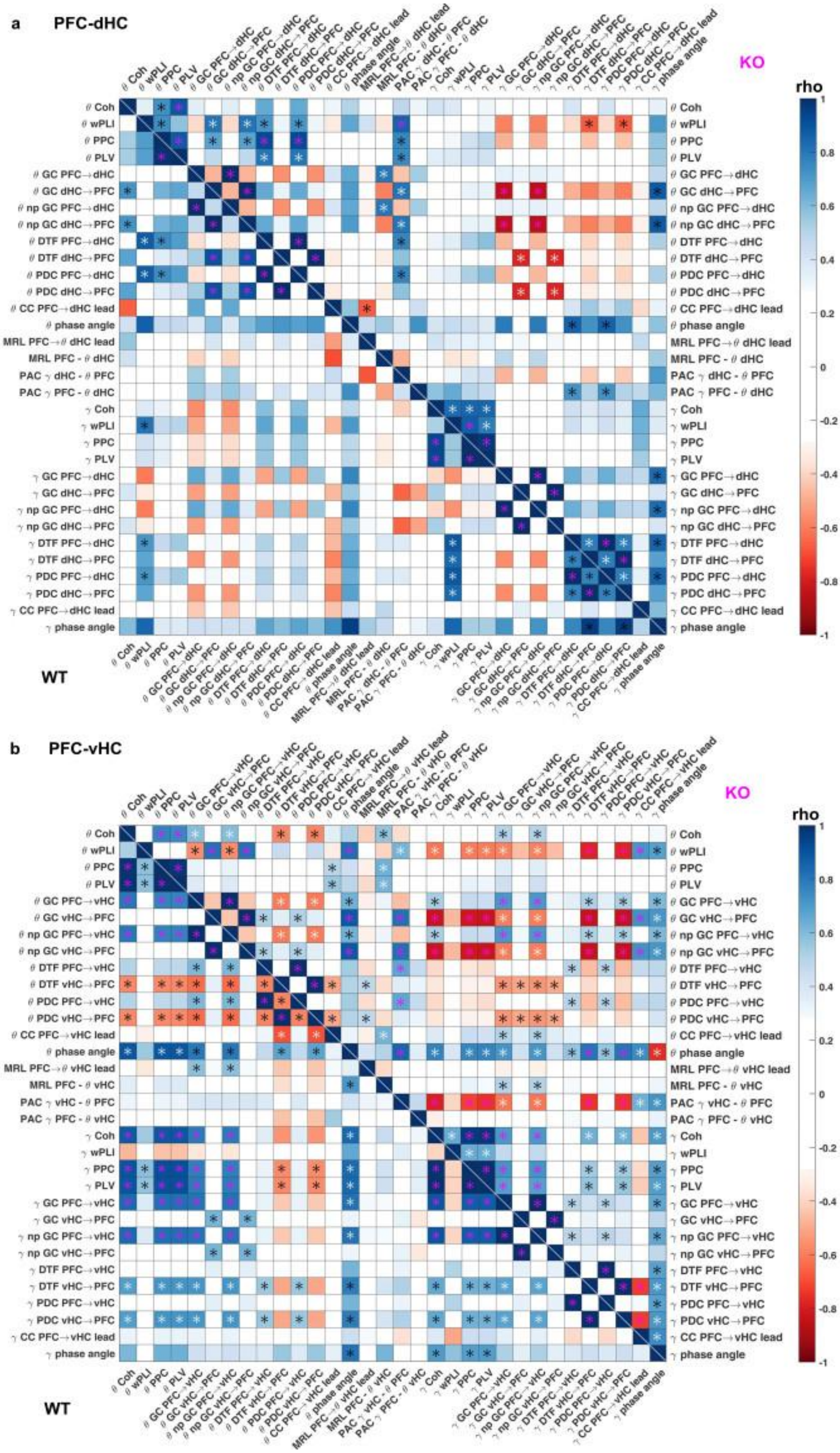
a
PFC-dHC
KO
WT
rho
1
0.8
0.6
0.4
0.2
0
-0.2
-0.4
-0.6
-0.8
-1
θ Coh
θ wPLI
θ PPC
θ PLV
θ GC PFC→dHC
θ GC dHC→PFC
θ np GC PFC→dHC
θ np GC dHC→PFC
θ DTF PFC→dHC
θ DTF dHC→PFC
θ PDC PFC→dHC
θ PDC dHC→PFC
θ CC PFC→dHC lead
θ phase angle
MRL PFC→θ dHC lead
MRL PFC - θ dHC
PAC γ dHC - θ PFC
PAC γ PFC - θ dHC
γ Coh
γ wPLI
γ PPC
γ PLV
γ GC PFC→dHC
γ GC dHC→PFC
γ np GC PFC→dHC
γ np GC dHC→PFC
γ DTF PFC→dHC
γ DTF dHC→PFC
γ PDC PFC→dHC
γ PDC dHC→PFC
γ CC PFC→dHC lead
γ phase angle
b
PFC-vHC
KO
WT
rho
1
0.8
0.6
0.4
0.2
0
-0.2
-0.4
-0.6
-0.8
-1
θ Coh
θ wPLI
θ PPC
θ PLV
θ GC PFC→vHC
θ GC vHC→PFC
θ np GC PFC→vHC
θ np GC vHC→PFC
θ DTF PFC→vHC
θ DTF vHC→PFC
θ PDC PFC→vHC
θ PDC vHC→PFC
θ CC PFC→vHC lead
θ phase angle
MRL PFC→θ vHC lead
MRL PFC - θ vHC
PAC γ vHC - θ PFC
PAC γ PFC - θ vHC
γ Coh
γ wPLI
γ PPC
γ PLV
γ GC PFC→vHC
γ GC vHC→PFC
γ np GC PFC→vHC
γ np GC vHC→PFC
γ DTF PFC→vHC
γ DTF vHC→PFC
γ PDC PFC→vHC
γ PDC vHC→PFC
γ CC PFC→vHC lead
γ phase angle

Figure 3.1.5: Correlations between individual measures of hippocampal-prefrontal connectivity
(**a, b**) Spearman's coefficient (rho, colour of squares) and significance (star within squares) of bivariate correlations between individual measures of connectivity in the PFC-dHC (a) and PFC-vHC (b) connections within KO (top-right) and WT (bottom-left) mice. White stars, $p < 0.01$; purple stars, $p < 0.001$. Theta- and gamma metrics are spatially separated, and delta and beta metrics are omitted. Adapted from [420], open access article: CC BY 4.0, https://creativecommons.org/licenses/by/4.0/

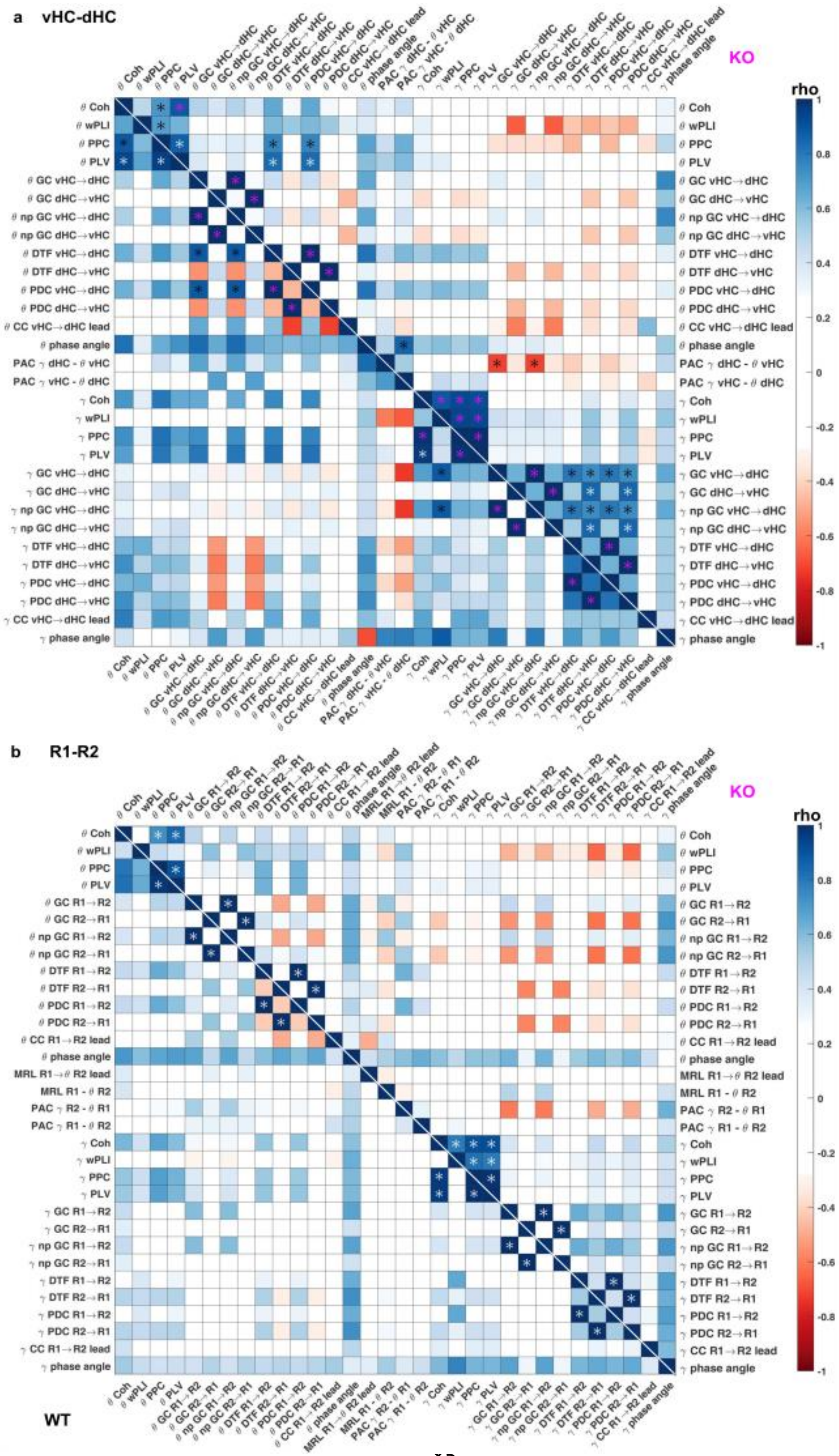
a vHC-dHC
KO
rho
1
0.8
0.6
0.4
0.2
0
-0.2
-0.4
-0.6
-0.8
-1
θ Coh
θ wPLI
θ PPC
θ PLV
θ GC vHC→dHC
θ GC dHC→vHC
θ np GC vHC→dHC
θ np GC dHC→vHC
θ DTF vHC→dHC
θ DTF dHC→vHC
θ PDC vHC→dHC
θ PDC dHC→vHC
θ CC vHC→dHC lead
θ phase angle
PAC γ dHC - θ vHC
PAC γ vHC - θ dHC
γ Coh
γ wPLI
γ PPC
γ PLV
γ GC vHC→dHC
γ GC dHC→vHC
γ np GC vHC→dHC
γ np GC dHC→vHC
γ DTF vHC→dHC
γ DTF dHC→vHC
γ PDC vHC→dHC
γ PDC dHC→vHC
γ CC vHC→dHC lead
γ phase angle
b R1-R2
KO
rho
1
0.8
0.6
0.4
0.2
0
-0.2
-0.4
-0.6
-0.8
-1
θ Coh
θ wPLI
θ PPC
θ PLV
θ GC R1→R2
θ GC R2→R1
θ np GC R1→R2
θ np GC R2→R1
θ DTF R1→R2
θ DTF R2→R1
θ PDC R1→R2
θ PDC R2→R1
θ CC R1→R2 lead
θ phase angle
MRL R1→θ R2 lead
MRL R1 - θ R2
PAC γ R2 - θ R1
PAC γ R1 - θ R2
γ Coh
γ wPLI
γ PPC
γ PLV
γ GC R1→R2
γ GC R2→R1
γ np GC R1→R2
γ np GC R2→R1
γ DTF R1→R2
γ DTF R2→R1
γ PDC R1→R2
γ PDC R2→R1
γ CC R1→R2 lead
γ phase angle
WT

Figure 3.1.6: Correlations between individual measures of intra-hippocampal and overall connectivity
(**a**) Spearman's coefficient (rho, colour of squares) and significance (star within squares) of bivariate correlations between individual measures of connectivity in the vHC-dHC connection within KO (top-right) and WT (bottom-left) mice. (**b**) Same display as in (a) but indicating the *average* correlation coefficient across the three connections (Figure 3.1.5a-b, Figure 3.1.6a) by the colour of a square and significance only if a significant correlation existed in every one of the three connections. White stars, $p < 0.01$; purple stars, $p < 0.001$. Theta- and gamma metrics are spatially separated, and delta and beta metrics are omitted. Adapted from [420], open access article: CC BY 4.0, https://creativecommons.org/licenses/by/4.0/

3.1.5 No differences in electrode placements, but in reference location

Additionally, for WT animals, we sorted the LFP power and coherence values obtained from each electrode according to its in different subdivisions of the PFC (PrL, Cg1 and Cg2), dHC (apical dendritic layers of CA1, CA1 pyramidal cells, CA1 stratum oriens) and vHC (apical dendritic layers of CA1/CA3, CA1 pyramidal cells, DG). While we did not conduct statistical analysis given the much smaller number of sites outside the target region (PrL in PFC and apical dendritic layers, including fissure, in the hippocampus), a qualitative inspection suggested that the placements inferred from lesion sites did not noticeably alter the obtained spectral LFP properties (Figure 3.1.7).

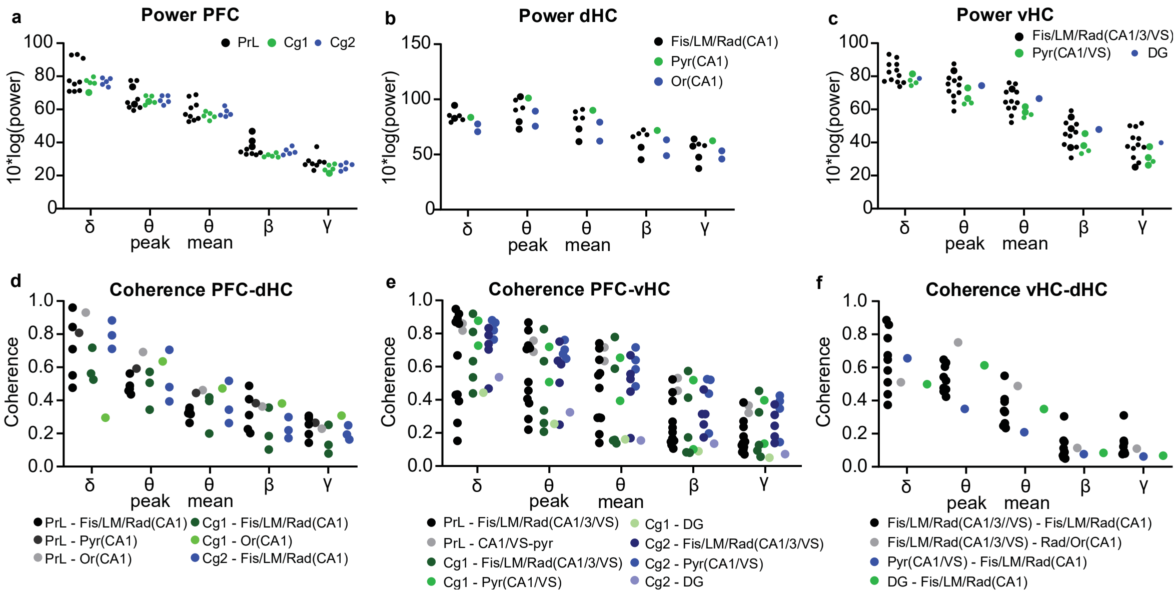

Figure 3.1.7: No qualitative differences in electrode placements
(a-c) Power of LFP in the indicated frequency bands (x-axis) and region (top of panel) displayed for each individual electrode that contributed to the WT-dataset colour-coded by the sub-division in which it was placed; hippocampal layers: pyramidal (Pyr), stratum oriens (Or), lacunosum-moleculare (LM), radiatum (Rad), fissure (Fis). **(d-f)** Coherence between all possible combinations of electrode pairs. No statistical analysis was done given some rare placements. Adapted from [420], open access article: CC BY 4.0, https://creativecommons.org/licenses/by/4.0/

The choice of placement site for the reference electrode varies considerably between studies, and both the referencing to the ground screw above the cerebellum (as done for all analyses in this work) and to the anterior part of the frontal cortex are widely used. In order to investigate the effect of this difference, we recorded a separate reference signal from a frontal reference screw [401, 434] and used it to digitally re-reference all recorded data by subtracting this signal from the recorded LFP traces before re-calculating local power, coherence, wPLI, and GC.

Using repeated-measures ANOVAs with the within-subject factor of re-referencing and the between-subject factor of genotype, we found that the location of the reference has quite a substantial influence on the results. In the lower frequency-ranges, there were significant effects of re-referencing on local power in the delta range in all brain regions (except for the MD) and in the theta range only in the dHC. For connectivity measures, there were also discrepancies between frequency bands: For delta, there were significant effects of re-referencing on coherence and GC in all connections, while the effect on wPLI was comparatively minor (but note that delta-wPLI is generally very low and entirely different from delta-coherence and GC; Figure 3.1.8a-m). In the theta-range, re-referencing strongly impacted coherence, wPLI, and GC alike along both hippocampal-prefrontal connections – not only in terms of significant effects of re-referencing, but also in terms of genotype-reference interactions, which indicate that the prior conclusions on theta-range connectivity are partly dependent on the position of the reference. In the GC measure, interactions were apparent in the d/vHC→PFC direction but not in the reverse (Figure 3.1.8k-l). Nevertheless, there were also significant effects of genotype in those connections and measures, suggesting that the fundamental observation of elevated hippocampal-prefrontal theta-connectivity in KOs still holds, especially for the PFC-dHC connection and the GC measure in general (Figure 3.1.8e-f, h-i, k-l). Intra-hippocampal theta-connectivity was not much affected by the reference placement, irrespective of measure (Figure 3.1.8g, j, m).

In the higher frequency-ranges the effects were more mixed. Beta power in the dHC and coherence – but only partly wPLI and GC – along its connections were affected by reference placement. In the gamma range, re-referencing impacted power in the PFC and dHC, wPLI in the PFC-d/vHC connections, and coherence along all three connections (Figure 3.1.8a-j). In fact, the formerly observed lower PFC-dHC gamma-coherence and wPLI in KOs (Figure 3.1.2d, j) was dependent on the reference placement for detection (interaction effect *only* for coherence and wPLI, Figure 3.1.8e, h). A similar observation holds for the PFC-vHC gamma connectivity, which was increased in KOs in the *wPLI*, but not the *coherence* measure (Figure 3.1.2e, k). Here again, an interaction indicated that the absence or presence of this difference in the coherence measure depends on the reference location (Figure 3.1.8f), while an effect of genotype is maintained when using wPLI even though an interaction is found in addition (Figure 3.1.8i). The impact of referencing on gamma-GC, in contrast, was limited to the dHC→PFC projection (Figure 3.1.8k-m).

In summary, a frontal reference electrode - as often used when studying prefrontal-hippocampal connectivity [401, 434] - may considerably alter the results obtained for LFP-based measurements of connectivity between the PFC and the hippocampus. Somewhat surprisingly, the wPLI measure does not eliminate this contingency but only reduces it, especially in the beta-gamma range. Referencing effects on GC are particularly visible in the low (delta/theta) frequency range and (as interactions) in the direction from hippocampus towards PFC.

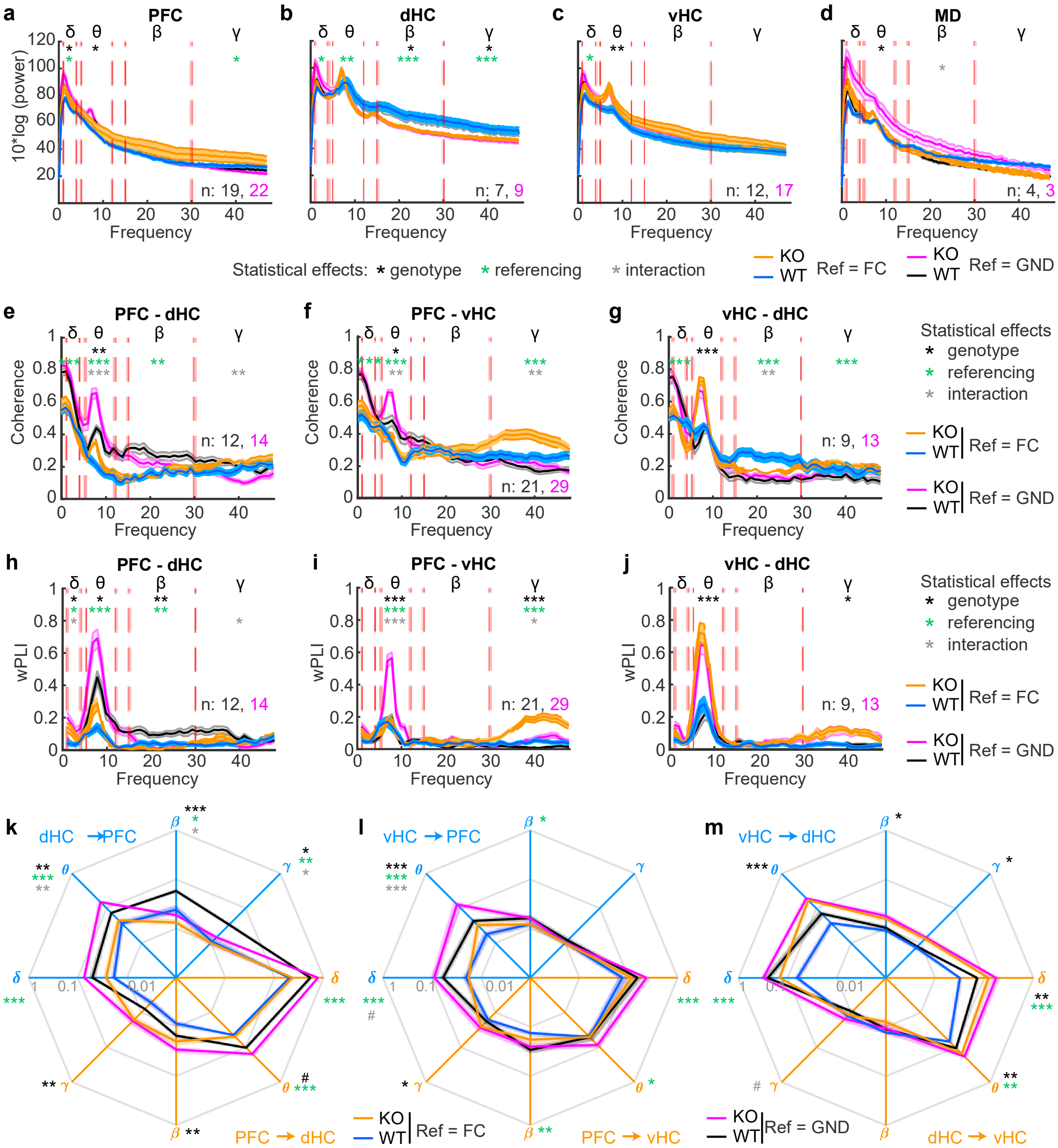

Figure 3.1.8: Assessment of the impact of the reference electrode placement on the measurement of power and connectivity

(**a-j**) Spectra for power (a-d), coherence (e-g) and wPLI (h-j) for the regions or connections indicated at the top of each panel, shown for standard referencing to the ground screw above the cerebellum (black, WT and purple, KO; as in Figure 3.1.2 and Figure 3.1.3) or digitally re-referencing to the reference screw above the frontal cortex (blue, WT and orange, KO). Red lines indicate the boundaries of the analysed frequency bands named by the Greek letters at the top. (**k-m**) GC in the frequency bands indicated by Greek letters and along the directed connections identified by the colour (blue: dHC→PFC (k), vHC→PFC (l), vHC→dHC (m); orange: reverse of the before; display as in Figure 3.1.3a-c). Throughout, shaded regions indicate SEM and stars indicate results of RM-ANOVA: black, effect of genotype; green, effect of chosen reference; grey, genotype-reference interaction. In the theta-range the statistics for coherence and wPLI refer to peak-theta. * $p < 0.05$; ** $p < 0.01$; *** $p \leq 0.001$. Adapted from [420], open access article: CC BY 4.0, https://creativecommons.org/licenses/by/4.0/

3.2 Highly task-specific and distributed neural connectivity in working memory in mice and humans

After identifying non-redundant measures of neural communication and the most suited reference location (3.1) we next aimed to apply those findings to recordings made in *Gria1* KO and WT mice and also in humans [225] to scrutinize the electrophysiological basis of WM. To this end, mice were tested in three WM tasks, and measures of neural communication at multiple time points during the tasks were calculated. We then established a ML-based approach and investigated the predictability of WM performance based on the calculated measures. We also extracted relevant electrophysiological features in order to compare different WM paradigms (3.2.1 - 3.2.6). A similar methodology was subsequently harnessed to analyse a publicly available dataset of humans performing various WM tasks [225] (3.2.7 - 3.2.8). We then turned to our *Gria1*$^{-/-}$ mice to translate our methodology to a mouse model of schizophrenia in order to identify potentially disease-related alterations (3.3).

3.2.1 Correct choices in DMTS working memory are associated with distinct signatures in connectivity

Mice were first trained across multiple training stages in an operant DMTS 5-choice SWM (5-CSWM) task before undergoing surgery for electrode implantation (Figure 3.2.1a-b). After recovery from surgery, neural activity was recorded during a 10 min open-field test. Results from this experiment and according analyses were presented in section 3.1 above and in [420] and guided the choice of metrics used for the subsequent analysis to include GC, PDC, coherence, theta-gamma PAC, and wPLI (i.e., largely mutually non-redundant metrics).

To evaluate associations between WM and electrophysiological measures of inter-regional connectivity, we first trained and tested mice implanted with chronic field electrodes in PFC, MD, vHC, and dHC in three SWM tasks (Figure 3.2.1a-f): First, the operant DMTS 5-choice SWM (5-CSWM) task in which mice were trained before implantation, subsequently the T-maze rewarded alternation task, and finally an operant DNMTS 2-choice SWM (2-CSWM) task. To allow for simultaneous LFP recordings during operant tasks, a recently developed custom-designed operant box optimized for implanted and tethered animals (Figure 3.2.1c) that is tightly integrated with electrophysiological recordings via pyControl software and microcontroller modules was used [7]. The set of three tasks (Figure 3.2.1d-f) was chosen to retain comparability due to their shared visuo-spatial nature and distinct individual differences (i.e., operant DMTS vs. DNMTS; maze-based DNMTS vs. operant DNMTS). In addition, the T-maze task was included due to its wide usage (see e.g., Table 1.6.1). The 5-CSWM task was specifically designed to limit the usage of non-WM mediation strategies by the animal - due the large number of choice configurations, requirement to shuttle between opposite walls of the box, and delay-periods in total darkness, as described in detail in [437]. Also, both operant tasks provide tight control over the timing of behavioural events and deliver intrinsic control variables for WM-enabling psychological functions like attention, measured by SP accuracy, and motivational drive, measured by reward latency. In each task, we applied extensions of the delay between the SP and the CP across which the memorized information needed to be maintained in order to strongly engage WM capacity. As expected for WM assays [21], such delay challenges significantly decreased WM choice accuracy of the mice (Figure 3.2.1g-i).

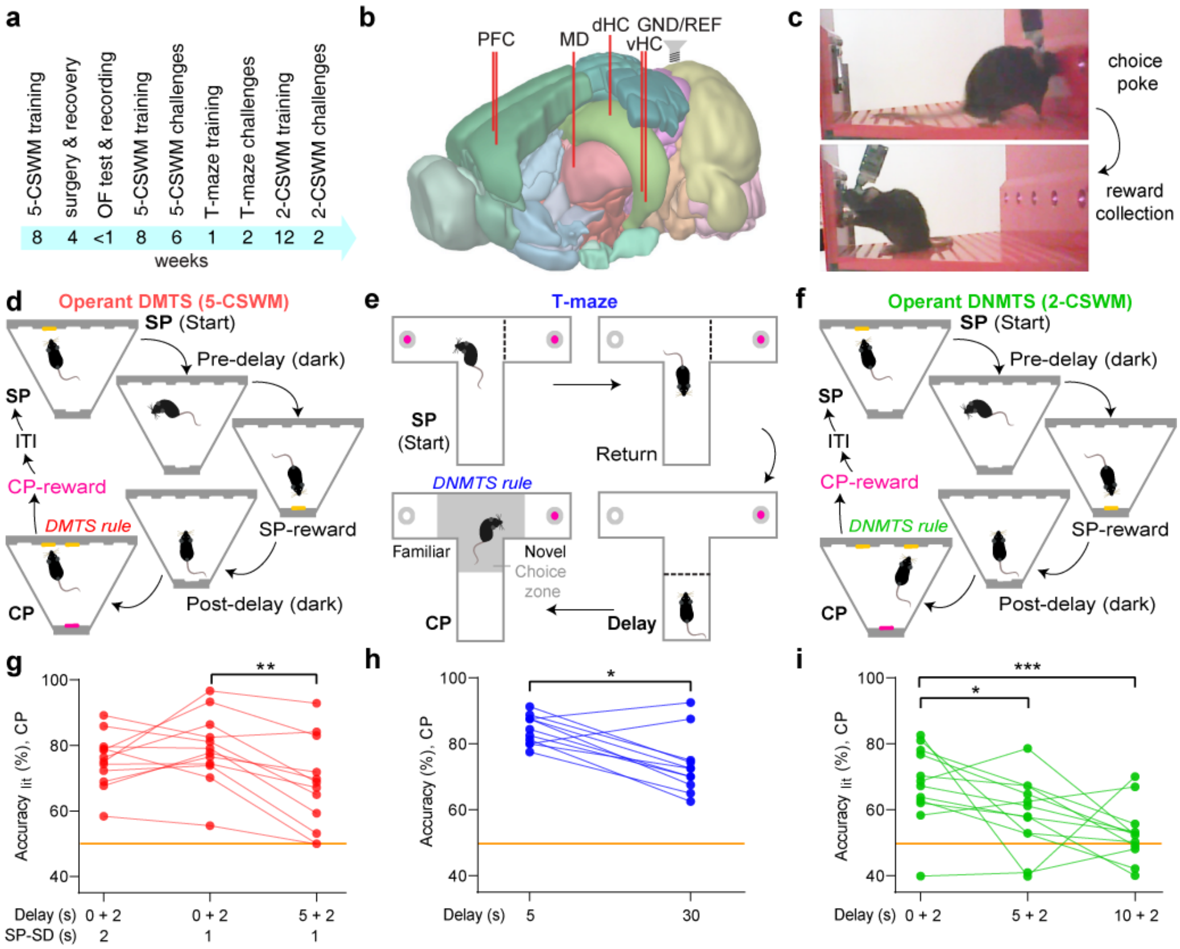

Figure 3.2.1: Behaviour in rodent WM

(**a**) Timeline of experiments in the analysed cohort (see Methods). (**b**) Illustration of electrode placements in in the mouse brain (image taken from the Allen Brain Atlas (http://connectivity.brain-map.org/static/brainexplorer)); pairs of electrodes were inserted into PFC and vHC. (**c**) Lack of obstruction of tethered mice with mounted head stage during poking of choice hole (top) and reward collection (bottom) in custom-made pyControl operant boxes. (**d-f**) Illustration of DMTS 5-CSWM [437] (d), T-maze rewarded alternation (e), and DNMTS 2-CSWM (f) tasks; in (d, f), choices in SP and CP need to be made at the 5-choice wall, while rewards for correct responses in each phase are collected on the opposite wall. (**g-i**) WM performance measured as response accuracy in the CP (% correct choices relative to available indicated options) in wildtype mice (N = 12) in each set of challenge conditions including their respective baseline with simultaneous electrophysiological recordings. Delay length determining the WM challenge stated on x-axes; for operant tasks (e, j) pre- + post-delay (referring to set delays before and after SP-reward collection) are indicated. SP-SD, stimulus duration in SP. Asterisks indicate differences between challenge, Sidak-post-hoc tests conducted after significant main effect of challenge, RM-ANOVA. Orange line, chance level performance. * $P < 0.05$; ** $P < 0.01$; *** $P \leq 0.001$. Training mice on the operant tasks and on the T-maze was supported by Sampath K.T. Kapanaiah. Adapted from [421], open access article: CC BY 4.0, https://creativecommons.org/licenses/by/4.0/

To elucidate possible correlates of WM among measures of neural connectivity, we computed time-resolved spectrograms of four largely non-redundant (see 3.1.4 and [420]) connectivity metrics aligned to the time of correct and incorrect CP and SP responses for the distinct phases of the 5-CSWM task (*non-directed*: coherence, Coh; wPLI; *directed*: GC; PDC; Suppl. Figure 1, Suppl. Figure 2). We subtracted spectra from *correct SP* responses or *incorrect CP* responses from those of *correct CP* responses to eliminate neural representations of poking action, execution of a reward-related response, or attention (Figure 3.2.2a-d, Suppl. Figure 3). In this qualitative analysis, we observed multiple changes associated with correct WM decisions including elevated hippocampal-prefrontal low gamma-range (30-48 Hz) activity immediately after the response (Figure 3.2.2a, b), and sustained theta-activity (5-12 Hz) during the delay in the PFC→MD and vHC→dHC connections (Figure 3.2.2c-d).

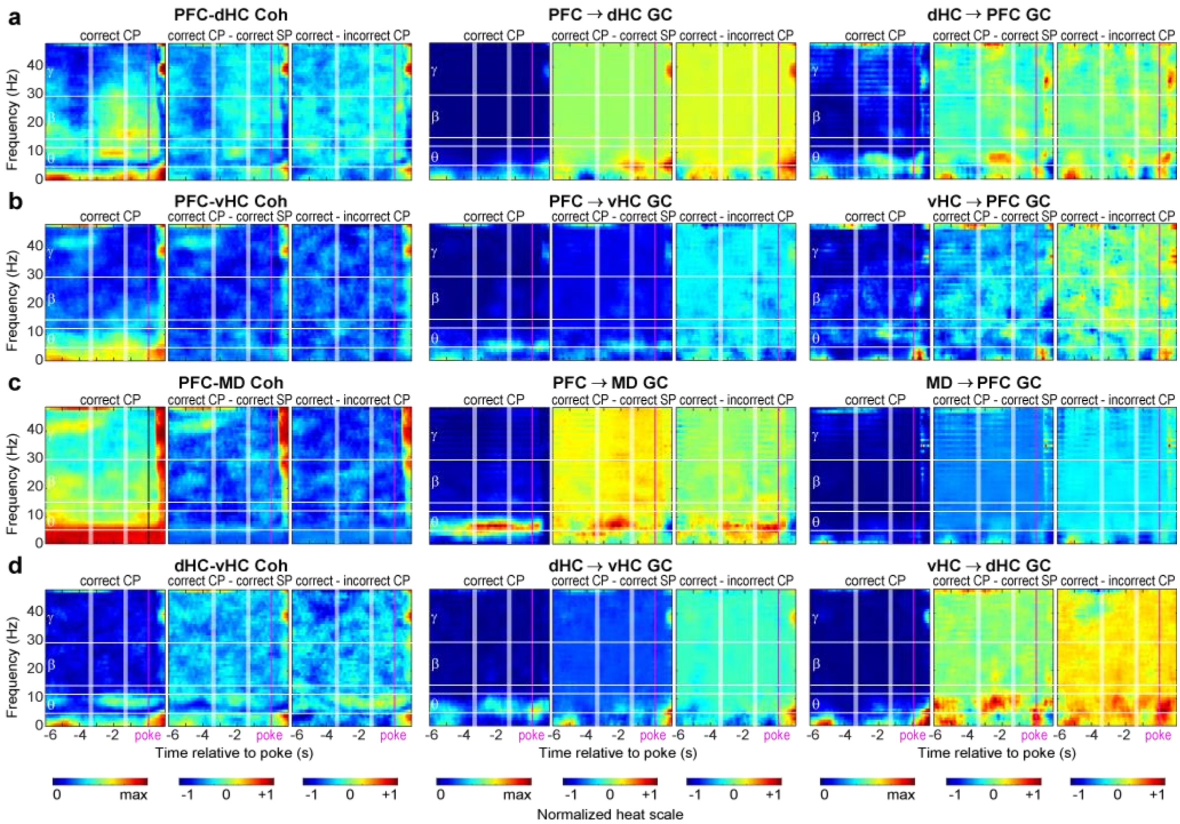

Figure 3.2.2: Connectivity in rodent WM during the 5-CSWM task
(**a-d**) Spectrograms depicting min-max normalized coherence and GC for the connections stated above each triplet panel for the delay and CP of the 5-CSWM task, temporally aligned to the choice poke entry (p, white vertical lines) showing 6 s before until 1 s after the poke; the start and end of the post-delay shown by white stripes corresponding to mean ± SD as determined by CP response latency. Each triplet shows the absolute value (left), the difference between the former and either the prior correct SP (middle), or incorrect CPs (right). Horizontal white lines show borders between analysed frequency bands, stated on the left. See Suppl. Figure 1 and Suppl. Figure 2 for spectrograms of absolute values in correct and incorrect trials of the CP and SP, respectively, and Suppl. Figure 3 for the same display as (a-d) for wPLI and PDC. Adapted from [421], open access article: CC BY 4.0, https://creativecommons.org/licenses/by/4.0/

3.2.2 Trial-by-trial prediction of WM-mediated choices from local and long-range neural activity

The ability to predict behavioural choices from neural activity may be regarded as proof that such activity encodes aspects of these choices [104, 410]. Even though individual LFP traces recorded on individual trials are unlikely to represent cleanly a certain behavioural state but instead are affected by various sources of noise and biological activity, we attempted to infer WM-based choice from metrics obtained from LFP traces to probe their predictive power using a ML approach. This data-driven approach is able to overcome the inherit hurdle of having too many data to analyse in a more classic, descriptive way as presented in Figure 3.2.2. Individual connectivity and activity variables were computed in four task phases (SP, pre-reward delay, post-reward delay, CP; see Figure 2.6.1), and four frequency bands (delta, 1-4 Hz, theta, 5-12 Hz, beta, 15-30 Hz, low-gamma, 30-48 Hz) along 4 connections (as shown in Figure 3.2.2a-d). In the same way, indicators of local activity (power and local PAC) were calculated in the four involved regions (dHC, vHC, PFC, MD). Additionally, all metrics were calculated in *relative* terms by dividing their obtained value by the value that specific metric had in the ITI before the start of the respective trial. This resulted in 240 variables for connections and 56 variables for local regions characterizing each 5-CSWM trial. Subspace discriminant classifiers – which proved superior among 25 different types of linear and non-linear classifiers (Figure 3.2.4) - were trained to predict WM-choice trial-by-trial using the parameters contributed by each connection or region separately for trials of the final 5-CSWM challenge (1 s SP-SD, 5 s delay; Figure 3.2.3a). Decoding models were generated across all subjects and trials and decoding accuracies were determined by predicting trials that were not part of the training dataset. This procedure was repeated separately 100 times to ensure that all trials were used as training and test data – but obviously not both in the same iteration – resulting in solid cross-validated prediction scores (see Figure 2.6.1 for graphical illustration of the ML analysis pipeline).

We found that individual DMTS 5-CSWM choices could be predicted with 79.4% and 79.8% average accuracy when using measures of neural connectivity along the PFC-MD or the PFC-dHC connection as predictors, respectively (Figure 3.2.3a). Using one-way ANOVA and pairwise Tukey post-hoc tests, we established a hierarchy between connections and regions revealing that the prediction accuracies obtained from PFC-MD, PFC-dHC, local dHC and MD activity did not differ from each other and were superior to the remainder (Figure 3.2.3a). Even though decoding accuracies varied by connection and region, they were always significantly better than those of control classifiers trained with shuffled labels ($P < 10^{-17}$, *t*-tests) which, in turn, decoded indistinguishably from chance level on average (Figure 3.2.3a). These data reveal that WM-based choice is encoded in LFP-based connectivity and activity measures in individual trials and that such information is widely distributed across multiple brain regions.

To evaluate the generality of the obtained classifiers, we assessed if they could also decode WM-based choices in data from other DMTS 5-CSWM challenge protocols. For this, we used data from one task protocol as training data and data from another protocol as test data to evaluate the predictive capabilities of the classifier. Even though prediction accuracies were generally lower compared to those achieved with data from the same protocol, they were still significantly higher than those of classifiers trained with shuffled labels (Figure 3.2.5). Note that for cross-paradigm prediction only task phases that were present in both paradigms were included (i.e., pre-delay was excluded in paradigms without extended delay).

To investigate if this conclusion applies generally to rodent WM, we repeated the same analysis for the operant DNMTS-data (final baseline sessions, 2 s delay). In this case, however, we obtained the maximum average prediction accuracy (86.1 %) from local dHC activity, rather than PFC-MD (66.1%, lowest rank of all classifiers) or PFC-dHC (73.5%) connections. Generally, in this task, local activities allowed relatively high decoding accuracies (72-77 % for PFC, MD, and vHC), while coupling metrics were significantly less predictive (66-68%, $P < 0.001$, Tukey; except for dHC-PFC, Figure 3.2.3a).

In reverse, trial-by-trial decoding of T-maze data achieved the highest average accuracies (82-88 %) when using connectivity data from either one of the four connections (with dHC-connections being most predictive), whereas local activities were significantly less predictive (62-79%; $P < 0.001$, Tukey, Figure 3.2.3b). However, decoding accuracies for information from all 4 connections decreased when analysing data from the 30 s delay challenge, in which these animals also showed lower behavioural performance (Figure 3.2.1h, Figure 3.2.3b), suggesting that not only task type but also task difficulty affect the information encoded in each connection.

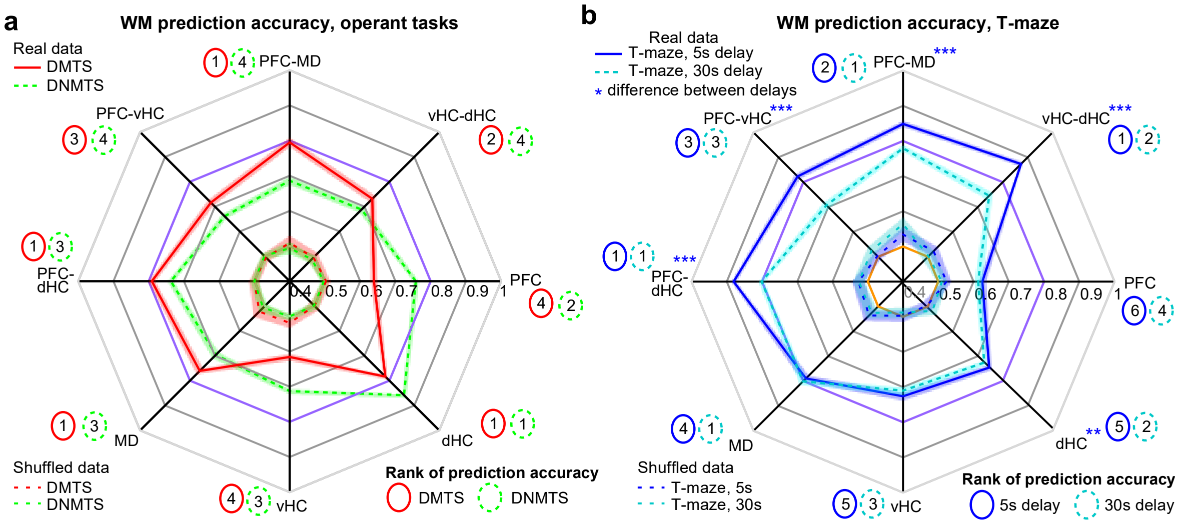

Figure 3.2.3: Trial-by-trial decoding of WM-based choice
(**a-b**) Cross-subject decoding accuracies achieved on average when using connectivity or local activity parameters of the indicated individual connections (black) or areas (grey), respectively to predict WM-based *correct* vs. *incorrect* choices in the DMTS 5-CSWM task (combined 1 s SP-SD, 5+2 s delay challenge, 2 sessions; red, a), the DNMTS 2-CSWM task (baseline, 2 sessions, green, a), the T-maze WM task with either 5s (solid blue, 4 sessions, b) or 30s (dashed blue, 4 sessions, b). Thinner dotted lines show decoding accuracies of corresponding classifiers trained with shuffled labels, remaining at chance level (0.5, orange). Classifiers trained with real labels perform better than those trained with shuffled labels in all cases ($P < 10^{-17}$, *t*-tests, not indicated). The accuracy of 0.8 is coloured in purple to aid comparison. Numbers in coloured ovals indicate the rank of the prediction accuracies achieved on average by using data from the respective connection or region. See Suppl. Table 2, Suppl. Table 3 and Suppl. Table 4 for confirmation of classifier quality by evaluation of various measures of decoding performance. Ranks have been generated from pairwise comparisons with Tukey post-doc tests conducted after significant effects of connection/region in one-way ANOVAs ($P < 0.0001$ in all cases); connections/regions that were not significantly different from each other were assigned the same rank. Blue stars in (b) indicate pairwise differences between the two delays (uncorrected *t*-tests). ** $P < 0.01$; *** $P \leq 0.001$. Shaded regions around mean show s.e.m. across 100 classifiers generated for each task and connection or region. Adapted from [421], open access article: CC BY 4.0, https://creativecommons.org/licenses/by/4.0/

To check for imbalances in the classifier performance, e.g., if only one class is driving the high prediction accuracy, we also analysed measures like the AUC of the ROC, the F1-score and sensitivity and specificity (for description see 2.6). For all three WM paradigms, high percentages were evenly distributed across all measures, indicating that the classifiers fitted the data well without any imbalances (Suppl. Table 2, Suppl. Table 3 and Suppl. Table 4).

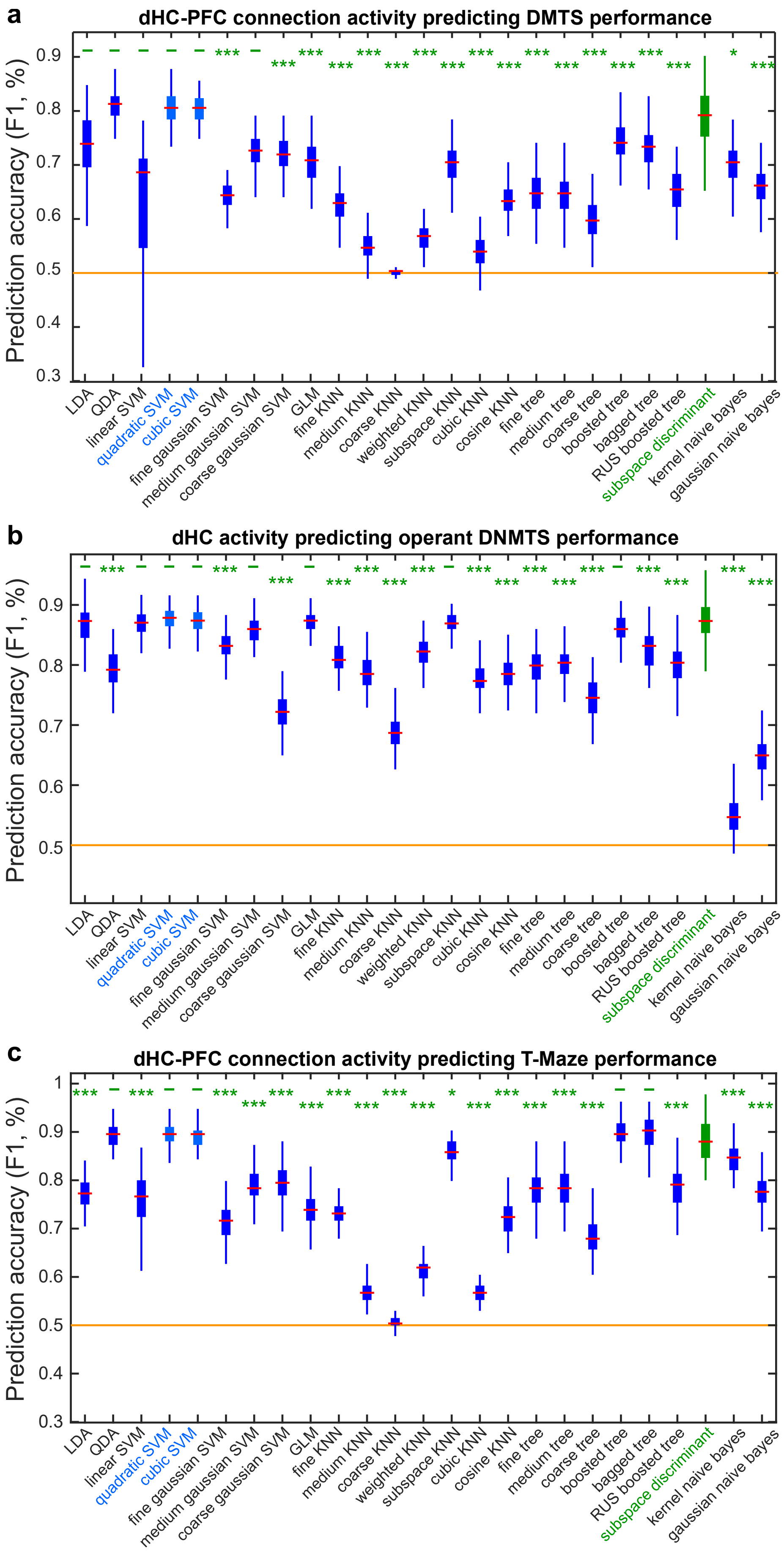
a
dHC-PFC connection activity predicting DMTS performance
Prediction accuracy (F1, %)
0.3
0.4
0.5
0.6
0.7
0.8
0.9
LDA
QDA
linear SVM
quadratic SVM
cubic SVM
fine gaussian SVM
medium gaussian SVM
coarse gaussian SVM
GLM
fine KNN
medium KNN
coarse KNN
weighted KNN
subspace KNN
cubic KNN
cosine KNN
fine tree
medium tree
coarse tree
boosted tree
bagged tree
RUS boosted tree
subspace discriminant
kernel naive bayes
gaussian naive bayes
b
dHC activity predicting operant DNMTS performance
Prediction accuracy (F1, %)
0.5
0.6
0.7
0.8
0.9
LDA
QDA
linear SVM
quadratic SVM
cubic SVM
fine gaussian SVM
medium gaussian SVM
coarse gaussian SVM
GLM
fine KNN
medium KNN
coarse KNN
weighted KNN
subspace KNN
cubic KNN
cosine KNN
fine tree
medium tree
coarse tree
boosted tree
bagged tree
RUS boosted tree
subspace discriminant
kernel naive bayes
gaussian naive bayes
c
dHC-PFC connection activity predicting T-Maze performance
Prediction accuracy (F1, %)
0.3
0.4
0.5
0.6
0.7
0.8
0.9
1
LDA
QDA
linear SVM
quadratic SVM
cubic SVM
fine gaussian SVM
medium gaussian SVM
coarse gaussian SVM
GLM
fine KNN
medium KNN
coarse KNN
weighted KNN
subspace KNN
cubic KNN
cosine KNN
fine tree
medium tree
coarse tree
boosted tree
bagged tree
RUS boosted tree
subspace discriminant
kernel naive bayes
gaussian naive bayes

Figure 3.2.4: Decoding performance of different types of classifiers
(**a-c**) Decoding accuracy displayed as the F1-score for the connections (**a, c**) or brain region activity (**b**) which yielded the highest predictive power in its respective task (see Figure 3.2.3), as named above each panel. The most commonly used classifiers implemented in MatLab were trained and tested with the same data, and prediction accuracies were compared. Yellow horizontal line depicts chance level. Red lines indicate mean, coloured boxes the 25th and 75th percentile and whiskers indicate data range across the 100 classifiers computed for each type and connection. The subspace discriminant analysis (green) was superior to all tested linear classifier types and therefore used for all analyses in this study. Only two of the tested non-linear classifier types, named in light blue font, yielded equivalent accuracies across all three comparisons (**a-c**), but non-linear classifiers do not allow to extract and compare predictor weights for individual metrics. Classifier performance was compared using pairwise Tukey post-hoc tests after a significant main effect of classifier type in a one-way ANOVA ($P < 0.0001$). Results of Tukey tests comparing each classifier type to the subspace discriminant type are indicated by green dashes ($P > 0.05$, n.s.) or stars, * $P < 0.05$, *** $P < 0.001$. Abbr.: QDA (Quadratic Discriminant Analysis), SVM (support vector machine), GLM (Generalized linear model), KNN (K-nearest neighbours), RUS (random under sampling). Adapted from [421], open access article: CC BY 4.0, https://creativecommons.org/licenses/by/4.0/

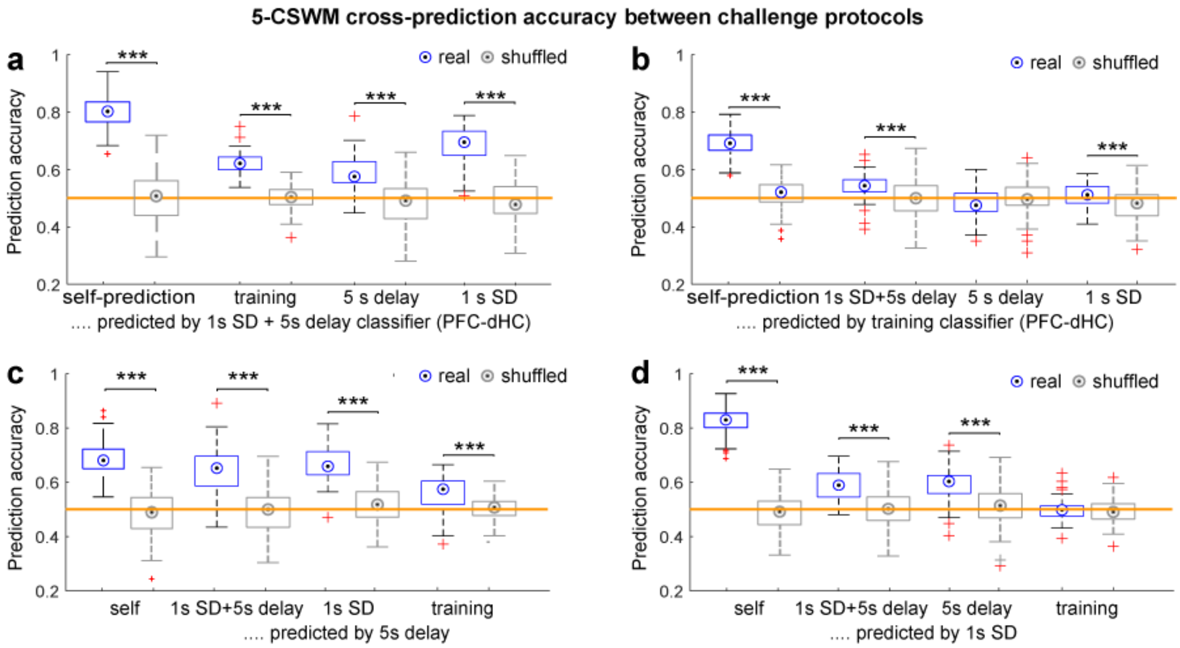

Figure 3.2.5: Cross-prediction accuracy for dHC-PFC classifiers trained on different challenges.
(**a-d**) Decoding accuracies achieved when using the classifiers trained on dHC-PFC connectivity data from the DMTS combined challenge (**a**), the training (**b**), the 5 s delay WM challenge (**c**), or the 1 s SP-SD attention challenge (**d**) on data from the other respective 5-CSWM protocols named on x-axes; blue and grey depicts performance of classifiers trained on trials with correct or incorrect (shuffled) labels (stars indicate *t*-test comparisons between them). Error bars, data range without identified outliers which are highlighted in red; boxes, range between 25th-75th percentile; dot, median. *** $P < 0.001$. Adapted from [421], open access article: CC BY 4.0, https://creativecommons.org/licenses/by/4.0/

3.2.3 Specific connections and regions are engaged differently in distinct phases of rodent WM tasks

The prior analyses entail at least two conclusions: Firstly, WM-related information in a single trial is not encoded in any single region or connection, although some of them bear higher predictive power regarding WM-choice than others. Secondly, the predictive power of a given region or connection is not uniform but strongly depends on the type of WM task and its difficulty, indicating that different mechanisms and regions are engaged to solve distinct behavioural demands. These conclusions re-emphasize the question as to what extent oscillatory processes in distinct frequency bands, of a distinct biological type, or in a specific task phase (encoding, delay, choice) can be regarded as correlates of WM (Table 1.6.1).

To answer this question, we took advantage of the fact that a linear classifier reveals the predictive power of each involved predictor variable according to its assigned weight. We performed Bonferroni-adjusted *t*-tests comparing the weights for each connectivity variable with the weights assigned by the classifiers trained on label-shuffled control data, and, additionally, conducted *t*-tests comparing the amplitudes of each variable between correct and incorrect trials that contributed to the classifiers. Variables for which both *t*-tests were significant were considered as bearing WM-related information (indicated by colour in Figure 3.2.6a). This analysis revealed a relatively small set of consistent WM-related feature-classes as correlates of DMTS 5-CSWM, a majority of them in the γ-range (Figure 3.2.6b): (*1*) PFC→MD δ- and γ-range connectivity in the *SP*, (*2*) MD→PFC β- and γ-range as well as dHC-vHC θ–range connectivity in the *delay*, (*3*) dHC→PFC and MD-PFC γ-range as well as vHC-PFC δ–θ-range coupling in the *CP,* and (*4*) intra-hippocampal δ-connectivity in *all phases* (Figure 3.2.6c-d).

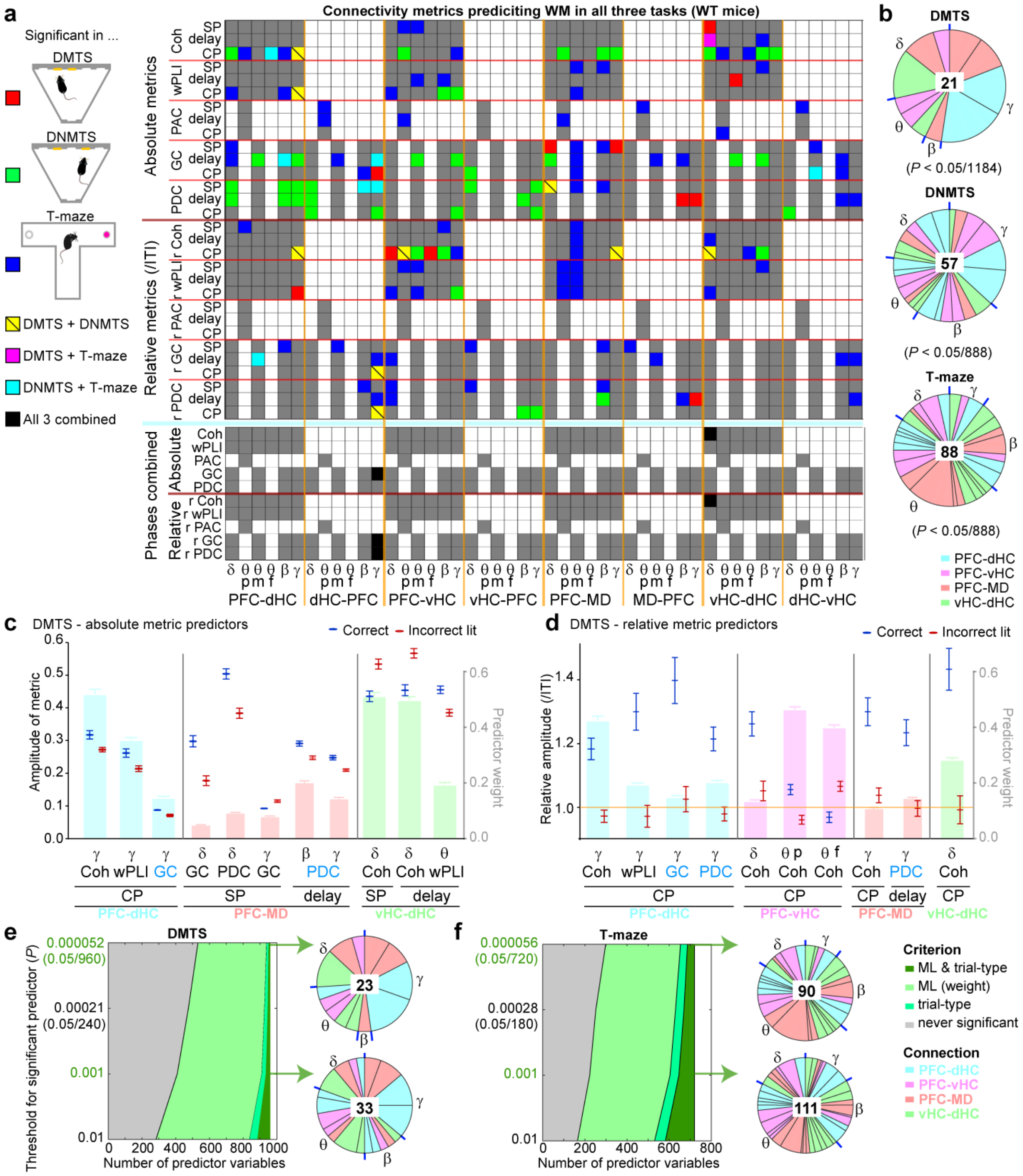

Figure 3.2.6: Individual connectivity measures predicting WM choice in wildtype mice.
(**a**) Matrix showing all connectivity predictor variables that contributed to the connection-based classifiers shown in Figure 3.2.3a,b. Variables that were significantly associated with WM-performance according to both their prediction weight and differences between correct and incorrect CP (*t*-tests, Bonferroni-adjusted for total number of variables, see (b) in any of the three WM tasks are indicated by the corresponding colour, remainder in grey (white squares have no corresponding variable). Variables from the pre- and post-delay in the 5-CSWM are combined in single lines. For theta, mean amplitude (m), peak amplitude (p) and frequency of peak (f) are shown, while for all other frequency bands only the mean amplitude is used due to the absence of a clear singular peak. At the bottom, all task phases are combined and only connectivity metrics that are predictive in all three tasks (in at least one phase) are indicated in black. (**b**) Share of each connection (coded by colour) and frequency band (stated around pie chart with separations in blue) among all significant predictors (*N* stated in centre) for the indicated task. (**c-d**) Values of absolute (c) or relative (d) predictor variables for DMTS WM (extracted from (a)) in correct (blue) and incorrect (red) trials (left axes). Bars in the background, referenced to by right axis, show absolute values of average predictor weights normalized within each classifier (i.e., connection) coded by their colour. Significance is not indicated as it

applies to all shown variables. Blue font, directed connectivity in the *opposite* direction compared to connection-name. Error bars, s.e.m. (**e, f**) Left: Number of variables identified as significant based on ML predictor weight (light green), difference between correct and incorrect trials (medium green), or both (dark green) in dependence on the *P*-value adjustment (y-axes) in the DNMTS (e) and T-maze (f) tasks. Right: Share of predictor variables as depicted in (b) for the *P*-levels indicated in green. Adapted from [421], open access article: CC BY 4.0, https://creativecommons.org/licenses/by/4.0/

Given the prominence and high predictor weights of *CP* parameters (Figure 3.2.6c, d) - which align with the arising γ-band connectivity immediately after the CP-poke (Figure 3.2.2a-d) - we wondered, if the predictability of WM-choice (Figure 3.2.3) actually relied mainly on identifying a representation of anticipated reward. Therefore, we replicated the decoding analysis for *SP* choices for which animals also expect reward. For the SP, however, average decoding accuracies were – although still above the 50% chance level - considerably smaller, namely 64-68 % and 54-59 % for predictions based on connectivity and local activity, respectively (Figure 3.2.7a).

While this result shows that the attentional element of the task is more difficult to predict from the available parameters than WM choice, it also demonstrates that the obtained *CP* prediction accuracy was not simply based on representations of motor-action (hole-poking), attention, or reward anticipation. We also repeated the decoding analysis for CP choice with complete omission of all CP parameters; even though decoding accuracies decreased significantly for some connections, including the most predictive ones (PFC-dHC, 72%; PFC-MD, 73.9%) - but not for vHC-dHC (72%) - overall accuracies remained far above those obtained from classifiers trained on shuffled labels, and hence above chance level ($P < 10^{-30}$ and $P < 0.002$ for classifiers trained on connectivity or local data, respectively; Figure 3.2.7b). Overall, these analyses demonstrate that activity along distinct connections and in distinct frequency bands represent encoding (SP), maintenance (delay), and recall (CP) of WM contents in the 5-CSWM task.

When omitting the CP predictors for decoding of correct choices on the T-maze, visual inspection of the overall distribution of accuracies revealed no major deviation from the original distribution (Figure 3.2.7c). Still, four regions or connections displayed significantly higher accuracies when including CP predictors, but not as pronounced as seen for the DMTS task (Figure 3.2.7b). Also, contrasting the DMTS findings, decoding accuracy for the PFC-MD connection was even higher when CP predictors were excluded (Figure 3.2.7c).

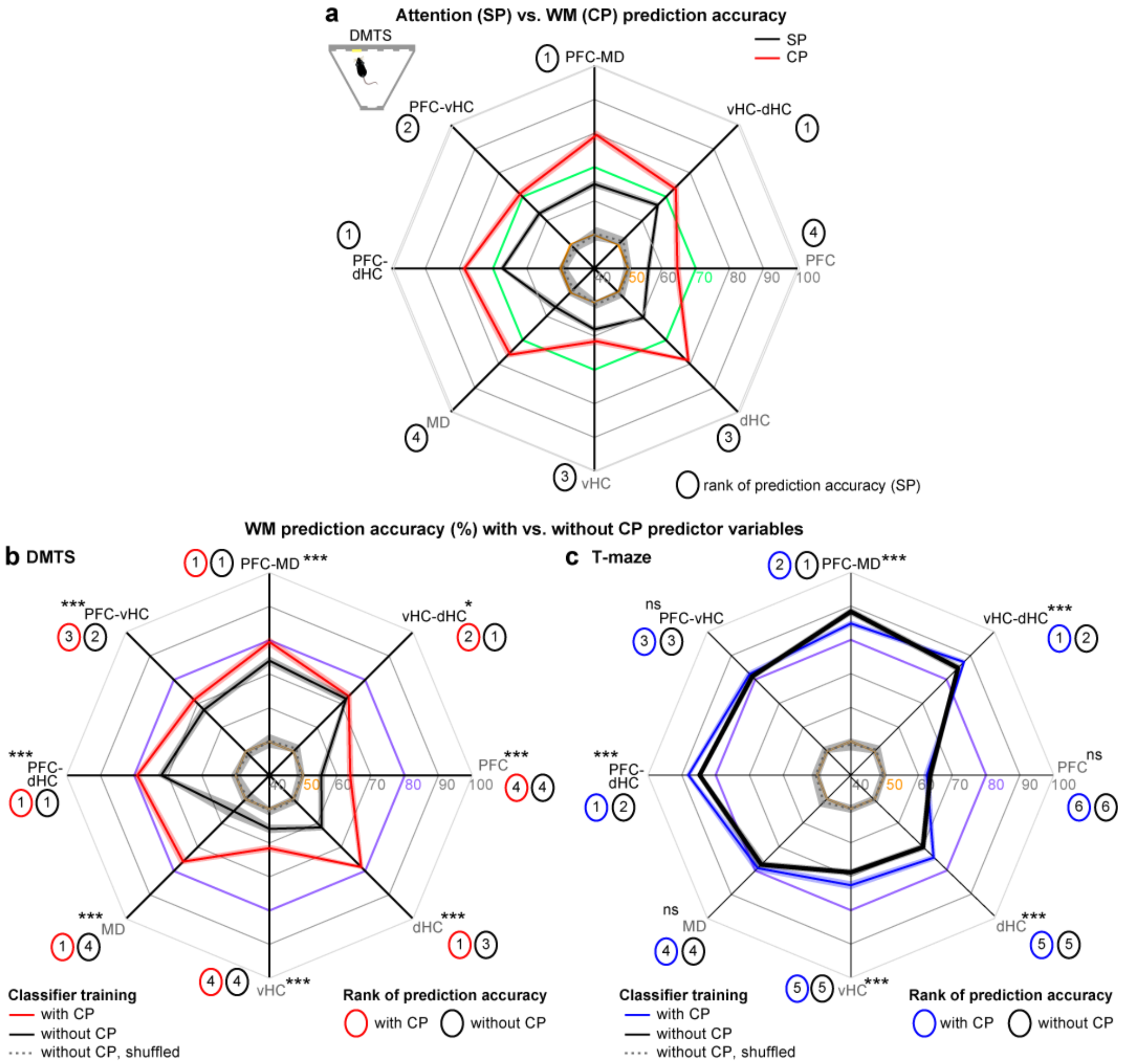

Figure 3.2.7: Prediction accuracies in the 5-CSWM SP and without CP predictors
(**a**) Cross-subject decoding accuracies for predicting of correct vs incorrect *SP*-choices (as a measure of sustained attention) from SP connectivity or local activity parameters of the indicated connections or areas in the 5-CSWM (black line; combined 1 s SP-SD, 5+2 s delay challenge, 2 sessions). A time window that ends 1 s after the SP-poke was used to retain equivalence to CP-based predictors contributing to WM-decoding accuracies in Figure 3.2.3a. The CP decoding accuracy (as in Figure 3.2.3a) is shown for comparison in red. (**b**) Same display as Figure 3.2.3a (5-CSWM DMTS data only, red) but showing equivalently determined WM decoding accuracies without including CP variables as predictors (black). Decoding accuracies were still significantly higher than what was achieved by classifiers trained on control datasets with shuffled labels (grey, $P < 10^{-30}$ and $P < 0.002$ for classifiers trained on connectivity or local data, respectively; *t*-test for each connection, not indicated), but are also lower than the accuracies obtained if CP variables are included (red) for all connections and regions (uncorrected *t*-test, indicated by black asterisks). Except for accuracies for MD-derived predictors, the rank order of decoding accuracies across connections/regions remained similar, however. (**c**) Same analysis as in (b) but for the T-maze (5 s delay protocol) and hence in relation to main Figure 3.2.3b. Note that, for several connections/regions, prediction accuracies remained roughly equal if CP predictor variables are omitted (black; uncorrected *t*-test, indicated by black asterisks). Also, decoding accuracies achieved without CP variables were significantly higher than those achieved with classifiers trained the same data but with shuffled labels in all cases (dotted line, $P < 10^{-40}$, *t*-tests, not indicated). Numbers in coloured ovals indicate the rank of the prediction accuracies achieved on average by using data from the respective connection or region. Ranks have been generated from pairwise comparisons with Tukey post-doc tests conducted after significant effects of connection/region in one-way ANOVAs ($P <$ 0.0001 in all cases); connections/regions that were not significantly different from each other were assigned

the same rank. ns, $P > 0.1$, * $P < 0.05$, ** $P < 0.01$, *** $P < 0.001$. Shaded regions represent s.e.m. Adapted from [421], open access article: CC BY 4.0, https://creativecommons.org/licenses/by/4.0/

3.2.4 WM-related functional connectivity is highly task-specific in mice

To uncover if such phase-specific connectivity generalizes across WM tasks, we performed the same analysis for the classifiers predicting performance in the operant DNMTS and the T-maze assays. In both cases, considerably more parameters carried WM-related information than in the 5-CSWM task (Figure 3.2.6a-b). Compared to DMTS WM, T-maze rewarded alternation choice was predicted by a much larger number of predictors, with a prominence of θ- and β-range (as opposed to γ-range) variables, and a considerable proportion of SP-parameters (Figure 3.2.6a-b).

Most astonishingly, the combined analysis of all three tasks revealed that *none* of the specific connectivity parameters identified in *one* task bore significant predictive power in both of the other tasks, revealing a remarkable task-specificity of such parameters (Figure 3.2.6a). It is possible that this finding is simply caused by a very conservative Bonferroni-adjustment of the *P*-value used as significance threshold (0.05/number of *all* connectivity and activity variables combined; 0.05/1184 for the 5-CSWM, 0.05/888 for the T-maze and 2-CSWM). Therefore, we repeated the above analysis while relaxing this adjustment incrementally over four orders of magnitude (Figure 3.2.6e-f). However, the number of identified significant parameters, the relative contribution of individual frequency bands, and especially the extreme sparseness of overlap between task-specific predictors changed relatively little (Figure 3.2.6e-f, Figure 3.2.8). This analysis also revealed that far more connectivity parameters are identified according to their prediction weight than according to their amplitude difference between correct and incorrect trials (Figure 3.2.6e-f). This suggests that the classical approach of correlating behavioural performance with amplitude of a given metric (Table 1.6.1) likely misses a sizeable proportion of WM-related functional connectivity.

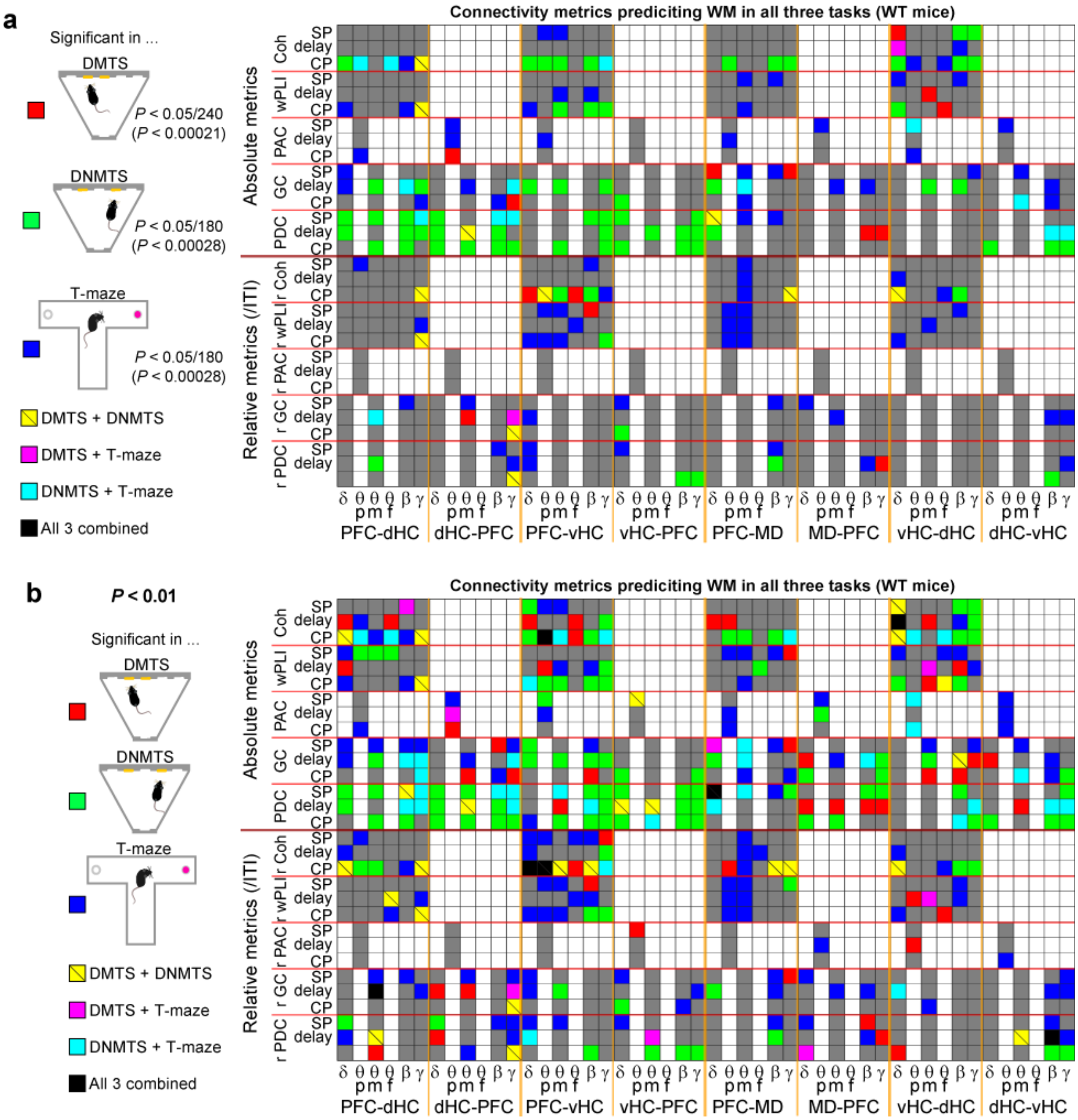

Figure 3.2.8: P-value adjustment of individual connectivity measures predicting WM choice across rodent tasks.

(**a-b**) Same display as in Figure 3.2.6a but for higher (less conservative) *P*-value thresholds: (**a**) Bonferroni-adjustment using the number of parameters per connection (240 for 5-CSWM DMTS, 180 for the other two tasks). (**b**) Use of 0.01 as a fixed threshold. Matrix showing all connectivity predictor variables that contributed to the connection-based classifiers shown in Figure 3.2.3a-b for the three rodent WM tasks (WT only) and were significantly associated with WM-performance according to their weight and differences between correct and incorrect CP. Note that variables from the pre- and post-delay in the 5-CSWM have been combined in single lines. Adapted from [421], open access article: CC BY 4.0, https://creativecommons.org/licenses/by/4.0/

To investigate potential differences or similarities between the time-course of individual parameters during the task, we extracted those spectral connectivity parameters that were predictive across all three assays albeit in different phases: directed dHC→PFC γ-connectivity and intra-hippocampal δ-range coupling (Figure 3.2.6a). Inspection of the time-course of these parameters over the delay and CP revealed that they behaved rather differently in the individual tasks: dHC→PFC γ-connectivity showed a transient increase during the delay of all three tasks, but only in the operant tasks a second increase occurred immediately after correct choices (but not after incorrect choices; Figure 3.2.9a-b). Intra-hippocampal δ-coupling even showed a different time course in every task, including a correct choice-specific decrease in the 2-CSWM delay which contrasted sharply with a steady rise during the T-maze delay (Figure 3.2.9a-b). Thus, even within the few predictor variables that are relevant across all tasks, the actual physiological activity relating to the behaviour differed markedly.

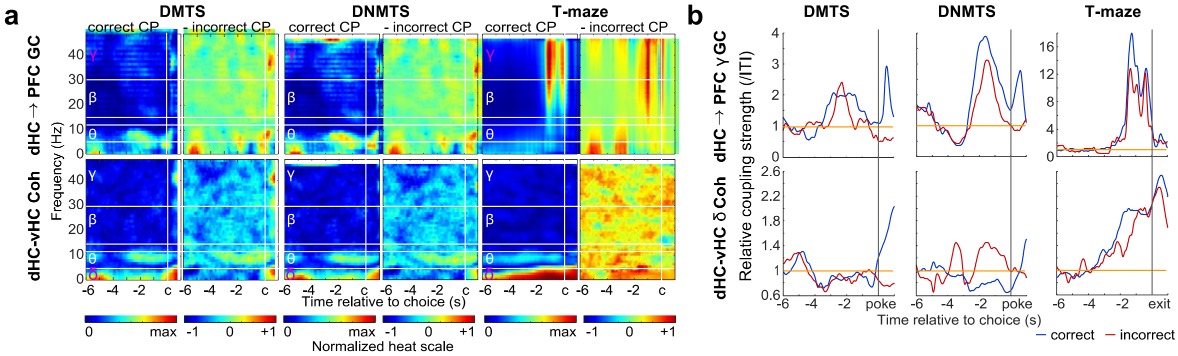

Figure 3.2.9: Time-frequency resolved connectivity measures predicting WM choice in all tasks in wildtype mice.
(**a**) Spectrograms for metrics (stated on the left) that were predictive in all three tasks (albeit in different phases; named at the top) are shown as absolute values and as difference between correct and incorrect CP responses, -6s until +1s around the choice; relevant frequency bands are gamma (top) and delta (bottom). (**b**) Average temporal evolution of those metrics in units of their value during the preceding ITI aligned to the choice point in each task (vertical grey line, poke or exit from decision zone) during correct (blue) and incorrect (red) trials. Adapted from [421], open access article: CC BY 4.0, https://creativecommons.org/licenses/by/4.0/

Given these results, we directly tested the hypothesis that distinct activity patterns underlie the different rodent WM tasks by rendering *task-type* a dependent variable: we trained classifiers to decode which one of the three tasks a subject is currently conducting using connectivity or local activity parameters from correct trials as input. Based on connectivity data, task-type could be decoded with average accuracies of 97-99% when discriminating between the two operant tasks (50% chance level) and with an accuracy >90-95% when discriminating between all three tasks simultaneously (33.3% chance level; Figure 3.2.10), underlining the high separability of these task paradigms.

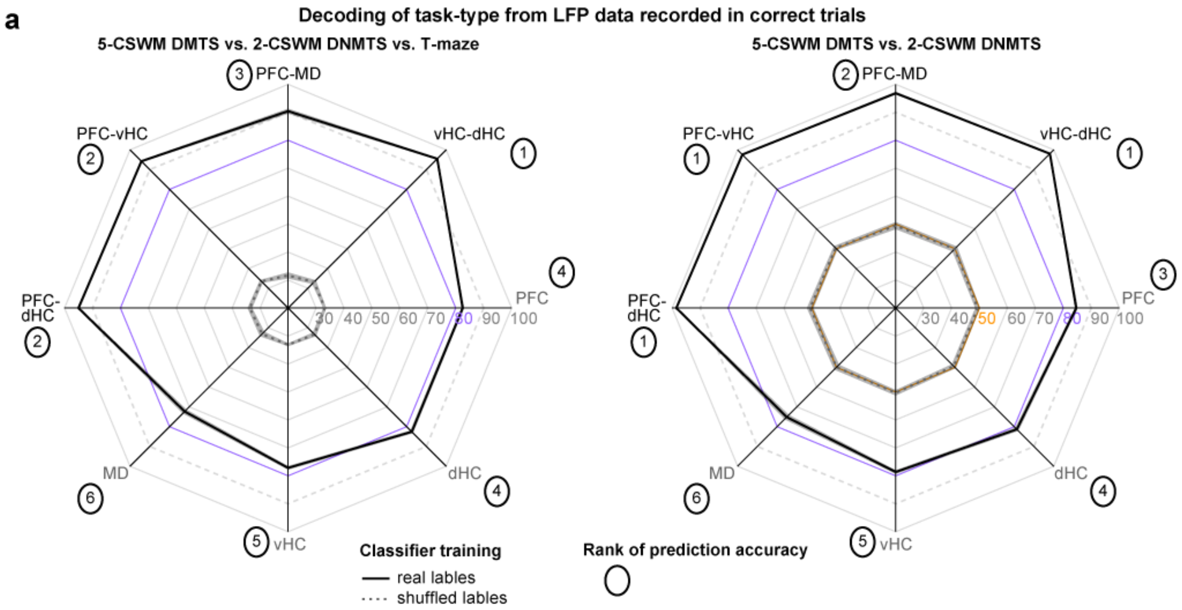

Figure 3.2.10: Prediction of task-type from connectivity and activity data recorded in correct trials.

(**a**) Cross-subject decoding accuracies for predicting the task during which the data was recorded using the connectivity or local activity predictor variables as in the other classifiers (main Figure 3.2.3a-b) albeit only from trials with correct choices. Either all three tasks had to be discriminated from each other (left) or only the two operant tasks (right), resulting in chance levels of 33.3% and 50% respectively. Lines for accuracy levels of 80% and 90% are emphasized by purple colour or dashed appearance, respectively, to aid comparison. Decoding accuracies were significantly higher than what was achieved by classifiers trained on control datasets with shuffled labels (dashed grey lines at chance level, P <0.0001; t-test for each connection, not indicated). Numbers in coloured ovals indicate the rank of the prediction accuracies achieved on average by using data from the respective connection or region. Ranks have been generated from pairwise comparisons with Tukey post-doc tests conducted after significant effects of connection/region in one-way ANOVAs (P < 0.0001 in all cases); connections/regions that were not significantly different from each other were assigned the same rank. Shaded regions represent s.e.m. Adapted from [421], open access article: CC BY 4.0, https://creativecommons.org/licenses/by/4.0/

3.2.5 Common hippocampal-prefrontal WM-related activity during the delay and CP of all WM tasks

To extract commonalities of connectivity between the three tasks, we aggregated predictive non-directed (coherence, wPLI) and directed (GC, PDC) metrics (extracted from Figure 3.2.6a) and depicted their amplitude increases relative to the preceding ITI for each task phase (Figure 3.2.11a-c). For the T-maze (the only task for which prior reference data exists), this revealed several connectivity patterns associated before with rewarded alternation performance, including vHC-PFC [410] and dHC-PFC [295] coupling during encoding and MD→PFC beta-range activity during maintenance across the delay [56, 349]. Importantly, MD-PFC β-range delay activity was also seen in the other two WM tasks, although their directionality differed (MD→PFC in the DMTS task; PFC→MD in the DNMTS task; Figure 3.2.11a-c). Likewise, further task-independent connectivity patterns emerged in this analysis: prominent vHC-PFC and vHC-dHC coupling in the CP of all tasks (especially in the delta and theta range), as well as MD→PFC delta and PFC→dHC/vHC multi-frequency directed connectivity during the SP and delay, respectively, of the two DNMTS tasks (Figure 3.2.11a-c). At the same time, this analysis also confirmed that the vast majority of WM-related connectivity was task-specific, especially when comparing the 5-CSWM DMTS to the other two tasks (Figure 3.2.11a-c).

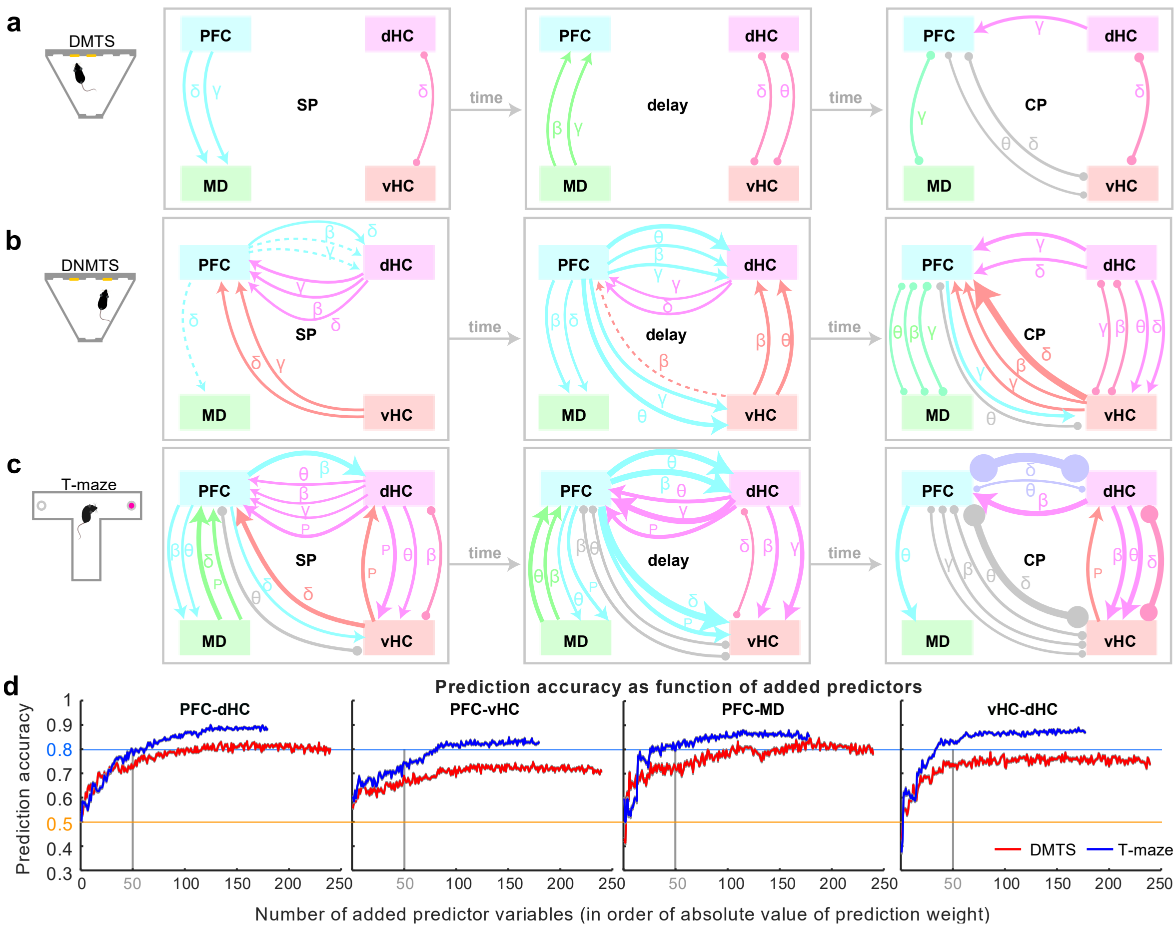

Figure 3.2.11: Connections in all tasks in wildtype mice
(**a-c**) Depictions of directed connectivity (arrows, derived from GC or PDC) or non-directed coupling (round-ended arcs, coherence or wPLI) during the three phases of each task identified on the left, derived from significant predictor variables shown in Figure 3.2.6a. Line weights indicate the increase of connectivity in the stated phase relative to the preceding ITI. Connectivity metrics for which only the absolute, but not the relative variable yielded significance are shown as dotted lines in (a, b), omitted in (c) for clarity, and their line thickness nevertheless represents relative increase. Measures that are significant but *decrease* in the respective phase relative to the ITI are omitted. (**d**) Average decoding accuracies obtained with classifiers calculated with a reduced number of predictor variables are shown as a function of the number of added predictors, whereby the addition was done in order of normalized prediction weight obtained with all variables (Figure 3.2.3a, b) for DMTS (red) and T-maze (blue) and the named connections. Chance level (50%) and 80% accuracy are indicated by coloured lines. Shaded area, s.e.m. Adapted from [421], open access article: CC BY 4.0, https://creativecommons.org/licenses/by/4.0/

An important aspect of this analytical approach is that none of these individually highlighted connectivity measures (Figure 3.2.6a, Figure 3.2.11a-c) is particularly predictive on its own: When performing decoding analysis with reduced sets of predictor variables – starting with the parameter with the single highest weight and adding variables incrementally – the inclusion of several dozen predictor variables was necessary to achieve maximum decoding accuracy (Figure 3.2.11d).

3.2.6 Predictive power of local activity in a single area varies by task phase and type

Local oscillatory activity in the four analysed regions also allowed considerable prediction accuracy in all three tasks - partly even exceeding that obtained from connectivity metrics (Figure 3.2.3a-b). Therefore, to reveal WM-related local activity metrics, we repeated the prior weight-based analysis for the respective variables (power, local PAC). In the 5-CSWM DMTS task – in line with connectivity predictors (Figure 3.2.6a) - only CP parameters, mostly in the β/γ-range, were significantly associated with WM (Figure 3.2.12a). For the two other tasks, in contrast, significant predictors came from all three phases and were somewhat less frequency-specific; the power of dHC-oscillations across all frequency bands and phases constituted the most prominent cluster of choice-predictors in both assays (Figure 3.2.12a). In agreement with the high decoding accuracy obtained with local activity (as opposed to connectivity) in the DNMTS 2-CSWM (Figure 3.2.3a), many more significant local predictor-variables were found for this task compared to the other two, irrespective of *P*-value threshold (Figure 3.2.12b). Importantly, however, there was again hardly any overlap between significant predictors from the three tasks. PFC and MD γ-power were identified as the only common variables when collapsing across task phases (Figure 3.2.12a) but displayed a different temporal evolution in each paradigm (Figure 3.2.12c). Also, while in DMTS WM all predictive activity parameters had *higher* amplitudes in correct trials compared to incorrect trials, this was not the case for the T-maze, where virtually all predictive hippocampal activity was *lower* in correct trials compared to incorrect trials – only PFC and MD power were higher in correct trials (Figure 3.2.12d, e). Hence, as observed in inter-regional connectivity, local activities related to WM-choice were highly task-specific in multiple respects.

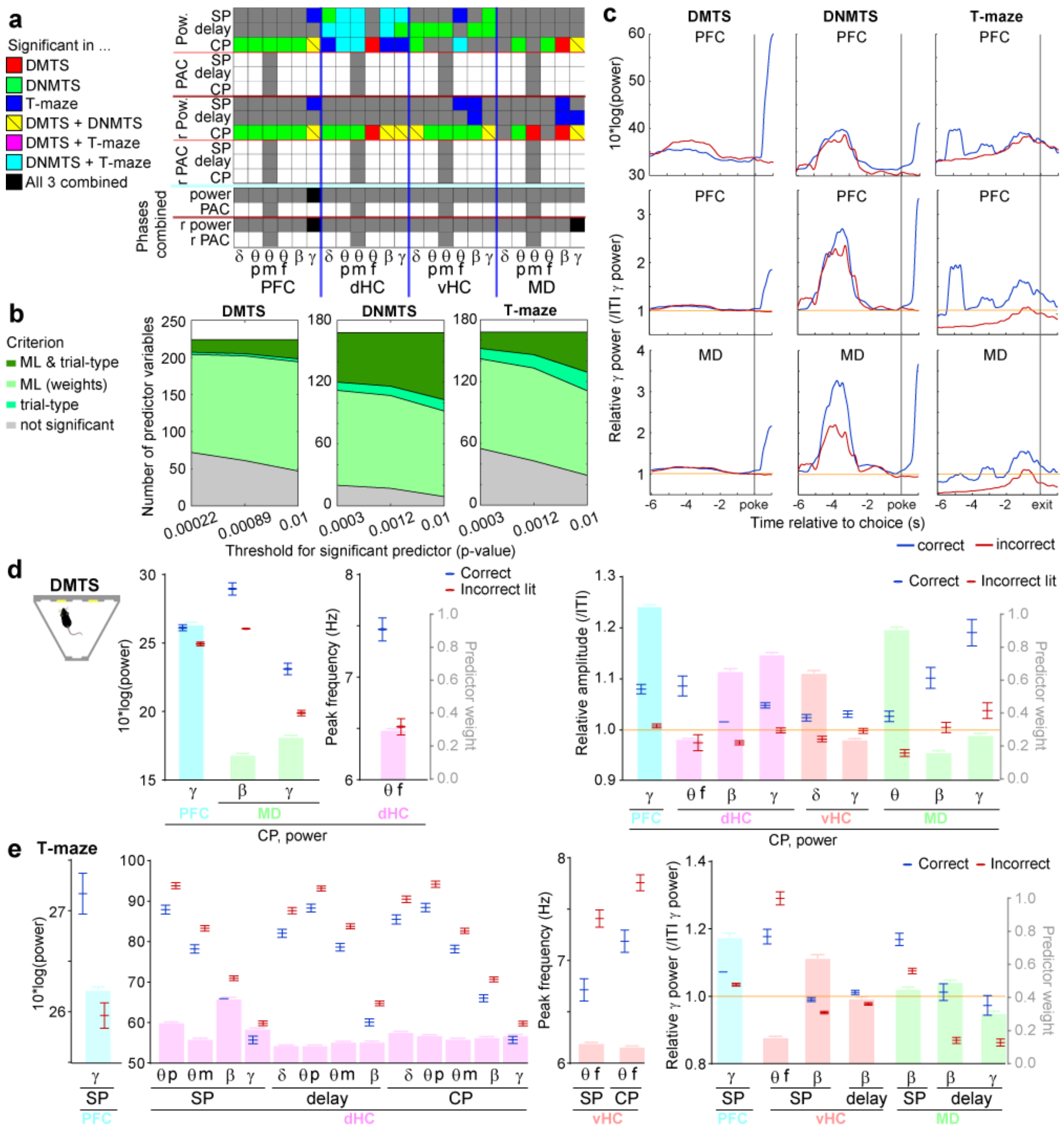

Figure 3.2.12: Local activity measures predicting WM choice in all tasks.
(**a**) Display and analysis as in Figure 3.2.6a, but for all local activity parameters that contributed to the classifiers shown in Figure 3.2.3a,b. Variables that were significantly associated with WM-performance according to both their prediction weight and differences between correct and incorrect CP (*t*-tests, Bonferroni-adjusted for total number of variables) in any of the three WM tasks are indicated by the corresponding colour, remainder in grey (white squares have no corresponding variable). At the bottom, all task phases are combined and only metrics that are predictive in all three tasks (in at least one phase) are indicated in black. (**b**) Number of variables identified as significant based on ML predictor weight (light green), difference between correct and incorrect trials (medium green), or both (dark green) in dependence on the *P*-value adjustment (x-axes) in the named tasks. (**c**) Average temporal metrics predictive in all three tasks absolute unite (top) or in units of their value during the preceding ITI (below) aligned to the choice point in each task (vertical grey line, poke or exit from decision zone) during correct (blue) and incorrect (red) trials. (**e-f**) Values of absolute (left) or relative (right) predictor variables for DMTS (e) or T-maze (f) WM (extracted from (a)) in correct (blue) and incorrect (red) trials (left axes). Bars in the background, referenced to by right axis, show absolute values of average predictor weights normalized within each classifier (i.e., connection) coded by their colour. Significance is not indicated as it applies to all shown variables. Error bars, s.e.m. Adapted from [421], open access article: CC BY 4.0, https://creativecommons.org/licenses/by/4.0/

3.2.7 Trial-by-trial prediction of WM-mediated choices from local and long-range neural activity in humans

It remains unclear if highly task-specific and widely distributed WM correlates are only found in rodents or also in human WM. To clarify this question, we used a dataset of intracranial LFP (iEEG) recordings made in 8 human subjects from three sites - PFC, OFC, and MTL (Figure 2.4.1b) – during three types of WM assays whose trials were intermixed within a single test session: identity-related WM (differentiating between identical and novel shapes), spatial WM (tell which of the two cues was presented above or below the other), and temporal WM (remembering the temporal order of two stimuli; Figure 2.4.1a) [225]. For each of the three tasks, we applied the same ML-approach as in mice, generating classifiers that use activity data from four phases (SP, pre-cue- and post-cue delay phases, CP; see task schedule in Figure 2.4.1a) from only a single connection (three connections in total: PFC-MTL, PFC-OFC and OFC-MTL) or region (see above) at a time.

Average decoding accuracies for trial-by-trial prediction of WM-choices were mostly higher than those achieved in mice, ranging consistently between 87-90% for predictions based on connectivity and between 72-82% for predictions based on local activity, whereas "predictions" based on shuffled control data remained significantly lower ($P < 10^{-40}$, *t*-tests) and were not different from chance level (50%; Figure 3.2.13a). We also trained classifiers on the combined data from all three inter-regional connections and three regions – either separately for each task-type or combining all types of trials indiscriminately. For task-specific classifiers, average encoding accuracies reached 87.6%, 90.8%, and 89.8% for identity-related, spatial, and temporal WM, respectively, i.e., no higher than what could be achieved by connectivity data from the single best connection in each task (Figure 3.2.13b). However, encoding accuracy dropped to 79.4% if task-paradigms were intermixed (Figure 3.2.13c) suggesting that functional connectivity is, at least partially, task-specific. Task-specific prediction accuracies of up to 91% could also be obtained without including CP connectivity measures (Figure 3.2.14a). Furthermore, in two cases, an average prediction accuracy of up to 81% could even be achieved if using connectivity data from only a single task phase – either the SP in temporal WM or the post-cue delay in spatial WM (Figure 3.2.14b). Strikingly, in both cases, prediction accuracies – and hence information contents - of all three connections were always similar to each other, suggesting a broad presence of WM-related neural substrates across the brain.

Also, neural communication between the three assessed regions bore more information on predicting WM performance than local activity in those brain regions as the prediction accuracy of the former was consistently higher in all paradigms (Figure 3.2.14b).

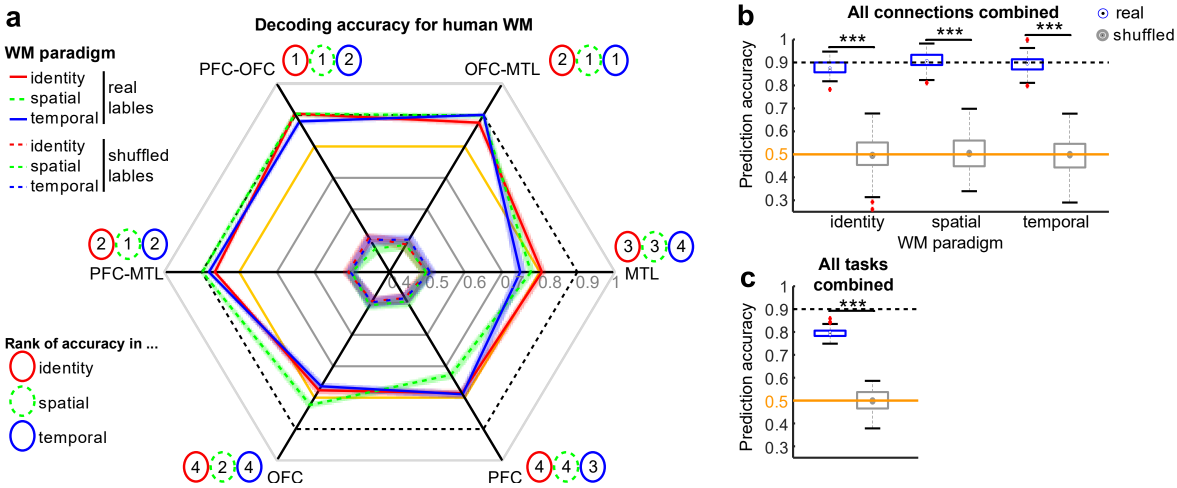

Figure 3.2.13: Single trial-based prediction of WM choice in humans.
(a) Cross-subject decoding accuracies achieved on average when using connectivity or local activity parameters of the indicated connections or areas, respectively, to predict WM-based *correct* vs. *incorrect* choices in the tasks coded by colour on the left. Accuracies achieved by classifiers trained with randomly shuffled labels are shown as coloured dotted lines; they are consistently lower than accuracies achieved by classifiers trained with real labels in all tasks and connections/regions ($P < 10^{-40}$, *t*-tests, not indicated) and assume chance level (50%, orange). Accuracies of 80% (yellow line) and 90% (black dotted line) are indicated to aid comparison. Shaded area represents s.e.m. See Suppl. Table 5, Suppl. Table 6 and Suppl. Table 7 for confirmation of classifier quality by evaluation of various measures of decoding performance. Numbers in circles colour-coded for the respective paradigm indicate the rank of the average decoding accuracies achieved using data from the respective connection or region. Ranks have been generated from pairwise comparisons with Tukey post-doc tests conducted after significant effects of connection/region in one-way ANOVAs ($P < 0.0001$ in all cases); connections/regions that were not significantly different from each other were assigned the same rank. (**b**) Decoding accuracies achieved when using the classifiers trained on predictors from all connections/regions combined (**c**) Similar analysis as (d) but with trials from all three paradigms inter-mixed. Blue and grey in (b-c) depicts performance of classifiers trained on trials with correct or incorrect (shuffled) labels (stars indicate *t*-test comparisons between them). Error bars, data range without identified outliers which are highlighted in red; boxes, range between 25th-75th percentile; dot, median. Red lines indicate mean, boxes the 25th and 75th percentile, whiskers indicate data range without outliers, and red crosses indicate outliers. See Figure 3.2.14 for analysis but using only predictors from single task-phases. Adapted from [421], open access article: CC BY 4.0, https://creativecommons.org/licenses/by/4.0/

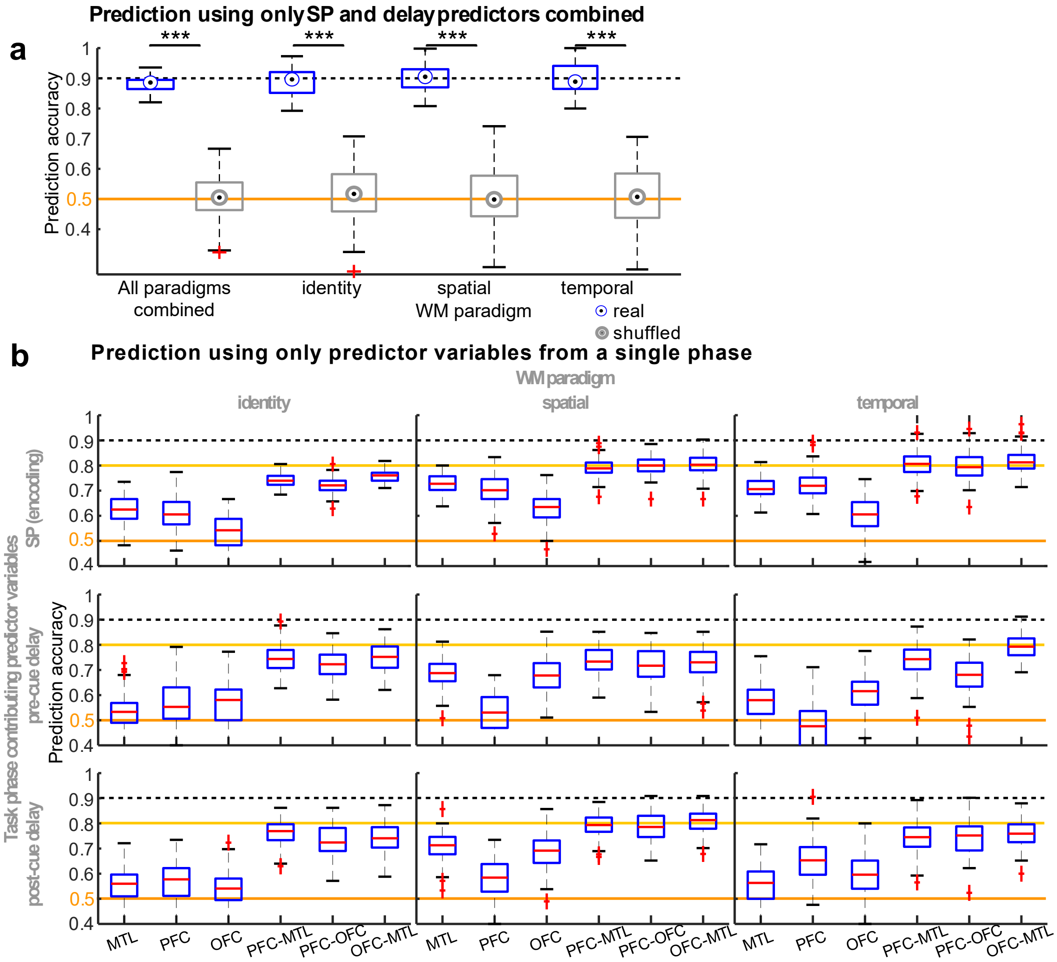

Figure 3.2.14: Decoding accuracy in human WM when using only predictors from the SP and delay.

(a) Decoding of human WM performance by including all trials irrespective of sub-task (left) and separately for the identity, spatial and temporal sub-task (as indicated on x-axis) and using variables from all 3 connections and 3 regions combined. In contrast to the primary analysis shown in Figure 3.2.13a-b, here, parameters from the CP and *relative* measures (that proved to carry little predictive weight in the main analysis, see Figure 3.2.15a) were not included as predictor variables. Blue and grey depict performance of classifiers trained on trials with correct or incorrect (shuffled) labels (stars indicate *t*-test comparisons between them). Error bars, data range without identified outliers which are highlighted in red; boxes, range between 25th-75th percentile; dot, median. **(b)** Separate classifiers were used to predict WM choice separately for the 3 sub-tasks (named at the top of each subpanel) and for each brain region or connection (named on the x-axis) separately, using exclusively absolute metrics obtained during the during the SP (top, same as main Figure 3.2.13f), the pre-cue delay (middle) or the post-cue delay phase (bottom, named on the left). Red lines indicate mean, boxes the 25th and 75th percentile, whiskers indicate data range without outliers, and red crosses indicate outliers. Accuracies of 50% (chance level, orange line), 80% (yellow line) and 90% (dotted line) are indicated to aid comparison in (a, b). Adapted from [421], open access article: CC BY 4.0, https://creativecommons.org/licenses/by/4.0/

Akin to the mouse data analysis (3.2.2), we checked for imbalances in the classifier performance by also analysing measures like the AUC of the ROC, the F1-score, sensitivity, and specificity (see 2.6). For all three human WM paradigms, high percentages were equally distributed across all measures, indicating that the classifiers fitted the data well without any imbalances (Suppl. Table 5, Suppl. Table 6 and Suppl. Table 7).

In order to identify possible individual correlates of WM in humans, we analysed the prediction weights of the connectivity metrics similarly as for the mouse dataset, again extracting WM-related metrics based on the two criteria of prediction weight and a different amplitude of the metric in correct trials compared to incorrect trials (Bonferroni-adjusted *t*-tests). As in mice, WM-related measures (185 out of 1344 connectivity predictor variables) were widely distributed across connections, frequency bands, and metric types. When inspecting the matrix of significant predictors more closely, some regularities emerged (Figure 3.2.15a):

(*a*) WM-related activity was highly task-specific with 88% of significantly WM-related connectivity metrics being relevant in only a single paradigm. If separating by task-phase, only a single metric was predictive in all three paradigms – OFC→PFC post-cue γ-PDC. Such principal task-specificity was maintained also with relaxed *P*-value thresholds (Suppl. Figure 4, Suppl. Figure 5). Similar to the mouse decoding analysis, the classical approach of correlating behavioural performance with the amplitude of a given metric would likely miss a substantial fraction of WM-related functional connectivity because the ML-approach identified predictors that were not detected when comparing between correct and incorrect trials (Suppl. Figure 5).

(*b*) By far the most – and the most common - predictors emerged in the γ-band, irrespective of significance threshold (Figure 3.2.15a-d, Suppl. Figure 4). In contrast to mice, the δ-band contributed almost no WM-related variables (only one each in spatial and temporal WM, confined to the OFC-MTL connection). Also, the θ-band bore relatively few WM-related connectivity parameters, and these were mostly relevant for spatial WM and to a lesser extent for identity WM, but hardly for temporal WM. In contrast to rodents, θ-γ-PAC appeared rather relevant (as found in the same data before [225]) in all three types of tasks, especially identity-related WM.

(*c*) *Changes* of a metric relative to the ITI before each trial were rarely predictive.

(*d*) Despite the relatively high encoding accuracy achieved for temporal WM (Figure 3.2.13a-b), the number of connectivity metrics related to this WM-type was considerably smaller (18 out of 1344 measures) than for the other two (72 and 95) and there was hardly any overlap between these metrics and those relevant for the other two WM-paradigms (only 3 each, mostly in the γ-band; Figure 3.2.15a-d).

In summary, the analysis in humans confirms the high-task specificity, and broad anatomical and frequency-range distribution of WM-related neural activity already seen in mice.

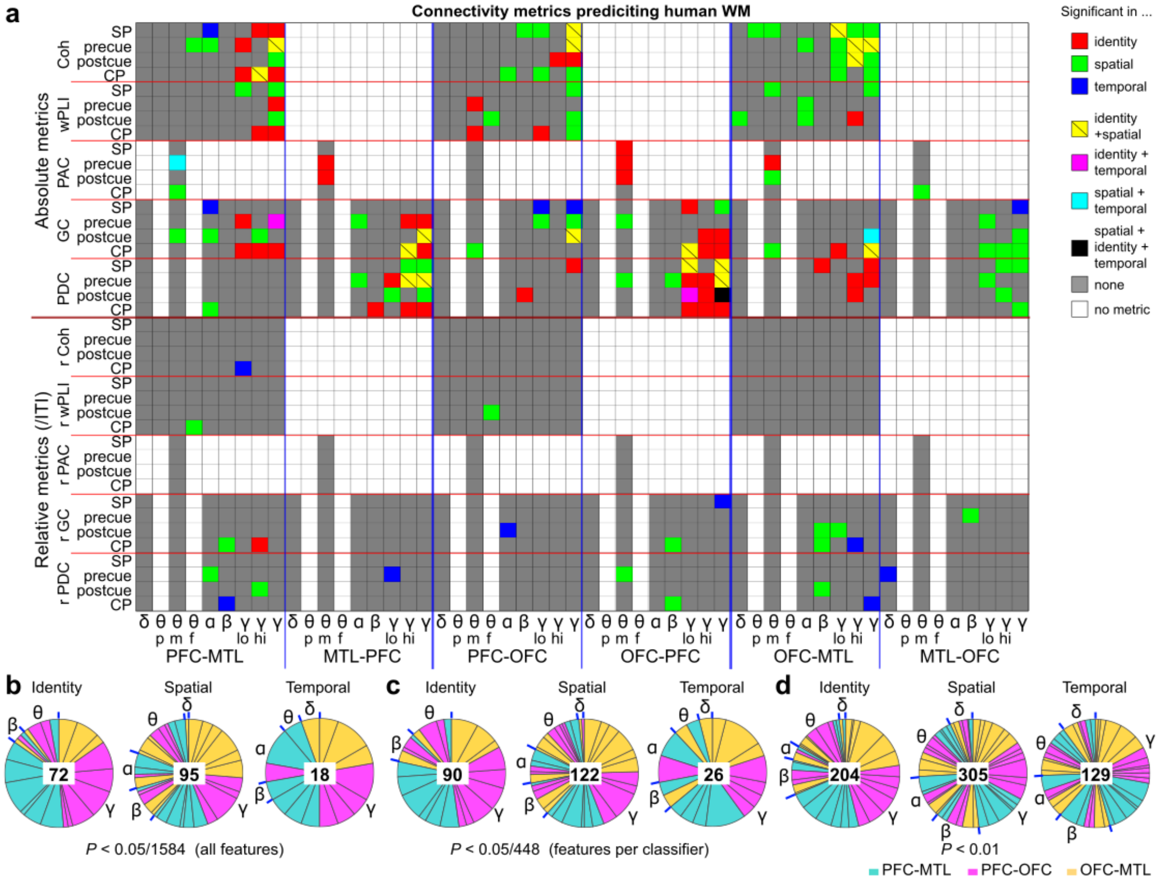

Figure 3.2.15: Highly task-specific and broadly distributed correlates of human WM
(**a**) Matrix showing all connectivity predictor variables that contributed to the classifiers shown in (Figure 3.2.13a) and were significantly associated with WM-performance according to their weight and differences between correct and incorrect CP in the paradigms coded by colour (see legend on the right). For theta, mean amplitude (m), peak amplitude (p), and frequency of peak (f) are shown, while for all other variables only the mean amplitude is used. The gamma-band contributed three predictors each as this frequency was split into a high- and low-gamma-range in addition to using the whole range (30-100 Hz). At the bottom, all task phases are combined and only connectivity metrics that are predictive in all three tasks (in at least one phase) are indicated in black. See Suppl. Figure 4 for the same analysis with relaxed *P*-value correction. (**b-d**) Share of each connection (coded by colour) and frequency band (stated around pie chart with separations in blue) among all significant predictors (*N* stated in centre) for the indicated task. The significance threshold has been Bonferroni-adjusted either by the total number of predictor variables from all connections and regions (1548, corresponding to analysis in panel (a); b), or by the number of connectivity variables for a single connection (448; c), or a standard threshold of 0.01 was chosen (d). Adapted from [421], open access article: CC BY 4.0, https://creativecommons.org/licenses/by/4.0/

3.2.8 Common γ-band connectivity across human WM tasks

To scrutinize this conclusion, we searched for commonalities between tasks by aggregating predictive non-directed (coherence, wPLI) and directed (GC, PDC) metrics as well as the multiple measures within the γ- and θ-bands (extracted from Figure 3.2.15a), and depicted their amplitude change relative to the preceding ITI for each task phase (Figure 3.2.16a-c), as previously done for the mouse dataset (Figure 3.2.11a-c). In this analysis, OFC-PFC γ-coupling during encoding and directed OFC→PFC/MTL γ-connectivity during the post-cue delay emerged as common patterns present in every task. There were also more commonalities between spatial and identity WM, namely gamma-coupling between all three regions that was elevated throughout encoding and delay phases and then decreased below ITI-levels in the CP (Figure 3.2.16a-b). Strikingly in fact, *all* significant predictors from the α–β–γ-range in these two tasks showed *elevated* amplitudes during encoding and delay, but *decreased* amplitudes during the CP, compared to their amplitude in the preceding ITI (Figure 3.2.16a-c). Only θ and θ–γ-PAC predictor variables *increased* in amplitude during the CP in spatial WM (Figure 3.2.16b). Finally, even with this aggregated analysis, not a single connectivity pattern that was shared between any two tasks emerged outside the γ-band in any task phase (Figure 3.2.16a-c). This analysis suggests that human WM generally relies on anatomically broad, task phase-specific modulation of γ-connectivity between several brain regions irrespective of task, while the engagement of oscillatory coupling in other frequency bands is task-specific.

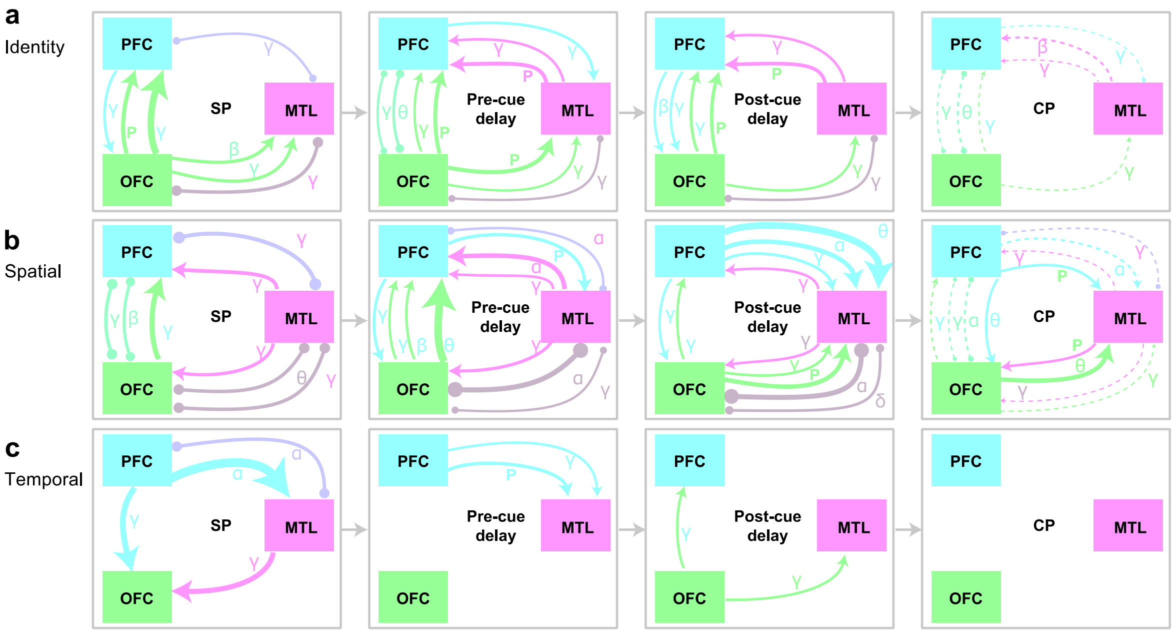

Figure 3.2.16: Neural communication during different WM paradigms in humans
(**a-c**) Depictions of directed connectivity (arrows, derived from GC or PDC) or non-directed coupling (round-ended arcs, coherence or wPLI) during the four phases of each task identified on the left, derived from significant predictor variables shown in Figure 3.2.15a. Line weights indicate the increase of connectivity in the stated phase relative to the preceding ITI. Measures that are significant but *decrease* in the respective phase relative to the ITI are shown as dashed lines. Significant coupling metrics are not depicted if directed measures are represented in both directions. P, θ–γ-PAC. Adapted from [421], open access article: CC BY 4.0, https://creativecommons.org/licenses/by/4.0/

3.3 Impairment of *Gria1*$^{-/-}$ mice in operant working memory assays

Several prior rodent studies investigated connectivity during T-maze testing in genetic mouse models that display a WM-deficit in order to reveal both putative WM correlates in general and causes of the given WM impairment of the model specifically (Table 1.6.1, [76, 401, 432]). In order to assess if the putative WM correlates identified with our ML-approach relate to potential pathological mechanisms of WM-deficits in schizophrenia, we extended our analysis to the *Gria1*$^{-/-}$ mouse model [488] that has genetic, cellular, and neuropsychological relevance to this disease (summarized in 1.5.2 and in [29]). The global ablation of the GluA1 AMPAR subunit (encoded by *Gria1*) in these mice entails a specific, complete, and persistent impairment in rewarded-alternation performance in the T-maze [76, 364] and radial maze [385], but their performance in non-maze WM assays is unknown. The WT mice used for the analysis presented so far were WT littermates of *Gria1*-KO mice, and the latter were trained, tested, and recorded alongside the former in order to allow direct comparisons of behaviour and physiology. As described in 2.3.5, mice were tested on the operant DMTS task and challenged by prolonging the delay period, by sound distraction, or by reducing the SD and simultaneously increasing the delay period (see column-wise arrangement in Figure 3.3.1 and Figure 3.3.3 for the resulting behavioural performance). For the operant DNMTS paradigm, mice were trained on the 2-CSWM task (see 2.3.6) and challenged by introducing a longer delay period. T-maze performance was assessed by first training mice for eight days and then challenging them by a longer delay period for four days, as stated in section 2.3.7.

In contrast to expectation, we found that *Gria1*-KO mice could actually perform the DMTS 5-CSWM task well above chance level. Before surgery, there was no significant difference between genotypes on the DMTS across training stages (Figure 3.3.1a, b). Interestingly, *Gria1*$^{-/-}$ mice initially even performed better than their WT littermates (Figure 3.3.1a). Nevertheless, when tested after full training (and with concomitant electrophysiological recordings), KO mice displayed significantly lower WM accuracy across the applied delay and distraction challenges compared to their WT littermates (Figure 3.3.2a, Figure 3.3.1c). In subsequent testing in the T-maze, we confirmed the chance level WM accuracy of *Gria1*$^{-/-}$ mice in this assay (Figure 3.3.2c). Finally, in the DNMTS 2-CSWM assay, *Gria1*$^{-/-}$ mice performed somewhat above chance level, but again worse than WT mice (Figure 3.3.2d-e, Figure 3.3.4a-b).

Their deficits in the DMTS paradigm were selective for the WM component of the task, and not mediated by impairments in more basic attentional or motivational functioning since SP accuracy, CP omission rate and CP reward latency were similar between groups (Figure 3.3.2b, Figure 3.3.1e, f). Note, however, that *SP* omission rates and correct latencies (time from illumination onset until correct poke) in SP and CP were even lower in KO mice (Figure 3.3.3b-d, Figure 3.3.1g). Also, *Gria1*$^{-/-}$ mice performed more correct SP trials in total (Figure 3.3.3c) and were faster in getting to the reward as their reward latency in SPs was slightly lower than in WT mice (Figure 3.3.3e). These behavioural anomalies suggest hyper-alertness, faster processing, and more task engagement (or motor drive) in this genotype during the SP which, however, does not translate to enhanced WM compared to WT mice in the CP.

Similar to the DMTS assay, WM-performance in the DNMTS task was also not confounded by motivational or attentional components as the SP accuracy, SP and CP omission rates, and CP reward latency were indistinguishable between genotypes (Figure 3.3.2e, Figure

3.3.4c, e, g). Also, even if not as pronounced as in the DMTS paradigm, *Gria1*$^{-/-}$ mice showed faster responding as indicated by lower SP correct latency (Figure 3.3.4i).

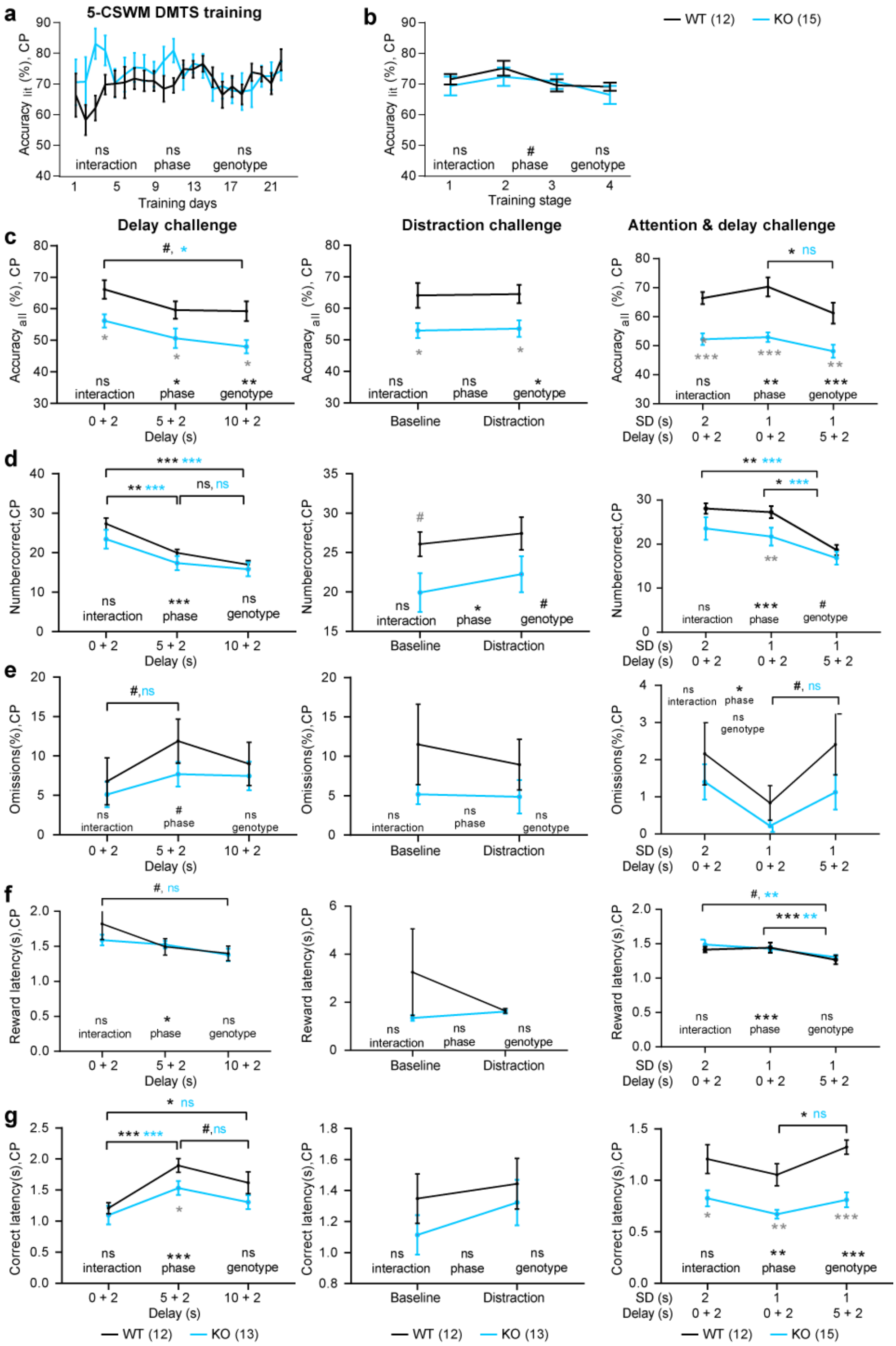

Figure 3.3.1: Behavioural performance in the CP of the 5-CSWM task
(**a**, **b**) Mean CP performance (accuracy$_{lit}$, number of correct CP responses into lit holes divided by number of all CP responses into lit holes) of WT and KO mice during initial 21 training days (**a**) and on 2-3 d of successively conducted training stages (b) in the 5-CSWM DMTS paradigm before surgery. **(c-g)** Performance parameters for three DMTS challenge series for which SP and CP accuracy data is shown in Figure 3.3.2a (parameters stated on x-axes) including their respective baseline. Parameters are accuracy$_{all}$ (number of correct

CP responses divided by number of all CP responses; c), absolute number of correct CP responses (d), relative number of CP omissions (e), CP reward latency as the mean duration between correct CP-poke (entry) and entry into the reward receptacle on the opposite site of the box (f), and CP correct response latency as mean time needed to enter the correct CP poke hole after the onset of its illumination. In each panel the results of a repeated-measures (RM) ANOVA of the data are shown a *P*-values of effects of phase (challenge condition), genotype, and interaction. Paired within-group post-hoc comparisons between phases are indicated on horizontal lines for each genotype and pairwise comparisons between genotypes at individual phases are indicated below the data points in grey. # $P < 0.1$, * $P < 0.05$; ** $P < 0.01$; *** $P \leq 0.001$; error bars display s.e.m.

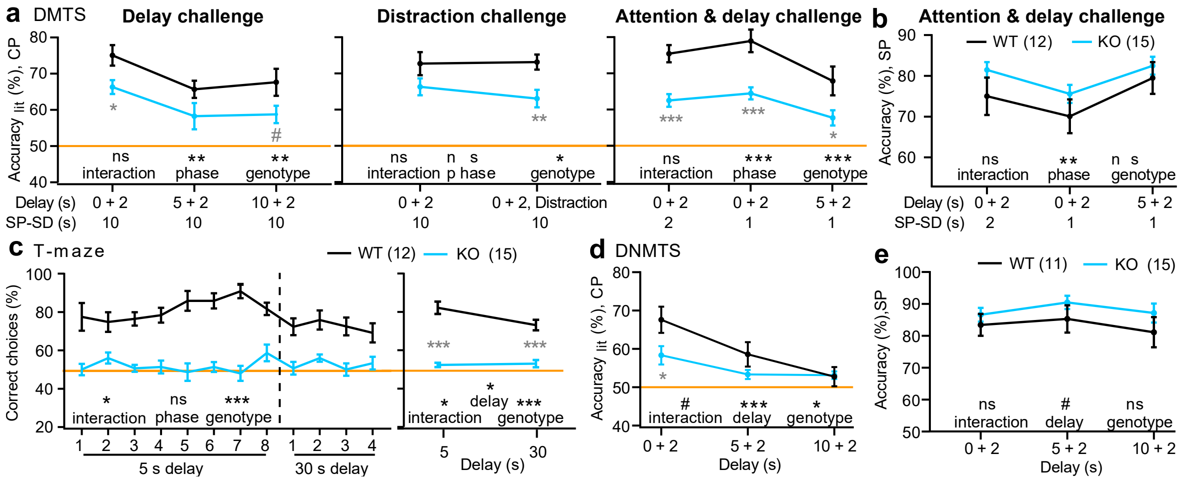

Figure 3.3.2: Impaired WM performance in *Gria1*$^{-/-}$ mice

(**a-e**) WM (a, c, d) and attentional (b, e) accuracy of *Gria1*$^{-/-}$ mice (KO, cyan) and littermate controls (WT, black) in each set of baseline and challenge conditions, as stated on the x-axes, of the tasks identified in (a,c,d; top left). Right panel in (c) shows same data as (the left panel) but averaged across the last 4 sessions of each delay, which were also used for ML-based analysis. All shown behavioural data was conducted with simultaneous electrophysiological recordings. Delay length in operant tasks (a-b, d-e) is indicated as pre- + post-delay (referring to set delays before and after SP-reward collection). SD, stimulus duration in SP. Orange line, chance level performance. *N* numbers for each dataset are stated in (b,c,e). Results of repeated-measures ANOVAs within each challenge set are stated at the bottom of each graph; grey stars indicate pairwise Sidak post-hoc comparisons between groups within protocol. See Figure 3.3.1 and Figure 3.3.3 for further behavioural parameters in the CP and SP of the two operant tasks.

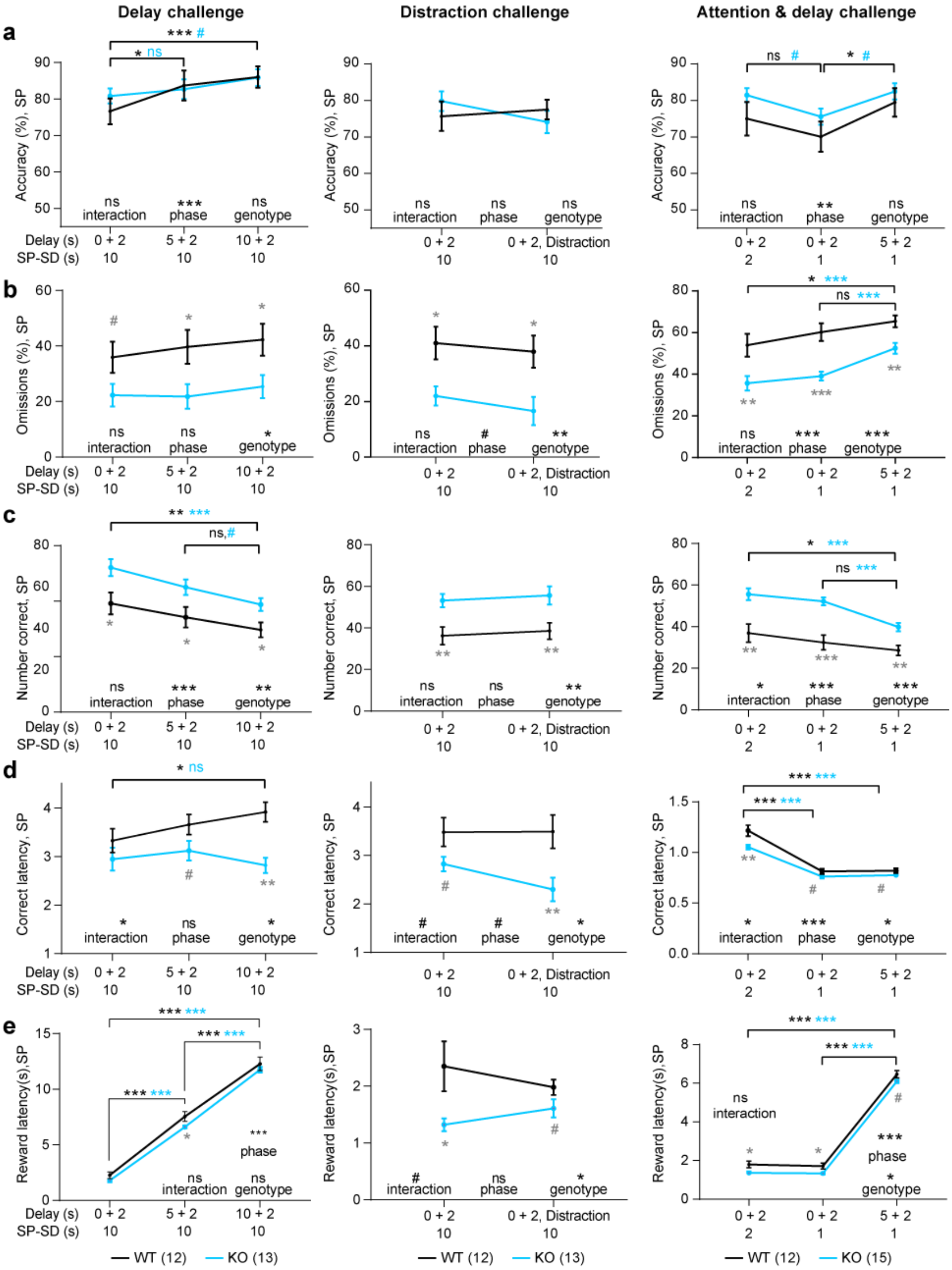

Figure 3.3.3: Behavioural performance in the SP of the 5-CSWM task

(a-e) Same display and analysis as in Figure 3.3.1c-g, but for behavioural SP parameters in the same 5-CSWM protocols (indicated on x-axes), namely (**a**) SP accuracy (main indicator of sustained attention in this task), relative number of SP omissions (**b**), number of corrects responses (**c**), correct response latency as time from illumination of poke-hole until the entry into the hole (d), and (**e**) SP reward latency (including the pre-reward delay where applied). Statistical analysis as in Figure 3.3.1. # $P < 0.1$, * $P < 0.05$; ** $P < 0.01$; *** $P \leq 0.001$; error bars display s.e.m.

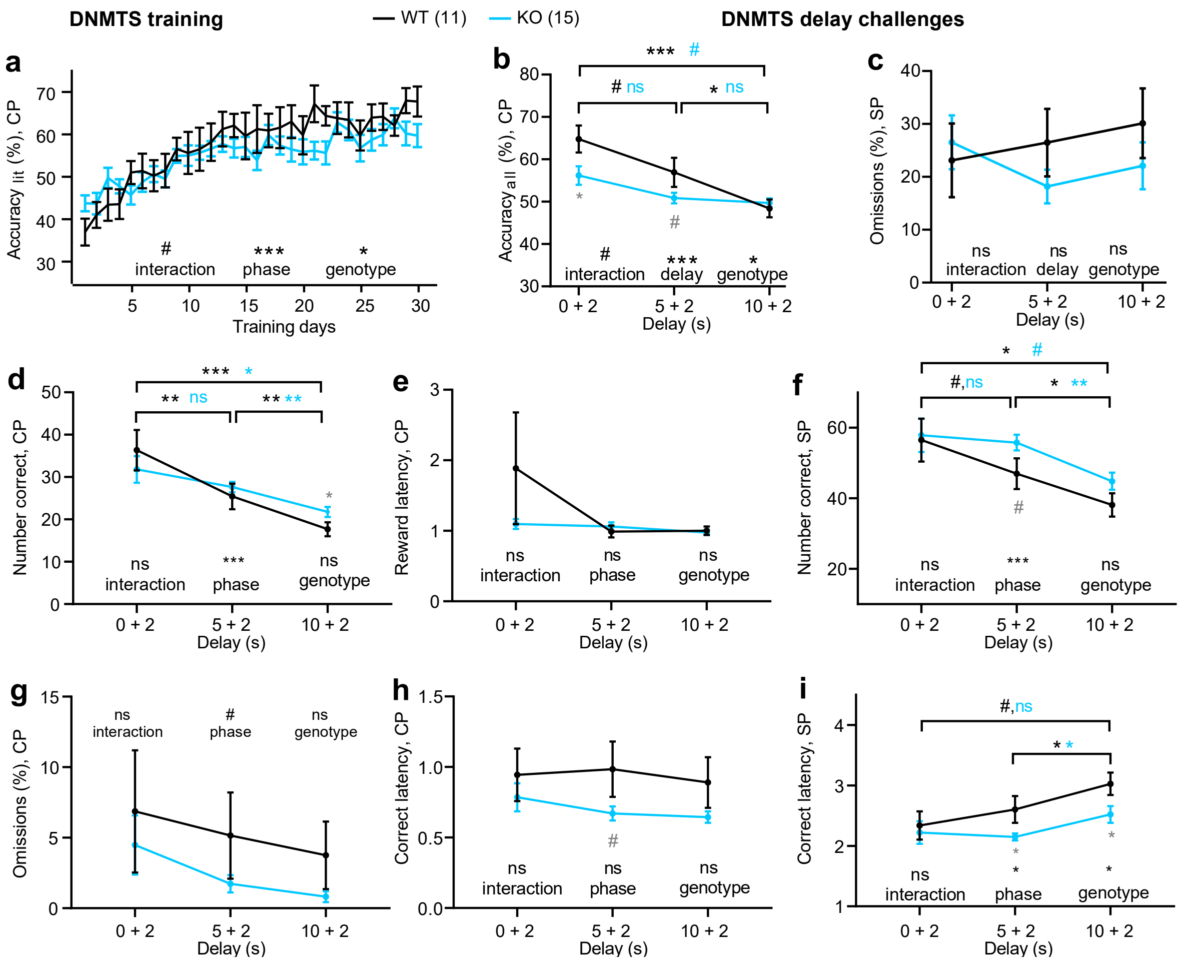

Figure 3.3.4: Behavioural performance on the DNMTS paradigm of the 5-CSWM task
(a) Accuracy$_{lit}$ of WT and KO mice over the course of the initial 30 training sessions in the operant DNMTS paradigm. **(b-i)** Behavioural parameters during DNMTS delay challenges and its baseline (indicated on x-axes), for which SP and CP accuracies are shown in Figure 3.3.2d,e as same display and analysis as in Figure 3.3.1 and Figure 3.3.3 for the DMTS task, namely for accuracy$_{all}$ (b), SP omission rate (c), total number of correct CP responses (d), CP reward latency (e), number of correct SP responses (f), CP omission rate (g), correct CP response latency (h), and correct SP response latency (i). # $P < 0.1$, * $P < 0.05$; ** $P < 0.01$; *** $P \leq 0.001$; error bars display s.e.m.

3.3.1 Absence of WM-related information underlies impaired rewarded alternation on the T-maze in *Gria1*$^{-/-}$ mice

To reveal possible physiological correlates of impaired WM performance in *Gria1*$^{-/-}$ mice, we firstly computed classifiers to predict WM-based choices in KOs as done before for WTs (Figure 3.2.3a-b, Figure 3.3.5a-c). For DMTS data, there were no obvious relations between predictability of WM choice and behavioural performance differences between the two groups: compared to WTs, in KOs, decoding accuracy was significantly lower if computed from PFC-dHC/vHC, MD, and dHC activity, but was higher if derived from the remaining regions and connections (Figure 3.3.5a). For DNMTS data, prediction accuracy was lower in KOs compared to WTs in five out of eight connections or regions, but the appearance in the spider plots upon visual inspection (Figure 3.3.5b) and the ranks obtained by genotype specific one-way ANOVAs were roughly similar between genotypes (e.g., dHC being the region with the high accuracy and MD and PFC being the only regions with differing ranks).

This pattern contrasted sharply with decoding accuracies on the T-maze, which were not only significantly lower than those obtained with WT data along all connections and regions but did not even exceed chance level in five out of eight of them and were *at* or *below* 60% in the remainder (Figure 3.3.5c). Thus, classifier accuracy mirrored the chance level performance of the animals in the task itself (Figure 3.3.2c) suggesting that their impairment is caused by a basic neural failure to store and communicate WM items. As a consequence, mice are likely unaware of what constitutes a correct choice even if they make one, and instead follow a different behavioural rule in this task - the simplest possibility being to always turn into the same direction. Indeed, we found that KO-mice exhibited a strong bias to turn to a specific side in the CP of any given session (Figure 3.3.5d).

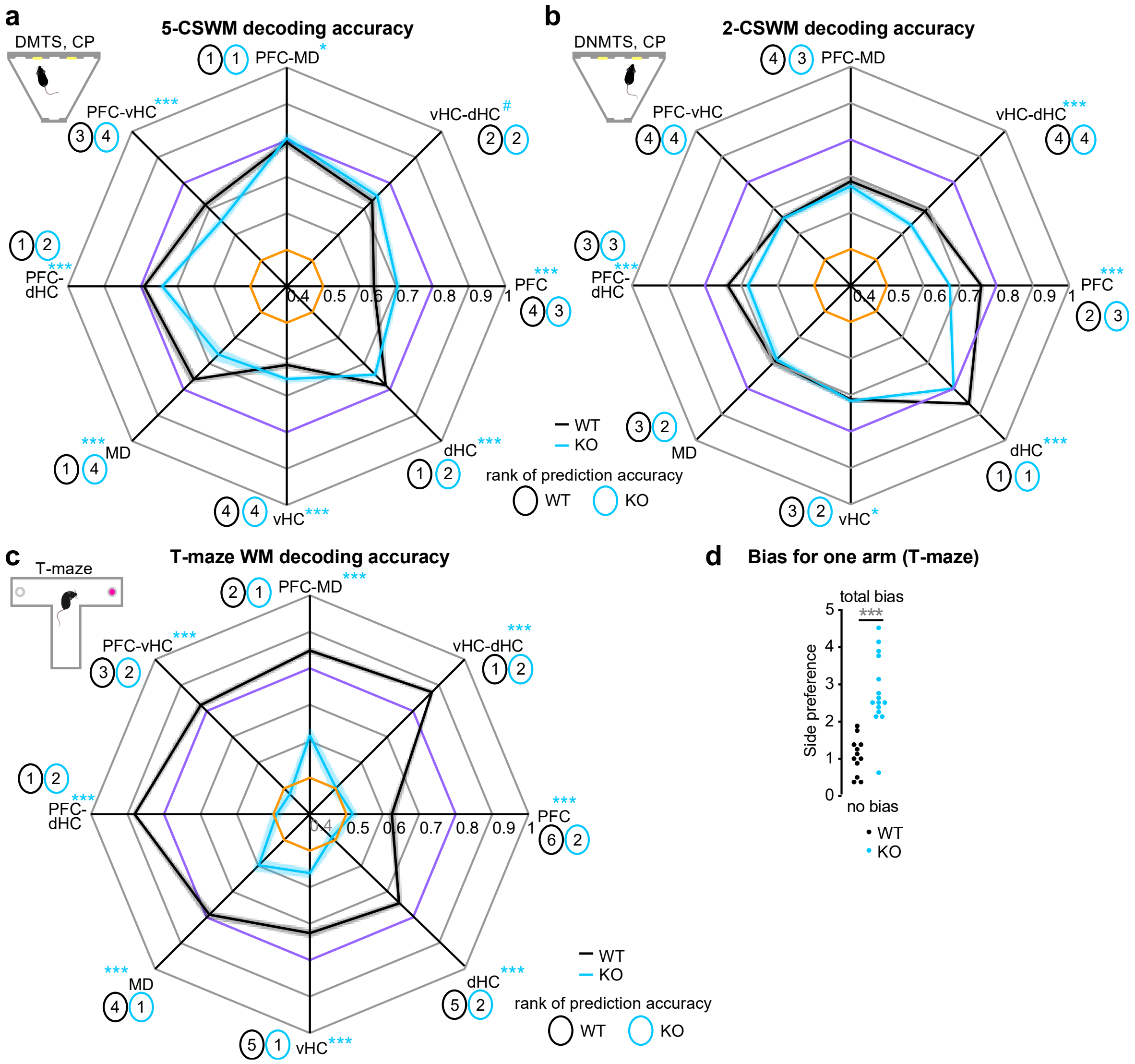

Figure 3.3.5: Decoding of WM in *Gria1*$^{-/-}$ mice.
(**a-c**) Cross-subject decoding accuracies when using indicated connectivity or local activity parameters to predict WM-based choices in *Gria1*-knockouts (cyan) and littermate wildtype controls (black) in the 5-CSWM DMTS (combined 1 s SP-SD, 5+2 s delay challenge, a), 2-CSWM DNMTS (b) and the T-maze (c). Wildtype data and respective ranks (numbers in ovals) are identical to Figure 3.2.3a, b. Similarly, ranks for KO (in cyan ovals) have been generated from pairwise comparisons with Tukey post-hoc tests conducted after significant effects of connection/region in one-way ANOVAs ($P < 0.0001$ in all cases); connections/regions that were not significantly different from each other were assigned the same rank. Genotype-related differences indicated by asterisks (unadjusted *t*-tests). Accuracies of classifiers trained on shuffled data are shown in the corresponding colour as dashed lines. Accuracies of all classifiers trained on real data in (a-c) exceeded chance level, except for those trained on *Gria1*-KO data in the T-maze for PFC-v/dHC connections, PFC, and dHC. (**d**) Average bias to turn to one of the two choice arms irrespective of correct choice. $^{\#}$ $P < 0.1$ * $P < 0.05$, ** $P < 0.01$; *** $P \leq 0.001$. Shaded regions around mean show s.e.m.

3.3.2 Simultaneous decoding of genotype and choice reveals aberrant WM-related connectivity in *Gria1*$^{-/-}$ mice

In order to find specific connectivity metrics that may underlie behavioural WM differences between genotypes, we extracted significant predictor weights from the obtained classifiers from KO data in all three tasks, as done before for the WT data from the same experiments. However, there was only minimal overlap between the sets of significant predictor variables of both genotypes in the operant WM tasks (Figure 3.3.6a, b). For the 5-CSWM assay, these were exclusively in the γ-range - namely MD→PFC γ-PDC in the delay and dHC→PFC γ-PDC (and coherence) in the CP – which may be taken as an indication for the importance of such connectivity for DMTS WM (Figure 3.3.6a). Likewise, for operant DNMTS, the few parameters highlighted as significant predictors in both genotypes were almost exclusively in the β- and γ-range (mainly PFC-vHC/dHC connectivity in the CP, Figure 3.3.6b). In the T-maze, virtually no significant predictors were found in KO mice, in line with the near chance level decoding accuracy of the respective classifiers (Figure 3.3.5c, Figure 3.3.6c).

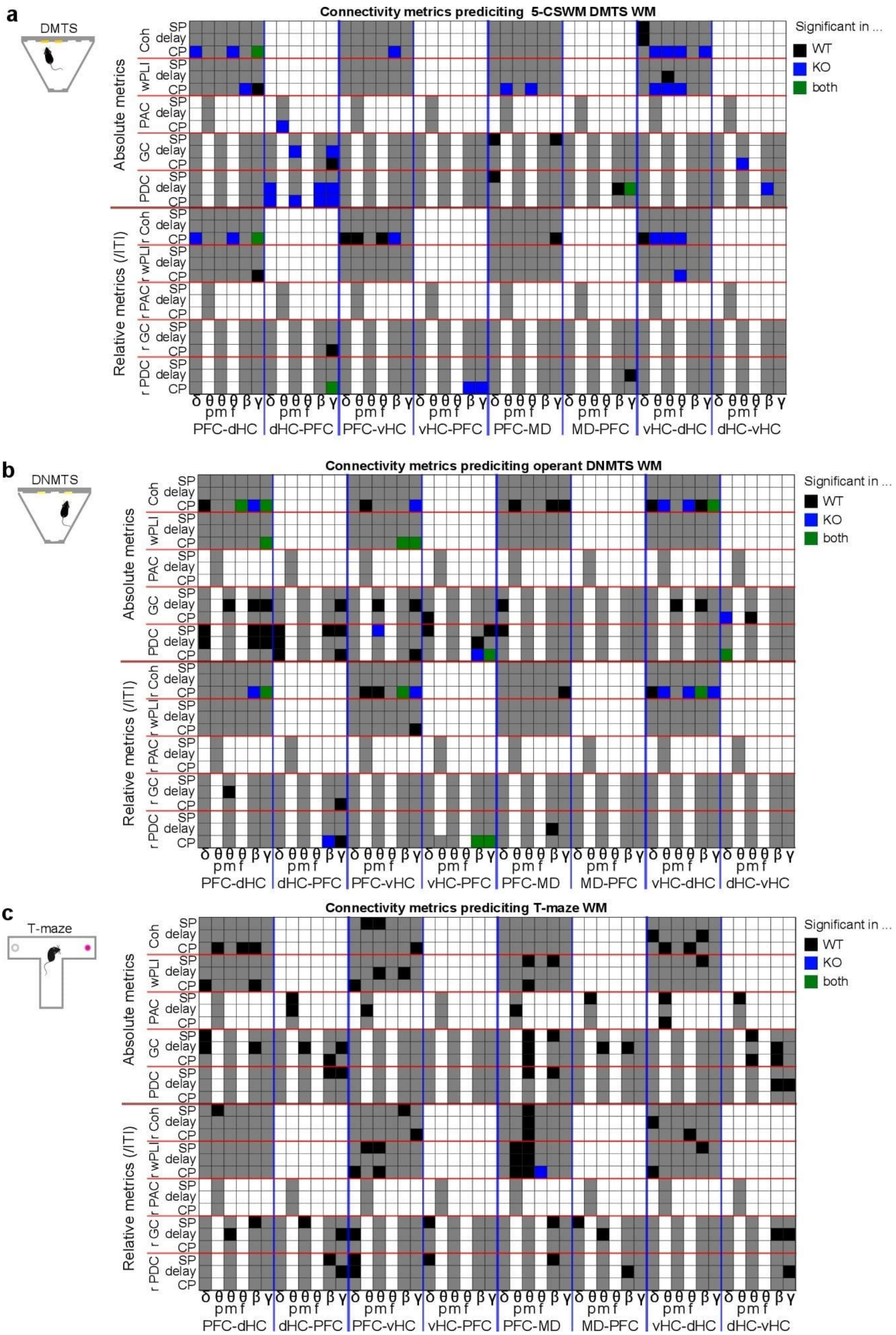

Figure 3.3.6: Individual connectivity measures predicting WM choice in all three rodent tasks in WT and KO.

(**a-c**) Matrix showing all connectivity predictor variables that contributed to the connection-based classifiers shown in Figure 3.2.3a-b (WT) and Figure 3.3.5a-c (WT and KO; DMTS, DNMTS and T-maze) and that were significantly associated with WM-performance according to their weight and differences between correct and incorrect CP in the dataset from WT (black), KO (blue), or both (green), or did not reach significance (grey). The same Bonferroni-adjustment as in Figure 3.2.6a was used: $P < 0.05/$ (total number of predictor variables across all phases, connections, and regions), i.e., $P < 0.05/1184$ for DMTS and $P < 0.05/888$ for DNMTS and T-maze. Variables from the pre- and post-delay of the DMTS 5-CSWM task have been combined in single lines. For theta, mean amplitude (m), peak amplitude (p) and frequency of peak (f) are shown, while for all other variables only the mean amplitude is used due to the absence of a clear singular peak. Note the relatively small overlap between sets of significant predictors in WT and KO mice, and the virtual absence of significant predictors for KO data in the T-maze, aligning with virtual lack of prediction accuracy of the respective classifiers (Figure 3.3.5c).

This broad lack of overlap between predictor matrices in KO and WT even in the operant tasks suggests that KO mice engage partly different neural mechanisms to perform above chance level in these assays. To identify *those* aberrations among the broad changes of connectivity in *Gria1*$^{-/-}$ mice, that are most directly related to their WM-deficit, we adapted our ML approach and trained classifiers to discriminate genotype (KO vs. WT) and trial-type (correct vs. incorrect) simultaneously (multi-class decoding). Average decoding accuracies of such multi-class classifiers were always far above chance level (25%; $P < 0.0001$, *t*-test; Figure 3.3.7a). By a wide margin, the highest average decoding accuracies were achieved when using data from the PFC-MD connection in the 5-CSWM (80%) and the T-maze (82%) assays, and from local dHC activity in the 2-CSWM task (79%), pointing to them as a likely source of WM deficits in *Gria1*$^{-/-}$ mice (Figure 3.3.7a). Analysis of the pairwise multi-class decoding accuracies (assessing four categories (WT/KO and correct/incorrect) against each other with either differing genotype or trial type, but not both (KO correct vs. WT incorrect or vice versa)) for 5-CSWM assay data revealed that genotype could be predicted with significantly higher accuracy (> 95% at maximum) than trial type, irrespective of which connection or region contributed the data used for decoding (Figure 3.3.7b).

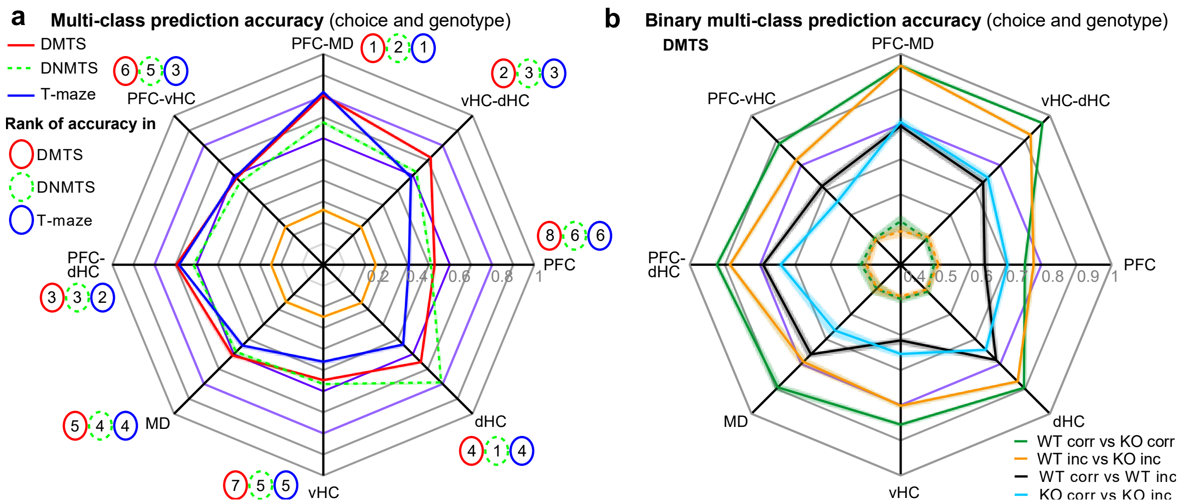

Figure 3.3.7: Multi-class decoding of WM in *Gria1$^{-/-}$* mice

(**a**) Multi-class decoding accuracy for simultaneous predictions of genotype and choice (25% chance level) in the three rodent tasks indicated by colour. Rank order of each connection and region determined as in Figure 3.2.3a, b. (**b**) Pairwise classification accuracy between the four relevant (out of six) comparisons for the 5-CSWM task. Accuracies of classifiers trained on shuffled data are shown in the corresponding colour as dashed lines. Accuracies of all classifiers trained on real data exceeded chance level. $^{\#}$ $P < 0.1$ * $P < 0.05$, ** $P < 0.01$; *** $P \leq 0.001$. Shaded regions around mean show s.e.m.

Analogously to our previous analysis, we extracted the most predictive connectivity metrics of the multi-class decoders in order to identify WM-related neurophysiological differences between the genotypes. Again, two criteria had to be fulfilled for such predictors: their absolute weights had to be significantly higher in classifiers trained with real labels than in those trained with shuffled labels (*t*-test), and, when analysing the effects of genotype and choice (correct vs. incorrect) on the amplitude of the metric with repeated-measures ANOVAs, the genotype-choice interaction had to be significant. Strikingly, there was no single common connectivity measure that was identified in every one of the three tasks as significant predictor. Only two common predictors – vHC-dHC δ-coherence in the delay and PFC-dHC β-wPLI in the CP – emerged when relaxing the *P*-value adjustment to $P < 0.01$ for genotype-choice interactions (Suppl. Figure 6). These results suggest that – in alignment with the high task-specificity of WM-correlates seen in WT mice (see 3.2.4) – the specific circuit-level origins of WM-deficits in *Gria1$^{-/-}$* mice are distinct between tasks. Indeed, the vast majority of significant multi-class predictor variables for the T-maze were found in the PFC-MD and, to a lesser extent, in the vHC-dHC connections. For the 5-CSWM task, in contrast, the most significant predictors were almost exclusively confined to the dHC→PFC connection (Figure 3.3.8a), although predictors in the PFC-MD and vHC-dHC connection emerged with lower p-value threshold (Suppl. Figure 6).

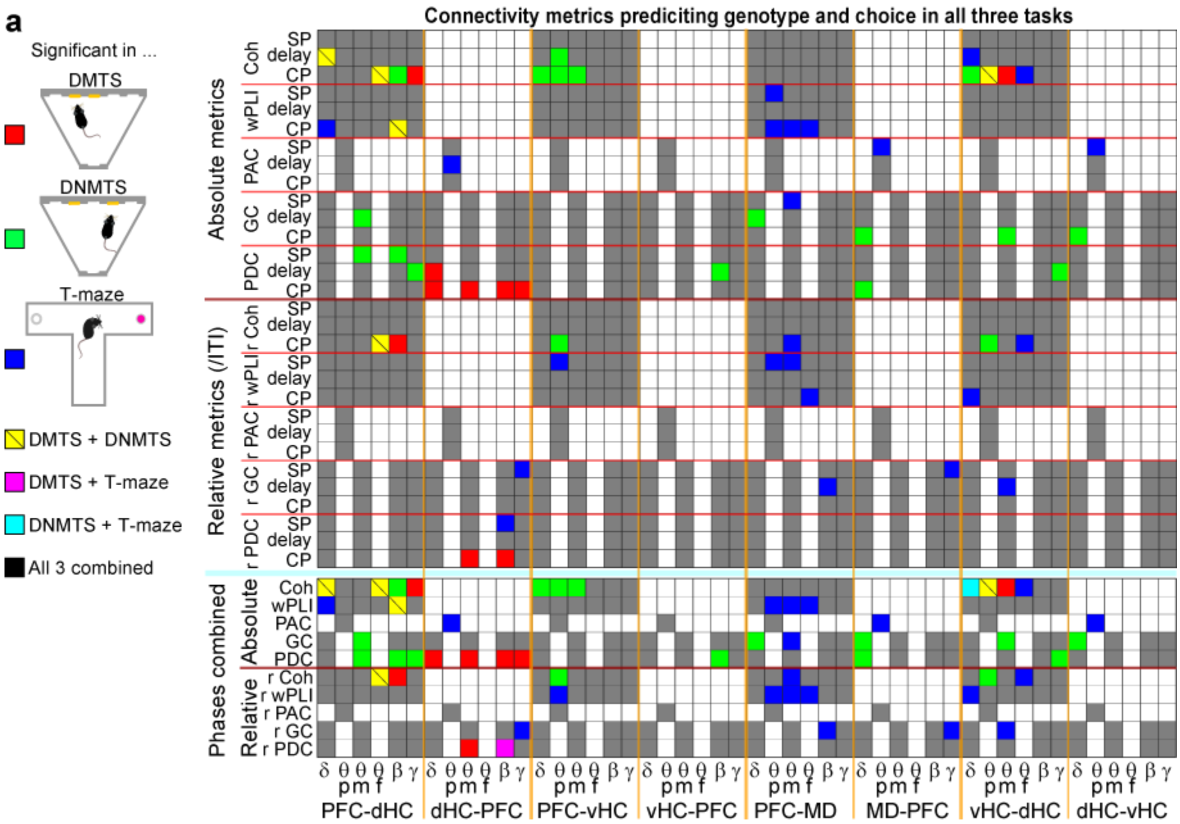

Figure 3.3.8: Distinct WM-related connectivity in *Gria1*$^{-/-}$ mice

(**a**) Matrix showing all connectivity predictor variables that contributed to the connection-based classifiers shown in Figure 3.3.7a. Variables that were significantly associated with WM-performance according to both their prediction weight (*t*-tests) and a significant genotype-choice interaction (RM-ANOVA, Bonferroni-adjusted for total number of variables) in any of the three WM tasks are indicated by the corresponding colour, remainder in grey (white squares have no corresponding variable). Variables from the pre- and post-delay in the 5-CSWM are combined in single lines. For theta, mean amplitude (m), peak amplitude (p) and frequency of peak (f) are shown, while for all other frequency bands only the mean amplitude is used due to the absence of a clear singular peak. At the bottom, all task phases are combined.

We further analysed the most predictive predictors depicted in Figure 3.3.8a by displaying the amplitudes for measures during the DMTS task (Figure 3.3.9). Interestingly, for the PFC-dHC connection, the classifier mainly used predictors in which KOs had always higher absolute or relative amplitudes during correct compared to incorrect trials whereas the picture was more variable for WT mice.

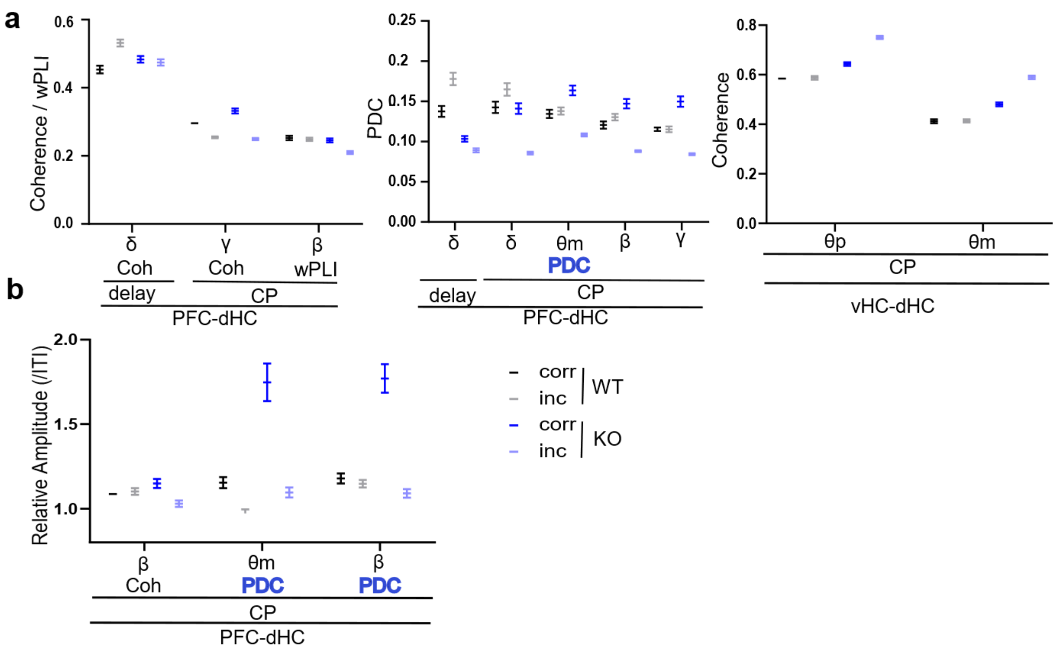

Figure 3.3.9: Significant multiclass predictors for DMTS
Mean values of absolute (**a**) or relative (**b**) predictor variables for DMTS WM (extracted from Figure 3.3.8a) for WT in correct (black) and incorrect (grey) trials and for KO in correct (dark blue) and incorrect (light blue) trials. X-axis contains significant features sorted by frequency band, measure, task phase and connection. Significance is not indicated as a significant genotype/choice interaction revealed by repeated-measures ANOVA applies to all shown variables. PDC in blue font, directed connectivity in the *opposite* direction compared to connection-name. Error bars, s.e.m.

These data suggest that there is no singular neural cause for the profound WM-deficits of *Gria1*$^{-/-}$ mice, but that the broad connectivity aberrations in this mouse-line, seen across multiple connections and all frequency bands [76, 420] affect the successful execution of each WM task in distinct ways, depending on the relative engagement of each brain region by each task's demands.

3.4 Normal anxiety in *Gria1*$^{-/-}$ mice

As described in the Introduction, the overarching goal of this thesis work was to elucidate GluA1-mediated circuit mechanisms of schizophrenia-related cognitive and affective functions. This centrally includes mechanisms of salience attribution in addition to those of WM. While a large plethora of alterations in *Gria1*-KOs under conditions of *spatial novelty* have already been described in section 1.5.2, we also sought to investigate other types of saliencies. For example, mutant mice with inactivated GluA1 phosphorylation sites [266] have shown a decrease in anxiety-like behaviours [250] - and so have *Gria1*$^{-/-}$ mice [141], which points to a role of GluA1 in assigning anxiogenic salience. To firstly recapitulate these findings and to validate the behavioural phenotype in this mouse model, unconditioned anxiety and exploration were tested on the EPM and in the open field (Figure 3.4.1) in the same cohort that underwent the WM tasks (15 *Gria1*$^{-/-}$ mice (10 males and 5 females) and 12 *Gria1* WT mice (8 males and 4 females)). On the EPM, more time spent *in* and more entries *to* the open arms relative to the closed arms is considered to represent either reduced anxiety or increased exploratory drive (or a combination of both) in rodents. The preference ratio calculated from visiting time – i.e., time spent in the open arm divided by time spent in all arms – revealed no significant differences between genotypes (Figure 3.4.1c). Also, the preference calculated from the number of entries– i.e., entries to the open arm divided by entries to all arms – showed no significant difference (Figure 3.4.1d). In line with the latter, in the open field test (10 minute exploration in a novel box; same experiment as in Figure 3.1.1b-c; see 2.3.1 and 3.1.1 for methodological description and further results, respectively), the distance mice kept to the border of the box was not significantly different between genotypes (Figure 3.4.1h), indicating no pronounced anxiety-related behavioural phenotype.

However, *Gria1*$^{-/-}$ mice showed hyperlocomotion on the EPM as also seen on the open field test (Figure 3.1.1b, c): The mean distance travelled on the EPM was higher in *Gria1*$^{-/-}$ mice than in *Gria1* WT mice (29.33 vs. 16.79m, Figure 3.4.1e) and *Gria1*$^{-/-}$ mice entered both of the closed arms more often than their WT littermates (71.40 vs. 39.08, Figure 3.4.1b). Additionally, *Gria1*$^{-/-}$ mice travelled at a higher speed during the experiment (0.049 vs. 0.028 cm/s, Figure 3.4.1f). These results are in line with previous descriptions of hyper locomotor activity in this mouse line (e.g. Figure 3.1.1b, c, or [76]). Since no robust anxiety-related phenotypes of *Gria1*$^{-/-}$ mice were found, no further electrophysiological analyses of potential correlates of anxiety-related salience were performed.

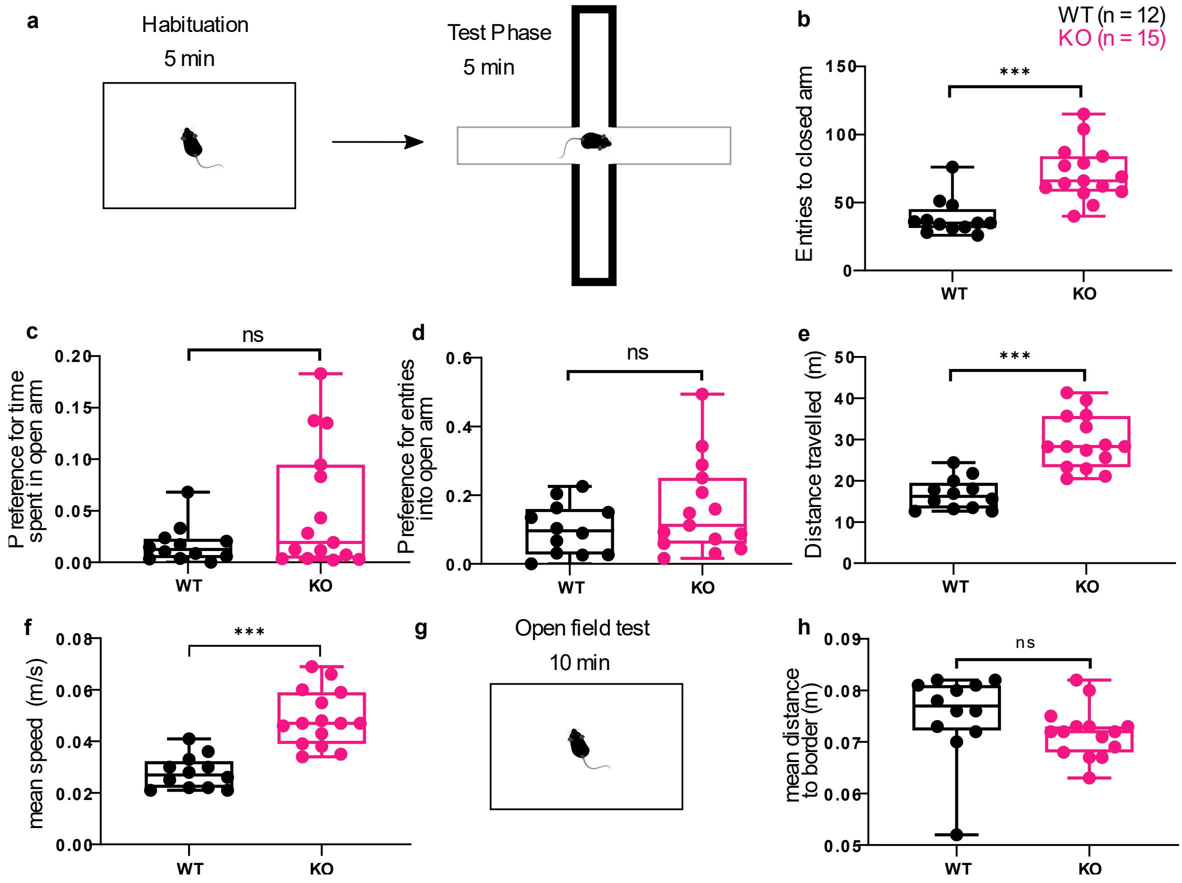

Figure 3.4.1: *Gria1*$^{-/-}$ mice show hyperactivity on the EPM, but no anxiety-related abnormalities. (**a**) Experimental setup for assessing anxiety in *Gria1* WT and KO mice, a 5min habituation time in a novel cage is followed by a 5min test phase on the EPM. Locomotion was measured by analysing the total entries to the closed arm (**b**) and the total distance travelled (**e**). (**c**) Preference for time spent in the open arm and preference for the number of entries to the open arm (**d**). (**f**) Mean travelling speed (m/s) on the EPM. (**g**) graphical depiction of the open field setup. (**h**) Mean distance to border during exploration in the open field test. Dots indicate all data points, boxes the 25th and 75th percentile, whiskers range and horizontal line median. *** p<0.001 (unpaired t-test; Wilcoxon rank-sum test was used where the normality of the data was not assumed).

3.5 Behavioural impact of GluA1 ablation from excitatory CA2/CA3 cells

A previous study of the lab has pointed to a crucial role of GluA1-containing AMPARs in either the CA2 or the CA3 subfield of the hippocampus in spatial novelty-related salience attribution (spatial short-term habituation, [76]). To further elucidate and clarify this role, we turned to a transgenic approach to ablate GluA1 from specific populations of excitatory cells of the CA2-subfield (targeted by the Amigo2-Cre driver line; *Gria1*$^{\Delta Amigo2}$) or of the CA3-subfield (targeted by the Grik4-Cre driver line; *Gria1*$^{\Delta Grik4}$). Inside the hippocampus, correct ablation was verified as *Gria1*$^{\Delta Amigo2}$ and *Gria1*$^{\Delta Grik4}$ mice showed a noticeable gap of GluA1-expression in the CA2 and CA3 subfields, respectively (Figure 3.5.1a).

3.5.1 *Gria1*-knockout from excitatory cells of CA2/CA3 causes mild hyperlocomotion

Both *Gria1*$^{\Delta\text{Amigo2}}$ and *Gria1*$^{\Delta\text{Grik4}}$ mice displayed a mild increase of novelty-induced locomotion in the open-field and EPM (Figure 3.5.1d-h) – although far from the pronounced hyperlocomotion phenotype consistently seen with global *Gria1*-knockout (see Figure 3.1.1b, c, Figure 3.4.1e and [53, 76, 471]). *Gria1*$^{\Delta\text{Amigo2}}$ – but not *Gria1*$^{\Delta\text{Grik4}}$ – mice showed marginally higher preference for entries into the open arm of the EPM compared to controls, indicating slightly reduced anxiety (Figure 3.5.1b). In contrast, they also displayed a reduced average distance from the wall of the open field, suggesting higher anxiety (Figure 3.5.1c). This mixed phenotype points to a subtle aberration in the processing of anxiogenic signals but argues against a clear phenotype of altered anxiety in this line.

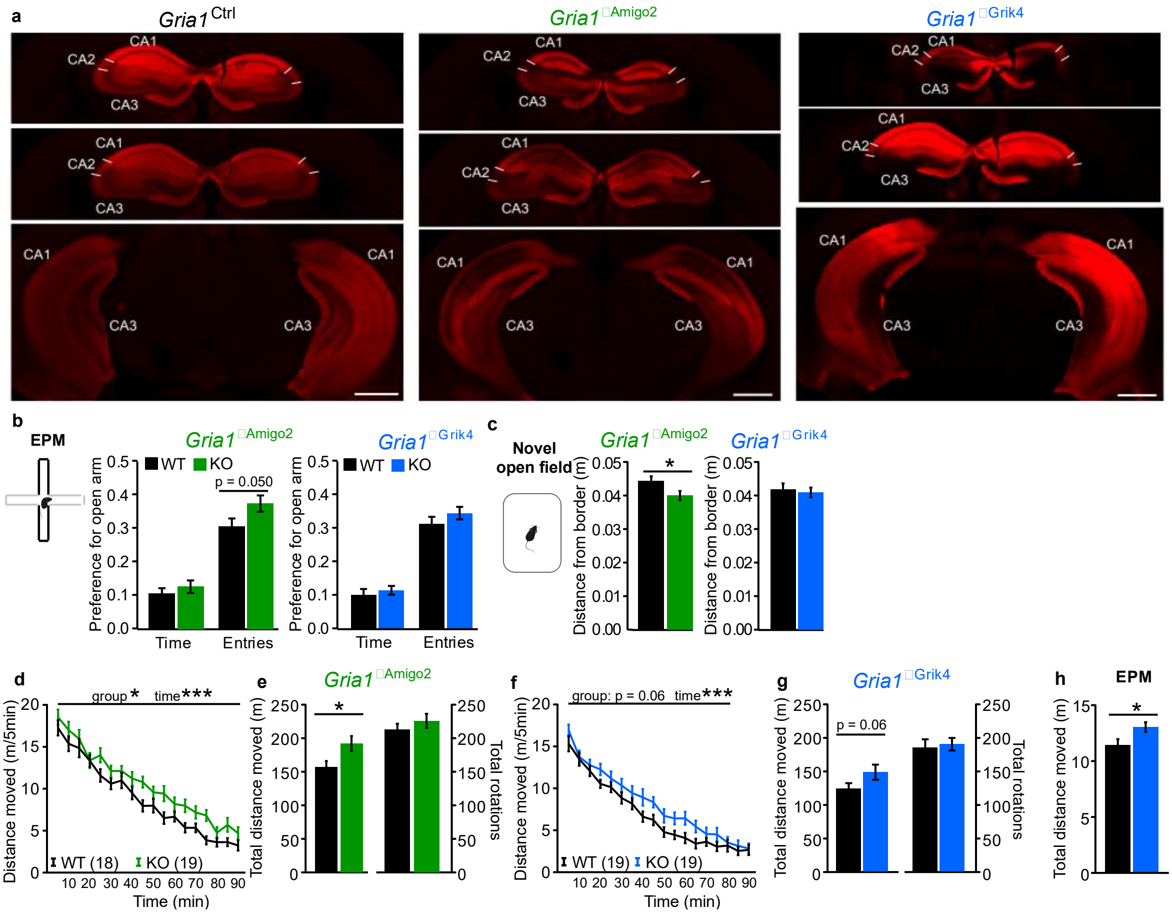

Figure 3.5.1: Ablation of GluA11 from CA2/CA3 mildly elevates locomotion.
(**a**) Confocal images of anti-GluA1 staining (red) of slices of dorsal (top) and ventral (bottom) hippocampus from the groups named above. Scale bar, 1 mm. (**b**) Preference (time and entries) for the open arm on the EPM. (**c**) Average distance from border during 90 min locomotor activity measurement in a novel open field. (**d-g**) Novelty-induced locomotor activity displayed in 5 min intervals (d, f) or as total distance moved (e, g). (**h**) Distance moved on the EPM. In (b-h), the cohort is identified above the panels and colour-coded, with KO-mice and control groups of each cohort in colour and black, respectively. *N*-numbers stated in (d, f). The two cohorts were treated separately for statistics. Repeated measures-ANOVA was used for analysing data over time (d, f), univariate ANOVAs for the remainder, ANOVAs used genotype and sex as independent

variables. All graphs represent mean ± s.e.m. *** $P < 0.001$, * $P < 0.05$. Post-mortem histology was conducted by Kasyoka Kilonzo, Dennis Kätzel, and Stefanie Schulz.

3.5.2 GluA1-hypofunction in CA2/CA3 impairs short-time habituation

Short-term habituation to sensory stimuli is strongly impaired by global *Gria1*-knockout, entailing deficits of object-related and spatial novelty-preference in the novel-object recognition and Y-maze tests, respectively [29, 380]. Both tests were conducted in *Gria1*$^{\Delta \mathrm{Amigo2}}$ and *Gria1*$^{\Delta \mathrm{Grik4}}$ mice. In the Y-maze, GluA1 ablation from CA3 excitatory cells caused reduced spatial novelty preference in terms of entries into the novel vs. the familiar arm at young age and in terms of time spent in the novel vs. the familiar arm at old age, whereas *Gria1*$^{\Delta \mathrm{Amigo2}}$ mice showed no significant alterations on the task (Figure 3.5.2a-c).

In addition, object-related short-term habituation was tested by assessing the preference for a novel object relative to an object that mice familiarized with immediately before the preference test. In contrast to spatial short-term habituation, a deficit of novel object recognition was seen both in *Gria1*$^{\Delta \mathrm{Amigo2}}$ and *Gria1*$^{\Delta \mathrm{Grik4}}$ mice as the preference index for the novel object was significantly lower in both groups compared to the respective control mice (Figure 3.5.2g). However, only *Gria1*$^{\Delta \mathrm{Amigo2}}$ mice displayed strongly increased exploration of all types of objects in all phases of the task, suggesting a profound deficit of object-related short-term habituation (Figure 3.5.2d-g).

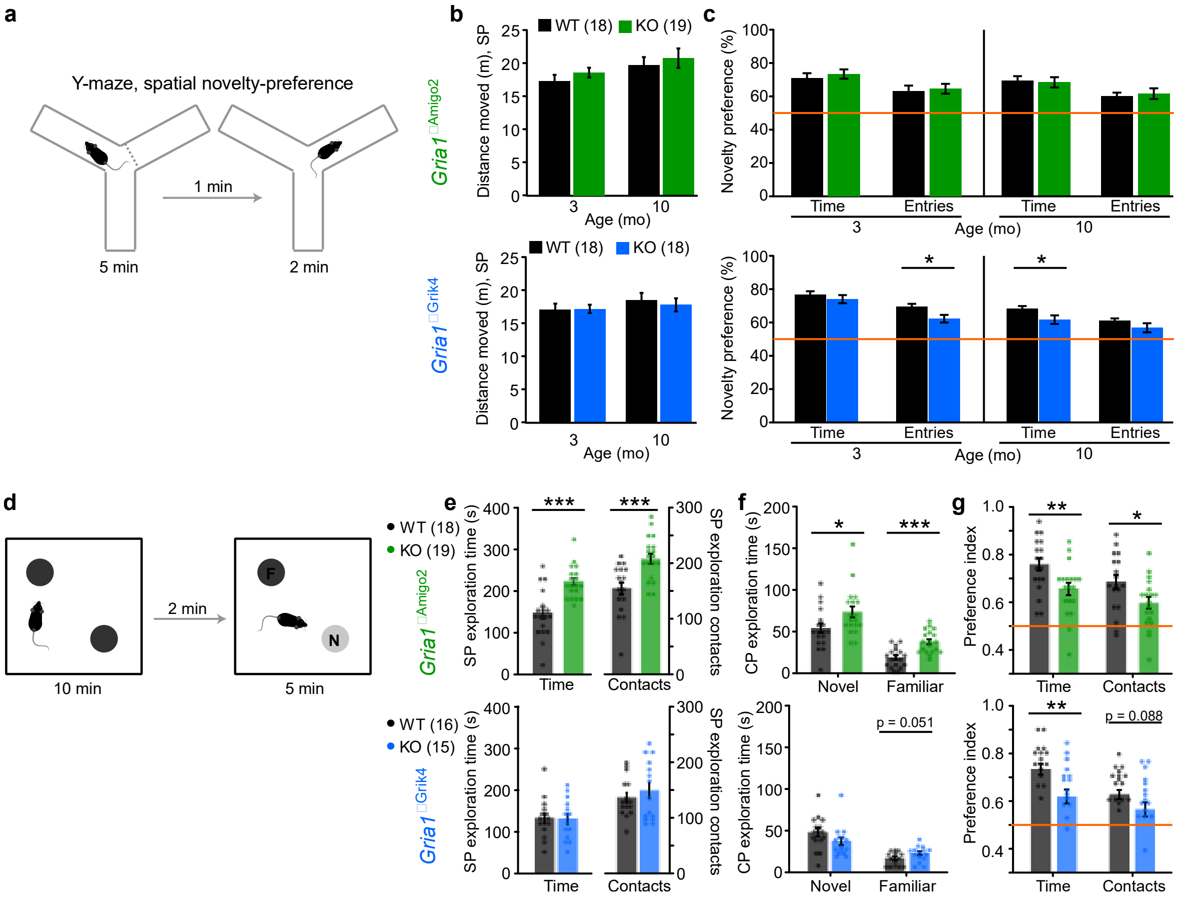

Figure 3.5.2: Ablation of GluA1 from CA2/CA3 impairs short time habituation.
(**a**) Illustration of Y-maze SNP task of spatial short-term habituation. (**b**) Locomotor-activity in the sample phase (SP) for the cohorts stated on the left test at different ages (x-axes). (**c**) Preference for the novel arm in the test phase of the Y-maze, conducted at the indicated ages, calculated from residence time or number of entries, as stated. Stated N (b) refer to the test at old age, while the full cohorts participated in the first test. (**d**) Illustration of the novel-object recognition test (NOR) of object-related short-term habituation. (**e**) Exploration of the two identical objects in the sample phase measured as interaction time (left) and number of contacts (right). (**f**) Interaction time with novel and familiar object in the NOR choice phase (CP). (**g**) Preference for the novel object calculated as interaction with novel object relative to interaction with both objects combined using interaction time or the number of contacts as indicator. In (b-c, e-g), the cohort is identified above the panels and colour-coded, with KO-mice and control groups of each cohort in colour and black, respectively. *N*-numbers stated in (b, e); the two cohorts were treated separately for statistics. Univariate ANOVAs were used for the remainder using genotype and sex as independent variables. Dot graphs represent individual mice, all other show mean ± s.e.m. Orange line indicates chance level, where applicable. *** *P* < 0.001, ** *P* < 0.01, * *P* < 0.05. The NOR-test was conducted by Vivien Prex and Dennis Kätzel, the Y-maze testing was supported by Sampath K.T. Kapanaiah.

3.5.3 Altered social behaviour in *Gria1*$^{\Delta Amigo2}$ mice

Ablation of synapses from Amigo2-positive cells in the hippocampus was shown to entail a deficit of social short-term memory [201] and of representation of social novelty by CA2-activity [127], but whether AMPARs are involved in these processes is unknown. Therefore, we conducted a reciprocal sociability test in a familiar environment at the beginning of the test battery, and found that, *Gria1*$^{\Delta Amigo2}$ – but not *Gria1*$^{\Delta Grik4}$ – mice showed a strongly reduced social interaction (Figure 3.5.3b-d). At older age, we repeated the test, albeit with an additional novelty-based social memory test an hour later (analogously to [201]; Figure 3.5.3a). At this later stage, sociability was normal, but the social novelty preference score was not different from chance level in both *Gria1*$^{\Delta\text{Amigo2}}$ and *Gria1*$^{\Delta\text{Grik4}}$ mice (but was also only marginally above chance level in controls; Figure 3.5.3b-e). For further exploration, we applied the 3-chamber task with a modification (analogously to [201]) that allowed to discriminate between social novelty- and genuine social memory effects by testing separately for social novelty-preference (using cage-mates as control stimulus condition; Figure 3.5.3f). Briefly summarised, *social preference* (sociability) was tested by introducing a cage mate and a mouse-sized dark sponge, *social novelty preference* by introducing an unfamiliar mouse together with the same cage mate, and *social short-term memory* by introducing another unfamiliar mouse together with the previously familiarised novel mouse (Figure 3.5.3f).

During the *sociability phase* we found that *Gria1*$^{\Delta\text{Amigo2}}$ mice were normal, but *Gria1*$^{\Delta\text{Grik4}}$ mice showed enhanced social interaction as they visited their cage mate more often (relative to investigations of the inanimate sponge) than their control group (Figure 3.5.3g). While both transgenic GluA1-ablation models showed normal social novelty-preference, only *Gria1*$^{\Delta\text{Amigo2}}$ mice showed a deficit in *social short-term memory* indicated by a chance level preference score ($P > 0.3$, one-sample t-test; note that due to high variability the difference to control mice reached only trend-level; Figure 3.5.3g).

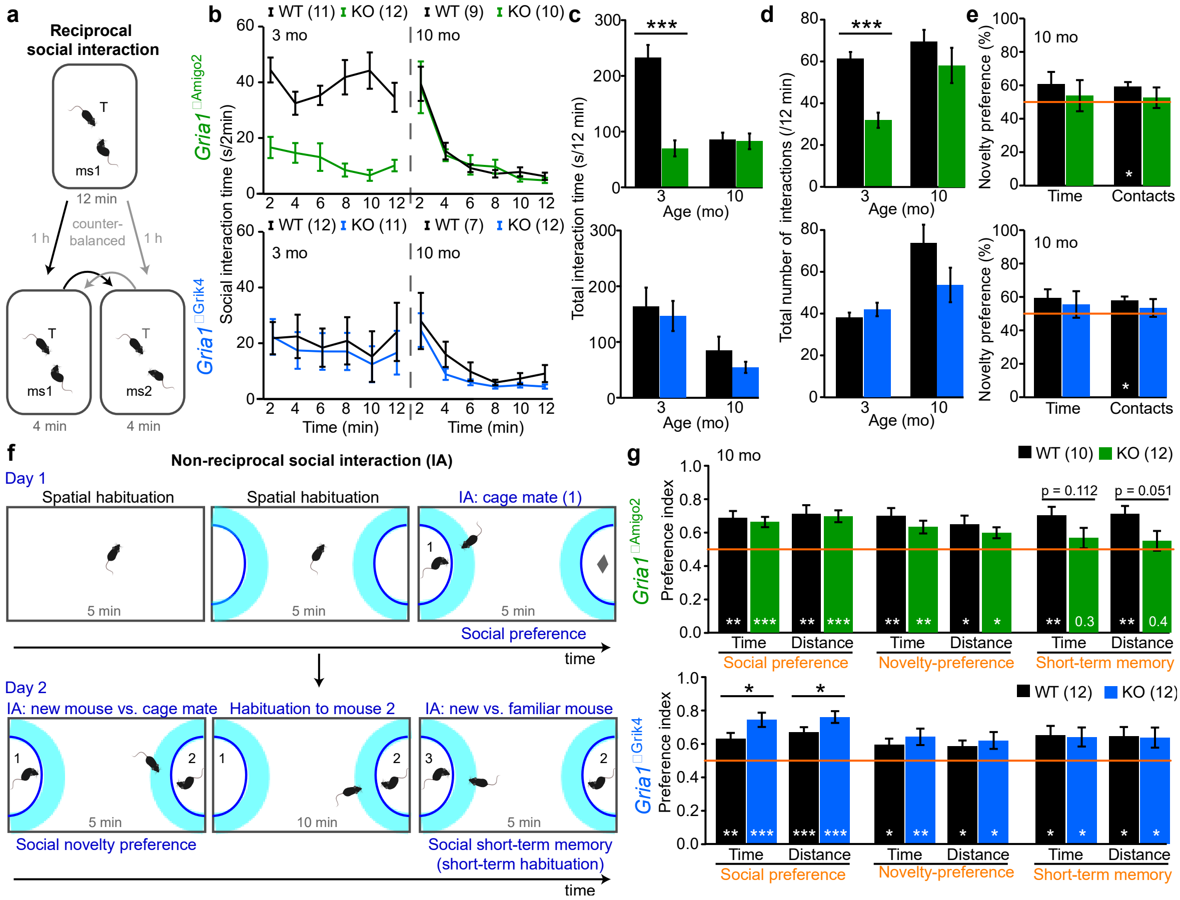

Figure 3.5.3: Ablation of GluA1 from CA2/CA3 alters social behaviour.
(**a**) Illustration of reciprocal social interaction assay with memory phase 1h later; see 2.3.3. (**b**) Social interaction time in 2 min intervals in the cohorts named on the left for the first 12 min exposure, tested at two different ages (stated in upper left corner). (**c**) Same as (b) but summed up total interaction time. (**d**) Total number of interactions in 12 min. (**e**) Preference for novel mouse calculated as interaction with novel mouse relative to sum of interaction with both mice using interaction time or the number of contacts as indicator. (**f**) Illustration of phases of 3-chamber task (omitting habituation to small compartments on the prior day and a 5 min habituation phase on day 2); see 2.3.3. (**g**) Preference indexes for the three test phases named in orange in (f) and (g) each calculated either from the time spent in the interaction zone around the lateral compartments (cyan in (f)), or from the distance the head of the animal moved inside the interaction zone, as stated. The *social preference* refers to the preference for the compartment with a cage-mate compared to the compartment with a mouse-sized object, as determined in the last phase of day 1. Novelty-preference refers to the preference for an unknown mouse compared to a cage-mate. Short-term memory refers to the preference for another novel mouse compared to the mouse that has become familiar across the two immediately prior phases on day 2. All data shown in (b-e, g) is from male mice and the cohort is identified on the left of (b, g) and colour-coded, with KO-mice and control groups of each cohort in colour and black, respectively. *N*-numbers stated in (b, g), although some mice were excluded for the memory test (e); the two cohorts were treated separately for statistical comparison between wildtype and control data with univariate ANOVAs. White stars and numbers indicate result of one-sample *t*-test against chance level (orange line). All graphs show mean ± s.e.m. *** $P < 0.001$, ** $P < 0.01$, * $P < 0.05$. Experiments were supported by Stefanie Schulz, Vivien Prex, and Dennis Kätzel.

4 DISCUSSION

The objectives of this thesis were to explore the neural basis of WM by analysing multiple measures of LFP-based connectivity in mice and humans using a novel ML approach and to further scrutinize the role of GluA1-containig AMPARs for various forms of short-term memory, including WM and short-term habituation. In addition - to allow for an optimal connectivity analysis in the first place - the most widely applied measures of interregional directed and non-directed neural connectivity were comparatively examined in awake mice recorded during the open field test with chronically implanted field electrodes.

To investigate WM-related connectivity, firstly, a cohort of *Gria1*-KO and WT mice was trained and tested on multiple WM paradigms using a novel operant box system and the conventional T-maze. Simultaneously, field recordings from frontal, temporal and thalamic brain regions were obtained, and measures of connectivity were calculated on a single-trial basis to investigate the neural basis of WM using a newly designed approach of ML-based decoding of individual WM-mediated choices. Additionally, this approach was also applied to a publicly available dataset of intracranial recordings made in human subjects while they performed three distinct visual WM tasks with transiently implanted surface field electrodes. In a separate project, various forms of short-term memory were assessed in two transgenic mouse lines, in which GluA1 was selectively ablated from excitatory cells of either the CA2 or the CA3 subfield of the hippocampus.

In the following, results from each part will be summarised and reviewed in context of the current literature regarding their relevance, limitations, and future implications.

4.1 ELEVATED THETA-BAND CONNECTIVITY ACROSS THE BRAIN DURING EXPLORATION IN *GRIA1*$^{-/-}$ MICE

Following up on a previous study from our laboratory [76], in which the coherence *between* and power and PAC *within* the PFC and dHC were examined during novelty-induced locomotion, we aimed to further elucidate the underlying pathophysiology of hyperlocomotion of *Gria1*$^{-/-}$ mice. This thesis work replicated this robust hyperactivity phenotype [53, 76, 471] and analysed LFP data from field electrodes chronically implanted in the PFC, dHC, and vHC by calculating a large number of commonly used measures of inter-regional neural connectivity. We found that elevated theta-band connectivity in *Gria1*$^{-/-}$ mice could be found in all examined connections and across all measures of non-directed synchrony (coherence, wPLI, PLV and PPC). Furthermore, the PFC-dHC connection showed reduced gamma-band connectivity in all measures. Bygrave et al. suggested a hippocampal origin of the theta hyperconnectivity phenotype since viral rescue of GluA1 in the hippocampus was able to restore normal theta coherence [76]. This hypothesis could be confirmed in the present work since theta-band GC departed in either subdivision of the hippocampus. However, other measures of directed synchrony (PDC, DTF, SPC) were only partly able to recapitulate these findings, calling for a cautious application of all of those measures in order to obtain a full and fine-grained picture of connectivity across the brain. Apart from the characterization of the pathological connectivity in *Gria1*-KO mice, we also investigated and discovered discrepancies between the various connectivity measures which is discussed in broader detail in 4.2.

Regarding clinical relevance of these findings, it is important to note that hyperconnectivity and EEG disturbances in general are reliably found in schizophrenia patients [146, 254] and might serve as potential biomarkers in the future [246, 268, 443]. To find proper treatment strategies it might therefore be crucial to find the underlying pathophysiology of these electrophysiological alterations, first and foremost in animal models. Growing evidence suggests that the *Gria1* mouse might serve as a suitable model for schizophrenia as it displays several behavioural abnormalities related to the disease such as hyperlocomotion and impaired SWM and attentional regulation of salience attribution to novel stimuli [28, 29].

4.2 Substantial lack of redundancy between a broad number of measures of connectivity

We examined the level of redundancy and experimental contingencies of the most widely applied measures of interregional directed and non-directed neural connectivity that are obtainable when recording LFP and MUA with chronically implanted field electrodes in awake mice. This analysis revealed a surprisingly large absence of redundancies between such metrics which suggests that the implicitly held belief that experimental results obtained with one metric of connectivity would allow *general* deductions about aberrations in inter-regional functional connectivity is problematic.

While this finding was somewhat expected *a priori* when regarding metrics of distinct conceptual foundation – e.g., non-directed synchrony vs. measures of causation – the lack of similarity even within the same analytical category is unreckoned. From a conceptual perspective, the results reveal the absence of a concrete empirical counterpart of the rather interchangeably used terms of inter-regional *communication*, *coupling*, *information transfer*, or *functional connectivity.* Given these contingencies of a result obtained with any single metric, it is difficult to equate it with the too generic concept of *neural communication*.

Intriguingly, a comparable conclusion has been reached by a recent study on connectivity measures applied on human EEG data [149]. In this study, the authors analysed a freely available resting-state EEG dataset and questioned the vast proliferation of different approaches and their capricious use in the literature in order to capture *functional connectivity*. To this end, they computed multiple measures of connectivity (for a brief review see 1.2.1 and Table 1.2.1) such as PLV, PPC and wPLI and concluded, similarly to our study, that the often arbitrary choice of the applied measure might have detrimental effects on the reported conclusions across different studies and that the term *functional connectivity* is misleading and should therefore be used much more carefully [149].

A particular analytical problem appears to be the lack of benchmarking of the sensitivity, specificity, and robustness of the individual measures against a ground truth of actual physiological trans-synaptic activity along anatomically verified connections. Notably, we here, like previous studies, found evidence for significant causal influence not only along the direct anatomical projections – dHC→vHC [47, 428], vHC→dHC [47] and vHC→PFC [47, 221, 410, 426] – but also along the PFC-dHC connection that is mediated only *indirectly* via the nucleus reuniens [452, 453], and even in the direction for which no obvious anatomical correlate has been described yet to our knowledge (PFC→vHC [47]), which complicates the validation and interpretation of the functional connectivity measurements.

In absence of such benchmarking and while facing considerable logistical limits in applying multiple referencing and multiple metrics for every experiment, our analysis at least qualitatively implies some guidelines on how to maximize the analytical advance from similar experiments by proposing a set of coupling metrics suited for a rather comprehensive, yet *non-redundant* analysis of inter-regional communication:

Firstly, we demonstrate that some mathematically related measures *do* actually show a pairwise redundancy and hence do not need to be included into the same analysis, namely PPC and PLV [36], parametric and non-parametric GC (allowing for considerably faster computation by using the non-parametric approach [121]), and PDC and DTF [19, 50, 233].

Secondly, beyond these reliable redundancies, we found further partial redundancies across connections, genotypes and frequencies helping to narrow the list of metrics to include in an analysis, further. Most importantly, PPC and PLV also showed considerable overlap with both the magnitude and (to a lesser degree) the phase angle of coherence, and medium average correlations with wPLI, PDC, and DTF. Also, coherence phase angle correlated broadly at a medium average level with coherence amplitude, PDC, DTF, GC and npGC in addition to PLV and PPC. Additionally, coherence magnitude often correlated with wPLI, suggesting, for practical purposes, that an assessment of two pairs of metrics – PPC and coherence phase angle, or coherence magnitude and wPLI – would be a useful first-pass approach to survey LFP data for possible aberrations in functional connectivity, which can then be followed up with mutually non-redundant directed metrics. However, it is important to note that coherence phase angle did not capture *between genotype* effects that were seen with other measures (Figure 3.1.3).

Thirdly, while in such further analysis GC and PDC (or DTF) may seem particularly attractive metrics given that they provide a more fine-grained picture of coupling in distinct directions and may be interpreted as indicators of causal influence between two brain regions, it is important to note that they do not yield similar results even though they are sometimes (erroneously [30]) equated. Despite some correlations between PDC (and DTF) with PLV, PPC, and coherence phase angle in the correlation analysis (Figure 3.1.5, Figure 3.1.6), there were actually considerable and irresolvable discrepancies between these measures in the genotype-comparison (compare Figure 3.1.2 with Figure 3.1.3d-f). For instance, genotype-related differences in PFC-dHC gamma-range coupling seen across all measures of synchrony and coherence phase angle, were not uncovered by PDC, while the reverse was true for the vHC-dHC connection. Therefore, PDC/DTF and GC may serve as complementary metrics rather than surrogates and are in combination suited for an educated assertion about directed communication.

Fourthly, spike-phase and phase-amplitude coupling take on a special role as they cannot be expected to be equivalent to any of the other parameters because they capture interdependencies between spikes and LFP and between distinct LFP frequencies respectively and are therefore useful to include to deliver a *different perspective* on functional connectivity. While this may have been expected given their distinct biological nature, the degree of absence of redundancy is nevertheless astonishing. Therefore, when adding further metrics to the analysis, SPC and PAC would be the measures of choice because they correlate least with the other measures, including GC, both in the bivariate correlational analysis within subjects and with respect to detecting genotype-related effects. It should be noted, however, that the presented SPC analysis using MUA [4] is likely far from optimal given that units cannot be chosen by movement of the electrodes and not properly sorted. The recording of single-unit activity from moveable electrode bundles or arrays [401, 434] will certainly improve the assessment of SPC and its related directed measures.

The analysis discussed in this section informed the choice of metrics for the analysis of the subsequent WM experiments. For non-directed measures, coherence and wPLI were included as they are largely non-redundant; for directed measures, GC and PDC were used for the same reason; PAC was included as it contains exclusive cross-frequency information and is non-redundant with almost all other measures. SPC was not applicable due to the short trial length leading to too few spikes per time frame to calculate reliable coupling. Amplitude cross-correlation and coherence phase angle were not applied because they were shown to be unsensitive to aberrations detected with other measures. The remaining measures were excluded because of obvious redundancies with the included measures.

4.3 Choice of reference location is crucial for identifying differences using LFP-based connectivity

A prefrontal or cerebellar placement are potential locations for a reference electrode in rodent studies. When analysing the PFC, the distance of the reference electrode to the analysed brain regions plays an important role because it might obscure biological effects. We therefore sought to systematically investigate this issue by recording from both reference locations in order to be able to digitally re-reference the recorded signals. We found a worrying contingency with respect to the location of the reference electrode and, as shown in Figure 3.1.8, connectivity involving the PFC is most strongly affected by the choice of reference location. These findings advocate, that experimental results obtained with one configuration for referencing do not deliver the complete picture of inter-regional functional connectivity. Therefore, for LFP-based measures, the reference electrode should be placed in a brain structure that is largely separate from the brain regions between which connectivity is studied. A frontal electrode may easily obscure phenotypes in prefrontal connectivity as it may pick-up field potential signals from the PFC [197, 230]. It was argued that the LFP might not be as local as its name suggests, therefore, it should be of high importance to keep enough distance between the recorded region of interest and the reference location [197, 230]. Contrary to this, Katzner et al. revealed that LFPs in the visual cortex mainly stem from sources within 100µm of the respective recording point, with evident influences coming from up to within 250µm [241] and Xing et al. found a spatial spread of around 200-400µm [482], both studies suggesting that LFPs are in general local phenomena. However, Kajikawa and Schroeder demonstrated that the lateral and vertical spread of the LFP can reach well beyond 400µm [230] which is in line with previous findings that propose a larger spatial spread up to 3mm [46, 327, 463]. These studies question the widely held belief that indirect currents picked up as LFP can be complementary to directly measured, local action potentials, because exact spatial localization of the LFP source is problematic [135, 230, 231].

The present study supports the notion that some reference locations may obscure biological changes while others are more favourable, as it provides a systematic comparison of two reference locations [1, 345, 401, 434].

4.4 Tests of working memory in mice

In this study, we were able to show for the first time that healthy mice are capable of learning several WM tasks with opposing rules consecutively, namely a DMTS 5-CSWM task, a DNMTS T-maze and a DNMTS 2-CSWM task (Figure 3.2.1). Previous studies implemented the DMTS 5-CSWM task (termed CAM task) in rats [97] and mice [437]. Here, *Gria1* KO and WT mice were first trained on this task until they reached solid above chance level performance, then they underwent surgery for electrode implantation and were subsequently retrained on the DMTS assay (for a timeline of WM experiments, see Figure 3.2.1). After successful completion of several challenges with simultaneous recordings, they were shifted to the T-maze where they effectively adopted a rewarded alternation (DNMTS) paradigm. (Implementing a *DMTS* paradigm in the T-maze is not possible because mice naturally tend to novelty-seeking behaviour by entering the previously unentered arm.) After that, mice were again transferred to the operant boxes where they learned the DNMTS 2-CSWM task with only the second and fourth hole being illuminated (making it similar to a task developed by [178]). This paradigm was then used for challenge experiments with simultaneous recordings because mice failed to acquire the 5-choice (5-CSWM) version of the DNMTS paradigm (in line with previous data, [437]). In contrast to the T-maze, spatial cues for exploration (or spatial novelty in general) do not play a major role since the mouse resides in the same box all the time and hence, choice options (illuminated holes) are presented within the same setting. Nevertheless, learning the DNMTS 2-CSWM task after the other two paradigms still has to be considered a challenging task for mice, as the stimulus that was previously presented has to be ignored in order to obtain a reward. These findings, together with the previous study that firstly proposed operant 5-CSWM testing in mice [437], add a valuable repertoire of tasks that capture different aspects of WM in mice. This is underlined by our electrophysiological findings that point to the fact that mice use different neural mechanisms to solve different tasks what makes them even harder to compare and makes them seem complementary rather than interchangeable (see 4.5.1). This is also supported by the finding that mice with NMDAR-hypofunction in excitatory cells in the PFC were impaired in the 5-CSWM paradigm but performed normally on the T-maze [245] whereas the reverse is the case for mice with hippocampal GluA1 ablation (Kilonzo et al., in preparation).

Though, it is noteworthy that training and testing mice on operant tasks requires a more extensive setup, custom-made equipment to measure electrophysiology simultaneously, and time and labour for several months of training compared to the conventional T-maze.

4.5 Working memory related choices can be predicted trial-by-trial by LFP-based measures

Using a combination of WM-testing, simultaneous electrophysiological multi-site recordings and ML, we reveal that WM-related choices can be predicted trial-by-trial in mice and humans by linear decoding of high-dimensional arrays of LFP-based measures of inter-regional connectivity or local activity (the *electome*). In mice, we analysed signals from the chronically implanted depth electrodes and calculated a largely non-redundant set of measures of inter-regional and local activity (4.2). In humans, an openly available dataset of recordings made with iEEG electrodes during WM testing were used and the same measures were calculated.

The high decoding accuracies of around 90% (compared to a chance level of 50%) achieved in both species are remarkable in multiple respects, including the spatially coarse nature of the extracted neural signal (see 4.3 and [230]), the short – often sub-second – data traces used to calculate predictors, the intrinsic variability caused by merging data from all analysed subjects with varying electrode placements, and the lack of precise neuronal information as encoded in spike trains of individual neurons [56, 410, 419, 475]. Our novel approach utilizes the trial-by-trial predictive capacity of physiological activity as an indicator for its association with WM, and thus enabled a largely unbiased top-down analysis to reveal an unexpectedly rich pattern of frequency-specific connectivity and activity changes during individual phases of distinct WM assays in mice and humans.

4.5.1 Prediction of working memory in healthy subjects

The comparative analysis of multiple WM assays in mice - including those that allow control over basic motivational and attentional parameters - provides the unique advantage that neurophysiological activity patterns that might be truly relevant to WM may be isolated. In this way, we could reveal MD-PFC δ– and β-range coupling during memory encoding and maintenance, respectively, as well as vHC-PFC and vHC-dHC δ/θ-coupling during retrieval as common connectivity patterns across all three rodent tasks - whereas the vast majority of connectivity proved to be task-specific (Figure 3.2.11a-c).

Against a backdrop of widely varying claims about which kind of neural connectivity underlies WM (Table 1.6.1), our initial intention was to establish an unbiased analytical pipeline to extract “true” anatomical and frequency-related WM-correlates using the predictor weights generated by the linear classifiers that decode WM-based choices with high accuracy. Our results, however, refute some implicit key assumptions of this endeavour – and, by extension, of many prior investigations of WM-correlates:

Firstly, there is no single – or small set of – anatomical regions or connections, types of directed information transmission, or frequency bands that can be regarded as a unique *WM correlate*. Recalling the streetlight effect (overestimation of already known, and neglect of possible other, electrophysiological features, see 1.6.2 and [111]), previously suggested *correlates*, especially in the rodent literature (Table 1.6.1), could be identified as such only because the whole quantity of connections and measures investigated in each study was rather small, as opposed to the minimum 888 metrics analysed here in mice. In our study virtually every analysed frequency band, metric, connection, and region bore some predictive power regarding WM-mediated choice and significantly differed between correct and incorrect choices in some instances.
Notably, when reconsidering the issue of volume conduction, one would expect that *activity in* and *connectivity between* all brain regions would be equally proficient in predicting behavioural outcome because similar information is allegedly recorded at each site due to spread across the brain. However, this is not the case since distinct differences in predictive performance between brain regions and connections emerged and the classifier apparently found distinctive features which yielded varying predictive power.

Secondly, there is no single behavioural WM-task that could be regarded as *representative* of the broad psychological construct termed “working memory” in order to allow the identification of *the* neurophysiological correlate of that construct. This is illustrated by the enormous variability in the patterns of predictive connections and metrics across task-paradigms in both species. In mice, the diversity of predictive parameters between the three tasks and the relative predominance of SP and delay parameters in the T-maze compared to the other tasks is reflective of the variety of connectivity parameters that have been associated with T-maze performance in prior studies (Table 1.6.1), and the relatively detrimental effects of optogenetic manipulations in the SP and delay of the T-maze, as compared to the CP [56, 295, 410]. In other words, a physiological variable that correlates with choice accuracy in the T-maze represents a neurophysiological correlate of T-maze performance, but not necessarily of WM. The same principle applies to our cross-species comparison, as the uncovered candidates for a generic (task-independent) WM correlate originated from different frequency bands in humans (γ) than in rodents (δ–θ–β). A translational implication of these findings is that it is likely impossible to define neurophysiological underpinnings of "working memory" as a uniform psychological construct. However, the *RDoC* explicitly assumes the existence of certain tasks that represent such a psychological function, i.e., that engage a physiological mechanism that is central to all WM tasks across species, and further envisions to apply those representative paradigms to identify WM-enhancing cellular and molecular targets (see 1.1 and [113, 114]). When trying to accommodate this approach, our data would suggest that the key target variable in the preclinical discovery of WM-enhancing compounds might be the appropriate regulation of γ-range connectivity (given its importance for human WM) rather than behavioural performance in any particular rodent task.

4.5.2 Working Memory is not tied to one area or connection

Compared to the presented rodent results, the analysis of the human dataset, in particular, paints a rather different picture of what a correlate of WM could look like – at least when searched for in LFP-data. In all three tasks, prediction accuracies calculated from connectivity (as opposed to local activity) metrics were not only very high, but it was also roughly *equal* between the three analysed connections, even though these are anatomically quite distinct. This was the case even with the limited analysis incorporating only SP or post-cue delay connectivity as predictors of spatial WM. These findings may be taken as an indication that WM-related information is extremely broadly distributed, and - rather than specific activity located in a specific connection or region - it is the ability to manipulate information flow across brain regions *as such*, that determines task performance [227, 293]. Matching this observation, the body of studies implicating several brain regions in WM including the superior frontal [296], anterior cingulate [330, 331] and sensory cortex [137, 169], VTA [130], and the nuclei of the midline and anterior thalamus [188, 262, 295] is constantly growing. Also, our results are consistent with findings from Gilad et al. who found that mice were able to adopt various strategies to solve short-term memory tasks which are linked to activity in different areas of the neocortex and that the disruption of one strategy led to the switch to another [169].

An unexpectedly broad anatomical representation of sensory and behavioural information has recently been uncovered also by decoding activity of individual neurons or EEG in multiple cortical areas [191, 216, 224, 307]. E.g., Insanally et al. investigated the predictive power of non-classically responsive cortical neurons – neurons that do not exhibit a discernible response to certain trigger events and are therefore often omitted from further analysis – and found that including activity traces of these neurons drastically improved decoding of sensory stimuli (two distinct tones) and behavioural decisions (poking into two separate holes depending on the presented tone) [216]. Indeed, they revealed that these non-classically responsive neurons do not show obvious correlation to the animal's behaviour, but, however, that the spike intervals contain valuable information and that the neurons seem to work together in groups to encode information - which was also uncovered using a ML based decoding algorithm [216]. So, their approach very much resembles our study as we also made no a priori assumptions about what frequency range and what connection to primarily focus on (in contrast to the studies displayed in Table 1.6.1) and used a purely data-driven ML algorithm to detect the underlying connectivity in the brain during WM.

Also, in movement decoding in Parkinson's patients, it was shown that grip force could be decoded with higher accuracy when considering whole brain activity based on EEG power and MRI connectivity than decoding from LFP-traces from the subthalamic nucleus alone [307]. This study widens the range of surgical treatment options because their approach enables clinicians to determine the best trajectory individually for each patient taking into account their whole brain activity [307].

With regards to schizophrenia, Johannesen et al. challenged and circumvented the commonly used approach of determining and selecting EEG features *a priori* in order to identify possible correlates of WM performance in schizophrenia and healthy adults by using a linear classifier which was trained with local, frequency-resolved power values from three scalp sites and predicted trial accuracy and diagnosis, respectively [224]. With their study, the authors were able to uncover already known and novel features which might have gone undetected when not considering whole brain dynamics which is why their study might serve as a role model for future studies trying to differentiate between conditions and diagnoses using EEG in an unrestricted and objective way.

The studies from Insanally et al., Hattori et al., Merk et al., Johannesen et al. and ours clearly demonstrate that complex behaviour such as decision making, complex motor function and WM most likely cannot be traced back to a single underlying region or process but are rather distributed across various circuits of the brain. To capture these dynamics, ML-based decoding algorithms as implemented in this thesis and in the other cited studies seem the most suited strategy to identify relevant circuits in a rather unbiased (top-down) manner.

On the other hand, somewhat arguing against the necessity of such a vast distribution of connectivity in WM for successful task performance, is a recent study which showed that WM could be revived in the elderly by applying transcranial alternating-current stimulation (tACS) broadly to the left dlPFC and temporal cortex of humans [363]. They found that stimulation with a subject-specific theta frequency recorded by EEG could increase prefrontal-temporal theta-gamma PAC and significantly improve WM function for about 50 min, indicating that, while it might prove difficult to trace the neural basis of WM back to single regions, connections or frequency bands (as described in this thesis), stimulation of a single connection in a single frequency may still be sufficient to augment it [363]. Also in patients with schizophrenia, non-invasive brain stimulation especially over the left dorsolateral PFC has been shown to be effective in improving WM [223]. The methods used in these studies can be considered a coarse and non-invasive form of Brain-Machine Interfaces (BMI) which individually monitor brain activity and stimulate accordingly (e.g., with a certain frequency or at certain phases of the theta cycle). Ultimately, the approach proposed in this thesis and in other studies that try to decode cognitive functions by applying ML to neural signals could be used to individually identify brain patterns of function and, importantly, malfunction in order to stimulate or inhibit them accordingly. By that, one could overcome the restriction of applying the same stimulation protocol to all patients and step towards a more individualised, patient-based, and non-pharmaceutical manner of treatment. A technical concern, however, would be to implement this in real time because the computation of the measures described in this work is computationally intense and time consuming. Also, while such direct applications in human patients may still be a little bit farfetched, the methods described in this work could be used to investigate causal neural connectivity in preclinical models of various diseases. E.g., effects of chemogenetic, optogenetic or pharmacological manipulations in animal models could be assessed to determine the underlying circuits and their coordination into distinct networks depending on the condition. Regarding the suitability of certain pharmacological approaches, one is often confronted with the situation that their physiological mechanism remains unknown. Here, our approach could be helpful to search for patterns in brain dynamics that underlie their therapeutic effect.

4.5.3 Specific impairment of working memory in *Gria1*$^{-/-}$ mice

The notion that WM is a complex construct which is difficult to capture in a single task and whose physiological correlates are widely distributed across the brain, is further supported by our analysis of the *Gria1*$^{-/-}$ mouse line, which models schizophrenia-related deficits of WM and salience attribution and has considerable construct validity for this disease at the genetic, cellular, and neurophysiological levels (see 1.5 and [28, 29, 141]). Despite these animals' uniquely selective [385] and robust chance-level accuracy in rewarded alternation WM tasks, which does not improve with training [76, 364] as reproduced here (see 3.3), it was unknown if this represents a *genuine* WM-deficit or whether it is, at least in part, driven by impaired preference for relative spatial novelty. Our assessment in the two operant tasks confirms that GluA1-ablation genuinely impairs WM-performance, in comparison to well-trained WT mice. However, in contrast to the T-maze, in the operant assays, performance was higher than chance level and already above chance level at the start of their training in the 5-CSWM DMTS task. For the DMTS assay, the preference of these animals for familiar (as opposed to novel) stimulus [380] might help them with the task – indeed on the first few days of training, they were qualitatively better than controls and, in contrast to them, they did not further improve their performance with training (Figure 3.3.1a). This supports their usage of passive "familiarity preference" (or sensory sensitization) [380] to solve the task, at least initially, when the spatial stimuli are still relatively novel. However, if this were the only mechanism to solve the operant WM task, these animals would not perform above chance level in the DNMTS assay – which they, however, consistently do (although on a lower level than on the DMTS assay). This confirms that these mice do actually have the potential to learn new forms of WM assays.

More convincingly, the decoding analysis strongly supports the notion that the performance differences between the tasks are not simply a matter of degree of the impairment: the classifier was able to predict WM-based choices in *Gria1*-KOs as well as in WT mice for many connections or regions in both operant assays but was virtually unable to predict them in the T-maze with any appreciable accuracy (Figure 3.3.5). This suggests that, in the T-maze, the brains of these animals are indeed clueless about what constitutes the correct choice. This conclusion is further supported by the strong bias of KO-mice to turn into the same arm across the trials of a session, suggesting the adoption of an ineffective strategy that does not engage WM. This divergence of the behavioural and electrophysiological phenotypes of *Gria1*$^{-/-}$ between the operant and the maze tasks reveals stark differences between the psychological requirements these tasks actually pose despite their uniform categorization as *spatial working memory* assays.

Besides the striking divergence between the tasks, *Gria1*$^{-/-}$ mice displayed fundamental differences in the regions and connections they engage within each task compared to their WT littermates. This was analysed by comparative assessment of the overlap of predictive features between *Gria1* KO and WT mice, which revealed hardly any commonalities suggesting different communication involved in WM (see Figure 3.3.6). The few features that predicted WM in both genotypes were mainly in the gamma frequency band. Also, multi-class decoding was feasible with high accuracies (>90%) which directly implies that there are fundamental differences between tasks and genotypes. Hence, our study found several previously unknown, WM-related aberrations in LFP-based neural communication of *Gria1*$^{-/-}$ mice [76]. In contrast to prior studies which investigated differences in LFP-based connectivity in rodent mouse models of schizophrenia [1, 76, 401, 434], we aimed for a more unbiased search for WM-related connectivity by assessing a large number of mostly non-redundant measures (see 3.1.4 and [420]) and recording from 4 brain regions (instead of 2) in order to paint a comprehensive picture of oscillatory abnormalities in our mouse model. Of course, it has to be noted that our study is also far from being completely unbiased as several more brain regions should be recorded from, if technically possible.

4.6 Behavioural impact of GluA1 ablation from the hippocampal CA2/CA3 subfields

Gria1$^{-/-}$ mice display various behavioural deficits that point to a failure of short-term habituation including impaired spatial novelty preference and excessive novelty induced hyperactivity (see 1.5 and [25, 141, 359]). This failure was hypothesized to drive their increased exploratory behaviour and also links their behavioural phenotype to the theory of aberrant salience introduced in 1.1.2. It remains elusive, however, in which brain (sub-)region reduced GluA1 expression leads to this deficit. Freudenberg et al. virally reintroduced GluA1 in all subfields of the hippocampus in *Gria1*$^{-/-}$ mice and with this could rescue novelty induced hyperactivity [152]. Schmitt et al., however, could not rescue novelty induced hyperactivity by reintroducing GluA1 into the forebrain and the CA1 subfield of the hippocampus, further highlighting the possible role of GluA1 in the hippocampus, and particularly in CA3 [386]. Considering these studies, Bygrave et al. showed that selective viral reintroduction of GluA1 into CA2/CA3 combined was sufficient to restore spatial novelty preference on the Y-maze and normalize novelty-induced locomotion [76].

In the present study, we aimed to further elucidate the role of GluA1 in the CA2 and CA3 subfields of the hippocampus by taking the opposite approach – transgenically mediated selective ablation of GluA1 from excitatory cells of either CA2 or CA3 by breeding Cre-dependent conditional GluA1 KO mice with either Amigo2-Cre (expressing in excitatory cells in CA2) or Grik4-Cre (expressing in excitatory cells in CA3) lines. It was previously shown that excitatory cells of CA2 are crucial for social memory [201] and impaired CA2 firing and social behaviour was found in a mouse model of the human 22q11.2 microdeletion, a prominent risk factor for schizophrenia [127]. Our results confirm this association as selective ablation of GluA1 from excitatory cells in CA2 led to reduced reciprocal social interaction in young *Gria1*$^{\Delta Amigo2}$ mice and to impaired social short-term memory (measured during non-reciprocal social interaction). However, CA2 specific GluA1 ablation seemed to have behavioural effects beyond social memory as *Gria1*$^{\Delta Amigo2}$ mice also demonstrated mildly elevated spatial novelty-induced hyperlocomotion, strong increases of object exploration and resulting impairments of object-related short-term habituation and task-dependent mild alterations of anxiety behaviour. In contrast, in *Gria1*$^{\Delta Grik4}$ mice *spatial* short-term habituation was impaired, in addition to a mild deficit object-related short-term habituation. In the context of the theory of aberrant salience, these results suggest that the mechanism of salience attribution by short-term habituation is not a singular function organized by a single hippocampal circuit but that different circuits are engaged in dependence on the type of stimulus.

Notably, given that Amigo2-expression is broader outside hippocampus early during development [201], our use of a transgenic approach (to ensure complete GluA1 ablation from CA2 at potential expense of specificity) entails the possibility that the aberrant processing of non-social stimuli results from GluA1–ablation *outside* CA2. The extent of such non-hippocampal distribution is difficult to evaluate due to the much lower GluA1 expression (and detectability) outside hippocampus (Figure 3.5.1a), the scattered and time-dependent distribution of Amigo2-expression during development [201], and the dependence of the stochastic Cre-lox-recombination on the distance between lox-sites [40] which is smaller in typical fluorescent reporter lines (e.g. 838 bp in the widely used Ai9 and Ai14 tdTomato Cre-reporter lines) [294] than in the floxed *Gria1* line (1628 bp) [160]. Therefore, the unexpected finding of a possible association between CA2 and processing of non-social stimuli needs to be evaluated further in the future using virally mediated local manipulations [212] in combination with the tasks described here.

Intriguingly, GluA1 ablation from CA3 excitatory cells led to an increase in social preference with no impact on social memory, while Finlay et al. found that CA3 NMDAR deletion caused decreased social novelty preference [140] and Chiang et al. found that chemogenetic silencing of the ventral, but not dorsal, CA3 or deletion of the NMDA receptor subunit 1 in CA3 pyramidal cells led to a deficit in social memory (with no effect on sociability) [93], indicating GluA1-independent mechanisms of social memory in CA3. Interestingly, apart from this novel observation described in this thesis, another opposition has also been observed – CA3 ablation of NMDARs *increases* premature responding which indicates disrupted sustained attention [140], while CA3 GluA1 ablation *decreases* premature responding, i.e., an improvement of sustained attention (Kilonzo et al., in preparation).

4.7 CONCLUSIONS AND FUTURE DIRECTIONS

The precise circuit mechanisms that are involved in WM and other cognitive processes are yet to be understood. By measuring the dynamic coordination of neural activity *within* and *between* several brain regions, we can associate specific neural correlates with specific cognitive processes. To this end, this thesis has explored the redundancies between measures of neural communication and the mechanisms by which brain circuits coordinate during WM in mice and humans. A main contribution of this thesis to the field is the ML-based decoding approach of identifying electrophysiological correlates of working memory, as it challenges previous, less comprehensive, and correlational studies by including an unusually wide variety of parameters of neural communication and linking them to behavioural outcome (correct or incorrect choices) in an unbiased manner. By using this method, future studies could benefit and identify so far unknown features from electrophysiological signals during any task in animals or humans. In rodents, one could even take it one step further by manipulating the involved circuits and surveying the effects on the behavioural phenotype and decoding accuracy. We hope that using these approaches, we will be able to form a more complete understanding of the neural circuits that underlie functional and dysfunctional cognitive behaviour.
A caveat in rodent research that was emphasized by this thesis is, that one should be cautious when generalising results from one task onto other tasks which supposedly measure the same psychological construct (e.g., WM). Therefore, future studies aiming to investigate WM performance would significantly benefit from using multiple different paradigms in order to cross-validate their findings between tasks and to filter out potential confounding or highly task-specific factors.

The robust deficits in schizophrenia-related cognitive functions like WM and attentional regulation displayed by *Gria1*-KO mice - in addition to the multiple associations between *Gria1* and schizophrenia in humans - render targeted manipulations of this gene a fruitful research tool to identify neural circuits underlying these functions. The targeted knockout of *Gria1* in excitatory cells of CA2 or CA3 (hippocampal subfields where GluA1-expression is also reduced in patients with schizophrenia) could pinpoint them as important circuits for multiple forms of short-term habituation relevant to aberrant salience assignment in schizophrenia. Following similar approaches but using local manipulations with viral vectors, circuits and neuronal populations involved in these functions could be further narrowed down. For example, the role of GluA1 in the dorsal vs. the ventral hippocampus could be investigated by selectively targeting these areas and analysing behavioural and electrophysiological effects. Further, using local and Cre-dependent CRISPR/Cas9-mediated knockout in adult animals, the limitations imposed by the broader expression of the Amigo2-Cre driver line in cells outside CA2 during development could be overcome to verify that the deficits observed in the *Gria1*$^{\Delta Amigo2}$ line are truly originating from GluA1-ablation in CA2 only. These targeted knockout studies could be combined with an extended set of tasks to assess aspects of attentional control and short-term habituation-mediated salience assignment like the HORNS task or auditory stimulation paradigms (as described in 1.4 and 1.5.2) while performing electrophysiological recordings not only in the 4 regions recorded in the present study but also in the relevant sensory areas.

Therefore, both the scientific discoveries as well as the analytical tools developed in this thesis open multiple opportunities for future investigations into potential circuit mechanisms of schizophrenia-related pathologies of cognition.

5 Summary

Communication between brain areas has been implicated in a wide range of cognitive and emotive functions and is impaired in numerous mental disorders. Various metrics have been used to quantify inter-regional neural communication. However, typically only few measures of coupling are reported and, hence, redundancy across such indicators is implicitly assumed. To, firstly, test this assumption, we applied these measures to simultaneous field recordings from the prefrontal cortex and dorsal and ventral hippocampus in the *Gria1*$^{-/-}$ mouse line which globally lacks the glutamate α-amino-3-hydroxy-5-methyl-4-isoxazolepropionic acid receptor (AMPAR) subunit GluA1 and serves as a model with relevance to schizophrenia as it displays several related phenotypic abnormalities such as impaired working memory (WM) and short-term habituation. Using the detectability of coupling deficits in *Gria1*$^{-/-}$ mice and bivariate correlations within animals as criteria, we found a considerable lack of redundancy across measures of neural communication. Our analysis highlights the difficulty of quantifying real correlates of inter-regional information transfer, underscores the need to assess multiple coupling measures, and provides some guidelines which metrics to choose for a comprehensive, yet non-redundant characterization of functional connectivity.

Secondly, based on these findings, we aimed to investigate the physiological basis of WM which is the capacity to encode, maintain and retrieve mental items for a brief time period. WM is thought to be key to successful goal-directed behaviour and is impaired in a range of psychiatric disorders, especially in schizophrenia. To date, several brain regions, connections, and types of neural activity have been correlatively associated with WM performance. However, no unifying framework to integrate these findings exits, as the degree of their species- and task-specificity remains unclear. Here, we investigate WM correlates in three task paradigms each in mice and humans, with simultaneous multi-site electrophysiological recordings. In mice, we deployed novel operant delayed-matching-to-sample and non-matching-to-sample protocols in addition to the widely used T-maze alternation assay to assess WM performance. *Gria1*$^{-/-}$ mice performed above chance level, but still worse than their wildtype littermates in the operant tasks and at chance level on the T-maze. This suggests that they use different neural processes to solve each task. We then developed an approach based on machine learning to decode WM-mediated choices in individual trials across subjects from over 800 electrophysiological measures of neural connectivity with up to ~90% prediction accuracy. Relying on *predictive power* as the ultimate indicator of correlates of psychological functions, we unveiled a large number of task phase-specific WM-related connectivity from analysis of predictor weights in an unbiased manner. Mostly, the predictive activity patterns were unexpectedly specific to each task and always widely distributed across brain regions. Furthermore, in *Gria1*$^{-/-}$ mice, we were able to reliably predict WM choices in the operant tasks but not in the T-maze (mimicking their chance-level performance in the latter task). This further emphasizes the stark differences between those tasks and the specific impairments in *Gria1*$^{-/-}$ mice. Also, we could uncover noticeable differences in WM-related connectivity between genotypes, indicating different neurophysiological strategies to solve each task's demands. These results suggest that individual tasks cannot be used to uncover *generic* physiological correlates of the psychological construct termed WM which also calls for a new conceptualization of this cognitive domain in translational psychiatry.

Hippocampal expression of GluA1 also seems to play an important role in short-term habituation, a form of short-term memory that denotes the ability to decrease attention to novel stimuli as they become familiar. However, the exact circuitry within the hippocampus mediating this process remains elusive. Building upon previous studies emphasizing the role of the hippocampal subfields CA2 and CA3 in this process, we used transgenically modified mouse cohorts with selective ablation of GluA1 from excitatory cells of either CA2 or CA3 and tested them on a battery of tasks assessing short-term habituation as short-term novelty preference. This revealed a complex dissociation of different forms of short-term habituation, as GluA1-ablation from CA3 entailed a deficit in *spatial* novelty-preference whereas the same manipulation in CA2 impaired *social* short-term habituation, while both manipulations affected object-related novelty-preference, albeit in different ways.

These findings collectively underline the importance of GluA1-containing AMPARs for controlling short-term habituation and spatial WM , while simultaneously revealing that both of these cognitive functions are not singular entities but entail distinct circuit mechanisms depending on the specific task and involved stimuli.

6 References

1. Abbas AI, Sundiang MJM, Henoch B, Morton MP, Bolkan SS, Park AJ, Harris AZ, Kellendonk C, Gordon JA (2018) Somatostatin Interneurons Facilitate Hippocampal-Prefrontal Synchrony and Prefrontal Spatial Encoding. Neuron 100:926-939.e3. doi: 10.1016/j.neuron.2018.09.029

2. Acosta FJ, Hernández JL, Pereira J, Herrera J, Rodríguez CJ (2012) Medication adherence in schizophrenia. World J Psychiatry 2:74–82. doi: 10.5498/wjp.v2.i5.74

3. Adhikari A, Sigurdsson T, Topiwala MA, Gordon JA (2010) Cross-correlation of instantaneous amplitudes of field potential oscillations: A straightforward method to estimate the directionality and lag between brain areas. J Neurosci Methods 191:191–200. doi: 10.1016/j.jneumeth.2010.06.019

4. Adhikari A, Topiwala MA, Gordon JA (2010) Synchronized Activity between the Ventral Hippocampus and the Medial Prefrontal Cortex during Anxiety. Neuron 65:257–269

5. Aitta-aho T, Maksimovic M, Dahl K, Sprengel R, Korpi ER (2019) Attenuation of Novelty-Induced Hyperactivity of Gria1-/- Mice by Cannabidiol and Hippocampal Inhibitory Chemogenetics. Front Pharmacol 10. doi: 10.3389/fphar.2019.00309

6. Akam T, Kullmann DM (2010) Oscillations and Filtering Networks Support Flexible Routing of Information. Neuron 67:308–320. doi: 10.1016/j.neuron.2010.06.019

7. Akam T, Lustig A, Rowland J, Kapanaiah SKT, Esteve-Agraz J, Panniello M, Márquez C, Kohl M, Kätzel D, Costa RM, Walton ME (2021) pyControl: Open source, Python based, hardware and software for controlling behavioural neuroscience experiments. bioRxiv 2021.02.22.432227. doi: 10.1101/2021.02.22.432227

8. Amaral DG (1993) Emerging principles of intrinsic hippocampal organization. Curr Opin Neurobiol 3:225–229. doi: 10.1016/0959-4388(93)90214-J

9. Andreasen NC, Arndt S, Swayze V, Cizadlo T, Flaum M, O'Leary D, Ehrhardt JC, Yuh WT (1994) Thalamic abnormalities in schizophrenia visualized through magnetic resonance image averaging. Science 266:294–298. doi: 10.1126/science.7939669

10. Andreasen NC, Olsen S (1982) Negative v positive schizophrenia. Definition and validation. Arch Gen Psychiatry 39:789–794. doi: 10.1001/archpsyc.1982.04290070025006

11. Andreou C, Leicht G, Nolte G, Polomac N, Moritz S, Karow A, Hanganu-Opatz IL, Engel AK, Mulert C (2015) Resting-state theta-band connectivity and verbal memory in schizophrenia and in the high-risk state. Schizophr Res 161:299–307. doi: 10.1016/j.schres.2014.12.018

12. Andrews J, Wang L, Csernansky JG, Gado MH, Barch DM (2006) Abnormalities of thalamic activation and cognition in schizophrenia. Am J Psychiatry 163:463–469. doi: 10.1176/appi.ajp.163.3.463

13. Angrist B, Sathananthan G, Wilk S, Gershon S (1974) Amphetamine psychosis: behavioral and biochemical aspects. J Psychiatr Res 11:13–23. doi: 10.1016/0022-3956(74)90064-8

14. Anticevic A, Haut K, Murray JD, Repovs G, Yang GJ, Diehl C, McEwen SC, Bearden CE, Addington J, Goodyear B, Cadenhead KS, Mirzakhanian H, Cornblatt BA, Olvet D, Mathalon DH, McGlashan TH, Perkins DO, Belger A, Seidman LJ, Tsuang MT, van Erp TGM, Walker EF, Hamann S, Woods SW, Qiu M, Cannon TD (2015) Association of Thalamic Dysconnectivity and Conversion to Psychosis in Youth and Young Adults at Elevated Clinical Risk. JAMA Psychiatry 72:882–891. doi: 10.1001/jamapsychiatry.2015.0566

15. Anticevic A, Hu X, Xiao Y, Hu J, Li F, Bi F, Cole MW, Savic A, Yang GJ, Repovs G, Murray JD, Wang X-J, Huang X, Lui S, Krystal JH, Gong Q (2015) Early-Course Unmedicated Schizophrenia Patients Exhibit Elevated Prefrontal Connectivity Associated with Longitudinal Change. J Neurosci 35:267–286. doi: 10.1523/JNEUROSCI.2310-14.2015

16. Arguello PA, Gogos JA (2006) Modeling Madness in Mice: One Piece at a Time. Neuron 52:179–196. doi: 10.1016/j.neuron.2006.09.023

17. Arnedo J, Svrakic DM, del Val C, Romero-Zaliz R, Hernández-Cuervo H, Molecular Genetics of Schizophrenia Consortium, Fanous AH, Pato MT, Pato CN, de Erausquin GA, Cloninger CR, Zwir I (2015) Uncovering the Hidden Risk Architecture of the Schizophrenias: Confirmation in Three Independent Genome-Wide Association Studies. Am J Psychiatry 172:139–153. doi: 10.1176/appi.ajp.2014.14040435

18. Axmacher N, Henseler MM, Jensen O, Weinreich I, Elger CE, Fell J (2010) Cross-frequency coupling supports multi-item working memory in the human hippocampus. Proc Natl Acad Sci 107:3228–3233. doi: 10.1073/pnas.0911531107

19. Baccalá LA, Sameshima K (2001) Partial directed coherence: a new concept in neural structure determination. Biol Cybern 84:463–474. doi: 10.1007/PL00007990

20. Bachiller A, Poza J, Gómez C, Molina V, Suazo V, Hornero R (2014) A comparative study of event-related coupling patterns during an auditory oddball task in schizophrenia. J Neural Eng 12:016007. doi: 10.1088/1741-2560/12/1/016007

21. Baddeley A (1992) Working memory. Science 255:556–559. doi: 10.1126/science.1736359

22. Baddeley AD, Hitch G (1974) Working Memory. In: Bower GH (ed) Psychology of Learning and Motivation. Academic Press, pp 47–89

23. Ballard TM, Pauly-Evers M, Higgins GA, Ouagazzal A-M, Mutel V, Borroni E, Kemp JA, Bluethmann H, Kew JNC (2002) Severe impairment of NMDA receptor function

in mice carrying targeted point mutations in the glycine binding site results in drug-resistant nonhabituating hyperactivity. J Neurosci Off J Soc Neurosci 22:6713–6723. doi: 20026610

24. Bannerman DM, Bus T, Taylor A, Sanderson DJ, Schwarz I, Jensen V, Hvalby Ø, Rawlins JNP, Seeburg PH, Sprengel R (2012) Dissecting spatial knowledge from spatial choice by hippocampal NMDA receptor deletion. Nat Neurosci 15:1153–1159. doi: 10.1038/nn.3166

25. Bannerman DM, Deacon RMJ, Brady S, Bruce A, Sprengel R, Seeburg PH, Rawlins JNP (2004) A comparison of GluR-A-deficient and wild-type mice on a test battery assessing sensorimotor, affective, and cognitive behaviors. Behav Neurosci 118:643–647. doi: 10.1037/0735-7044.118.3.643

26. Bannerman DM, Grubb M, Deacon RMJ, Yee BK, Feldon J, Rawlins JNP (2003) Ventral hippocampal lesions affect anxiety but not spatial learning. Behav Brain Res 139:197–213. doi: 10.1016/S0166-4328(02)00268-1

27. Bari A, Dalley JW, Robbins TW (2008) The application of the 5-choice serial reaction time task for the assessment of visual attentional processes and impulse control in rats. Nat Protoc 3:759–767. doi: 10.1038/nprot.2008.41

28. Barkus C, Feyder M, Graybeal C, Wright T, Wiedholz L, Izquierdo A, Kiselycznyk C, Schmitt W, Sanderson DJ, Rawlins JNP, Saksida LM, Bussey TJ, Sprengel R, Bannerman D, Holmes A (2012) Do GluA1 knockout mice exhibit behavioral abnormalities relevant to the negative or cognitive symptoms of schizophrenia and schizoaffective disorder? Neuropharmacology 62:1263–1272. doi: 10.1016/j.neuropharm.2011.06.005

29. Barkus C, Sanderson DJ, Rawlins JNP, Walton ME, Harrison PJ, Bannerman DM (2014) What causes aberrant salience in schizophrenia? A role for impaired short-term habituation and the GRIA1 (GluA1) AMPA receptor subunit. Mol Psychiatry 19:1060–1070. doi: 10.1038/mp.2014.91

30. Barnett L, Barrett AB, Seth AK (2018) Solved problems for Granger causality in neuroscience: A response to Stokes and Purdon. NeuroImage 178:744–748. doi: 10.1016/j.neuroimage.2018.05.067

31. Barnett L, Seth AK (2011) Behaviour of Granger causality under filtering: Theoretical invariance and practical application. J Neurosci Methods 201:404–419. doi: 10.1016/j.jneumeth.2011.08.010

32. Barnett L, Seth AK (2014) The MVGC multivariate Granger causality toolbox: a new approach to Granger-causal inference. J Neurosci Methods 223:50–68. doi: 10.1016/j.jneumeth.2013.10.018

33. Barnett L, Seth AK (2017) Detectability of Granger causality for subsampled continuous-time neurophysiological processes. J Neurosci Methods 275:93–121. doi: 10.1016/j.jneumeth.2016.10.016

34. Barr MS, Rajji TK, Zomorrodi R, Radhu N, George TP, Blumberger DM, Daskalakis ZJ (2017) Impaired theta-gamma coupling during working memory performance in schizophrenia. Schizophr Res 189:104–110. doi: 10.1016/j.schres.2017.01.044

35. Barth C, Fein D, Waterhouse L (1995) Delayed match-to-sample performance in autistic children. Dev Neuropsychol 11:53–69. doi: 10.1080/87565649509540603

36. Bastos AM, Schoffelen J-M (2016) A Tutorial Review of Functional Connectivity Analysis Methods and Their Interpretational Pitfalls. Front Syst Neurosci 9. doi: 10.3389/fnsys.2015.00175

37. Basu J, Siegelbaum SA (2015) The Corticohippocampal Circuit, Synaptic Plasticity, and Memory. Cold Spring Harb Perspect Biol 7:a021733. doi: 10.1101/cshperspect.a021733

38. Bayes T, Price null (1763) LII. An essay towards solving a problem in the doctrine of chances. By the late Rev. Mr. Bayes, F. R. S. communicated by Mr. Price, in a letter to John Canton, A. M. F. R. S. Philos Trans R Soc Lond 53:370–418. doi: 10.1098/rstl.1763.0053

39. Beaulieu J-M, Gainetdinov RR (2011) The physiology, signaling, and pharmacology of dopamine receptors. Pharmacol Rev 63:182–217. doi: 10.1124/pr.110.002642

40. Belforte JE, Zsiros V, Sklar ER, Jiang Z, Yu G, Li Y, Quinlan EM, Nakazawa K (2010) Postnatal NMDA receptor ablation in corticolimbic interneurons confers schizophrenia-like phenotypes. Nat Neurosci 13:76–83. doi: 10.1038/nn.2447

41. Benchenane K, Peyrache A, Khamassi M, Tierney PL, Gioanni Y, Battaglia FP, Wiener SI (2010) Coherent Theta Oscillations and Reorganization of Spike Timing in the Hippocampal- Prefrontal Network upon Learning. Neuron 66:921–936. doi: 10.1016/j.neuron.2010.05.013

42. Bender F, Gorbati M, Cadavieco MC, Denisova N, Gao X, Holman C, Korotkova T, Ponomarenko A (2015) Theta oscillations regulate the speed of locomotion via a hippocampus to lateral septum pathway. Nat Commun 6:8521. doi: 10.1038/ncomms9521

43. Benes FM, Kwok EW, Vincent SL, Todtenkopf MS (1998) A reduction of nonpyramidal cells in sector CA2 of schizophrenics and manic depressives. Biol Psychiatry 44:88–97. doi: 10.1016/S0006-3223(98)00138-3

44. Beracochea DJ, Jaffard R, Jarrard LE (1989) Effects of anterior or dorsomedial thalamic ibotenic lesions on learning and memory in rats. Behav Neural Biol 51:364–376. doi: 10.1016/S0163-1047(89)91000-5

45. Berens P (2009) **CircStat** : A *MATLAB* Toolbox for Circular Statistics. J Stat Softw 31. doi: 10.18637/jss.v031.i10

46. Berens P, Keliris GA, Ecker AS, Logothetis NK, Tolias AS (2008) Feature selectivity of the gamma-band of the local field potential in primate primary visual cortex. Front Neurosci 2:199–207. doi: 10.3389/neuro.01.037.2008

47. Bienkowski MS, Bowman I, Song MY, Gou L, Ard T, Cotter K, Zhu M, Benavidez NL, Yamashita S, Abu-Jaber J, Azam S, Lo D, Foster NN, Hintiryan H, Dong H-W (2018) Integration of gene expression and brain-wide connectivity reveals the multiscale organization of mouse hippocampal networks. Nat Neurosci 21:1628–1643. doi: 10.1038/s41593-018-0241-y

48. Black JE, Kodish IM, Grossman AW, Klintsova AY, Orlovskaya D, Vostrikov V, Uranova N, Greenough WT (2004) Pathology of layer V pyramidal neurons in the prefrontal cortex of patients with schizophrenia. Am J Psychiatry 161:742–744. doi: 10.1176/appi.ajp.161.4.742

49. Bleuler E (1950) Dementia praecox or the group of schizophrenias. International Universities Press, Oxford, England

50. Blinowska KJ (2011) Review of the methods of determination of directed connectivity from multichannel data. Med Biol Eng Comput 49:521–529. doi: 10.1007/s11517-011-0739-x

51. Bliss TVP, Collingridge GL (1993) A synaptic model of memory: long-term potentiation in the hippocampus. Nature 361:31–39. doi: 10.1038/361031a0

52. Boehme R, Deserno L, Gleich T, Katthagen T, Pankow A, Behr J, Buchert R, Roiser JP, Heinz A, Schlagenhauf F (2015) Aberrant Salience Is Related to Reduced Reinforcement Learning Signals and Elevated Dopamine Synthesis Capacity in Healthy Adults. J Neurosci Off J Soc Neurosci 35:10103–10111. doi: 10.1523/JNEUROSCI.0805-15.2015

53. Boerner T, Bygrave AM, Chen J, Fernando A, Jackson S, Barkus C, Sprengel R, Seeburg PH, Harrison PJ, Gilmour G, Bannerman DM, Sanderson DJ (2017) The group II metabotropic glutamate receptor agonist LY354740 and the D2 receptor antagonist haloperidol reduce locomotor hyperactivity but fail to rescue spatial working memory in GluA1 knockout mice. Eur J Neurosci 45:912–921. doi: 10.1111/ejn.13539

54. Bogerts B, Meertz E, Schönfeldt-Bausch R (1985) Basal Ganglia and Limbic System Pathology in Schizophrenia: A Morphometric Study of Brain Volume and Shrinkage. Arch Gen Psychiatry 42:784–791. doi: 10.1001/archpsyc.1985.01790310046006

55. Bokil H, Andrews P, Kulkarni JE, Mehta S, Mitra PP (2010) Chronux: A platform for analyzing neural signals. J Neurosci Methods 192:146–151. doi: 10.1016/j.jneumeth.2010.06.020

56. Bolkan SS, Stujenske JM, Parnaudeau S, Spellman TJ, Rauffenbart C, Abbas AI, Harris AZ, Gordon JA, Kellendonk C (2017) Thalamic projections sustain prefrontal activity during working memory maintenance. Nat Neurosci 20:987–996. doi: 10.1038/nn.4568

57. Boran E, Fedele T, Klaver P, Hilfiker P, Stieglitz L, Grunwald T, Sarnthein J (2019) Persistent hippocampal neural firing and hippocampal-cortical coupling predict verbal working memory load. Sci Adv 5:eaav3687. doi: 10.1126/sciadv.aav3687

58. Braff D, Stone C, Callaway E, Geyer M, Glick I, Bali L (1978) Prestimulus Effects on Human Startle Reflex in Normals and Schizophrenics. Psychophysiology 15:339–343. doi: 10.1111/j.1469-8986.1978.tb01390.x

59. Braff DL, Geyer MA (1990) Sensorimotor gating and schizophrenia. Human and animal model studies. Arch Gen Psychiatry 47:181–188. doi: 10.1001/archpsyc.1990.01810140081011

60. Braga RJ, Reynolds GP, Siris SG (2013) Anxiety comorbidity in schizophrenia. Psychiatry Res 210:1–7. doi: 10.1016/j.psychres.2013.07.030

61. Bragin A, Jandó G, Nádasdy Z, Hetke J, Wise K, Buzsáki G (1995) Gamma (40-100 Hz) oscillation in the hippocampus of the behaving rat. J Neurosci Off J Soc Neurosci 15:47–60

62. Bressler SL, Seth AK (2011) Wiener–Granger Causality: A well established methodology. NeuroImage 58:323–329. doi: 10.1016/j.neuroimage.2010.02.059

63. Brovelli A, Ding M, Ledberg A, Chen Y, Nakamura R, Bressler SL (2004) Beta oscillations in a large-scale sensorimotor cortical network: Directional influences revealed by Granger causality. Proc Natl Acad Sci 101:9849–9854. doi: 10.1073/pnas.0308538101

64. Bugarski-Kirola D, Iwata N, Sameljak S, Reid C, Blaettler T, Millar L, Marques TR, Garibaldi G, Kapur S (2016) Efficacy and safety of adjunctive bitopertin versus placebo in patients with suboptimally controlled symptoms of schizophrenia treated with antipsychotics: results from three phase 3, randomised, double-blind, parallel-group, placebo-controlled, multicentre studies in the SearchLyte clinical trial programme. Lancet Psychiatry 3:1115–1128. doi: 10.1016/S2215-0366(16)30344-3

65. Burgess N, Barry C, O’Keefe J (2007) An oscillatory interference model of grid cell firing. Hippocampus 17:801–812. doi: 10.1002/hipo.20327

66. Burton BG, Hok V, Save E, Poucet B (2009) Lesion of the ventral and intermediate hippocampus abolishes anticipatory activity in the medial prefrontal cortex of the rat. Behav Brain Res 199:222–234. doi: 10.1016/j.bbr.2008.11.045

67. Buzsáki G (2002) Theta Oscillations in the Hippocampus. Neuron 33:325–340. doi: 10.1016/S0896-6273(02)00586-X

68. Buzsáki G (2005) Theta rhythm of navigation: link between path integration and landmark navigation, episodic and semantic memory. Hippocampus 15:827–840. doi: 10.1002/hipo.20113

69. Buzsáki G (2006) Rhythms of the Brain. Oxford University Press

70. Buzsáki G, Anastassiou CA, Koch C (2012) The origin of extracellular fields and currents — EEG, ECoG, LFP and spikes. Nat Rev Neurosci 13:407–420. doi: 10.1038/nrn3241

71. Buzsáki G, Draguhn A (2004) Neuronal oscillations in cortical networks. Science 304:1926–1929. doi: 10.1126/science.1099745

72. Buzsáki G, Moser EI (2013) Memory, navigation and theta rhythm in the hippocampal-entorhinal system. Nat Neurosci 16:130–138. doi: 10.1038/nn.3304

73. Buzsáki G, Rappelsberger P, Kellényi L (1985) Depth profiles of hippocampal rhythmic slow activity ('theta rhythm') depend on behaviour. Electroencephalogr Clin Neurophysiol 61:77–88. doi: 10.1016/0013-4694(85)91075-2

74. Buzsáki G, Schomburg EW (2015) What does gamma coherence tell us about interregional neural communication? Nat Neurosci 18:484–489. doi: 10.1038/nn.3952

75. Buzsáki G, Wang X-J (2012) Mechanisms of Gamma Oscillations. Annu Rev Neurosci 35:203–225. doi: 10.1146/annurev-neuro-062111-150444

76. Bygrave AM, Jahans-Price T, Wolff AR, Sprengel R, Kullmann DM, Bannerman DM, Kätzel D (2019) Hippocampal-prefrontal coherence mediates working memory and selective attention at distinct frequency bands and provides a causal link between schizophrenia and its risk gene GRIA1. Transl Psychiatry 9:142. doi: 10.1038/s41398-019-0471-0

77. Bygrave AM, Masiulis S, Nicholson E, Berkemann M, Barkus C, Sprengel R, Harrison PJ, Kullmann DM, Bannerman DM, Kätzel D (2016) Knockout of NMDA-receptors from parvalbumin interneurons sensitizes to schizophrenia-related deficits induced by MK-801. Transl Psychiatry 6:e778–e778. doi: 10.1038/tp.2016.44

78. Cahusac PMB, Miyashita Y, Rolls ET (1989) Responses of hippocampal formation neurons in the monkey related to delayed spatial response and object-place memory tasks. Behav Brain Res 33:229–240. doi: 10.1016/S0166-4328(89)80118-4

79. Cahusac PMB, Miyashita Y, Rolls ET (1989) Responses of hippocampal formation neurons in the monkey related to delayed spatial response and object-place memory tasks. Behav Brain Res 33:229–240. doi: 10.1016/S0166-4328(89)80118-4

80. Canolty RT, Edwards E, Dalal SS, Soltani M, Nagarajan SS, Kirsch HE, Berger MS, Barbaro NM, Knight RT (2006) High Gamma Power Is Phase-Locked to Theta Oscillations in Human Neocortex. Science 313:1626–1628. doi: 10.1126/science.1128115

81. Canolty RT, Knight RT (2010) The functional role of cross-frequency coupling. Trends Cogn Sci 14:506–515. doi: 10.1016/j.tics.2010.09.001

82. Cantor-Graae E (2007) The contribution of social factors to the development of schizophrenia: a review of recent findings. Can J Psychiatry Rev Can Psychiatr 52:277–286. doi: 10.1177/070674370705200502

83. Cardin JA, Carlén M, Meletis K, Knoblich U, Zhang F, Deisseroth K, Tsai L-H, Moore CI (2009) Driving fast-spiking cells induces gamma rhythm and controls sensory responses. Nature 459:663–667. doi: 10.1038/nature08002

84. Cardno AG, Owen MJ (2014) Genetic relationships between schizophrenia, bipolar disorder, and schizoaffective disorder. Schizophr Bull 40:504–515. doi: 10.1093/schbul/sbu016

85. Cardoso-Cruz H, Lima D, Galhardo V (2013) Impaired Spatial Memory Performance in a Rat Model of Neuropathic Pain Is Associated with Reduced Hippocampus–Prefrontal Cortex Connectivity. J Neurosci 33:2465–2480. doi: 10.1523/JNEUROSCI.5197-12.2013

86. Carlén M, Meletis K, Siegle JH, Cardin JA, Futai K, Vierling-Claassen D, Rühlmann C, Jones SR, Deisseroth K, Sheng M, Moore CI, Tsai L-H (2012) A critical role for NMDA receptors in parvalbumin interneurons for gamma rhythm induction and behavior. Mol Psychiatry 17:537–548. doi: 10.1038/mp.2011.31

87. Carlsson M, Carlsson A (1989) The NMDA antagonist MK-801 causes marked locomotor stimulation in monoamine-depleted mice. J Neural Transm 75:221–226. doi: 10.1007/BF01258633

88. Catanese J, Carmichael JE, van der Meer MAA (2016) Low- and high-gamma oscillations deviate in opposite directions from zero-phase synchrony in the limbic corticostriatal loop. J Neurophysiol 116:5–17. doi: 10.1152/jn.00914.2015

89. Chadman KK, Yang M, Crawley JN (2009) Criteria for Validating Mouse Models of Psychiatric Diseases. Am J Med Genet Part B Neuropsychiatr Genet Off Publ Int Soc Psychiatr Genet 150B:1–11. doi: 10.1002/ajmg.b.30777

90. Chand GB, Dwyer DB, Erus G, Sotiras A, Varol E, Srinivasan D, Doshi J, Pomponio R, Pigoni A, Dazzan P, Kahn RS, Schnack HG, Zanetti MV, Meisenzahl E, Busatto GF, Crespo-Facorro B, Pantelis C, Wood SJ, Zhuo C, Shinohara RT, Shou H, Fan Y, Gur RC, Gur RE, Satterthwaite TD, Koutsouleris N, Wolf DH, Davatzikos C (2020) Two distinct neuroanatomical subtypes of schizophrenia revealed using machine learning. Brain 143:1027–1038. doi: 10.1093/brain/awaa025

91. Chawla NV, Bowyer KW, Hall LO, Kegelmeyer WP (2002) SMOTE: synthetic minority over-sampling technique. J Artif Intell Res 16:321–357

92. Chevaleyre V, Siegelbaum SA (2010) Strong CA2 pyramidal neuron synapses define a powerful disynaptic cortico-hippocampal loop. Neuron 66:560–572. doi: 10.1016/j.neuron.2010.04.013

93. Chiang M-C, Huang AJY, Wintzer ME, Ohshima T, McHugh TJ (2018) A role for CA3 in social recognition memory. Behav Brain Res 354:22–30. doi: 10.1016/j.bbr.2018.01.019

94. Cho KKA, Davidson TJ, Bouvier G, Marshall JD, Schnitzer MJ, Sohal VS (2020) Cross-hemispheric gamma synchrony between prefrontal parvalbumin interneurons sup-

ports behavioral adaptation during rule shift learning. Nat Neurosci 23:892–902. doi: 10.1038/s41593-020-0647-1

95. Chourbaji S, Vogt MA, Fumagalli F, Sohr R, Frasca A, Brandwein C, Hörtnagl H, Riva MA, Sprengel R, Gass P (2008) AMPA receptor subunit 1 (GluR-A) knockout mice model the glutamate hypothesis of depression. FASEB J. doi: 10.1096/fj.08-106450

96. Chudasama Y, Dalley JW, Nathwani F, Bouger P, Robbins TW, Nathwani F (2004) Cholinergic modulation of visual attention and working memory: dissociable effects of basal forebrain 192-IgG-saporin lesions and intraprefrontal infusions of scopolamine. Learn Mem Cold Spring Harb N 11:78–86. doi: 10.1101/lm.70904

97. Chudasama Y, Robbins TW (2004) Dopaminergic modulation of visual attention and working memory in the rodent prefrontal cortex. Neuropsychopharmacol Off Publ Am Coll Neuropsychopharmacol 29:1628–1636. doi: 10.1038/sj.npp.1300490

98. Clark A (2013) Whatever next? Predictive brains, situated agents, and the future of cognitive science. Behav Brain Sci 36:181–204. doi: 10.1017/S0140525X12000477

99. Cohen MX (2014) Analyzing Neural Time Series Data: Theory and Practice. The MIT Press

100. Cole MW, Anticevic A, Repovs G, Barch D (2011) Variable Global Dysconnectivity and Individual Differences in Schizophrenia. Biol Psychiatry 70:43–50. doi: 10.1016/j.biopsych.2011.02.010

101. Cole MW, Pathak S, Schneider W (2010) Identifying the brain's most globally connected regions. NeuroImage 49:3132–3148. doi: 10.1016/j.neuroimage.2009.11.001

102. Colgin LL, Denninger T, Fyhn M, Hafting T, Bonnevie T, Jensen O, Moser M-B, Moser EI (2009) Frequency of gamma oscillations routes flow of information in the hippocampus. Nature 462:353–357. doi: 10.1038/nature08573

103. Combrisson E, Jerbi K (2015) Exceeding chance level by chance: The caveat of theoretical chance levels in brain signal classification and statistical assessment of decoding accuracy. J Neurosci Methods 250:126–136. doi: 10.1016/j.jneumeth.2015.01.010

104. Combrisson E, Perrone-Bertolotti M, Soto JL, Alamian G, Kahane P, Lachaux J-P, Guillot A, Jerbi K (2017) From intentions to actions: Neural oscillations encode motor processes through phase, amplitude and phase-amplitude coupling. NeuroImage 147:473–487. doi: 10.1016/j.neuroimage.2016.11.042

105. Conn PJ, Lindsley CW, Jones CK (2009) Activation of metabotropic glutamate receptors as a novel approach for the treatment of schizophrenia. Trends Pharmacol Sci 30:25–31. doi: 10.1016/j.tips.2008.10.006

106. Conn PJ, Pin J-P (1997) Pharmacology and Functions of Metabotropic Glutamate Receptors. Annu Rev Pharmacol Toxicol 37:205–237. doi: 10.1146/annurev.pharmtox.37.1.205

107. Corlett PR, Frith CD, Fletcher PC (2009) From drugs to deprivation: a Bayesian framework for understanding models of psychosis. Psychopharmacology (Berl) 206:515–530. doi: 10.1007/s00213-009-1561-0

108. Correll CU, Davis RE, Weingart M, Saillard J, O'Gorman C, Kane JM, Lieberman JA, Tamminga CA, Mates S, Vanover KE (2020) Efficacy and Safety of Lumateperone for Treatment of Schizophrenia: A Randomized Clinical Trial. JAMA Psychiatry 77:349. doi: 10.1001/jamapsychiatry.2019.4379

109. Cryan JF, Mombereau C (2004) In search of a depressed mouse: utility of models for studying depression-related behavior in genetically modified mice. Mol Psychiatry 9:326–357. doi: 10.1038/sj.mp.4001457

110. Csicsvari J, Jamieson B, Wise KD, Buzsáki G (2003) Mechanisms of Gamma Oscillations in the Hippocampus of the Behaving Rat. Neuron 37:311–322. doi: 10.1016/S0896-6273(02)01169-8

111. Cunniff MM, Markenscoff-Papadimitriou E, Ostrowski J, Rubenstein JL, Sohal VS (2020) Altered hippocampal-prefrontal communication during anxiety-related avoidance in mice deficient for the autism-associated gene Pogz. eLife 9:e54835. doi: 10.7554/eLife.54835

112. Curtis CE, Rao VY, D'Esposito M (2004) Maintenance of spatial and motor codes during oculomotor delayed response tasks. J Neurosci 24:3944–3952. doi: 10.1523/JNEUROSCI.5640-03.2004

113. Cuthbert BN, Insel TR (2013) Toward the future of psychiatric diagnosis: the seven pillars of RDoC. BMC Med 11:126. doi: 10.1186/1741-7015-11-126

114. Cuthbert BN, Morris SE (2021) Evolving Concepts of the Schizophrenia Spectrum: A Research Domain Criteria Perspective. Front Psychiatry 12. doi: 10.3389/fpsyt.2021.641319

115. Davis KL, Kahn RS, Ko G, Davidson M (1991) Dopamine in schizophrenia: a review and reconceptualization. Am J Psychiatry 148:1474–1486. doi: 10.1176/ajp.148.11.1474

116. Deacon RMJ, Rawlins JNP (2006) T-maze alternation in the rodent. Nat Protoc 1:7–12. doi: 10.1038/nprot.2006.2

117. DeLisi LE, Hoff AL, Schwartz JE, Shields GW, Halthore SN, Gupta SM, Henn FA, Anand AK (1991) Brain morphology in first-episode schizophrenic-like psychotic patients: A quantitative magnetic resonance imaging study. Biol Psychiatry 29:159–175. doi: 10.1016/0006-3223(91)90044-M

118. Delorme A, Makeig S (2004) EEGLAB: an open source toolbox for analysis of single-trial EEG dynamics including independent component analysis. J Neurosci Methods 134:9–21. doi: 10.1016/j.jneumeth.2003.10.009

119. D'Esposito M, Detre JA, Alsop DC, Shin RK, Atlas S, Grossman M (1995) The neural basis of the central executive system of working memory. Nature 378:279–281. doi: 10.1038/378279a0

120. Dhamala M, Liang H, Bressler SL, Ding M (2018) Granger-Geweke causality: Estimation and interpretation. NeuroImage 175:460–463. doi: 10.1016/j.neuroimage.2018.04.043

121. Dhamala M, Rangarajan G, Ding M (2008) Analyzing information flow in brain networks with nonparametric Granger causality. NeuroImage 41:354–362. doi: 10.1016/j.neuroimage.2008.02.020

122. Dhamala M, Rangarajan G, Ding M (2008) Estimating Granger Causality from Fourier and Wavelet Transforms of Time Series Data. Phys Rev Lett 100:018701. doi: 10.1103/PhysRevLett.100.018701

123. Dickerson DD, Wolff AR, Bilkey DK (2010) Abnormal long-range neural synchrony in a maternal immune activation animal model of schizophrenia. J Neurosci 30:12424–31

124. DiLuca M, Olesen J (2014) The Cost of Brain Diseases: A Burden or a Challenge? Neuron 82:1205–1208. doi: 10.1016/j.neuron.2014.05.044

125. Dimitriadis SI, Marimpis AD (2018) Enhancing Performance and Bit Rates in a Brain–Computer Interface System With Phase-to-Amplitude Cross-Frequency Coupling: Evidences From Traditional c-VEP, Fast c-VEP, and SSVEP Designs. Front Neuroinformatics 12. doi: 10.3389/fninf.2018.00019

126. Ding M, Chen Y, Bressler SL (2006) Granger Causality: Basic Theory and Application to Neuroscience. ArXivq-Bio0608035

127. Donegan ML, Stefanini F, Meira T, Gordon JA, Fusi S, Siegelbaum SA (2020) Coding of social novelty in the hippocampal CA2 region and its disruption and rescue in a 22q11.2 microdeletion mouse model. Nat Neurosci 23:1365–1375. doi: 10.1038/s41593-020-00720-5

128. Douglas RJ (1967) The hippocampus and behavior. Psychol Bull 67:416–442. doi: 10.1037/h0024599

129. Dunnett SB (1985) Comparative effects of cholinergic drugs and lesions of nucleus basalis or fimbria-fornix on delayed matching in rats. Psychopharmacology (Berl) 87:357–363. doi: 10.1007/BF00432721

130. Duvarci S, Simpson EH, Schneider G, Kandel ER, Roeper J, Sigurdsson T (2018) Impaired recruitment of dopamine neurons during working memory in mice with stri-

atal D2 receptor overexpression. Nat Commun 9:2822. doi: 10.1038/s41467-018-05214-4

131. Eastwood SL, Kerwin RW, Harrison PJ (1997) Immunoautoradiographic evidence for a loss of alpha-amino-3-hydroxy-5-methyl-4-isoxazole propionate-preferring non-N-methyl-D-aspartate glutamate receptors within the medial temporal lobe in schizophrenia. Biol Psychiatry 41:636–643. doi: 10.1016/S0006-3223(96)00220-X

132. Eastwood SL, McDonald B, Burnet PW, Beckwith JP, Kerwin RW, Harrison PJ (1995) Decreased expression of mRNAs encoding non-NMDA glutamate receptors GluR1 and GluR2 in medial temporal lobe neurons in schizophrenia. Brain Res Mol Brain Res 29:211–223. doi: 10.1016/0169-328x(94)00247-c

133. Eastwood SL, Story P, Burnet PWJ, Heath P, Harrison PJ (1994) Differential changes in glutamate receptor subunit messenger RNAs in rat brain after haloperidol treatment. J Psychopharmacol (Oxf) 8:196–203. doi: 10.1177/026988119400800402

134. Eckhorn R, Bauer R, Jordan W, Brosch M, Kruse W, Munk M, Reitboeck HJ (1988) Coherent oscillations: a mechanism of feature linking in the visual cortex? Multiple electrode and correlation analyses in the cat. Biol Cybern 60:121–130. doi: 10.1007/BF00202899

135. Einevoll GT, Kayser C, Logothetis NK, Panzeri S (2013) Modelling and analysis of local field potentials for studying the function of cortical circuits. Nat Rev Neurosci 14:770–785. doi: 10.1038/nrn3599

136. Erickson MA, Maramara LA, Lisman J (2009) A Single Brief Burst Induces GluR1-dependent Associative Short-term Potentiation: A Potential Mechanism for Short-term Memory. J Cogn Neurosci 22:2530–2540. doi: 10.1162/jocn.2009.21375

137. Esmaeili V, Diamond ME (2019) Neuronal Correlates of Tactile Working Memory in Prefrontal and Vibrissal Somatosensory Cortex. Cell Rep 27:3167-3181.e5. doi: 10.1016/j.celrep.2019.05.034

138. Fell J, Klaver P, Lehnertz K, Grunwald T, Schaller C, Elger CE, Fernández G (2001) Human memory formation is accompanied by rhinal–hippocampal coupling and decoupling. Nat Neurosci 4:1259–1264. doi: 10.1038/nn759

139. File SE, Hyde JR (1978) Can social interaction be used to measure anxiety? Br J Pharmacol 62:19–24. doi: 10.1111/j.1476-5381.1978.tb07001.x

140. Finlay JM, Dunham GA, Isherwood AM, Newton CJ, Nguyen TV, Reppar PC, Snitkovski I, Paschall SA, Greene RW (2015) Effects of prefrontal cortex and hippocampal NMDA NR1-subunit deletion on complex cognitive and social behaviors. Brain Res 1600:70–83. doi: 10.1016/j.brainres.2014.10.037

141. Fitzgerald PJ, Barkus C, Feyder M, Wiedholz LM, Chen Y-C, Karlsson R-M, Machado-Vieira R, Graybeal C, Sharp T, Zarate C, Harvey-White J, Du J, Sprengel R, Gass P, Bannerman D, Holmes A (2010) Does gene deletion of AMPA GluA1 phenocopy fea-

tures of schizoaffective disorder? Neurobiol Dis 40:608–621. doi: 10.1016/j.nbd.2010.08.005

142. Fleischhacker WW, Podhorna J, Gröschl M, Hake S, Zhao Y, Huang S, Keefe RSE, Desch M, Brenner R, Walling DP, Mantero-Atienza E, Nakagome K, Pollentier S (2021) Efficacy and safety of the novel glycine transporter inhibitor BI 425809 once daily in patients with schizophrenia: a double-blind, randomised, placebo-controlled phase 2 study. Lancet Psychiatry 8:191–201. doi: 10.1016/S2215-0366(20)30513-7

143. Fletcher PC, Frith CD (2009) Perceiving is believing: a Bayesian approach to explaining the positive symptoms of schizophrenia. Nat Rev Neurosci 10:48–58. doi: 10.1038/nrn2536

144. Floresco SB, Braaksma DN, Phillips AG (1999) Thalamic–Cortical–Striatal Circuitry Subserves Working Memory during Delayed Responding on a Radial Arm Maze. J Neurosci 19:11061–11071. doi: 10.1523/JNEUROSCI.19-24-11061.1999

145. Florian G, Pfurtscheller G (1995) Dynamic spectral analysis of event-related EEG data. Electroencephalogr Clin Neurophysiol 95:393–396. doi: 10.1016/0013-4694(95)00198-8

146. Ford JM, Mathalon DH (2005) Corollary discharge dysfunction in schizophrenia: Can it explain auditory hallucinations? Int J Psychophysiol 58:179–189. doi: 10.1016/j.ijpsycho.2005.01.014

147. Ford JM, Mathalon DH, Whitfield S, Faustman WO, Roth WT (2002) Reduced communication between frontal and temporal lobes during talking in schizophrenia. Biol Psychiatry 51:485–492. doi: 10.1016/S0006-3223(01)01335-X

148. Frank LM, Brown EN, Wilson MA (2001) A Comparison of the Firing Properties of Putative Excitatory and Inhibitory Neurons From CA1 and the Entorhinal Cortex. J Neurophysiol 86:2029–2040. doi: 10.1152/jn.2001.86.4.2029

149. Fraschini M, La Cava SM, Didaci L, Barberini L (2020) On the Variability of Functional Connectivity and Network Measures in Source-Reconstructed EEG Time-Series. Entropy Basel Switz 23. doi: 10.3390/e23010005

150. Freeman W, Watts JW (1942) Psychosurgery: Intelligence, emotion, and social behavior following prefrontal lobotomy for mental disorders. Baillière, Tindall & Cox, London, England

151. Freudenberg F, Marx V, Seeburg PH, Sprengel R, Celikel T (2013) Circuit mechanisms of GluA1-dependent spatial working memory. Hippocampus 23:1359–1366. doi: 10.1002/hipo.22184

152. Freudenberg F, Resnik E, Kolleker A, Celikel T, Sprengel R, Seeburg PH (2016) Hippocampal GluA1 expression in Gria1−/− mice only partially restores spatial memory performance deficits. Neurobiol Learn Mem 135:83–90. doi: 10.1016/j.nlm.2016.07.005

153. Friedman HR, Goldman-Rakic PS (1988) Activation of the hippocampus and dentate gyrus by working-memory: a 2- deoxyglucose study of behaving rhesus monkeys. J Neurosci 8:4693–4706. doi: 10.1523/JNEUROSCI.08-12-04693.1988

154. Fries P (2005) A mechanism for cognitive dynamics: neuronal communication through neuronal coherence. Trends Cogn Sci 9:474–480. doi: 10.1016/j.tics.2005.08.011

155. Fries P (2015) Rhythms for Cognition: Communication through Coherence. Neuron 88:220–235. doi: 10.1016/j.neuron.2015.09.034

156. Friston K (2003) Learning and inference in the brain. Neural Netw Off J Int Neural Netw Soc 16:1325–1352. doi: 10.1016/j.neunet.2003.06.005

157. Friston KJ (1994) Functional and effective connectivity in neuroimaging: A synthesis. Hum Brain Mapp 2:56–78. doi: 10.1002/hbm.460020107

158. Friston KJ (2011) Functional and Effective Connectivity: A Review. Brain Connect 1:13–36. doi: 10.1089/brain.2011.0008

159. Friston KJ, Frith CD (1995) Schizophrenia: a disconnection syndrome? Clin Neurosci N Y N 3:89–97

160. Fuchs EC, Zivkovic AR, Cunningham MO, Middleton S, LeBeau FEN, Bannerman DM, Rozov A, Whittington MA, Traub RD, Rawlins JNP, Monyer H (2007) Recruitment of Parvalbumin-Positive Interneurons Determines Hippocampal Function and Associated Behavior. Neuron 53:591–604. doi: 10.1016/j.neuron.2007.01.031

161. Funahashi S, Bruce CJ, Goldman-Rakic PS (1989) Mnemonic coding of visual space in the monkey’s dorsolateral prefrontal cortex. J Neurophysiol 61:331–349. doi: 10.1152/jn.1989.61.2.331

162. Fuster JM, Alexander GE (1971) Neuron Activity Related to Short-Term Memory. Science 173:652–654. doi: 10.1126/science.173.3997.652

163. Fuster JM, Bressler SL (2015) Past makes future: role of pFC in prediction. J Cogn Neurosci 27:639–654. doi: 10.1162/jocn_a_00746

164. Gainetdinov RR, Wetsel WC, Jones SR, Levin ED, Jaber M, Caron MG (1999) Role of serotonin in the paradoxical calming effect of psychostimulants on hyperactivity. Science 283:397–401. doi: 10.1126/science.283.5400.397

165. Gallinat J, Winterer G, Herrmann CS, Senkowski D (2004) Reduced oscillatory gamma-band responses in unmedicated schizophrenic patients indicate impaired frontal network processing. Clin Neurophysiol Off J Int Fed Clin Neurophysiol 115:1863–1874. doi: 10.1016/j.clinph.2004.03.013

166. Gao R, van den Brink RL, Pfeffer T, Voytek B (2020) Neuronal timescales are functionally dynamic and shaped by cortical microarchitecture. eLife 9:e61277. doi: 10.7554/eLife.61277

167. Gerstein GL, Clark WA (1964) Simultaneous Studies of Firing Patterns in Several Neurons. Science 143:1325–1327. doi: 10.1126/science.143.3612.1325

168. Geweke JF (1984) Measures of Conditional Linear Dependence and Feedback between Time Series. J Am Stat Assoc 79:907–915. doi: 10.1080/01621459.1984.10477110

169. Gilad A, Gallero-Salas Y, Groos D, Helmchen F (2018) Behavioral Strategy Determines Frontal or Posterior Location of Short-Term Memory in Neocortex. Neuron 99:814-828.e7. doi: 10.1016/j.neuron.2018.07.029

170. Giraldo-Chica M, Woodward ND (2017) Review of thalamocortical resting-state fMRI studies in schizophrenia. Schizophr Res 180:58–63. doi: 10.1016/j.schres.2016.08.005

171. Glahn DC, Laird AR, Ellison-Wright I, Thelen SM, Robinson JL, Lancaster JL, Bullmore E, Fox PT (2008) Meta-Analysis of Gray Matter Anomalies in Schizophrenia: Application of Anatomic Likelihood Estimation and Network Analysis. Biol Psychiatry 64:774–781. doi: 10.1016/j.biopsych.2008.03.031

172. Glaser JI, Benjamin AS, Farhoodi R, Kording KP (2019) The roles of supervised machine learning in systems neuroscience. Prog Neurobiol 175:126–137. doi: 10.1016/j.pneurobio.2019.01.008

173. Goff DC, Lamberti JS, Leon AC, Green MF, Miller AL, Patel J, Manschreck T, Freudenreich O, Johnson SA (2008) A Placebo-Controlled Add-On Trial of the Ampakine, CX516, for Cognitive Deficits in Schizophrenia. Neuropsychopharmacology 33:465–472. doi: 10.1038/sj.npp.1301444

174. Goldman-Rakic PS (1999) The physiological approach: functional architecture of working memory and disordered cognition in schizophrenia. Biol Psychiatry 46:650–661. doi: 10.1016/S0006-3223(99)00130-4

175. Goldman-Rakic PS, Cools AR, Srivastava K, Roberts AC, Robbins TW, Weiskrantz L (1996) The prefrontal landscape: implications of functional architecture for understanding human mentation and the central executive. Philos Trans R Soc Lond B Biol Sci 351:1445–1453. doi: 10.1098/rstb.1996.0129

176. Gonzalez-Burgos G, Lewis DA (2008) GABA Neurons and the Mechanisms of Network Oscillations: Implications for Understanding Cortical Dysfunction in Schizophrenia. Schizophr Bull 34:944–961. doi: 10.1093/schbul/sbn070

177. Gore FM, Bloem PJN, Patton GC, Ferguson J, Joseph V, Coffey C, Sawyer SM, Mathers CD (2011) Global burden of disease in young people aged 10-24 years: a systematic analysis. Lancet Lond Engl 377:2093–2102. doi: 10.1016/S0140-6736(11)60512-6

178. Goto K, Ito I (2017) The asymmetry defect of hippocampal circuitry impairs working memory in β2-microglobulin deficient mice. Neurobiol Learn Mem 139:50–55. doi: 10.1016/j.nlm.2016.12.020

179. Gould LN (1949) Auditory hallucinations and subvocal speech; objective study in a case of schizophrenia. J Nerv Ment Dis 109:418–427. doi: 10.1097/00005053-194910950-00005

180. Granger CWJ (1969) Investigating Causal Relations by Econometric Models and Cross-spectral Methods. Econometrica 37:424–438. doi: 10.2307/1912791

181. Gray CM, König P, Engel AK, Singer W (1989) Oscillatory responses in cat visual cortex exhibit inter-columnar synchronization which reflects global stimulus properties. Nature 338:334–337. doi: 10.1038/338334a0

182. Gray CM, Singer W (1989) Stimulus-specific neuronal oscillations in orientation columns of cat visual cortex. Proc Natl Acad Sci U S A 86:1698–1702

183. Green IW, Glausier JR (2016) Different Paths to Core Pathology: The Equifinal Model of the Schizophrenia Syndrome. Schizophr Bull 42:542–549. doi: 10.1093/schbul/sbv136

184. Green JD, Arduini AA (1954) Hippocampal electrical activity in arousal. J Neurophysiol 17:533–557. doi: 10.1152/jn.1954.17.6.533

185. Greenamyre JT (1986) The Role of Glutamate in Neurotransmission and in Neurologic Disease. Arch Neurol 43:1058–1063. doi: 10.1001/archneur.1986.00520100062016

186. Guldin WO, Pritzel M, Markowitsch HJ (1981) Prefrontal cortex of the mouse defined as cortical projection area of the thalamic mediodorsal nucleus. Brain Behav Evol 19:93–107. doi: 10.1159/000121636

187. Hallock HL, Arreola AC, Shaw CL, Griffin AL (2013) Dissociable roles of the dorsal striatum and dorsal hippocampus in conditional discrimination and spatial alternation T-maze tasks. Neurobiol Learn Mem 100:108–116. doi: 10.1016/j.nlm.2012.12.009

188. Hallock HL, Wang A, Griffin AL (2016) Ventral Midline Thalamus Is Critical for Hippocampal–Prefrontal Synchrony and Spatial Working Memory. J Neurosci 36:8372–8389. doi: 10.1523/JNEUROSCI.0991-16.2016

189. Hamm JP, Gilmore CS, Picchetti NAM, Sponheim SR, Clementz BA (2011) Abnormalities of neuronal oscillations and temporal integration to low- and high-frequency auditory stimulation in schizophrenia. Biol Psychiatry 69:989–996. doi: 10.1016/j.biopsych.2010.11.021

190. Harrison PJ, McLaughlin D, Kerwin RW (1991) Decreased hippocampal expression of a glutamate receptor gene in schizophrenia. The Lancet 337:450–452. doi: 10.1016/0140-6736(91)93392-M

191. Hattori R, Danskin B, Babic Z, Mlynaryk N, Komiyama T (2019) Area-Specificity and Plasticity of History-Dependent Value Coding During Learning. Cell 177:1858-1872.e15. doi: 10.1016/j.cell.2019.04.027

192. Heckers S, Konradi C (2015) GABAergic mechanisms of hippocampal hyperactivity in schizophrenia. Schizophr Res 167:4–11. doi: 10.1016/j.schres.2014.09.041

193. Heckers S, Rauch S, Goff D, Savage C, Schacter D, Fischman A, Alpert N (1998) Impaired recruitment of the hippocampus during conscious recollection in schizophrenia. Nat Neurosci 1:318–323. doi: 10.1038/1137

194. Heckers S, Stone D, Walsh J, Shick J, Koul P, Benes FM (2002) Differential Hippocampal Expression of Glutamic Acid Decarboxylase 65 and 67 Messenger RNA in Bipolar Disorder and Schizophrenia. Arch Gen Psychiatry 59:521–529. doi: 10.1001/archpsyc.59.6.521

195. Heinz A, Schlagenhauf F (2010) Dopaminergic dysfunction in schizophrenia: salience attribution revisited. Schizophr Bull 36:472–485. doi: 10.1093/schbul/sbq031

196. Helmholtz H von (1867) Handbuch der physiologischen Optik. Voss

197. Herreras O (2016) Local Field Potentials: Myths and Misunderstandings. Front Neural Circuits 10. doi: 10.3389/fncir.2016.00101

198. Hesse W, Möller E, Arnold M, Schack B (2003) The use of time-variant EEG Granger causality for inspecting directed interdependencies of neural assemblies. J Neurosci Methods 124:27–44. doi: 10.1016/S0165-0270(02)00366-7

199. Hirabayashi T, Takeuchi D, Tamura K, Miyashita Y (2013) Functional Microcircuit Recruited during Retrieval of Object Association Memory in Monkey Perirhinal Cortex. Neuron 77:192–203. doi: 10.1016/j.neuron.2012.10.031

200. Hirano Y, Oribe N, Kanba S, Onitsuka T, Nestor PG, Spencer KM (2015) Spontaneous Gamma Activity in Schizophrenia. JAMA Psychiatry 72:813–821. doi: 10.1001/jamapsychiatry.2014.2642

201. Hitti FL, Siegelbaum SA (2014) The hippocampal CA2 region is essential for social memory. Nature 508:88–92. doi: 10.1038/nature13028

202. Hodgkin AL, Huxley AF (1939) Action Potentials Recorded from Inside a Nerve Fibre. Nature 144:710–711. doi: 10.1038/144710a0

203. Hoffman DA, Sprengel R, Sakmann B (2002) Molecular dissection of hippocampal theta-burst pairing potentiation. Proc Natl Acad Sci 99:7740–7745. doi: 10.1073/pnas.092157999

204. Holt DJ, Weiss AP, Rauch SL, Wright CI, Zalesak M, Goff DC, Ditman T, Welsh RC, Heckers S (2005) Sustained activation of the hippocampus in response to fearful faces in schizophrenia. Biol Psychiatry 57:1011–1019. doi: 10.1016/j.biopsych.2005.01.033

205. Honey RC, Watt A, Good M (1998) Hippocampal lesions disrupt an associative mismatch process. J Neurosci Off J Soc Neurosci 18:2226–2230

206. Horvitz JC (2000) Mesolimbocortical and nigrostriatal dopamine responses to salient non-reward events. Neuroscience 96:651–656. doi: 10.1016/s0306-4522(00)00019-1

207. Howes OD, Kapur S (2009) The Dopamine Hypothesis of Schizophrenia: Version III—The Final Common Pathway. Schizophr Bull 35:549–562. doi: 10.1093/schbul/sbp006

208. Hubel DH (1957) Tungsten Microelectrode for Recording from Single Units. Science 125:549–550. doi: 10.1126/science.125.3247.549

209. Hulse SH, Fowler H, Honig WK (2018) Cognitive Processes in Animal Behavior. Routledge

210. Hultman R, Mague SD, Li Q, Katz BM, Michel N, Lin L, Wang J, David LK, Blount C, Chandy R, Carlson D, Ulrich K, Carin L, Dunson D, Kumar S, Deisseroth K, Moore SD, Dzirasa K (2016) Dysregulation of Prefrontal Cortex-Mediated Slow-Evolving Limbic Dynamics Drives Stress-Induced Emotional Pathology. Neuron 91:439–452. doi: 10.1016/j.neuron.2016.05.038

211. Hultman R, Ulrich K, Sachs BD, Blount C, Carlson DE, Ndubuizu N, Bagot RC, Parise EM, Vu M-AT, Gallagher NM, Wang J, Silva AJ, Deisseroth K, Mague SD, Caron MG, Nestler EJ, Carin L, Dzirasa K (2018) Brain-wide Electrical Spatiotemporal Dynamics Encode Depression Vulnerability. Cell 173:166-180.e14. doi: 10.1016/j.cell.2018.02.012

212. Hunker AC, Soden ME, Krayushkina D, Heymann G, Awatramani R, Zweifel LS (2020) Conditional Single Vector CRISPR/SaCas9 Viruses for Efficient Mutagenesis in the Adult Mouse Nervous System. Cell Rep 30:4303-4316.e6. doi: 10.1016/j.celrep.2020.02.092

213. Hyman JM, Zilli EA, Paley AM, Hasselmo ME (2010) Working memory performance correlates with prefrontal-hippocampal theta interactions but not with prefrontal neuron firing rates. Front Integr Neurosci 4. doi: 10.3389/neuro.07.002.2010

214. Ingvar DH, Franzén G (1974) Abnormalities of Cerebral Blood Flow Distribution in Patients with Chronic Schizophrenia. Acta Psychiatr Scand 50:425–462. doi: 10.1111/j.1600-0447.1974.tb09707.x

215. Ingvar M, Ambros-Ingerson J, Davis M, Granger R, Kessler M, Rogers GA, Schehr RS, Lynch G (1997) Enhancement by an ampakine of memory encoding in humans. Exp Neurol 146:553–559. doi: 10.1006/exnr.1997.6581

216. Insanally MN, Carcea I, Field RE, Rodgers CC, DePasquale B, Rajan K, DeWeese MR, Albanna BF, Froemke RC (2019) Spike-timing-dependent ensemble encoding by non-classically responsive cortical neurons. eLife 8:e42409. doi: 10.7554/eLife.42409

217. Jablensky A (2010) The diagnostic concept of schizophrenia: its history, evolution, and future prospects. Dialogues Clin Neurosci 12:271–287

218. Jablensky A (2015) Schizophrenia or Schizophrenias? The Challenge of Genetic Parsing of a Complex Disorder. Am J Psychiatry 172:105–107. doi: 10.1176/appi.ajp.2014.14111452

219. Jaeseung Jeong, Gore JC, Peterson BS (2002) A method for determinism in short time series, and its application to stationary EEG. IEEE Trans Biomed Eng 49:1374–1379. doi: 10.1109/TBME.2002.804581

220. Jafakesh S, Jahromy FZ, Daliri MR (2016) Decoding of object categories from brain signals using cross frequency coupling methods. Biomed Signal Process Control 27:60–67. doi: 10.1016/j.bspc.2016.01.013

221. Jay TM, Glowinski J, Thierry A-M (1989) Selectivity of the hippocampal projection to the prelimbic area of the prefrontal cortex in the rat. Brain Res 505:337–340. doi: 10.1016/0006-8993(89)91464-9

222. Jensen V, Kaiser KMM, Borchardt T, Adelmann G, Rozov A, Burnashev N, Brix C, Frotscher M, Andersen P, Hvalby Ø, Sakmann B, Seeburg PH, Sprengel R (2003) A juvenile form of postsynaptic hippocampal long-term potentiation in mice deficient for the AMPA receptor subunit GluR-A. J Physiol 553:843–856. doi: 10.1113/jphysiol.2003.053637

223. Jiang Y, Guo Z, Xing G, He L, Peng H, Du F, McClure MA, Mu Q (2019) Effects of High-Frequency Transcranial Magnetic Stimulation for Cognitive Deficit in Schizophrenia: A Meta-Analysis. Front Psychiatry 10. doi: 10.3389/fpsyt.2019.00135

224. Johannesen JK, Bi J, Jiang R, Kenney JG, Chen C-MA (2016) Machine learning identification of EEG features predicting working memory performance in schizophrenia and healthy adults. Neuropsychiatr Electrophysiol 2:3. doi: 10.1186/s40810-016-0017-0

225. Johnson EL, Adams JN, Solbakk A-K, Endestad T, Larsson PG, Ivanovic J, Meling TR, Lin JJ, Knight RT (2018) Dynamic frontotemporal systems process space and time in working memory. PLOS Biol 16:e2004274. doi: 10.1371/journal.pbio.2004274

226. Johnson EL, Dewar CD, Solbakk A-K, Endestad T, Meling TR, Knight RT (2017) Bidirectional Frontoparietal Oscillatory Systems Support Working Memory. Curr Biol 27:1829-1835.e4. doi: 10.1016/j.cub.2017.05.046

227. Johnson EL, Kam JWY, Tzovara A, Knight RT (2020) Insights into human cognition from intracranial EEG: A review of audition, memory, internal cognition, and causality. J Neural Eng 17:051001. doi: 10.1088/1741-2552/abb7a5

228. Johnson EL, King-Stephens D, Weber PB, Laxer KD, Lin JJ, Knight RT (2019) Spectral Imprints of Working Memory for Everyday Associations in the Frontoparietal Network. Front Syst Neurosci 12. doi: 10.3389/fnsys.2018.00065

229. Jones MW, Wilson MA (2005) Theta Rhythms Coordinate Hippocampal–Prefrontal Interactions in a Spatial Memory Task. PLOS Biol 3:e402. doi: 10.1371/journal.pbio.0030402

230. Kajikawa Y, Schroeder CE (2011) How local is the local field potential? Neuron 72:847–858. doi: 10.1016/j.neuron.2011.09.029

231. Kajikawa Y, Schroeder CE (2015) Generation of field potentials and modulation of their dynamics through volume integration of cortical activity. J Neurophysiol 113:339–351. doi: 10.1152/jn.00914.2013

232. Kamiński J, Sullivan S, Chung JM, Ross IB, Mamelak AN, Rutishauser U (2017) Persistently active neurons in human medial frontal and medial temporal lobe support working memory. Nat Neurosci 20:590–601. doi: 10.1038/nn.4509

233. Kaminski MJ, Blinowska KJ (1991) A new method of the description of the information flow in the brain structures. Biol Cybern 65:203–210. doi: 10.1007/BF00198091

234. Kane J, Honigfeld G, Singer J, Meltzer H (1988) Clozapine for the Treatment-Resistant Schizophrenic: A Double-blind Comparison With Chlorpromazine. Arch Gen Psychiatry 45:789–796. doi: 10.1001/archpsyc.1988.01800330013001

235. Kapur S (2003) Psychosis as a state of aberrant salience: a framework linking biology, phenomenology, and pharmacology in schizophrenia. Am J Psychiatry 160:13–23. doi: 10.1176/appi.ajp.160.1.13

236. Kapur S, Mizrahi R, Li M (2005) From dopamine to salience to psychosis—linking biology, pharmacology and phenomenology of psychosis. Schizophr Res 79:59–68. doi: 10.1016/j.schres.2005.01.003

237. Karimi S, Shamsollahi MB (2020) Tractable Inference and Observation Likelihood Evaluation in Latent Structure Influence Models. IEEE Trans Signal Process 68:5736–5745. doi: 10.1109/TSP.2020.3025522

238. Katthagen T, Dammering F, Kathmann N, Kaminski J, Walter H, Heinz A, Schlagenhauf F (2016) Validating the construct of aberrant salience in schizophrenia — Behavioral evidence for an automatic process. Schizophr Res Cogn 6:22–27. doi: 10.1016/j.scog.2016.10.001

239. Katthagen T, Mathys C, Deserno L, Walter H, Kathmann N, Heinz A, Schlagenhauf F (2018) Modeling subjective relevance in schizophrenia and its relation to aberrant salience. PLOS Comput Biol 14:e1006319. doi: 10.1371/journal.pcbi.1006319

240. Kätzel D, Wolff AR, Bygrave AM, Bannerman DM (2020) Hippocampal Hyperactivity as a Druggable Circuit-Level Origin of Aberrant Salience in Schizophrenia. Front Pharmacol 11. doi: 10.3389/fphar.2020.486811

241. Katzner S, Nauhaus I, Benucci A, Bonin V, Ringach DL, Carandini M (2009) Local origin of field potentials in visual cortex. Neuron 61:35–41. doi: 10.1016/j.neuron.2008.11.016

242. Keefe RSE, Vinogradov S, Medalia A, Silverstein SM, Bell MD, Dickinson D, Ventura J, Marder SR, Stroup TS (2011) Report from the working group conference on mul-

tisite trial design for cognitive remediation in schizophrenia. Schizophr Bull 37:1057–1065. doi: 10.1093/schbul/sbq010

243. Keinanen K, Wisden W, Sommer B, Werner P, Herb A, Verdoorn T, Sakmann B, Seeburg P (1990) A family of AMPA-selective glutamate receptors. Science 249:556–560. doi: 10.1126/science.2166337

244. Kellendonk C, Simpson EH, Kandel ER (2009) Modeling cognitive endophenotypes of schizophrenia in mice. Trends Neurosci 32:347–358. doi: 10.1016/j.tins.2009.02.003

245. Kilonzo K, van der Veen B, Teutsch J, Schulz S, Kapanaiah SKT, Liss B, Kätzel D (2021) Delayed-matching-to-position working memory in mice relies on NMDA-receptors in prefrontal pyramidal cells. Sci Rep 11:8788. doi: 10.1038/s41598-021-88200-z

246. Kim HK, Blumberger DM, Daskalakis ZJ (2020) Neurophysiological Biomarkers in Schizophrenia—P50, Mismatch Negativity, and TMS-EMG and TMS-EEG. Front Psychiatry 11. doi: 10.3389/fpsyt.2020.00795

247. Kim JJ, Fanselow MS (1992) Modality-specific retrograde amnesia of fear. Science 256:675–677. doi: 10.1126/science.1585183

248. Kirkby LA, Luongo FJ, Lee MB, Nahum M, Vleet TMV, Rao VR, Dawes HE, Chang EF, Sohal VS (2018) An Amygdala-Hippocampus Subnetwork that Encodes Variation in Human Mood. Cell 175:1688-1700.e14. doi: 10.1016/j.cell.2018.10.005

249. Kirov G, Pocklington AJ, Holmans P, Ivanov D, Ikeda M, Ruderfer D, Moran J, Chambert K, Toncheva D, Georgieva L, Grozeva D, Fjodorova M, Wollerton R, Rees E, Nikolov I, van de Lagemaat LN, Bayés À, Fernandez E, Olason PI, Böttcher Y, Komiyama NH, Collins MO, Choudhary J, Stefansson K, Stefansson H, Grant SGN, Purcell S, Sklar P, O'Donovan MC, Owen MJ (2012) De novo CNV analysis implicates specific abnormalities of postsynaptic signalling complexes in the pathogenesis of schizophrenia. Mol Psychiatry 17:142–153. doi: 10.1038/mp.2011.154

250. Kiselycznyk C, Zhang X, Huganir RL, Holmes A, Svenningsson P (2013) Reduced phosphorylation of GluA1 subunits relates to anxiety-like behaviours in mice. Int J Neuropsychopharmacol 16:919–924. doi: 10.1017/S1461145712001174

251. Knapp M, Mangalore R, Simon J (2004) The Global Costs of Schizophrenia. Schizophr Bull 30:15

252. Körding KP, Wolpert DM (2004) Bayesian integration in sensorimotor learning. Nature 427:244–247. doi: 10.1038/nature02169

253. Kornblith S, Quian Quiroga R, Koch C, Fried I, Mormann F (2017) Persistent Single-Neuron Activity during Working Memory in the Human Medial Temporal Lobe. Curr Biol CB 27:1026–1032. doi: 10.1016/j.cub.2017.02.013

254. Koshiyama D, Miyakoshi M, Tanaka-Koshiyama K, Joshi YB, Molina JL, Sprock J, Braff DL, Light GA (2020) Neurophysiologic Characterization of Resting State Connectivity

Abnormalities in Schizophrenia Patients. Front Psychiatry 11:608154. doi: 10.3389/fpsyt.2020.608154

255. Krystal J, Karper L, Bennett A, Abi-Saab D, D'Souza C, Abi-Dargham A, Charney D (1995) Modulating ketamine-induced thought disorder with lorazepam and haloperidol in humans. Schizophr Res 1–2:156–157. doi: 10.1016/0920-9964(95)95485-R

256. Krystal JH, Abi-Saab W, Perry E, D'Souza DC, Liu N, Gueorguieva R, McDougall L, Hunsberger T, Belger A, Levine L, Breier A (2005) Preliminary evidence of attenuation of the disruptive effects of the NMDA glutamate receptor antagonist, ketamine, on working memory by pretreatment with the group II metabotropic glutamate receptor agonist, LY354740, in healthy human subjects. Psychopharmacology (Berl) 179:303–309. doi: 10.1007/s00213-004-1982-8

257. Krystal JH, Karper LP, Seibyl JP, Freeman GK, Delaney R, Bremner JD, Heninger GR, Bowers MB, Charney DS (1994) Subanesthetic Effects of the Noncompetitive NMDA Antagonist, Ketamine, in Humans: Psychotomimetic, Perceptual, Cognitive, and Neuroendocrine Responses. Arch Gen Psychiatry 51:199–214. doi: 10.1001/archpsyc.1994.03950030035004

258. Kullback S, Leibler RA (1951) On Information and Sufficiency. Ann Math Stat 22:79–86

259. Kwon JS, O'Donnell BF, Wallenstein GV, Greene RW, Hirayasu Y, Nestor PG, Hasselmo ME, Potts GF, Shenton ME, McCarley RW (1999) Gamma frequency-range abnormalities to auditory stimulation in schizophrenia. Arch Gen Psychiatry 56:1001–1005. doi: 10.1001/archpsyc.56.11.1001

260. Lachaux J-P, Rodriguez E, Martinerie J, Varela FJ (1999) Measuring phase synchrony in brain signals. Hum Brain Mapp 8:194–208. doi: 10.1002/(SICI)1097-0193(1999)8:4<194::AID-HBM4>3.0.CO;2-C

261. Lahti AC, Koffel B, LaPorte D, Tamminga CA (1995) Subanesthetic doses of ketamine stimulate psychosis in schizophrenia. Neuropsychopharmacol Off Publ Am Coll Neuropsychopharmacol 13:9–19. doi: 10.1016/0893-133X(94)00131-I

262. Lalonde R (2002) The neurobiological basis of spontaneous alternation. Neurosci Biobehav Rev 26:91–104. doi: 10.1016/S0149-7634(01)00041-0

263. Lane H-Y, Lin C-H, Green MF, Hellemann G, Huang C-C, Chen P-W, Tun R, Chang Y-C, Tsai GE (2013) Add-on treatment of benzoate for schizophrenia: a randomized, double-blind, placebo-controlled trial of D-amino acid oxidase inhibitor. JAMA Psychiatry 70:1267–1275. doi: 10.1001/jamapsychiatry.2013.2159

264. Laurent A, Saoud M, Bougerol T, d'Amato T, Anchisi AM, Biloa-Tang M, Dalery J, Rochet T (1999) Attentional deficits in patients with schizophrenia and in their non-psychotic first-degree relatives. Psychiatry Res 89:147–159. doi: 10.1016/s0165-1781(99)00109-2

265. Le Merre P, Ährlund-Richter S, Carlén M (2021) The mouse prefrontal cortex: Unity in diversity. Neuron. doi: 10.1016/j.neuron.2021.03.035

266. Lee H-K, Takamiya K, Han J-S, Man H, Kim C-H, Rumbaugh G, Yu S, Ding L, He C, Petralia RS, Wenthold RJ, Gallagher M, Huganir RL (2003) Phosphorylation of the AMPA Receptor GluR1 Subunit Is Required for Synaptic Plasticity and Retention of Spatial Memory. Cell 112:631–643. doi: 10.1016/S0092-8674(03)00122-3

267. Lee J, Park S (2005) Working Memory Impairments in Schizophrenia: A Meta-Analysis. J Abnorm Psychol 114:599–611. doi: 10.1037/0021-843X.114.4.599

268. Lee M, Balla A, Sershen H, Sehatpour P, Lakatos P, Javitt DC (2018) Rodent Mismatch Negativity/theta Neuro-Oscillatory Response as a Translational Neurophysiological Biomarker for N-Methyl-D-Aspartate Receptor-Based New Treatment Development in Schizophrenia. Neuropsychopharmacol Off Publ Am Coll Neuropsychopharmacol 43:571–582. doi: 10.1038/npp.2017.176

269. Lee PH, Anttila V, Won H, Feng Y-CA, Rosenthal J, Zhu Z, Tucker-Drob EM, Nivard MG, Grotzinger AD, Posthuma D, Wang MM-J, Yu D, Stahl EA, Walters RK, Anney RJL, Duncan LE, Ge T, Adolfsson R, Banaschewski T, Belangero S, Cook EH, Coppola G, Derks EM, Hoekstra PJ, Kaprio J, Keski-Rahkonen A, Kirov G, Kranzler HR, Luykx JJ, Rohde LA, Zai CC, Agerbo E, Arranz MJ, Asherson P, Bækvad-Hansen M, Baldursson G, Bellgrove M, Belliveau RA, Buitelaar J, Burton CL, Bybjerg-Grauholm J, Casas M, Cerrato F, Chambert K, Churchhouse C, Cormand B, Crosbie J, Dalsgaard S, Demontis D, Doyle AE, Dumont A, Elia J, Grove J, Gudmundsson OO, Haavik J, Hakonarson H, Hansen CS, Hartman CA, Hawi Z, Hervás A, Hougaard DM, Howrigan DP, Huang H, Kuntsi J, Langley K, Lesch K-P, Leung PWL, Loo SK, Martin J, Martin AR, McGough JJ, Medland SE, Moran JL, Mors O, Mortensen PB, Oades RD, Palmer DS, Pedersen CB, Pedersen MG, Peters T, Poterba T, Poulsen JB, Ramos-Quiroga JA, Reif A, Ribasés M, Rothenberger A, Rovira P, Sánchez-Mora C, Satterstrom FK, Schachar R, Artigas MS, Steinberg S, Stefansson H, Turley P, Walters GB, Werge T, Zayats T, Arking DE, Bettella F, Buxbaum JD, Christensen JH, Collins RL, Coon H, Rubeis SD, Delorme R, Grice DE, Hansen TF, Holmans PA, Hope S, Hultman CM, Klei L, Ladd-Acosta C, Magnusson P, Nærland T, Nyegaard M, Pinto D, Qvist P, Rehnström K, Reichenberg A, Reichert J, Roeder K, Rouleau GA, Saemundsen E, Sanders SJ, Sandin S, Pourcain BS, Stefansson K, Sutcliffe JS, Talkowski ME, Weiss LA, Willsey AJ, Agartz I, Akil H, Albani D, Alda M, Als TD, Anjorin A, Backlund L, Bass N, Bauer M, Baune BT, Bellivier F, Bergen SE, Berrettini WH, Biernacka JM, Blackwood DHR, Bøen E, Budde M, Bunney W, Burmeister M, Byerley W, Byrne EM, Cichon S, Clarke T-K, Coleman JRI, Craddock N, Curtis D, Czerski PM, Dale AM, Dalkner N, Dannlowski U, Degenhardt F, Florio AD, Elvsåshagen T, Etain B, Fischer SB, Forstner AJ, Forty L, Frank J, Frye M, Fullerton JM, Gade K, Gaspar HA, Gershon ES, Gill M, Goes FS, Gordon SD, Gordon-Smith K, Green MJ, Greenwood TA, Grigoroiu-Serbanescu M, Guzman-Parra J, Hauser J, Hautzinger M, Heilbronner U, Herms S, Hoffmann P, Holland D, Jamain S, Jones I, Jones LA, Kandaswamy R, Kelsoe JR, Kennedy JL, Joachim OK, Kittel-Schneider S, Kogevinas M, Koller AC, Lavebratt C, Lewis CM, Li QS, Lissowska J, Loohuis LMO, Lucae S, Maaser A, Malt UF, Martin NG, Martinsson L, McElroy SL, McMahon FJ, McQuillin A, Melle I, Metspalu A, Millischer V, Mitchell PB, Montgomery GW, Morken G, Morris DW, Müller-Myhsok B, Mullins N,

Myers RM, Nievergelt CM, Nordentoft M, Adolfsson AN, Nöthen MM, Ophoff RA, Owen MJ, Paciga SA, Pato CN, Pato MT, Perlis RH, Perry A, Potash JB, Reinbold CS, Rietschel M, Rivera M, Roberson M, Schalling M, Schofield PR, Schulze TG, Scott LJ, Serretti A, Sigurdsson E, Smeland OB, Stordal E, Streit F, Strohmaier J, Thorgeirsson TE, Treutlein J, Turecki G, Vaaler AE, Vieta E, Vincent JB, Wang Y, Witt SH, Zandi P, Adan RAH, Alfredsson L, Ando T, Aschauer H, Baker JH, Bencko V, Bergen AW, Birgegård A, Perica VB, Brandt H, Burghardt R, Carlberg L, Cassina M, Clementi M, Courtet P, Crawford S, Crow S, Crowley JJ, Danner UN, Davis OSP, Degortes D, DeSocio JE, Dick DM, Dina C, Docampo E, Egberts K, Ehrlich S, Espeseth T, Fernández-Aranda F, Fichter MM, Foretova L, Forzan M, Gambaro G, Giegling I, Gonidakis F, Gorwood P, Mayora MG, Guo Y, Halmi KA, Hatzikotoulas K, Hebebrand J, Helder SG, Herpertz-Dahlmann B, Herzog W, Hinney A, Imgart H, Jiménez-Murcia S, Johnson C, Jordan J, Julià A, Kaminská D, Karhunen L, Karwautz A, Kas MJH, Kaye WH, Kennedy MA, Kim Y-R, Klareskog L, Klump KL, Knudsen GPS, Landén M, Hellard SL, Levitan RD, Li D, Lichtenstein P, Maj M, Marsal S, McDevitt S, Mitchell J, Monteleone P, Monteleone AM, Munn-Chernoff MA, Nacmias B, Navratilova M, O'Toole JK, Padyukov L, Pantel J, Papezova H, Rabionet R, Raevuori A, Ramoz N, Reichborn-Kjennerud T, Ricca V, Roberts M, Rujescu D, Rybakowski F, Scherag A, Schmidt U, Seitz J, Slachtova L, Landt MCTS-O, Slopien A, Sorbi S, Southam L, Strober M, Tortorella A, Tozzi F, Treasure J, Tziouvas K, Elburg AA van, Wade TD, Wagner G, Walton E, Watson HJ, Wichmann H-E, Woodside DB, Zeggini E, Zerwas S, Zipfel S, Adams MJ, Andlauer TFM, Berger K, Binder EB, Boomsma DI, Castelao E, Colodro-Conde L, Direk N, Docherty AR, Domenici E, Domschke K, Dunn EC, Foo JC, Geus EJC de, Grabe HJ, Hamilton SP, Horn C, Hottenga J-J, Howard D, Ising M, Kloiber S, Levinson DF, Lewis G, Magnusson PKE, Mbarek H, Middeldorp CM, Mostafavi S, Nyholt DR, Penninx BW, Peterson RE, Pistis G, Porteous DJ, Preisig M, Quiroz JA, Schaefer C, Schulte EC, Shi J, Smith DJ, Thomson PA, Tiemeier H, Uher R, Auwera S van der, Weissman MM, Alexander M, Begemann M, Bramon E, Buccola NG, Cairns MJ, Campion D, Carr VJ, Cloninger CR, Cohen D, Collier DA, Corvin A, DeLisi LE, Donohoe G, Dudbridge F, Duan J, Freedman R, Gejman PV, Golimbet V, Godard S, Ehrenreich H, Hartmann AM, Henskens FA, Ikeda M, Iwata N, Jablensky AV, Joa I, Jönsson EG, Kelly BJ, Knight J, Konte B, Laurent-Levinson C, Lee J, Lencz T, Lerer B, Loughland CM, Malhotra AK, Mallet J, McDonald C, Mitjans M, Mowry BJ, Murphy KC, Murray RM, O'Neill FA, Oh S-Y, Palotie A, Pantelis C, Pulver AE, Petryshen TL, Quested DJ, Riley B, Sanders AR, Schall U, Schwab SG, Scott RJ, Sham PC, Silverman JM, Sim K, Steixner AA, Tooney PA, Os J van, Vawter MP, Walsh D, Weiser M, Wildenauer DB, Williams NM, Wormley BK, Zhang F, Androutsos C, Arnold PD, Barr CL, Barta C, Bey K, Bienvenu OJ, Black DW, Brown LW, Budman C, Cath D, Cheon K-A, Ciullo V, Coffey BJ, Cusi D, Davis LK, Denys D, Depienne C, Dietrich A, Eapen V, Falkai P, Fernandez TV, Garcia-Delgar B, Geller DA, Gilbert DL, Grados MA, Greenberg E, Grünblatt E, Hagstrøm J, Hanna GL, Hartmann A, Hedderly T, Heiman GA, Heyman I, Hong HJ, Huang A, Huyser C, Ibanez-Gomez L, Khramtsova EA, Kim YK, Kim Y-S, King RA, Koh Y-J, Konstantinidis A, Kook S, Kuperman S, Leventhal BL, Lochner C, Ludolph AG, Madruga-Garrido M, Malaty I, Maras A, McCracken JT, Meijer IA, Mir P, Morer A, Müller-Vahl KR, Münchau A, Murphy TL, Naarden A, Nagy P, Nestadt G, Nestadt PS, Nicolini H, Nurmi EL, Okun MS, Paschou P, Piras F, Piras F, Pittenger C, Plessen KJ, Richter MA, Rizzo R, Robertson M, Roessner V, Ruhrmann S, Samuels JF, Sandor P, Schlögelhofer M, Shin E-Y, Singer H, Song D-H, Song J, Spalletta G, Stein DJ, Stewart SE, Storch EA, Stranger B, Stuhrmann M, Tarnok Z, Tischfield JA, Tübing J, Visscher F, Vulink N, Wagner M, Walitza S, Wanderer S, Woods M, Worbe Y, Zai G, Zinner SH, Sullivan PF, Franke B, Daly MJ, Bulik CM, Lewis CM, McIntosh AM, O'Donovan MC, Zheutlin A, Andreassen OA, Børglum AD, Breen G, Edenberg HJ, Fanous AH, Faraone SV, Gelernter J, Mathews CA, Mattheisen M, Mitchell KS, Neale MC, Nurnberger JI, Ripke S, Santangelo SL, Scharf JM, Stein MB, Thornton LM, Walters JTR, Wray NR, Geschwind DH, Neale BM, Kendler KS, Smoller JW (2019) Genomic Relationships, Novel Loci, and Pleiotropic Mechanisms across Eight Psychiatric Disorders. Cell 179:1469-1482.e11. doi: 10.1016/j.cell.2019.11.020

270. Lee S-H, Wynn JK, Green MF, Kim H, Lee K-J, Nam M, Park J-K, Chung Y-C (2006) Quantitative EEG and low resolution electromagnetic tomography (LORETA) imaging of patients with persistent auditory hallucinations. Schizophr Res 83:111–119. doi: 10.1016/j.schres.2005.11.025

271. Lencz T, Bilder RM, Turkel E, Goldman RS, Robinson D, Kane JM, Lieberman JA (2003) Impairments in perceptual competency and maintenance on a visual delayed match-to-sample test in first-episode schizophrenia. Arch Gen Psychiatry 60:238–243. doi: 10.1001/archpsyc.60.3.238

272. Lencz T, Malhotra AK (2015) Targeting the schizophrenia genome: a fast track strategy from GWAS to clinic. Mol Psychiatry 20:820–826. doi: 10.1038/mp.2015.28

273. Leucht S, Cipriani A, Spineli L, Mavridis D, Örey D, Richter F, Samara M, Barbui C, Engel RR, Geddes JR, Kissling W, Stapf MP, Lässig B, Salanti G, Davis JM (2013) Comparative efficacy and tolerability of 15 antipsychotic drugs in schizophrenia: a multiple-treatments meta-analysis. The Lancet 382:951–962. doi: 10.1016/S0140-6736(13)60733-3

274. Lichtenstein P, Yip BH, Björk C, Pawitan Y, Cannon TD, Sullivan PF, Hultman CM (2009) Common genetic determinants of schizophrenia and bipolar disorder in Swedish families: a population-based study. 373:6

275. Liddle PF, Friston KJ, Frith CD, Hirsch SR, Jones T, Frackowiak RSJ (1992) Patterns of Cerebral Blood Flow in Schizophrenia. Br J Psychiatry 160:179–186. doi: 10.1192/bjp.160.2.179

276. Lieberman JA, Girgis RR, Brucato G, Moore H, Provenzano F, Kegeles L, Javitt D, Kantrowitz J, Wall MM, Corcoran CM, Schobel SA, Small SA (2018) Hippocampal dysfunction in the pathophysiology of schizophrenia: a selective review and hypothesis for early detection and intervention. Mol Psychiatry 23:1764–1772. doi: 10.1038/mp.2017.249

277. Lieberman JA, Kane JM, Alvir J (1987) Provocative tests with psychostimulant drugs in schizophrenia. Psychopharmacology (Berl) 91:415–433. doi: 10.1007/BF00216006

278. Lieberman JA, Perkins D, Belger A, Chakos M, Jarskog F, Boteva K, Gilmore J (2001) The early stages of schizophrenia: speculations on pathogenesis, pathophysiology,

and therapeutic approaches. Biol Psychiatry 50:884–897. doi: 10.1016/S0006-3223(01)01303-8

279. Lieberman JA, Rosenheck RA, Davis SM, Hsiao JK (2005) Effectiveness of Antipsychotic Drugs in Patients with Chronic Schizophrenia. N Engl J Med 15

280. Likhtik E, Stujenske JM, Topiwala MA, Harris AZ, Gordon JA (2014) Prefrontal entrainment of amygdala activity signals safety in learned fear and innate anxiety. Nat Neurosci 17:106–113. doi: 10.1038/nn.3582

281. Lindner A, Thier P, Kircher TTJ, Haarmeier T, Leube DT (2005) Disorders of agency in schizophrenia correlate with an inability to compensate for the sensory consequences of actions. Curr Biol CB 15:1119–1124. doi: 10.1016/j.cub.2005.05.049

282. Lips ES, Cornelisse LN, Toonen RF, Min JL, Hultman CM, Holmans PA, O'Donovan MC, Purcell SM, Smit AB, Verhage M, Sullivan PF, Visscher PM, Posthuma D (2012) Functional gene group analysis identifies synaptic gene groups as risk factor for schizophrenia. Mol Psychiatry 17:996–1006. doi: 10.1038/mp.2011.117

283. Lisman J (2016) Low-Frequency Brain Oscillations in Schizophrenia. JAMA Psychiatry 73:298–299. doi: 10.1001/jamapsychiatry.2015.2320

284. Lisman J, Buzsáki G (2008) A neural coding scheme formed by the combined function of gamma and theta oscillations. Schizophr Bull 34:974–980. doi: 10.1093/schbul/sbn060

285. Lisman JE, Coyle JT, Green RW, Javitt DC, Benes FM, Heckers S, Grace AA (2008) Circuit-based framework for understanding neurotransmitter and risk gene interactions in schizophrenia. Trends Neurosci 31:234–242. doi: 10.1016/j.tins.2008.02.005

286. Lisman JE, Idiart MA (1995) Storage of 7 +/- 2 short-term memories in oscillatory subcycles. Science 267:1512–1515. doi: 10.1126/science.7878473

287. Lisman JE, Jensen O (2013) The Theta-Gamma Neural Code. Neuron 77:1002–1016. doi: 10.1016/j.neuron.2013.03.007

288. López-Bendito G, Molnár Z (2003) Thalamocortical development: how are we going to get there? Nat Rev Neurosci 4:276–289. doi: 10.1038/nrn1075

289. Luby ED, Cohen BD, Rosenbaum G, Gottlieb JS, Kelley R (1959) Study of a New Schizophrenomimetic Drug—Sernyl. AMA Arch Neurol Psychiatry 81:363–369. doi: 10.1001/archneurpsyc.1959.02340150095011

290. Luby ED, Gottlieb JS, Cohen BD, Rosenbaum G, Domino EF (1962) Model psychoses and schizophrenia. Am J Psychiatry 119:61–67. doi: 10.1176/ajp.119.1.61

291. Luo AH, Tahsili-Fahadan P, Wise RA, Lupica CR, Aston-Jones G (2011) Linking context with reward: a functional circuit from hippocampal CA3 to ventral tegmental area. Science 333:353–357. doi: 10.1126/science.1204622

292. Lynch G (2004) AMPA receptor modulators as cognitive enhancers. Curr Opin Pharmacol 4:4–11. doi: 10.1016/j.coph.2003.09.009

293. Ma WJ, Husain M, Bays PM (2014) Changing concepts of working memory. Nat Neurosci 17:347–356. doi: 10.1038/nn.3655

294. Madisen L, Zwingman TA, Sunkin SM, Oh SW, Zariwala HA, Gu H, Ng LL, Palmiter RD, Hawrylycz MJ, Jones AR, Lein ES, Zeng H (2010) A robust and high-throughput Cre reporting and characterization system for the whole mouse brain. Nat Neurosci 13:133–140. doi: 10.1038/nn.2467

295. Maisson DJ-N, Gemzik ZM, Griffin AL (2018) Optogenetic suppression of the nucleus reuniens selectively impairs encoding during spatial working memory. Neurobiol Learn Mem 155:78–85. doi: 10.1016/j.nlm.2018.06.010

296. Majerus S, Cowan N, Péters F, Van Calster L, Phillips C, Schrouff J (2016) Cross-Modal Decoding of Neural Patterns Associated with Working Memory: Evidence for Attention-Based Accounts of Working Memory. Cereb Cortex N Y NY 26:166–179. doi: 10.1093/cercor/bhu189

297. Malinow R, Malenka RC (2002) AMPA Receptor Trafficking and Synaptic Plasticity. Annu Rev Neurosci 25:103–126. doi: 10.1146/annurev.neuro.25.112701.142758

298. von der Malsburg C (1995) Binding in models of perception and brain function. Curr Opin Neurobiol 5:520–526. doi: 10.1016/0959-4388(95)80014-x

299. von der Malsburg C, Buhmann J (1992) Sensory segmentation with coupled neural oscillators. Biol Cybern 67:233–242. doi: 10.1007/BF00204396

300. Mann EO, Suckling JM, Hajos N, Greenfield SA, Paulsen O (2005) Perisomatic feedback inhibition underlies cholinergically induced fast network oscillations in the rat hippocampus in vitro. Neuron 45:105–117. doi: 10.1016/j.neuron.2004.12.016

301. McCarthy G, Blamire AM, Puce A, Nobre AC, Bloch G, Hyder F, Goldman-Rakic P, Shulman RG (1994) Functional magnetic resonance imaging of human prefrontal cortex activation during a spatial working memory task. Proc Natl Acad Sci 91:8690–8694. doi: 10.1073/pnas.91.18.8690

302. McClain K, Tingley D, Heeger DJ, Buzsáki G (2019) Position–theta-phase model of hippocampal place cell activity applied to quantification of running speed modulation of firing rate. Proc Natl Acad Sci 116:27035–27042. doi: 10.1073/pnas.1912792116

303. McGlashan TH (1996) Early Detection and Intervention in Schizophrenia: Research. Schizophr Bull 22:327–345. doi: 10.1093/schbul/22.2.327

304. McGrath J, Saha S, Chant D, Welham J (2008) Schizophrenia: a concise overview of incidence, prevalence, and mortality. Epidemiol Rev 30:67–76. doi: 10.1093/epirev/mxn001

305. McNally JM, McCarley RW (2016) Gamma band oscillations: a key to understanding schizophrenia symptoms and neural circuit abnormalities. Curr Opin Psychiatry 29:202–210. doi: 10.1097/YCO.0000000000000244

306. Medoff DR, Holcomb HH, Lahti AC, Tamminga CA (2001) Probing the human hippocampus using rCBF: contrasts in schizophrenia. Hippocampus 11:543–550. doi: 10.1002/hipo.1070

307. Merk T, Peterson V, Lipski W, Blankertz B, Turner RS, Li N, Horn A, Kuehn A, Richardson M, Neumann W-J (2021) Electrocorticography is superior to subthalamic local field potentials for movement decoding in Parkinson's disease. bioRxiv 2021.04.24.441207. doi: 10.1101/2021.04.24.441207

308. Millan MJ, Agid Y, Brüne M, Bullmore ET, Carter CS, Clayton NS, Connor R, Davis S, Deakin B, DeRubeis RJ, Dubois B, Geyer MA, Goodwin GM, Gorwood P, Jay TM, Joëls M, Mansuy IM, Meyer-Lindenberg A, Murphy D, Rolls E, Saletu B, Spedding M, Sweeney J, Whittington M, Young LJ (2012) Cognitive dysfunction in psychiatric disorders: characteristics, causes and the quest for improved therapy. Nat Rev Drug Discov 11:141–168. doi: 10.1038/nrd3628

309. Miller EK, Lundqvist M, Bastos AM (2018) Working Memory 2.0. Neuron 100:463–475. doi: 10.1016/j.neuron.2018.09.023

310. Minzenberg MJ, Laird AR, Thelen S, Carter CS, Glahn DC (2009) Meta-analysis of 41 functional neuroimaging studies of executive function in schizophrenia. Arch Gen Psychiatry 66:811–822. doi: 10.1001/archgenpsychiatry.2009.91

311. Mitelman SA, Byne W, Kemether EM, Hazlett EA, Buchsbaum MS (2005) Metabolic Disconnection Between the Mediodorsal Nucleus of the Thalamus and Cortical Brodmann's Areas of the Left Hemisphere in Schizophrenia. Am J Psychiatry 162:1733–1735. doi: 10.1176/appi.ajp.162.9.1733

312. Mitzdorf U (1985) Current source-density method and application in cat cerebral cortex: investigation of evoked potentials and EEG phenomena. Physiol Rev 65:37–100. doi: 10.1152/physrev.1985.65.1.37

313. Miyakawa T, Leiter LM, Gerber DJ, Gainetdinov RR, Sotnikova TD, Zeng H, Caron MG, Tonegawa S (2003) Conditional calcineurin knockout mice exhibit multiple abnormal behaviors related to schizophrenia. Proc Natl Acad Sci U S A 100:8987–8992. doi: 10.1073/pnas.1432926100

314. Moghaddam B, Adams BW (1998) Reversal of Phencyclidine Effects by a Group II Metabotropic Glutamate Receptor Agonist in Rats. Science 281:1349–1352. doi: 10.1126/science.281.5381.1349

315. Mohn AR, Gainetdinov RR, Caron MG, Koller BH (1999) Mice with reduced NMDA receptor expression display behaviors related to schizophrenia. Cell 98:427–436. doi: 10.1016/s0092-8674(00)81972-8

316. Montgomery SM, Buzsáki G (2007) Gamma oscillations dynamically couple hippocampal CA3 and CA1 regions during memory task performance. Proc Natl Acad Sci 104:14495–14500. doi: 10.1073/pnas.0701826104

317. Monyer H, Seeburg PH, Wisden W (1991) Glutamate-operated channels: Developmentally early and mature forms arise by alternative splicing. Neuron 6:799–810. doi: 10.1016/0896-6273(91)90176-Z

318. Moran LV, Hong LE (2011) High vs Low Frequency Neural Oscillations in Schizophrenia. Schizophr Bull 37:659–663. doi: 10.1093/schbul/sbr056

319. Morris R (1983) Developments of a water-maze procedure for

320. Morrison PD, Nottage J, Stone JM, Bhattacharyya S, Tunstall N, Brenneisen R, Holt D, Wilson D, Sumich A, McGuire P, Murray RM, Kapur S, ffytche DH (2011) Disruption of Frontal Theta Coherence by Δ9-Tetrahydrocannabinol is Associated with Positive Psychotic Symptoms. Neuropsychopharmacology 36:827–836. doi: 10.1038/npp.2010.222

321. Mullins N, Forstner AJ, O’Connell KS, Coombes B, Coleman JRI, Qiao Z, Als TD, Bigdeli TB, Børte S, Bryois J, Charney AW, Drange OK, Gandal MJ, Hagenaars SP, Ikeda M, Kamitaki N, Kim M, Krebs K, Panagiotaropoulou G, Schilder BM, Sloofman LG, Steinberg S, Trubetskoy V, Winsvold BS, Won H-H, Abramova L, Adorjan K, Agerbo E, Eissa MA, Albani D, Alliey-Rodriguez N, Anjorin A, Antilla V, Antoniou A, Awasthi S, Baek JH, Bækvad-Hansen M, Bass N, Bauer M, Beins EC, Bergen SE, Birner A, Pedersen CB, Bøen E, Boks MP, Bosch R, Brum M, Brumpton BM, Brunkhorst-Kanaan N, Budde M, Bybjerg-Grauholm J, Byerley W, Cairns M, Casas M, Cervantes P, Clarke T-K, Cruceanu C, Cuellar-Barboza A, Cunningham J, Curtis D, Czerski PM, Dale AM, Dalkner N, David FS, Degenhardt F, Djurovic S, Dobbyn AL, Douzenis A, Elvsåshagen T, Escott-Price V, Ferrier IN, Fiorentino A, Foroud TM, Forty L, Frank J, Frei O, Freimer NB, Frisén L, Gade K, Garnham J, Gelernter J, Pedersen MG, Gizer IR, Gordon SD, Gordon-Smith K, Greenwood TA, Grove J, Guzman-Parra J, Ha K, Haraldsson M, Hautzinger M, Heilbronner U, Hellgren D, Herms S, Hoffmann P, Holmans PA, Huckins L, Jamain S, Johnson JS, Kalman JL, Kamatani Y, Kennedy JL, Kittel-Schneider S, Knowles JA, Kogevinas M, Koromina M, Kranz TM, Kranzler HR, Kubo M, Kupka R, Kushner SA, Lavebratt C, Lawrence J, Leber M, Lee H-J, Lee PH, Levy SE, Lewis C, Liao C, Lucae S, Lundberg M, MacIntyre DJ, Magnusson SH, Maier W, Maihofer A, Malaspina D, Maratou E, Martinsson L, Mattheisen M, McCarroll SA, McGregor NW, McGuffin P, McKay JD, Medeiros H, Medland SE, Millischer V, Montgomery GW, Moran JL, Morris DW, Mühleisen TW, O’Brien N, O’Donovan C, Loohuis LMO, Oruc L, Papiol S, Pardiñas AF, Perry A, Pfennig A, Porichi E, Potash JB, Quested D, Raj T, Rapaport MH, DePaulo JR, Regeer EJ, Rice JP, Rivas F, Rivera M, Roth J, Roussos P, Ruderfer DM, Sánchez-Mora C, Schulte EC, Senner F, Sharp S, Shilling PD, Sigurdsson E, Sirignano L, Slaney C, Smeland OB, Smith DJ, Sobell JL, Hansen CS, Artigas MS, Spijker AT, Stein DJ, Strauss JS, Świątkowska B, Terao C, Thorgeirsson TE, Toma C, Tooney P, Tsermpini E-E, Vawter MP, Vedder H, Walters JTR, Witt SH, Xi S, Xu W, Yang JMK, Young AH, Young H, Zandi PP, Zhou H, Zillich L, Adolfsson R, Agartz I, Alda M, Alfredsson L, Babadjanova G, Backlund L, Baune BT, Bellivier F, Bengesser S, Berrettini WH, Blackwood DHR, Boehnke M, Børglum AD,

Breen G, Carr VJ, Catts S, Corvin A, Craddock N, Dannlowski U, Dikeos D, Esko T, Etain B, Ferentinos P, Frye M, Fullerton JM, Gawlik M, Gershon ES, Goes FS, Green MJ, Grigoroiu-Serbanescu M, Hauser J, Henskens F, Hillert J, Hong KS, Hougaard DM, Hultman CM, Hveem K, Iwata N, Jablensky AV, Jones I, Jones LA, Kahn RS, Kelsoe JR, Kirov G, Landén M, Leboyer M, Lewis CM, Li QS, Lissowska J, Lochner C, Loughland C, Martin NG, Mathews CA, Mayoral F, McElroy SL, McIntosh AM, McMahon FJ, Melle I, Michie P, Milani L, Mitchell PB, Morken G, Mors O, Mortensen PB, Mowry B, Müller-Myhsok B, Myers RM, Neale BM, Nievergelt CM, Nordentoft M, Nöthen MM, O'Donovan MC, Oedegaard KJ, Olsson T, Owen MJ, Paciga SA, Pantelis C, Pato C, Pato MT, Patrinos GP, Perlis RH, Posthuma D, Ramos-Quiroga JA, Reif A, Reininghaus EZ, Ribasés M, Rietschel M, Ripke S, Rouleau GA, Saito T, Schall U, Schalling M, Schofield PR, Schulze TG, Scott LJ, Scott RJ, Serretti A, Weickert CS, Smoller JW, Stefansson H, Stefansson K, Stordal E, Streit F, Sullivan PF, Turecki G, Vaaler AE, Vieta E, Vincent JB, Waldman ID, Weickert TW, Werge T, Wray NR, Zwart J-A, Biernacka JM, Nurnberger JI, Cichon S, Edenberg HJ, Stahl EA, McQuillin A, Florio AD, Ophoff RA, Andreassen OA (2021) Genome-wide association study of more than 40,000 bipolar disorder cases provides new insights into the underlying biology. Nat Genet 1–13. doi: 10.1038/s41588-021-00857-4

322. Murray RM, Lewis SW (1987) Is schizophrenia a neurodevelopmental disorder? Br Med J Clin Res Ed 295:681–682. doi: 10.1136/bmj.295.6600.681

323. Nakashiba T, Cushman JD, Pelkey KA, Renaudineau S, Buhl DL, McHugh TJ, Barrera VR, Chittajallu R, Iwamoto KS, McBain CJ, Fanselow MS, Tonegawa S (2012) Young Dentate Granule Cells Mediate Pattern Separation, whereas Old Granule Cells Facilitate Pattern Completion. Cell 149:188–201. doi: 10.1016/j.cell.2012.01.046

324. Nakashiba T, Young JZ, McHugh TJ, Buhl DL, Tonegawa S (2008) Transgenic Inhibition of Synaptic Transmission Reveals Role of CA3 Output in Hippocampal Learning. Science 319:1260–1264. doi: 10.1126/science.1151120

325. Nakazawa K, Quirk MC, Chitwood RA, Watanabe M, Yeckel MF, Sun LD, Kato A, Carr CA, Johnston D, Wilson MA, Tonegawa S (2002) Requirement for Hippocampal CA3 NMDA Receptors in Associative Memory Recall. Science 297:211–218. doi: 10.1126/science.1071795

326. Nandi B, Swiatek P, Kocsis B, Ding M (2019) Inferring the direction of rhythmic neural transmission via inter-regional phase-amplitude coupling (ir-PAC). Sci Rep 9:1–13. doi: 10.1038/s41598-019-43272-w

327. Nauhaus I, Busse L, Carandini M, Ringach DL (2009) Stimulus contrast modulates functional connectivity in visual cortex. Nat Neurosci 12:70–76. doi: 10.1038/nn.2232

328. Neher E, Sakmann B (1976) Single-channel currents recorded from membrane of denervated frog muscle fibres. Nature 260:799–802. doi: 10.1038/260799a0

329. Nemani K, Li C, Olfson M, Blessing EM, Razavian N, Chen J, Petkova E, Goff DC (2021) Association of Psychiatric Disorders With Mortality Among Patients With COVID-19. JAMA Psychiatry. doi: 10.1001/jamapsychiatry.2020.4442

330. Niki H, Watanabe M (1976) Cingulate unit activity and delayed response. Brain Res 110:381–386. doi: 10.1016/0006-8993(76)90412-1

331. Niki H, Watanabe M (1979) Prefrontal and cingulate unit activity during timing behavior in the monkey. Brain Res 171:213–224. doi: 10.1016/0006-8993(79)90328-7

332. Nolte G, Bai O, Wheaton L, Mari Z, Vorbach S, Hallett M (2004) Identifying true brain interaction from EEG data using the imaginary part of coherency. Clin Neurophysiol 115:2292–2307. doi: 10.1016/j.clinph.2004.04.029

333. Noorbala AA, Akhondzadeh S, Davari-Ashtiani R, Amini-Nooshabadi H (1999) Piracetam in the treatment of schizophrenia: implications for the glutamate hypothesis of schizophrenia. J Clin Pharm Ther 24:369–374. doi: 10.1046/j.1365-2710.1999.00238.x

334. Oberauer K (2019) Working Memory and Attention – A Conceptual Analysis and Review. J Cogn 2:36. doi: 10.5334/joc.58

335. O'Keefe J, Dostrovsky J (1971) The hippocampus as a spatial map. Preliminary evidence from unit activity in the freely-moving rat. Brain Res 34:171–175. doi: 10.1016/0006-8993(71)90358-1

336. O'Keefe J, Recce ML (1993) Phase relationship between hippocampal place units and the EEG theta rhythm. Hippocampus 3:317–330. doi: 10.1002/hipo.450030307

337. O'Keefe J, Speakman A (1987) Single unit activity in the rat hippocampus during a spatial memory task. Exp Brain Res 68:1–27. doi: 10.1007/bf00255230

338. Olin SS, Mednick SA (1996) Risk Factors of Psychosis: Identifying Vulnerable Populations Premorbidly. Schizophr Bull 22:223–240. doi: 10.1093/schbul/22.2.223

339. Olton DS, Papas BC (1979) Spatial memory and hippocampal function. Neuropsychologia 17:669–682. doi: 10.1016/0028-3932(79)90042-3

340. O'Neill MF, Shaw G (1999) Comparison of dopamine receptor antagonists on hyperlocomotion induced by cocaine, amphetamine, MK-801 and the dopamine D1 agonist C-APB in mice. Psychopharmacology (Berl) 145:237–250. doi: 10.1007/s002130051055

341. O'Neill P-K, Gordon JA, Sigurdsson T (2013) Theta Oscillations in the Medial Prefrontal Cortex Are Modulated by Spatial Working Memory and Synchronize with the Hippocampus through Its Ventral Subregion. J Neurosci 33:14211–14224. doi: 10.1523/JNEUROSCI.2378-13.2013

342. Oostenveld R, Fries P, Maris E, Schoffelen J-M (2011) FieldTrip: Open Source Software for Advanced Analysis of MEG, EEG, and Invasive Electrophysiological Data. Comput Intell Neurosci 2011:1–9. doi: 10.1155/2011/156869

343. Oretti RG, Spurlock G, Buckland PR, McGuffin P (1994) Lack of effect of antipsychotic and antidepressant drugs on glutamate receptor mRNA levels in rat brains. Neurosci Lett 177:39–43. doi: 10.1016/0304-3940(94)90039-6

344. Owen MJ, Sawa A, Mortensen PB (2016) Schizophrenia. The Lancet 388:86–97. doi: 10.1016/S0140-6736(15)01121-6

345. Padilla-Coreano N, Canetta S, Mikofsky RM, Alway E, Passecker J, Myroshnychenko MV, Garcia-Garcia AL, Warren R, Teboul E, Blackman DR, Morton MP, Hupalo S, Tye KM, Kellendonk C, Kupferschmidt DA, Gordon JA (2019) Hippocampal-Prefrontal Theta Transmission Regulates Avoidance Behavior. Neuron 104:601-610.e4. doi: 10.1016/j.neuron.2019.08.006

346. Pardo JV, Fox PT, Raichle ME (1991) Localization of a human system for sustained attention by positron emission tomography. Nature 349:61–64. doi: 10.1038/349061a0

347. Paré D, Gaudreau H (1996) Projection Cells and Interneurons of the Lateral and Basolateral Amygdala: Distinct Firing Patterns and Differential Relation to Theta and Delta Rhythms in Conscious Cats. J Neurosci 16:3334–3350. doi: 10.1523/JNEUROSCI.16-10-03334.1996

348. Park AJ, Harris AZ, Martyniuk KM, Chang C-Y, Abbas AI, Lowes DC, Kellendonk C, Gogos JA, Gordon JA (2021) Reset of hippocampal–prefrontal circuitry facilitates learning. Nature 591:615–619. doi: 10.1038/s41586-021-03272-1

349. Parnaudeau S, O'Neill P-K, Bolkan SS, Ward RD, Abbas AI, Roth BL, Balsam PD, Gordon JA, Kellendonk C (2013) Inhibition of Mediodorsal Thalamus Disrupts Thalamofrontal Connectivity and Cognition. Neuron 77:1151–1162. doi: 10.1016/j.neuron.2013.01.038

350. Parto Dezfouli M, Zarei M, Constantinidis C, Daliri MR (2021) Task-specific modulation of PFC activity for matching-rule governed decision-making. Brain Struct Funct. doi: 10.1007/s00429-020-02191-7

351. Parwani A, Duncan EJ, Bartlett E, Madonick SH, Efferen TR, Rajan R, Sanfilipo M, Chappell PB, Chakravorty S, Gonzenbach S, Ko GN, Rotrosen JP (2000) Impaired prepulse inhibition of acoustic startle in schizophrenia. Biol Psychiatry 47:662–669. doi: 10.1016/S0006-3223(99)00148-1

352. Patil ST, Zhang L, Martenyi F, Lowe SL, Jackson KA, Andreev BV, Avedisova AS, Bardenstein LM, Gurovich IY, Morozova MA, Mosolov SN, Neznanov NG, Reznik AM, Smulevich AB, Tochilov VA, Johnson BG, Monn JA, Schoepp DD (2007) Activation of mGlu2/3 receptors as a new approach to treat schizophrenia: a randomized Phase 2 clinical trial. Nat Med 13:1102–1107. doi: 10.1038/nm1632

353. Pelkey KA, Barksdale E, Craig MT, Yuan X, Sukumaran M, Vargish GA, Mitchell RM, Wyeth MS, Petralia RS, Chittajallu R, Karlsson R-M, Cameron HA, Murata Y, Colonnese MT, Worley PF, McBain CJ (2015) Pentraxins Coordinate Excitatory Synapse Maturation and Circuit Integration of Parvalbumin Interneurons. Neuron 85:1257–1272. doi: 10.1016/j.neuron.2015.02.020

354. Pellow S, Chopin P, File SE, Briley M (1985) Validation of open:closed arm entries in an elevated plus-maze as a measure of anxiety in the rat. J Neurosci Methods 14:149–167. doi: 10.1016/0165-0270(85)90031-7

355. Pinault D (2008) N-methyl d-aspartate receptor antagonists ketamine and MK-801 induce wake-related aberrant gamma oscillations in the rat neocortex. Biol Psychiatry 63:730–735. doi: 10.1016/j.biopsych.2007.10.006

356. Post RM, Fink E, Carpenter WT, Goodwin FK (1975) Cerebrospinal Fluid Amine Metabolites in Acute Schizophrenia. Arch Gen Psychiatry 32:1063–1069. doi: 10.1001/archpsyc.1975.01760260127011

357. Potter D, Summerfelt A, Gold J, Buchanan RW (2006) Review of Clinical Correlates of P50 Sensory Gating Abnormalities in Patients with Schizophrenia. Schizophr Bull 32:692–700. doi: 10.1093/schbul/sbj050

358. Procaccini C, Aitta-aho T, Jaako-Movits K, Zharkovsky A, Panhelainen A, Sprengel R, Linden A-M, Korpi ER (2011) Excessive novelty-induced c-Fos expression and altered neurogenesis in the hippocampus of GluA1 knockout mice. Eur J Neurosci 33:161–174. doi: 10.1111/j.1460-9568.2010.07485.x

359. Procaccini C, Maksimovic M, Aitta-Aho T, Korpi ER, Linden A-M (2013) Reversal of novelty-induced hyperlocomotion and hippocampal c-Fos expression in GluA1 knockout male mice by the mGluR2/3 agonist LY354740. Neuroscience 250:189–200. doi: 10.1016/j.neuroscience.2013.07.010

360. Pycock CJ, Kerwin RW, Carter CJ (1980) Effect of lesion of cortical dopamine terminals on subcortical dopamine receptors in rats. Nature 286:74–77. doi: 10.1038/286074a0

361. Ranganathan M, DeMartinis N, Huguenel B, Gaudreault F, Bednar MM, Shaffer CL, Gupta S, Cahill J, Sherif MA, Mancuso J, Zumpano L, D'Souza DC (2017) Attenuation of ketamine-induced impairment in verbal learning and memory in healthy volunteers by the AMPA receptor potentiator PF-04958242. Mol Psychiatry 22:1633–1640. doi: 10.1038/mp.2017.6

362. Rao N, Northoff G, Tagore A, Rusjan P, Kenk M, Wilson A, Houle S, Strafella A, Remington G, Mizrahi R (2019) Impaired Prefrontal Cortical Dopamine Release in Schizophrenia During a Cognitive Task: A [11C]FLB 457 Positron Emission Tomography Study. Schizophr Bull 45:670–679. doi: 10.1093/schbul/sby076

363. Reinhart RMG, Nguyen JA (2019) Working memory revived in older adults by synchronizing rhythmic brain circuits. Nat Neurosci 22:820–827. doi: 10.1038/s41593-019-0371-x

364. Reisel D, Bannerman DM, Schmitt WB, Deacon RMJ, Flint J, Borchardt T, Seeburg PH, Rawlins JNP (2002) Spatial memory dissociations in mice lacking GluR1. Nat Neurosci 5:868–873. doi: 10.1038/nn910

365. Reith J, Benkelfat C, Sherwin A, Yasuhara Y, Kuwabara H, Andermann F, Bachneff S, Cumming P, Diksic M, Dyve SE, Etienne P, Evans AC, Lal S, Shevell M, Savard G, Wong DF, Chouinard G, Gjedde A (1994) Elevated dopa decarboxylase activity in living brain of patients with psychosis. Proc Natl Acad Sci U S A 91:11651–11654. doi: 10.1073/pnas.91.24.11651

366. Riedel G, Micheau J, Lam AGM, Roloff E v L, Martin SJ, Bridge H, Hoz L de, Poeschel B, McCulloch J, Morris RGM (1999) Reversible neural inactivation reveals hippocampal participation in several memory processes. Nat Neurosci 2:898–905. doi: 10.1038/13202

367. Ripke S, O'Dushlaine C, Chambert K, Moran JL, Kähler AK, Akterin S, Bergen SE, Collins AL, Crowley JJ, Fromer M, Kim Y, Lee SH, Magnusson PKE, Sanchez N, Stahl EA, Williams S, Wray NR, Xia K, Bettella F, Borglum AD, Bulik-Sullivan BK, Cormican P, Craddock N, de Leeuw C, Durmishi N, Gill M, Golimbet V, Hamshere ML, Holmans P, Hougaard DM, Kendler KS, Lin K, Morris DW, Mors O, Mortensen PB, Neale BM, O'Neill FA, Owen MJ, Milovancevic MP, Posthuma D, Powell J, Richards AL, Riley BP, Ruderfer D, Rujescu D, Sigurdsson E, Silagadze T, Smit AB, Stefansson H, Steinberg S, Suvisaari J, Tosato S, Verhage M, Walters JT, Multicenter Genetic Studies of Schizophrenia Consortium, Levinson DF, Gejman PV, Kendler KS, Laurent C, Mowry BJ, O'Donovan MC, Owen MJ, Pulver AE, Riley BP, Schwab SG, Wildenauer DB, Dudbridge F, Holmans P, Shi J, Albus M, Alexander M, Campion D, Cohen D, Dikeos D, Duan J, Eichhammer P, Godard S, Hansen M, Lerer FB, Liang K-Y, Maier W, Mallet J, Nertney DA, Nestadt G, Norton N, O'Neill FA, Papadimitriou GN, Ribble R, Sanders AR, Silverman JM, Walsh D, Williams NM, Wormley B, Psychosis Endophenotypes International Consortium, Arranz MJ, Bakker S, Bender S, Bramon E, Collier D, Crespo-Facorro B, Hall J, Iyegbe C, Jablensky A, Kahn RS, Kalaydjieva L, Lawrie S, Lewis CM, Lin K, Linszen DH, Mata I, McIntosh A, Murray RM, Ophoff RA, Powell J, Rujescu D, Van Os J, Walshe M, Weisbrod M, Wiersma D, Wellcome Trust Case Control Consortium 2, Donnelly P, Barroso I, Blackwell JM, Bramon E, Brown MA, Casas JP, Corvin AP, Deloukas P, Duncanson A, Jankowski J, Markus HS, Mathew CG, Palmer CNA, Plomin R, Rautanen A, Sawcer SJ, Trembath RC, Viswanathan AC, Wood NW, Spencer CCA, Band G, Bellenguez C, Freeman C, Hellenthal G, Giannoulatou E, Pirinen M, Pearson RD, Strange A, Su Z, Vukcevic D, Donnelly P, Langford C, Hunt SE, Edkins S, Gwilliam R, Blackburn H, Bumpstead SJ, Dronov S, Gillman M, Gray E, Hammond N, Jayakumar A, McCann OT, Liddle J, Potter SC, Ravindrarajah R, Ricketts M, Tashakkori-Ghanbaria A, Waller MJ, Weston P, Widaa S, Whittaker P, Barroso I, Deloukas P, Mathew CG, Blackwell JM, Brown MA, Corvin AP, McCarthy MI, Spencer CCA, Bramon E, Corvin AP, O'Donovan MC, Stefansson K, Scolnick E, Purcell S, McCarroll SA, Sklar P, Hultman CM, Sullivan PF (2013) Genome-wide association analysis identifies 13 new risk loci for schizophrenia. Nat Genet 45:1150–1159. doi: 10.1038/ng.2742

368. Robbins T (2002) The 5-choice serial reaction time task: behavioural pharmacology and functional neurochemistry. Psychopharmacology (Berl) 163:362–380. doi: 10.1007/s00213-002-1154-7

369. Rodrigues-Amorim D, Rivera-Baltanás T, Regueiro B, Spuch C, de las Heras ME, Vázquez-Noguerol Méndez R, Nieto-Araujo M, Barreiro-Villar C, Olivares JM, Agís-Balboa RC (2018) The role of the gut microbiota in schizophrenia: Current and future perspectives. World J Biol Psychiatry 19:571–585. doi: 10.1080/15622975.2018.1433878

370. Roiser JP, Howes OD, Chaddock CA, Joyce EM, McGuire P (2013) Neural and behavioral correlates of aberrant salience in individuals at risk for psychosis. Schizophr Bull 39:1328–1336. doi: 10.1093/schbul/sbs147

371. Roiser JP, Stephan KE, den Ouden HEM, Barnes TRE, Friston KJ, Joyce EM (2009) Do patients with schizophrenia exhibit aberrant salience? Psychol Med 39:199–209. doi: 10.1017/S0033291708003863

372. Romberg C, Raffel J, Martin L, Sprengel R, Seeburg PH, Rawlins JNP, Bannerman DM, Paulsen O (2009) Induction and expression of GluA1 (GluR-A)-independent LTP in the hippocampus. Eur J Neurosci 29:1141–1152. doi: 10.1111/j.1460-9568.2009.06677.x

373. Rose JE, Woolsey CN (1948) Structure and relations of limbic cortex and anterior thalamic nuclei in rabbit and cat. J Comp Neurol 89:279–347. doi: https://doi.org/10.1002/cne.900890307

374. Rosenbrock H, Desch M, Kleiner O, Dorner-Ciossek C, Schmid B, Keller S, Schlecker C, Moschetti V, Goetz S, Liesenfeld K-H, Fillon G, Giovannini R, Ramael S, Wunderlich G, Wind S (2018) Evaluation of Pharmacokinetics and Pharmacodynamics of BI 425809, a Novel GlyT1 Inhibitor: Translational Studies. Clin Transl Sci 11:616–623. doi: https://doi.org/10.1111/cts.12578

375. van Rossum JM (1966) The significance of dopamine-receptor blockade for the mechanism of action of neuroleptic drugs. Arch Int Pharmacodyn Ther 160:492–494

376. Sahakian BJ, Morris RG, Evenden JL, Heald A, Levy R, Philpot M, Robbins TW (1988) A comparative study of visuospatial memory and learning in Alzheimer-type dementia and Parkinson's disease. Brain J Neurol 111 (Pt 3):695–718. doi: 10.1093/brain/111.3.695

377. Sanderson DJ, Bannerman DM (2012) The role of habituation in hippocampus-dependent spatial working memory tasks: evidence from GluA1 AMPA receptor subunit knockout mice. Hippocampus 22:981–994. doi: 10.1002/hipo.20896

378. Sanderson DJ, Good MA, Skelton K, Sprengel R, Seeburg PH, Rawlins JNP, Bannerman DM (2009) Enhanced long-term and impaired short-term spatial memory in GluA1 AMPA receptor subunit knockout mice: Evidence for a dual-process memory model. Learn Mem 16:379–386. doi: 10.1101/lm.1339109

379. Sanderson DJ, Gray A, Simon A, Taylor AM, Deacon RMJ, Seeburg PH, Sprengel R, Good MA, Rawlins JNP, Bannerman DM (2007) Deletion of glutamate receptor-A (GluR-A) AMPA receptor subunits impairs one-trial spatial memory. Behav Neurosci 121:559–569. doi: 10.1037/0735-7044.121.3.559

380. Sanderson DJ, Hindley E, Smeaton E, Denny N, Taylor A, Barkus C, Sprengel R, Seeburg PH, Bannerman DM (2011) Deletion of the GluA1 AMPA receptor subunit impairs recency-dependent object recognition memory. Learn Mem Cold Spring Harb N 18:181–190. doi: 10.1101/lm.2083411

381. Sanderson DJ, Sprengel R, Seeburg PH, Bannerman DM (2011) Deletion of the GluA1 AMPA receptor subunit alters the expression of short-term memory. Learn Mem 18:128–131. doi: 10.1101/lm.2014911

382. Schizophrenia Working Group of the Psychiatric Genomics Consortium, Ripke S, Neale BM, Corvin A, Walters JTR, Farh K-H, Holmans PA, Lee P, Bulik-Sullivan B, Collier DA, Huang H, Pers TH, Agartz I, Agerbo E, Albus M, Alexander M, Amin F, Bacanu SA, Begemann M, Belliveau Jr RA, Bene J, Bergen SE, Bevilacqua E, Bigdeli TB, Black DW, Bruggeman R, Buccola NG, Buckner RL, Byerley W, Cahn W, Cai G, Campion D, Cantor RM, Carr VJ, Carrera N, Catts SV, Chambert KD, Chan RCK, Chen RYL, Chen EYH, Cheng W, Cheung EFC, Ann Chong S, Robert Cloninger C, Cohen D, Cohen N, Cormican P, Craddock N, Crowley JJ, Curtis D, Davidson M, Davis KL, Degenhardt F, Del Favero J, Demontis D, Dikeos D, Dinan T, Djurovic S, Donohoe G, Drapeau E, Duan J, Dudbridge F, Durmishi N, Eichhammer P, Eriksson J, Escott-Price V, Essioux L, Fanous AH, Farrell MS, Frank J, Franke L, Freedman R, Freimer NB, Friedl M, Friedman JI, Fromer M, Genovese G, Georgieva L, Giegling I, Giusti-Rodríguez P, Godard S, Goldstein JI, Golimbet V, Gopal S, Gratten J, de Haan L, Hammer C, Hamshere ML, Hansen M, Hansen T, Haroutunian V, Hartmann AM, Henskens FA, Herms S, Hirschhorn JN, Hoffmann P, Hofman A, Hollegaard MV, Hougaard DM, Ikeda M, Joa I, Julià A, Kahn RS, Kalaydjieva L, Karachanak-Yankova S, Karjalainen J, Kavanagh D, Keller MC, Kennedy JL, Khrunin A, Kim Y, Klovins J, Knowles JA, Konte B, Kucinskas V, Ausrele Kucinskiene Z, Kuzelova-Ptackova H, Kähler AK, Laurent C, Lee Chee Keong J, Hong Lee S, Legge SE, Lerer B, Li M, Li T, Liang K-Y, Lieberman J, Limborska S, Loughland CM, Lubinski J, Lönnqvist J, Macek Jr M, Magnusson PKE, Maher BS, Maier W, Mallet J, Marsal S, Mattheisen M, Mattingsdal M, McCarley RW, McDonald C, McIntosh AM, Meier S, Meijer CJ, Melegh B, Melle I, Mesholam-Gately RI, Metspalu A, Michie PT, Milani L, Milanova V, Mokrab Y, Morris DW, Mors O, Murphy KC, Murray RM, Myin-Germeys I, Müller-Myhsok B, Nelis M, Nenadic I, Nertney DA, Nestadt G, Nicodemus KK, Nikitina-Zake L, Nisenbaum L, Nordin A, O'Callaghan E, O'Dushlaine C, O'Neill FA, Oh S-Y, Olincy A, Olsen L, Van Os J, Pantelis C, Papadimitriou GN, Papiol S, Parkhomenko E, Pato MT, Paunio T, Pejovic-Milovancevic M, Perkins DO, Pietiläinen O, Pimm J, Pocklington AJ, Powell J, Price A, Pulver AE, Purcell SM, Quested D, Rasmussen HB, Reichenberg A, Reimers MA, Richards AL, Roffman JL, Roussos P, Ruderfer DM, Salomaa V, Sanders AR, Schall U, Schubert CR, Schulze TG, Schwab SG, Scolnick EM, Scott RJ, Seidman LJ, Shi J, Sigurdsson E, Silagadze T, Silverman JM, Sim K, Slominsky P, Smoller JW, So H-C, Spencer CA, Stahl EA, Stefansson H, Steinberg S, Stogmann E, Straub RE, Strengman E, Strohmaier J, Scott Stroup T, Subramaniam M, Suvisaari J, Svrakic DM, Szat-

kiewicz JP, Söderman E, Thirumalai S, Toncheva D, Tosato S, Veijola J, Waddington J, Walsh D, Wang D, Wang Q, Webb BT, Weiser M, Wildenauer DB, Williams NM, Williams S, Witt SH, Wolen AR, Wong EHM, Wormley BK, Simon Xi H, Zai CC, Zheng X, Zimprich F, Wray NR, Stefansson K, Visscher PM, Trust Case-Control Consortium W, Adolfsson R, Andreassen OA, Blackwood DHR, Bramon E, Buxbaum JD, Børglum AD, Cichon S, Darvasi A, Domenici E, Ehrenreich H, Esko T, Gejman PV, Gill M, Gurling H, Hultman CM, Iwata N, Jablensky AV, Jönsson EG, Kendler KS, Kirov G, Knight J, Lencz T, Levinson DF, Li QS, Liu J, Malhotra AK, McCarroll SA, McQuillin A, Moran JL, Mortensen PB, Mowry BJ, Nöthen MM, Ophoff RA, Owen MJ, Palotie A, Pato CN, Petryshen TL, Posthuma D, Rietschel M, Riley BP, Rujescu D, Sham PC, Sklar P, St Clair D, Weinberger DR, Wendland JR, Werge T, Daly MJ, Sullivan PF, O'Donovan MC (2014) Biological insights from 108 schizophrenia-associated genetic loci. Nature 511:421–427. doi: 10.1038/nature13595

383. Schmack K, Bosc M, Ott T, Sturgill JF, Kepecs A (2021) Striatal dopamine mediates hallucination-like perception in mice. Science 372. doi: 10.1126/science.abf4740

384. Schmitt LI, Wimmer RD, Nakajima M, Happ M, Mofakham S, Halassa MM (2017) Thalamic amplification of cortical connectivity sustains attentional control. Nature 545:219–223. doi: 10.1038/nature22073

385. Schmitt WB, Deacon RMJ, Seeburg PH, Rawlins JNP, Bannerman DM (2003) A Within-Subjects, Within-Task Demonstration of Intact Spatial Reference Memory and Impaired Spatial Working Memory in Glutamate Receptor-A-Deficient Mice. J Neurosci 23:3953–3959. doi: 10.1523/JNEUROSCI.23-09-03953.2003

386. Schmitt WB, Sprengel R, Mack V, Draft RW, Seeburg PH, Deacon RMJ, Rawlins JNP, Bannerman DM (2005) Restoration of spatial working memory by genetic rescue of GluR-A–deficient mice. Nat Neurosci 8:270–272. doi: 10.1038/nn1412

387. Schneider CW, Chenoweth MB (1970) Effects of hallucinogenic and other drugs on the nest-building behaviour of mice. Nature 225:1262–1263. doi: 10.1038/2251262a0

388. Schobel SA, Chaudhury NH, Khan UA, Paniagua B, Styner MA, Asllani I, Inbar BP, Corcoran CM, Lieberman JA, Moore H, Small SA (2013) Imaging patients with psychosis and a mouse model establishes a spreading pattern of hippocampal dysfunction and implicates glutamate as a driver. Neuron 78:81–93. doi: 10.1016/j.neuron.2013.02.011

389. Schobel SA, Kelly MA, Corcoran CM, Van Heertum K, Seckinger R, Goetz R, Harkavy-Friedman J, Malaspina D (2009) Anterior hippocampal and orbitofrontal cortical structural brain abnormalities in association with cognitive deficits in schizophrenia. Schizophr Res 114:110–118. doi: 10.1016/j.schres.2009.07.016

390. Schwarz G (1978) Estimating the Dimension of a Model. Ann Stat 6:461–464

391. Scoville WB, Milner B (1957) LOSS OF RECENT MEMORY AFTER BILATERAL HIPPOCAMPAL LESIONS. J Neurol Neurosurg Psychiatry 20:11–21

392. Seager MA, Johnson LD, Chabot ES, Asaka Y, Berry SD (2002) Oscillatory brain states and learning: Impact of hippocampal theta-contingent training. Proc Natl Acad Sci U S A 99:1616–1620. doi: 10.1073/pnas.032662099

393. Seeman P, Chau-Wong M, Tedesco J, Wong K (1975) Brain receptors for antipsychotic drugs and dopamine: direct binding assays. Proc Natl Acad Sci 72:4376–4380. doi: 10.1073/pnas.72.11.4376

394. Seidenbecher T, Laxmi TR, Stork O, Pape HC (2003) Amygdalar and hippocampal theta rhythm synchronization during fear memory retrieval. Science 301:846–50. doi: 10.1126/science.1085818

395. Selemon LD, Rajkowska G, Goldman-Rakic PS (1995) Abnormally high neuronal density in the schizophrenic cortex. A morphometric analysis of prefrontal area 9 and occipital area 17. Arch Gen Psychiatry 52:805–818; discussion 819-820. doi: 10.1001/archpsyc.1995.03950220015005

396. Seth A (2017) Your brain hallucinates your conscious reality, https://www.ted.com/talks/anil_seth_your_brain_hallucinates_your_conscious_reality, accessed: 2021-06-19 10:20:38

397. Seth AK, Barrett AB, Barnett L (2015) Granger Causality Analysis in Neuroscience and Neuroimaging. J Neurosci 35:3293–3297. doi: 10.1523/JNEUROSCI.4399-14.2015

398. Sherman SM, Guillery RW (2002) The role of the thalamus in the flow of information to the cortex. Philos Trans R Soc B Biol Sci 357:1695–1708. doi: 10.1098/rstb.2002.1161

399. Shi S-H, Hayashi Y, Esteban JA, Malinow R (2001) Subunit-Specific Rules Governing AMPA Receptor Trafficking to Synapses in Hippocampal Pyramidal Neurons. Cell 105:331–343. doi: 10.1016/S0092-8674(01)00321-X

400. Siapas AG, Lubenov EV, Wilson MA (2005) Prefrontal Phase Locking to Hippocampal Theta Oscillations. Neuron 46:141–151. doi: 10.1016/j.neuron.2005.02.028

401. Sigurdsson T, Stark KL, Karayiorgou M, Gogos JA, Gordon JA (2010) Impaired hippocampal–prefrontal synchrony in a genetic mouse model of schizophrenia. Nature 464:763–767. doi: 10.1038/nature08855

402. Simonsen A, Fusaroli R, Petersen ML, Vermillet A-Q, Bliksted V, Mors O, Roepstorff A, Campbell-Meiklejohn D (2021) Taking others into account: combining directly experienced and indirect information in schizophrenia. Brain. doi: 10.1093/brain/awab065

403. Sirota A, Montgomery S, Fujisawa S, Isomura Y, Zugaro M, Buzsáki G (2008) Entrainment of Neocortical Neurons and Gamma Oscillations by the Hippocampal Theta Rhythm. Neuron 60:683–697. doi: 10.1016/j.neuron.2008.09.014

404. Skurichina M, Duin RPW (2002) Bagging, Boosting and the Random Subspace Method for Linear Classifiers. Pattern Anal Appl 5:121–135. doi: 10.1007/s100440200011

405. Smith JW, Gastambide F, Gilmour G, Dix S, Foss J, Lloyd K, Malik N, Tricklebank M (2011) A comparison of the effects of ketamine and phencyclidine with other antagonists of the NMDA receptor in rodent assays of attention and working memory. Psychopharmacology (Berl) 217:255–269. doi: 10.1007/s00213-011-2277-5

406. Sohal VS, Zhang F, Yizhar O, Deisseroth K (2009) Parvalbumin neurons and gamma rhythms enhance cortical circuit performance. Nature 459:698–702. doi: 10.1038/nature07991

407. Soltesz I, Deschênes M (1993) Low- and high-frequency membrane potential oscillations during theta activity in CA1 and CA3 pyramidal neurons of the rat hippocampus under ketamine-xylazine anesthesia. J Neurophysiol 70:97–116. doi: 10.1152/jn.1993.70.1.97

408. Sommer B, Köhler M, Sprengel R, Seeburg PH (1991) RNA editing in brain controls a determinant of ion flow in glutamate-gated channels. Cell 67:11–19. doi: 10.1016/0092-8674(91)90568-J

409. Sommer IE, Bearden CE, van Dellen E, Breetvelt EJ, Duijff SN, Maijer K, van Amelsvoort T, de Haan L, Gur RE, Arango C, Díaz-Caneja CM, Vinkers CH, Vorstman JA (2016) Early interventions in risk groups for schizophrenia: what are we waiting for? Npj Schizophr 2:1–9. doi: 10.1038/npjschz.2016.3

410. Spellman T, Rigotti M, Ahmari SE, Fusi S, Gogos JA, Gordon JA (2015) Hippocampal-prefrontal input supports spatial encoding in working memory. Nature 522:309–314. doi: 10.1038/nature14445

411. Spencer KM, Nestor PG, Niznikiewicz MA, Salisbury DF, Shenton ME, McCarley RW (2003) Abnormal neural synchrony in schizophrenia. J Neurosci Off J Soc Neurosci 23:7407–7411

412. Spencer KM, Niznikiewicz MA, Nestor PG, Shenton ME, McCarley RW (2009) Left auditory cortex gamma synchronization and auditory hallucination symptoms in schizophrenia. BMC Neurosci 10:85. doi: 10.1186/1471-2202-10-85

413. Spencer KM, Salisbury DF, Shenton ME, McCarley RW (2008) Gamma-Band Auditory Steady-State Responses Are Impaired in First Episode Psychosis. Biol Psychiatry 64:369–375. doi: 10.1016/j.biopsych.2008.02.021

414. Spitzer M (1995) A neurocomputational approach to delusions. Compr Psychiatry 36:83–105. doi: 10.1016/S0010-440X(95)90103-5

415. Sponheim SR, Clementz BA, Iacono WG, Beiser M (1994) Resting EEG in first-episode and chronic schizophrenia. Psychophysiology 31:37–43. doi: 10.1111/j.1469-8986.1994.tb01023.x

416. Stam CJ, Nolte G, Daffertshofer A (2007) Phase lag index: Assessment of functional connectivity from multi channel EEG and MEG with diminished bias from common sources. Hum Brain Mapp 28:1178–1193. doi: 10.1002/hbm.20346

417. Stein A von, Chiang C, König P (2000) Top-down processing mediated by interareal synchronization. Proc Natl Acad Sci 97:14748–14753. doi: 10.1073/pnas.97.26.14748

418. Stevenson EL, Caldwell HK (2014) Lesions to the CA2 region of the hippocampus impair social memory in mice. Eur J Neurosci 40:3294–3301. doi: 10.1111/ejn.12689

419. Stout JJ, Griffin AL (2020) Representations of On-Going Behavior and Future Actions During a Spatial Working Memory Task by a High Firing-Rate Population of Medial Prefrontal Cortex Neurons. Front Behav Neurosci 14. doi: 10.3389/fnbeh.2020.00151

420. Strahnen D, Kapanaiah SKT, Bygrave AM, Kätzel D (2021) Lack of redundancy between electrophysiological measures of long-range neuronal communication. BMC Biol 19:24. doi: 10.1186/s12915-021-00950-4

421. Strahnen D, Kapanaiah SKT, Bygrave AM, Liss B, Bannerman DM, Akam T, Grewe BF, Johnson EL, Kätzel D (2021) Highly task-specific and distributed neural connectivity in working memory revealed by single-trial decoding in mice and humans. bioRxiv 2021.04.20.440621. doi: 10.1101/2021.04.20.440621

422. Strange BA, Witter MP, Lein ES, Moser EI (2014) Functional organization of the hippocampal longitudinal axis. Nat Rev Neurosci 15:655–669. doi: 10.1038/nrn3785

423. Stujenske JM, Likhtik E, Topiwala MA, Gordon JA (2014) Fear and Safety Engage Competing Patterns of Theta-Gamma Coupling in the Basolateral Amygdala. Neuron 83:919–933. doi: 10.1016/j.neuron.2014.07.026

424. Suh J, Rivest AJ, Nakashiba T, Tominaga T, Tonegawa S (2011) Entorhinal Cortex Layer III Input to the Hippocampus Is Crucial for Temporal Association Memory. Science 334:1415–1420. doi: 10.1126/science.1210125

425. Sullivan PF, Kendler KS, Neale MC (2003) Schizophrenia as a complex trait: evidence from a meta-analysis of twin studies. Arch Gen Psychiatry 60:1187–1192. doi: 10.1001/archpsyc.60.12.1187

426. Swanson LW (1981) A direct projection from Ammon's horn to prefrontal cortex in the rat. Brain Res 217:150–154. doi: 10.1016/0006-8993(81)90192-X

427. Szczepanski SM, Crone NE, Kuperman RA, Auguste KI, Parvizi J, Knight RT (2014) Dynamic Changes in Phase-Amplitude Coupling Facilitate Spatial Attention Control in Fronto-Parietal Cortex. PLOS Biol 12:e1001936. doi: 10.1371/journal.pbio.1001936

428. Takata N, Yoshida K, Komaki Y, Xu M, Sakai Y, Hikishima K, Mimura M, Okano H, Tanaka KF (2015) Optogenetic Activation of CA1 Pyramidal Neurons at the Dorsal and Ventral Hippocampus Evokes Distinct Brain-Wide Responses Revealed by Mouse fMRI. PloS One 10:e0121417. doi: 10.1371/journal.pone.0121417

429. Talati P, Rane S, Donahue MJ, Heckers S (2016) Hippocampal arterial cerebral blood volume in early psychosis. Psychiatry Res Neuroimaging 256:21–25. doi: 10.1016/j.pscychresns.2016.09.002

430. Talati P, Rane S, Kose S, Blackford JU, Gore J, Donahue MJ, Heckers S (2014) Increased hippocampal CA1 cerebral blood volume in schizophrenia. NeuroImage Clin 5:359–364. doi: 10.1016/j.nicl.2014.07.004

431. Talati P, Rane S, Skinner J, Gore J, Heckers S (2015) Increased hippocampal blood volume and normal blood flow in schizophrenia. Psychiatry Res 232:219–225. doi: 10.1016/j.pscychresns.2015.03.007

432. Tamura M, Mukai J, Gordon JA, Gogos JA (2016) Developmental Inhibition of Gsk3 Rescues Behavioral and Neurophysiological Deficits in a Mouse Model of Schizophrenia Predisposition. Neuron 89:1100–1109. doi: 10.1016/j.neuron.2016.01.025

433. Tamura M, Spellman TJ, Rosen AM, Gogos JA, Gordon JA (2017) Hippocampal-prefrontal theta-gamma coupling during performance of a spatial working memory task. Nat Commun 8:2182. doi: 10.1038/s41467-017-02108-9

434. Tan Z, Robinson HL, Yin D-M, Liu Y, Liu F, Wang H, Lin TW, Xing G, Gan L, Xiong W-C, Mei L (2018) Dynamic ErbB4 Activity in Hippocampal-Prefrontal Synchrony and Top-Down Attention in Rodents. Neuron 98:380-393.e4. doi: 10.1016/j.neuron.2018.03.018

435. Tanaka M, Kunugi A, Suzuki A, Suzuki N, Suzuki M, Kimura H (2019) Preclinical characterization of AMPA receptor potentiator TAK-137 as a therapeutic drug for schizophrenia. Pharmacol Res Perspect 7:e00479. doi: https://doi.org/10.1002/prp2.479

436. Teeters JL, Harris KD, Millman KJ, Olshausen BA, Sommer FT (2008) Data Sharing for Computational Neuroscience. Neuroinformatics 6:47–55. doi: 10.1007/s12021-008-9009-y

437. Teutsch J, Kätzel D (2019) Operant Assessment of DMTP Spatial Working Memory in Mice. Front Behav Neurosci 13:193. doi: 10.3389/fnbeh.2019.00193

438. Thuné H, Recasens M, Uhlhaas PJ (2016) The 40-Hz Auditory Steady-State Response in Patients With Schizophrenia: A Meta-analysis. JAMA Psychiatry 73:1145–1153. doi: 10.1001/jamapsychiatry.2016.2619

439. Timms AE, Dorschner MO, Wechsler J, Choi KY, Kirkwood R, Girirajan S, Baker C, Eichler EE, Korvatska O, Roche KW, Horwitz MS, Tsuang DW (2013) Support for the N -Methyl-D-Aspartate Receptor Hypofunction Hypothesis of Schizophrenia From Exome Sequencing in Multiplex Families. JAMA Psychiatry 70:582–590. doi: 10.1001/jamapsychiatry.2013.1195

440. Tin Kam Ho (1998) The random subspace method for constructing decision forests. IEEE Trans Pattern Anal Mach Intell 20:832–844. doi: 10.1109/34.709601

441. Tort ABL, Komorowski RW, Manns JR, Kopell NJ, Eichenbaum H (2009) Theta–gamma coupling increases during the learning of item–context associations. Proc Natl Acad Sci 106:20942–20947. doi: 10.1073/pnas.0911331106

442. Tort ABL, Kramer MA, Thorn C, Gibson DJ, Kubota Y, Graybiel AM, Kopell NJ (2008) Dynamic cross-frequency couplings of local field potential oscillations in rat striatum and hippocampus during performance of a T-maze task. Proc Natl Acad Sci 105:20517–20522. doi: 10.1073/pnas.0810524105

443. Tregellas JR, Smucny J, Harris JG, Olincy A, Maharajh K, Kronberg E, Eichman LC, Lyons E, Freedman R (2014) Intrinsic Hippocampal Activity as a Biomarker for Cognition and Symptoms in Schizophrenia. Am J Psychiatry 171:549–556. doi: 10.1176/appi.ajp.2013.13070981

444. Tsien JZ, Huerta PT, Tonegawa S (1996) The Essential Role of Hippocampal CA1 NMDA Receptor–Dependent Synaptic Plasticity in Spatial Memory. Cell 87:1327–1338. doi: 10.1016/S0092-8674(00)81827-9

445. Uhlhaas PJ (2013) Dysconnectivity, large-scale networks and neuronal dynamics in schizophrenia. Curr Opin Neurobiol 23:283–290. doi: 10.1016/j.conb.2012.11.004

446. Uhlhaas PJ, Linden DEJ, Singer W, Haenschel C, Lindner M, Maurer K, Rodriguez E (2006) Dysfunctional Long-Range Coordination of Neural Activity during Gestalt Perception in Schizophrenia. J Neurosci 26:8168–8175. doi: 10.1523/JNEUROSCI.2002-06.2006

447. Uhlhaas PJ, Singer W (2010) Abnormal neural oscillations and synchrony in schizophrenia. Nat Rev Neurosci 11:100–113. doi: 10.1038/nrn2774

448. Uylings HBM, Groenewegen HJ, Kolb B (2003) Do rats have a prefrontal cortex? Behav Brain Res 146:3–17. doi: 10.1016/j.bbr.2003.09.028

449. Vanderwolf CH (1969) Hippocampal electrical activity and voluntary movement in the rat. Electroencephalogr Clin Neurophysiol 26:407–418. doi: 10.1016/0013-4694(69)90092-3

450. Vardigan JD, Huszar SL, McNaughton CH, Hutson PH, Uslaner JM (2010) MK-801 produces a deficit in sucrose preference that is reversed by clozapine, d-serine, and the metabotropic glutamate 5 receptor positive allosteric modulator CDPPB: Relevance to negative symptoms associated with schizophrenia? Pharmacol Biochem Behav 95:223–229. doi: 10.1016/j.pbb.2010.01.010

451. Vekovischeva OY, Aitta-aho T, Echenko O, Kankaanpää A, Seppälä T, Honkanen A, Sprengel R, Korpi ER (2004) Reduced aggression in AMPA-type glutamate receptor GluR-A subunit-deficient mice. Genes Brain Behav 3:253–265. doi: 10.1111/j.1601-1848.2004.00075.x

452. Vertes RP (2004) Differential projections of the infralimbic and prelimbic cortex in the rat. Synapse 51:32–58. doi: 10.1002/syn.10279

453. Vertes RP (2006) Interactions among the medial prefrontal cortex, hippocampus and midline thalamus in emotional and cognitive processing in the rat. Neuroscience 142:1–20

454. Vinck M, Oostenveld R, van Wingerden M, Battaglia F, Pennartz CMA (2011) An improved index of phase-synchronization for electrophysiological data in the presence of volume-conduction, noise and sample-size bias. NeuroImage 55:1548–1565. doi: 10.1016/j.neuroimage.2011.01.055

455. Vinck M, van Wingerden M, Womelsdorf T, Fries P, Pennartz CMA (2010) The pairwise phase consistency: A bias-free measure of rhythmic neuronal synchronization. NeuroImage 51:112–122. doi: 10.1016/j.neuroimage.2010.01.073

456. Vinogradova OS (2001) Hippocampus as comparator: Role of the two input and two output systems of the hippocampus in selection and registration of information. Hippocampus 11:578–598. doi: 10.1002/hipo.1073

457. Voloh B, Valiante TA, Everling S, Womelsdorf T (2015) Theta–gamma coordination between anterior cingulate and prefrontal cortex indexes correct attention shifts. Proc Natl Acad Sci. doi: 10.1073/pnas.1500438112

458. Voytek B (2010) Shifts in gamma phase–amplitude coupling frequency from theta to alpha over posterior cortex during visual tasks. Front Hum Neurosci 4. doi: 10.3389/fnhum.2010.00191

459. Voytek B, D’Esposito M, Crone N, Knight RT (2013) A method for event-related phase/amplitude coupling. NeuroImage 64:416–424. doi: 10.1016/j.neuroimage.2012.09.023

460. Vu M-AT, Adalı T, Ba D, Buzsáki G, Carlson D, Heller K, Liston C, Rudin C, Sohal VS, Widge AS, Mayberg HS, Sapiro G, Dzirasa K (2018) A Shared Vision for Machine Learning in Neuroscience. J Neurosci 38:1601–1607. doi: 10.1523/JNEUROSCI.0508-17.2018

461. Wagner AR (2014) SOP: A Model of Automatic Memory Processing in Animal Behavior. In: Inf. Process. Anim. https://www.taylorfrancis.com/. Accessed 3 May 2020

462. Walf AA, Frye CA (2007) The use of the elevated plus maze as an assay of anxiety-related behavior in rodents. Nat Protoc 2:322–328. doi: 10.1038/nprot.2007.44

463. Wang C, Ulbert I, Schomer DL, Marinkovic K, Halgren E (2005) Responses of human anterior cingulate cortex microdomains to error detection, conflict monitoring, stimulus-response mapping, familiarity, and orienting. J Neurosci Off J Soc Neurosci 25:604–613. doi: 10.1523/JNEUROSCI.4151-04.2005

464. Wang X, Pinto-Duarte A, Behrens MM, Zhou X, Sejnowski TJ (2018) Ketamine independently modulated power and phase-coupling of theta oscillations in Sp4 hypomorphic mice. PLOS ONE 13:e0193446. doi: 10.1371/journal.pone.0193446

465. Watanabe T, Niki H (1985) Hippocampal unit activity and delayed response in the monkey. Brain Res 325:241–254. doi: 10.1016/0006-8993(85)90320-8

466. Watanabe T, Niki H (1985) Hippocampal unit activity and delayed response in the monkey. Brain Res 325:241–254. doi: 10.1016/0006-8993(85)90320-8

467. Weinberger DR (1987) Implications of Normal Brain Development for the Pathogenesis of Schizophrenia. Arch Gen Psychiatry 44:660–669. doi: 10.1001/archpsyc.1987.01800190080012

468. Weinberger DR, Berman KF, Zec RF (1986) Physiologic dysfunction of dorsolateral prefrontal cortex in schizophrenia. I. Regional cerebral blood flow evidence. Arch Gen Psychiatry 43:114–124. doi: 10.1001/archpsyc.1986.01800020020004

469. Weinberger DR, Gallhofer B (1997) Cognitive function in schizophrenia. Int Clin Psychopharmacol 12 Suppl 4:S29-36. doi: 10.1097/00004850-199709004-00006

470. Wenthold RJ, Petralia RS, Blahos J II, Niedzielski AS (1996) Evidence for multiple AMPA receptor complexes in hippocampal CA1/CA2 neurons. J Neurosci Off J Soc Neurosci 16:1982–1989

471. Wiedholz LM, Owens WA, Horton RE, Feyder M, Karlsson R-M, Hefner K, Sprengel R, Celikel T, Daws LC, Holmes A (2008) Mice lacking the AMPA GluR1 receptor exhibit striatal hyperdopaminergia and “schizophrenia-related” behaviors. Mol Psychiatry 13:631–640. doi: 10.1038/sj.mp.4002056

472. Wiener N (1956) The theory of prediction. Mod Math Eng

473. Witham CL, Riddle CN, Baker MR, Baker SN (2011) Contributions of descending and ascending pathways to corticomuscular coherence in humans. J Physiol 589:3789–3800. doi: 10.1113/jphysiol.2011.211045

474. Witter MP, Amaral DG (1991) Entorhinal cortex of the monkey: V. Projections to the dentate gyrus, hippocampus, and subicular complex. J Comp Neurol 307:437–459. doi: 10.1002/cne.903070308

475. Woloszyn L, Sheinberg DL (2009) Neural Dynamics in Inferior Temporal Cortex during a Visual Working Memory Task. J Neurosci 29:5494–5507. doi: 10.1523/JNEUROSCI.5785-08.2009

476. Womelsdorf T, Schoffelen J-M, Oostenveld R, Singer W, Desimone R, Engel AK, Fries P (2007) Modulation of Neuronal Interactions Through Neuronal Synchronization. Science 316:1609–1612. doi: 10.1126/science.1139597

477. Woodward ND, Heckers S (2016) Mapping Thalamocortical Functional Connectivity in Chronic and Early Stages of Psychotic Disorders. Biol Psychiatry 79:1016–1025. doi: 10.1016/j.biopsych.2015.06.026

478. Woodward ND, Karbasforoushan H, Heckers S (2012) Thalamocortical dysconnectivity in schizophrenia. Am J Psychiatry 169:1092–1099. doi: 10.1176/appi.ajp.2012.12010056

479. Woodward TS, Moritz S, Menon M, Klinge R (2008) Belief inflexibility in schizophrenia. Cognit Neuropsychiatry 13:267–277. doi: 10.1080/13546800802099033

480. Wright IC, Ellison ZR, Sharma T, Friston KJ, Murray RM, McGuire PK (1999) Mapping of grey matter changes in schizophrenia1This work was presented, in part, at the VIth International Congress on Schizophrenia Research, Colorado Springs, Colorado, USA, April 1997.1. Schizophr Res 35:1–14. doi: 10.1016/S0920-9964(98)00094-2

481. Wyatt RJ (1991) 13. Early intervention with neuroleptics may decrease the l long-term morbidity of schizophrenia. Schizophr Res 5:201–202. doi: 10.1016/0920-9964(91)90073-Z

482. Xing D, Yeh C-I, Shapley RM (2009) Spatial spread of the local field potential and its laminar variation in visual cortex. J Neurosci Off J Soc Neurosci 29:11540–11549. doi: 10.1523/JNEUROSCI.2573-09.2009

483. Yamamoto J, Suh J, Takeuchi D, Tonegawa S (2014) Successful Execution of Working Memory Linked to Synchronized High-Frequency Gamma Oscillations. Cell 157:845–857. doi: 10.1016/j.cell.2014.04.009

484. Yhnell E, Dunnett SB, Brooks SP (2016) The utilisation of operant delayed matching and non-matching to position for probing cognitive flexibility and working memory in mouse models of Huntington’s disease. J Neurosci Methods 265:72–80. doi: 10.1016/j.jneumeth.2015.08.022

485. Yoon T, Okada J, Jung MW, Kim JJ (2008) Prefrontal cortex and hippocampus subserve different components of working memory in rats. Learn Mem 15:97–105. doi: 10.1101/lm.850808

486. Yui K, Goto K, Ikemoto S, Ishiguro T, Angrist B, Duncan GE, Sheitman BB, Lieberman JA, Bracha SH, Ali SF (1999) Neurobiological basis of relapse prediction in stimulant-induced psychosis and schizophrenia: the role of sensitization. Mol Psychiatry 4:512–523. doi: 10.1038/sj.mp.4000575

487. Yuste R (2015) From the neuron doctrine to neural networks. Nat Rev Neurosci 16:487–497. doi: 10.1038/nrn3962

488. Zamanillo D, Sprengel R, Hvalby Ø, Jensen V, Burnashev N, Rozov A, Kaiser KMM, Köster HJ, Borchardt T, Worley P, Lübke J, Frotscher M, Kelly PH, Sommer B, Andersen P, Seeburg PH, Sakmann B (1999) Importance of AMPA Receptors for Hippocampal Synaptic Plasticity But Not for Spatial Learning. Science 284:1805–1811. doi: 10.1126/science.284.5421.1805

489. Zhang X, Zhong W, Brankačk J, Weyer SW, Müller UC, Tort ABL, Draguhn A (2016) Impaired theta-gamma coupling in APP-deficient mice. Sci Rep 6:1–10. doi: 10.1038/srep21948

490. Zheng L, Chai H, Yu S, Xu Y, Chen W, Wang W (2015) EEG Theta Power and Coherence to Octave Illusion in First-Episode Paranoid Schizophrenia with Auditory Hallucinations. Psychopathology 48:36–46. doi: 10.1159/000366104

491. Zhu JJ, Esteban JA, Hayashi Y, Malinow R (2000) Postnatal synaptic potentiation: Delivery of GluR4-containing AMPA receptors by spontaneous activity. Nat Neurosci 3:1098–1106. doi: 10.1038/80614

APPENDIX

Suppl. Table 1: Number of electrodes, connections, mice, and trials in mouse experiments.
Adapted from [421], open access article: CC BY 4.0, https://creativecommons.org/licenses/by/4.0/

	# of electrodes	**# of mice**	**Number of trials in ...**			
			5-CSWM, 1s SD + 5s delay	DNMTS, baseli-ne	T-maze, 5s	T-maze, 30s
PFC electrodes	19	12	758	1431	732	674
dHC electrodes	7	7	464	1320	448	408
vHC electrodes	12	9	584	1700	544	480
MD electrodes	4	7	236	694	246	224
PFC-dHC	7	7	464	1320	448	408
PFC-vHC	9	9	584	1700	544	480
vHC-dHC	6	6	400	1172	318	334
MD-PFC	4	4	236	694	246	224

Suppl. Table 2: Classifier parameters for prediction of operant DMTS 5-CSWM in wildtype mice
Measures of classification performance, the prediction accuracy, the AUC of the ROC the F1 and F2-score, sensitivity, specificity, and precision and recall for both classes (for definition of these parameters see 2.6). Rows represent respective brain region or connection. Adapted from [421], open access article: CC BY 4.0, https://creativecommons.org/licenses/by/4.0/

	Accuracy	AUC	F1	F2	sensitivity	specificity	cl1-precision	cl1-recall	cl2-precision	cl2-recall
PFC	0.66	0.66	0.66	0.65	0.65	0.67	0.68	0.65	0.64	0.67
dHC	0.79	0.79	0.79	0.78	0.79	0.79	0.79	0.79	0.78	0.79
vHC	0.61	0.61	0.62	0.58	0.60	0.62	0.65	0.60	0.56	0.62
MD	0.76	0.77	0.77	0.74	0.73	0.81	0.83	0.73	0.69	0.81
PFC-dHC	0.78	0.79	0.80	0.76	0.75	0.84	0.86	0.75	0.70	0.84
PFC-vHC	0.71	0.71	0.71	0.70	0.70	0.72	0.73	0.70	0.68	0.72
PFC-MD	0.77	0.79	0.79	0.74	0.74	0.85	0.87	0.74	0.67	0.85
vHC-dHC	0.73	0.74	0.74	0.71	0.71	0.76	0.78	0.71	0.68	0.76

Suppl. Table 3: Classifier parameters for prediction of operant DNMTS 2-CSWM in wildtype mice
Displays same as in Suppl. Table 2 but for the operant DNMTS task. Adapted from [421], open access article: CC BY 4.0, https://creativecommons.org/licenses/by/4.0/

	Accuracy	AUC	F1	F2	sensitivity	specificity	cl1-precision	cl1-recall	cl2-precision	cl2-recall
PFC	0.77	0.77	0.77	0.76	0.75	0.79	0.80	0.75	0.74	0.79
dHC	0.87	0.87	0.87	0.86	0.85	0.89	0.89	0.85	0.84	0.89
vHC	0.71	0.72	0.73	0.69	0.69	0.74	0.77	0.69	0.65	0.74
MD	0.73	0.74	0.74	0.72	0.72	0.75	0.77	0.72	0.69	0.75
PFC-dHC	0.70	0.71	0.73	0.67	0.67	0.75	0.80	0.67	0.61	0.75
PFC-vHC	0.63	0.63	0.65	0.61	0.62	0.65	0.68	0.62	0.58	0.65
PFC-MD	0.67	0.68	0.69	0.63	0.65	0.71	0.76	0.65	0.58	0.71
vHC-dHC	0.65	0.66	0.67	0.63	0.64	0.68	0.71	0.64	0.59	0.68

Suppl. Table 4: Classifier parameters for prediction of T-maze SWM in wildtype mice
Displays same as in Suppl. Table 2 but for T-maze. Adapted from [421], open access article: CC BY 4.0, https://creativecommons.org/licenses/by/4.0/

	Accuracy	AUC	F1	F2	sensitivity	specificity	cl1-precision	cl1-recall	cl2-precision	cl2-recall
PFC	0.63	0.63	0.62	0.63	0.64	0.62	0.61	0.64	0.64	0.62
dHC	0.70	0.73	0.75	0.64	0.65	0.82	0.88	0.65	0.53	0.82
vHC	0.67	0.67	0.66	0.67	0.68	0.67	0.66	0.68	0.68	0.67
MD	0.77	0.82	0.81	0.71	0.70	0.94	0.96	0.70	0.58	0.94
PFC-dHC	0.87	0.90	0.89	0.85	0.80	1.00	1.00	0.80	0.74	1.00
PFC-vHC	0.82	0.83	0.82	0.82	0.82	0.83	0.83	0.82	0.82	0.83
PFC-MD	0.84	0.88	0.86	0.80	0.77	1.00	1.00	0.77	0.68	1.00
vHC-dHC	0.83	0.85	0.84	0.81	0.79	0.91	0.91	0.79	0.75	0.91

Suppl. Table 5: Classifier parameters for prediction of identity task in humans
Displays same as in Suppl. Table 2 but for identity task in humans. Adapted from [421], open access article: CC BY 4.0, https://creativecommons.org/licenses/by/4.0/

	Accuracy	AUC	F1	F2	sensitivity	specificity	cl1-precision	cl1-recall	cl2-precision	cl2-recall
PFC	0.78	0.78	0.79	0.77	0.76	0.8	0.82	0.76	0.74	0.8
OFC	0.77	0.78	0.78	0.77	0.77	0.79	0.79	0.77	0.75	0.79
MTL	0.8	0.81	0.81	0.8	0.8	0.82	0.82	0.8	0.79	0.82
PFC-MTL	0.84	0.88	0.87	0.81	0.76	1	1	0.76	0.69	1
PFC-OFC	0.89	0.91	0.9	0.88	0.83	1	1	0.83	0.79	1
OFC-MTL	0.86	0.88	0.88	0.84	0.79	0.98	0.98	0.79	0.74	0.98

Suppl. Table 6: Classifier parameters for prediction of spatial task in humans
Displays same as in Suppl. Table 2 but for spatial task in humans. Adapted from [421], open access article: CC BY 4.0, https://creativecommons.org/licenses/by/4.0/

	Accuracy	AUC	F1	F2	sensitivity	specificity	cl1-precision	cl1-recall	cl2-precision	cl2-recall
PFC	0.71	0.72	0.73	0.68	0.68	0.75	0.79	0.68	0.63	0.75
OFC	0.82	0.82	0.82	0.81	0.81	0.84	0.85	0.81	0.79	0.84
MTL	0.76	0.77	0.78	0.74	0.73	0.81	0.83	0.73	0.7	0.81
PFC-MTL	0.89	0.91	0.9	0.87	0.82	1	1	0.82	0.77	1
PFC-OFC	0.89	0.91	0.9	0.88	0.83	1	1	0.83	0.79	1
OFC-MTL	0.89	0.91	0.9	0.87	0.82	1	1	0.82	0.77	1

Suppl. Table 7: Classifier parameters for prediction of temporal task in humans
Displays same as in Suppl. Table 2 but for temporal task in humans. Adapted from [421], open access article: CC BY 4.0, https://creativecommons.org/licenses/by/4.0/

	Accuracy	AUC	F1	F2	sensitivity	specificity	cl1-precision	cl1-recall	cl2-precision	cl2-recall
PFC	0.78	0.79	0.79	0.78	0.77	0.81	0.81	0.77	0.76	0.81
OFC	0.75	0.76	0.76	0.73	0.72	0.79	0.81	0.72	0.69	0.79
MTL	0.73	0.74	0.75	0.72	0.71	0.77	0.8	0.71	0.67	0.77
PFC-MTL	0.86	0.89	0.88	0.84	0.79	1	1	0.79	0.73	1
PFC-OFC	0.86	0.89	0.88	0.84	0.79	0.99	1	0.79	0.73	0.99
OFC-MTL	0.89	0.91	0.9	0.87	0.82	1	1	0.82	0.78	1

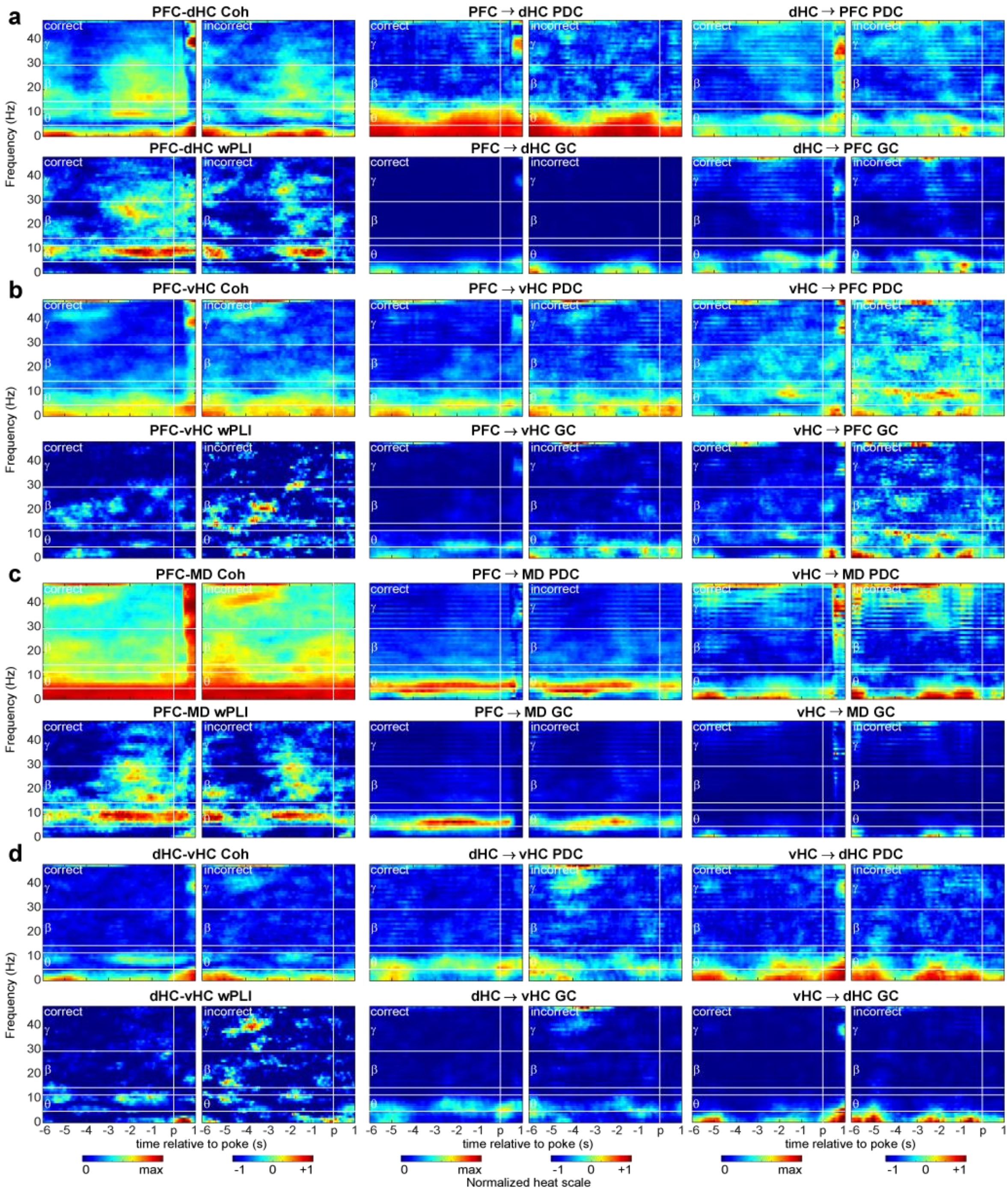

Suppl. Figure 1: Spectrograms of connectivity during the 5-CSWM delay and CP (1s SD+5s delay challenge)

(a-d) Spectrograms displayed from 6s before to 1s after a CP poke for the connections and metrics named in subpanel titles. Left and right graphs of each subpanel correspond to connectivity during correct and incorrect responses, respectively. White vertical lines indicate time of CP poke, while white horizontal lines differentiate between frequency ranges named on the left. Adapted from [421], open access article: CC BY 4.0, https://creativecommons.org/licenses/by/4.0/

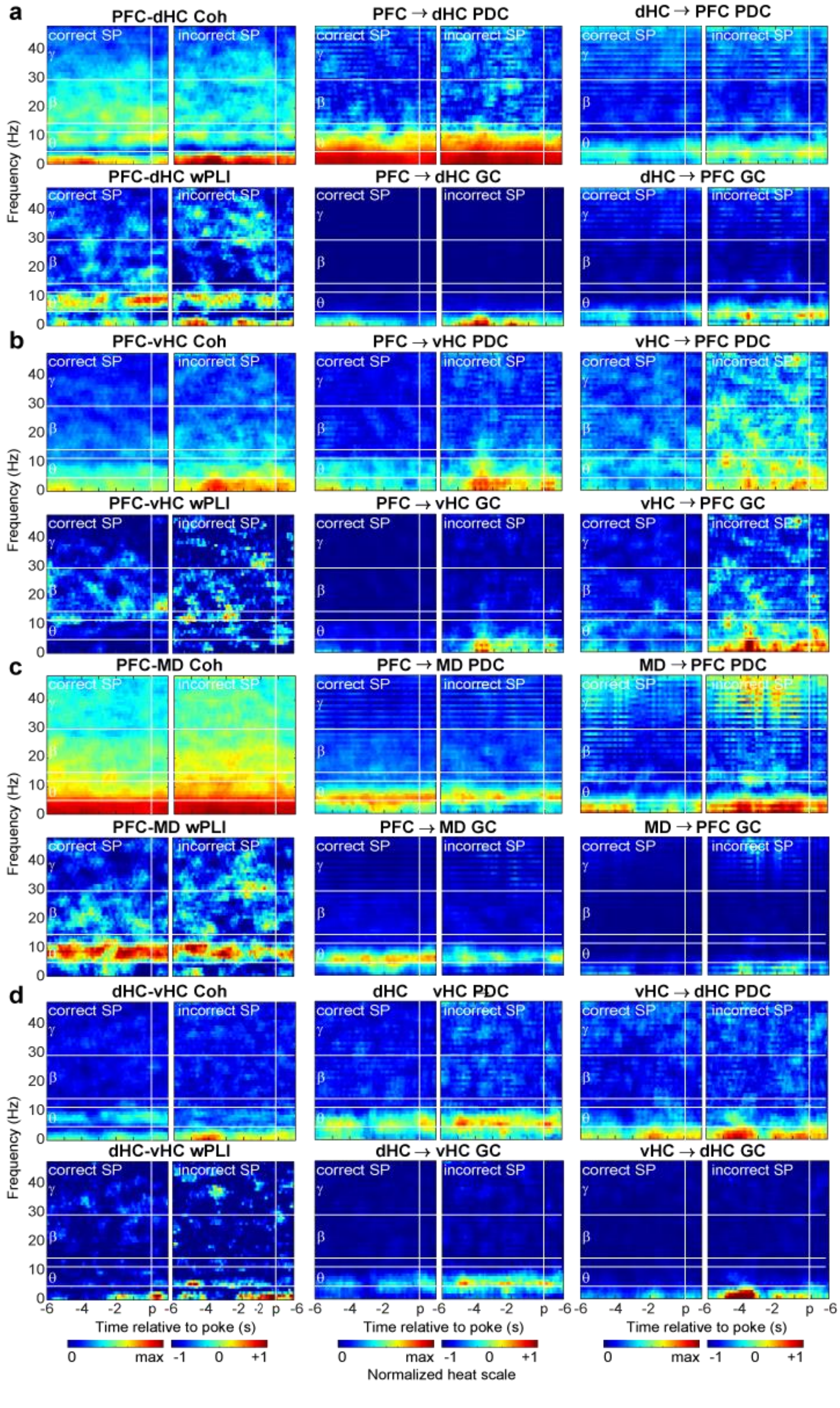

Suppl. Figure 2: Spectrograms of connectivity during the 5-CSWM SP (1s SD+5s delay challenge)
Same display as in Suppl. Figure 1, but for SP. Analogously, left, and right graphs of each subpanel correspond to connectivity during correct and incorrect SP responses, respectively. White vertical lines indicate SP poke. Adapted from [421], open access article: CC BY 4.0, https://creativecommons.org/licenses/by/4.0/

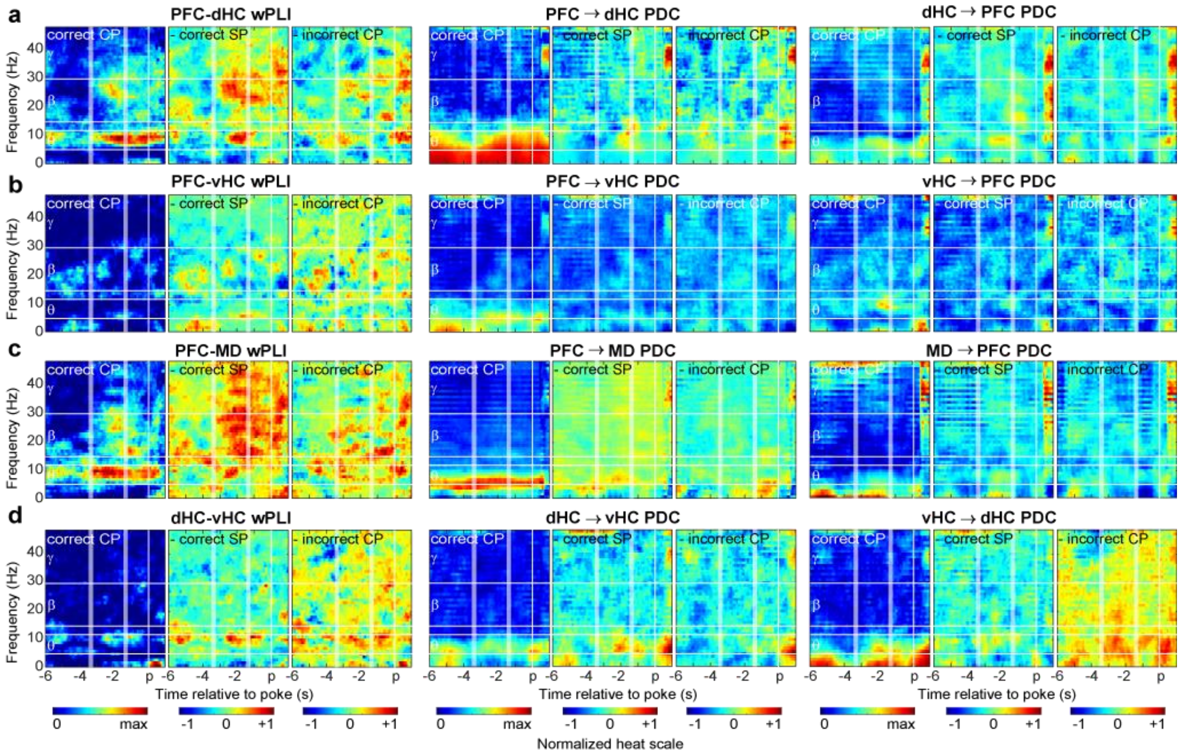

Suppl. Figure 3: Spectrograms of differential connectivity during the 5-CSWM delay and CP (1s SD+5s delay challenge)

(a-d) Same display as in main Figure 3.2.2a-d, but for wPLI and PDC. Spectrograms depicting min-max normalized coherence and GC for the connections stated above each triplet panel for the delay and CP of the 5-CSWM task, temporally aligned to the choice poke entry (p, white vertical lines; showing 6 s before until 1 s after the poke); the start and end of the post-delay shown by white stripes corresponding to mean ± SD as determined by CP response latency. Each triplet shows the absolute value (left), the difference between the former and either the prior correct SP (controlling for representations of attention and reward, middle), or incorrect CPs (showing differences of WM engagement and subtracting motor representations of poking; right). Horizontal white lines show borders between analysed frequency bands, stated on the left. Adapted from [421], open access article: CC BY 4.0, https://creativecommons.org/licenses/by/4.0/

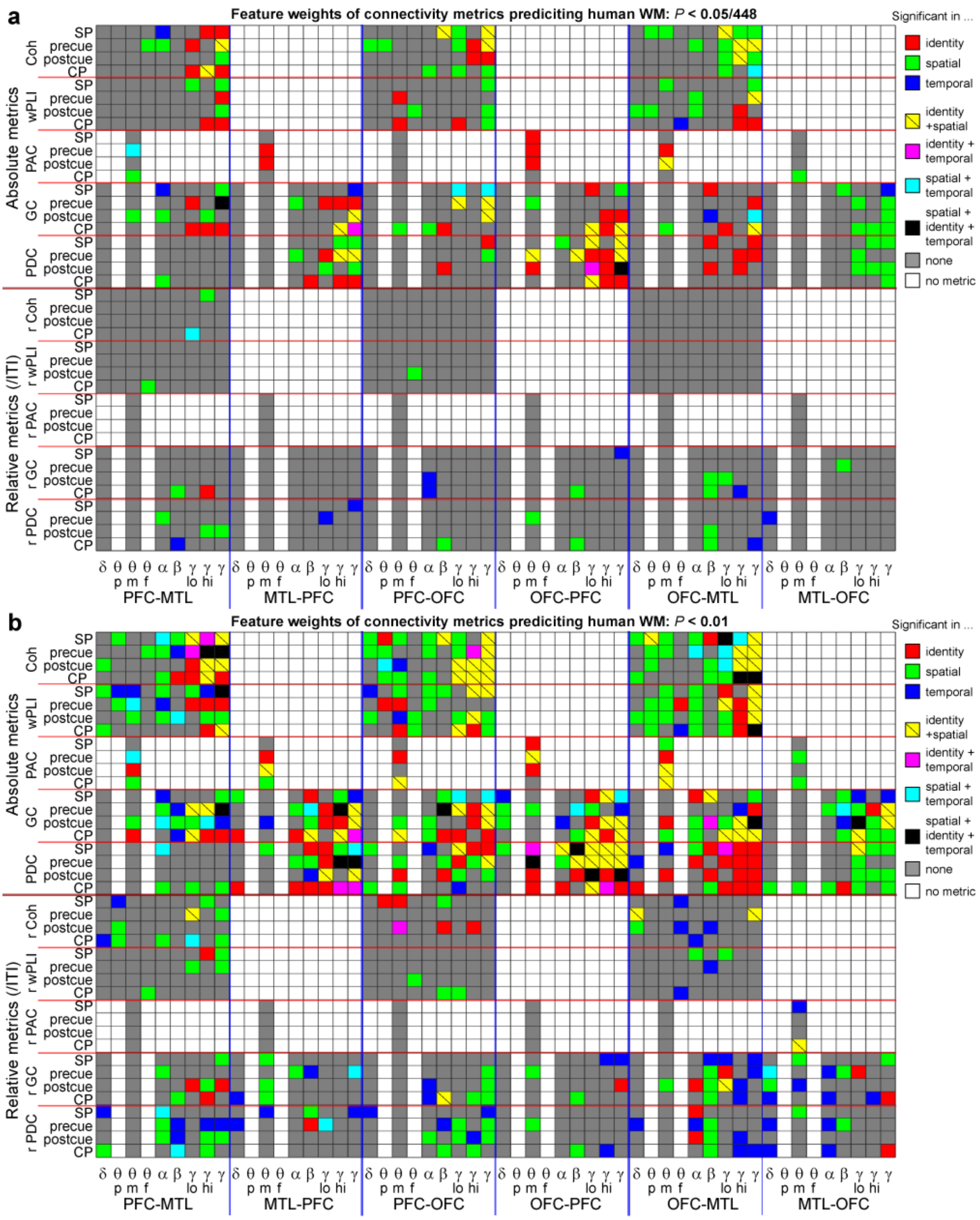

Suppl. Figure 4: Individual connectivity measures predicting WM choice in humans selected at lower *P*-value threshold.

(**a-b**) Matrix showing all connectivity predictor variables that contributed to the classifiers for which performance is shown in main Figure 3.2.13a (one classifier using all regional and local variables of all phases, *N* = 1584, as predictors). Indicated by colour are variables that were significantly associated with WM-performance according to their weight and differences between correct and incorrect CP in the paradigms coded by colour (see legend on the right). Same display as in main Figure 3.2.15a but using less conservative *P*-values: (**a**) Bonferroni-adjustment using the number of predictor variables of each single connection (448), $P < 0.05/448$. (**b**) Standard *P*-value of 0.01, $P < 0.01$. For theta, mean amplitude (m), peak amplitude (p), and frequency of peak (f) are shown, while for all other variables only the mean amplitude is used. The gamma-band contributed three predictors each as this frequency was split into a high- and low-gamma-range in addition to using the whole range (30-100 Hz). Adapted from [421], open access article: CC BY 4.0, https://creativecommons.org/licenses/by/4.0/

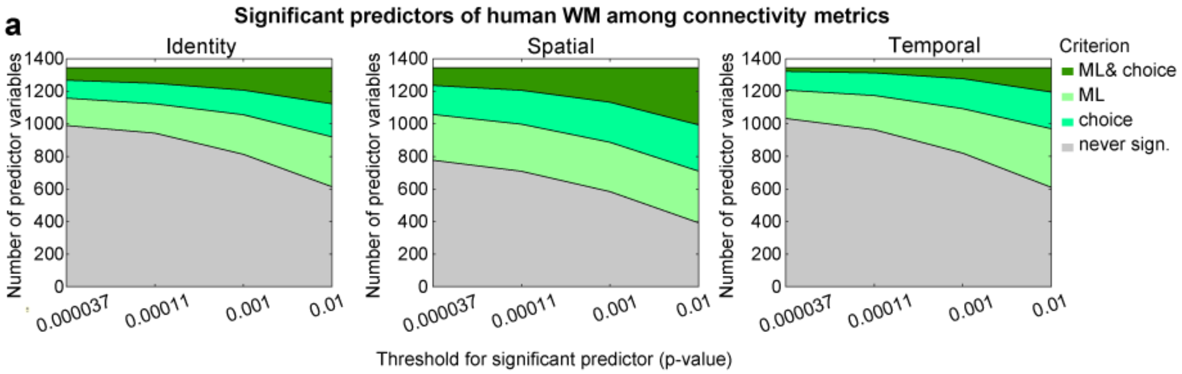

Suppl. Figure 5: Number of connectivity measures predicting WM choice in humans in dependence on *P*-value.

(**a**) The number of connectivity variables that are associated with WM-performance as the *P*-value adjustment for the selection of significant predictors is relaxed. The first value in each sub-panel corresponds to the adjustment by the number of *all* connectivity variables ($P < 0.05/1344$), the second value corresponds to the adjustment by number variables in a single connection ($P < 0.05/448$). Adapted from [421], open access article: CC BY 4.0, https://creativecommons.org/licenses/by/4.0/

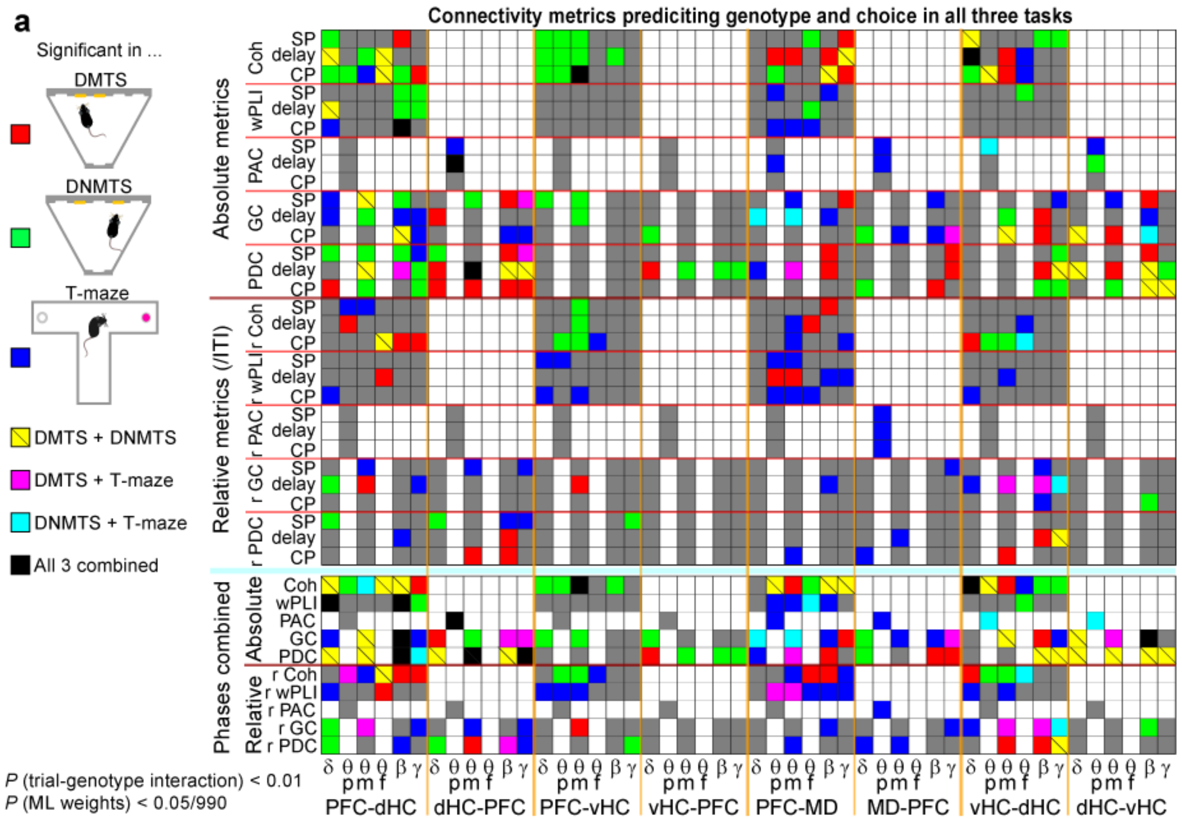

Suppl. Figure 6: Individual connectivity measures predicting WM choice and genotype in multi-class classifiers across rodent tasks.

(**a**) Same display as in main Figure 3.3.8a but for higher (less conservative) *P*-value thresholds: Bonferroni-adjustment using the number of parameters for all connections (990 for 5-CSWM DMTS, 720 for the other two tasks) for the comparison of predictor weights (real vs. shuffled, *t*-test) and $P < 0.01$ used as threshold for significant interactions between genotype (KO/WT) and trial-type (correct vs. incorrect). In the lower sub-panel, the display is reproduced but with all task-phases combined. Note that variables from the pre- and post-delay in the 5-CSWM have been combined in single lines.

FIGURES AND TABLES

ACKNOWLEDGEMENTS

Diese Arbeit wurde am Institut für Angewandte Physiologie der Universität Ulm unter der Betreuung von Prof. Dennis Kätzel angefertigt, dem ich allem voran für die Möglichkeit danken möchte meine Arbeit in seinem Labor durchzuführen. Vielen Dank für die unermüdliche Unterstützung und die außergewöhnlich motivierende und hingebungsvolle Art mit der du wissenschaftliches Denken und Arbeit vermittelst. Dein konstanter Enthusiasmus für die Wissenschaft war stets inspirierend und hat auch in mir die Leidenschaft zur Forschung geweckt.

My special thanks go to Sampath K. T. Kapanaiah who introduced me to working in the lab and had tremendous influence on the results presented in this thesis. Without his mastermind behind the operant boxes, I would have been left clueless more than once. Thank you for showing me how to carry out experiments, your help in general and our fruitful discussions!

I am also thankful for the unlimited help I received from Stefanie Schulz during my time in the lab and her guidance on how best to care of the mice.

I would also like to thank the other members of the group during my time in the lab. Kasyoka, Bas, Uwe, Peter, and Martin, thank you for your constant support and our inspiring lunch and coffee breaks!

CURRICULUM VITAE

The curriculum vitae has been removed for data protection reasons.